MEASURED RESULTS FOR A NEW HOLE-PATTERN ANNULAR GAS SEAL INCORPORATING LARGER DIAMETER HOLES, COMPARISONS TO RESULTS FOR A TRADITIONAL HOLE-PATTERN SEAL, AND PREDICTIONS

A Thesis

by

MICHAEL LLOYD VANNARSDALL

Submitted to the Office of Graduate Studies of
Texas A&M University
in partial fulfillment of the requirements for the degree of

MASTER OF SCIENCE

August 2011

Major Subject: Mechanical Engineering

MEASURED RESULTS FOR A NEW HOLE-PATTERN ANNULAR GAS SEAL INCORPORATING LARGER DIAMETER HOLES, COMPARISONS TO RESULTS FOR A TRADITIONAL HOLE-PATTERN SEAL, AND PREDICTIONS

A Thesis

by

MICHAEL LLOYD VANNARSDALL

Submitted to the Office of Graduate Studies of
Texas A&M University
in partial fulfillment of the requirements for the degree of

MASTER OF SCIENCE

Approved by:

Chair of Committee,	Dara W. Childs
Committee Members,	Gerald Morrison
	James Morgan
Head of Department,	Dennis L. O'Neal

August 2011

Major Subject: Mechanical Engineering

ABSTRACT

Measured Results for a New Hole-Pattern Annular Gas Seal Incorporating Larger Diameter Holes, Comparisons to Results for a Traditional Hole-Pattern Seal, and Predictions. (August 2011)

Michael Lloyd Vannarsdall, B.S., University of Kentucky

Chair of Advisory Committee: Dr. Dara W. Childs

To reduce manufacturing cost and time, a hole-pattern seal incorporating holes of larger diameter (12.19 mm (0.48 inches)) has been proposed. Experimental leakage and rotordynamic coefficients for this "new" seal design are presented. This experimental data was compared to theoretical results generated by ISOTSEAL a program developed by Kleynhans and Childs. Finally, the performance of this new hole-pattern seal was compared to a hole-pattern seal tested by Wade.

The experiments are configured to investigate the influence of changes in pressure ratio, preswirl, rotor speed, and clearances on seal characteristics. Due to stator stability issues, the peak inlet pressures had to be varied to allow for testing. Consequently, to study the effect of inlet preswirl and clearance, data were non-dimensionalized or normalized.

Cross-coupled coefficients were relatively frequency-independent while direct coefficients were functions of excitation frequency.

For all test cases, the seal developed negative direct stiffness at low frequencies.

Tests showed that pressure ratio had minimal effect on rotordynamic coefficients.

Non-dimensional cross-coupled stiffness increased with increasing preswirl causing the seal to become less stable with increasing preswirl.

Cross coupled stiffness increased with increasing running speed.

Two clearances: 0.1 mm (4 mils) and 0.2 mm (8 mils) were tested. The results demonstrated that non-dimensionalized stiffness is greater for the smaller clearance. The

larger clearance develops larger normalized direct damping values, and has enhanced stability.

Rotordynamic predictions are poor for cross-coupled coefficients. Generally, ISOTSEAL over-predicts direct stiffness and under-predicts direct damping. Negative stiffness was not predicted by ISOTSEAL. Predictions do improve for the smaller clearance.

ISOTSEAL does a good job of predicting non-dimensional leakage.

Non-dimensionalized direct and effective stiffness were greater for the "old" hole-pattern seal tested by Wade. However, the "new" seal generally developed greater normalized direct damping and exhibited a lower *cross-over frequency*. Non-dimensionalized leakage was greater for the seal tested here.

Production of this new seal proved to be more difficult than originally thought. The price of the new seal cost approximately the same as an original hole-pattern seal.

DEDICATION

This thesis is dedicated to my parents whom I love and respect very deeply.

ACKNOWLEDGEMENTS

I would like to thank Dr. Childs for allowing me the opportunity to continue my education, and work at the Turbomachinery Laboratory.

At the Turbomachinery Laboratory I would like to thank Stephen Phillips, Eddie Denk, and Ray Matthews.

I would also like to acknowledge fellow students Phillip Brown, Jason Wilkes, Chris Kulhanek, Paola Mahecha, and Naitik Mehta for their help.

Finally, I wish to thank my committee members: Dr. Morrison and Dr. Morgan.

NOMENCLATURE

a	Eccentricity value [L]
A	Whirling amplitude [L]
$\boldsymbol{A_i}$	Fourier transformation of acceleration [L/t^2]
c	Cross-coupled damping coefficients [F.t/L]
c^*	Non-dimensional cross-coupled damping coefficient [-]
$\bar{c}$	Non-dimensional cross-coupled damping coefficient [-]
C	Direct damping coefficients [F.t/L]
C^*	Non-dimensional direct damping coefficient [-]
$\bar{C}$	Non-dimensional direct damping coefficient [-]
C_{eff}	$C_{eff} = C(\Omega) - \frac{k(\Omega)}{\Omega}$ effective damping [F.t/L]
C_{ij}	Direct and cross-coupled damping coefficients [F.t/L]
$C(\Omega)_{ij}$	Frequency dependent direct and cross-coupled frequency dependent damping coefficients [F.t/L]
C_r	Radial clearance [L]
C^*_{eff}	Normalized effective damping [F.t/L]
C^*_{ij}	Normalized direct and cross-coupled stiffness [s]
dw	Incremental work [J]
D	Diameter of seal [L]
$\mathbf{D}$	Direct complex dynamic stiffness [F/L]
$\boldsymbol{D_i}$	Fourier transformation of displacement [L]
$\mathbf{E}$	Cross-coupled complex dynamic stiffness [F.t/L]
f	Non-dimensional frequency [-]
$f_{bearing_i}$	Bearing reaction force components [F]
f_f	Friction factor [-]
$f_{liquid\,seal_i}$	Seal reaction force components [F]
f_{seal_i}	Seal reaction force components [F]

$\mathbf{F_i}$	Seal reaction forces [F]
$\boldsymbol{F_i}$	Fourier transformation of external force [F]
h_d	Non-dimensional honeycomb cell-depth [-]
h_{ij}	Complex dynamic stiffness for individual shake [F/L] and [F.t/L]
h_0	Non-dimensional zeroth order clearance [-]
H_d	Effective cell depth [L]
$\boldsymbol{H}_{ij}$	Test seal complex dynamic stiffness [F/L] and [F.t/L]
$\tilde{\boldsymbol{H}}_{\boldsymbol{ij}}$	Test complex dynamic stiffness [F/L] and [F.t/L]
$\boldsymbol{H}_{ij,BASELINE}$	Baseline complex dynamic stiffness [F/L] and [F.t/L]
$\boldsymbol{H}_{ij,TEST\ SEAL}$	Test seal complex dynamic stiffness [F/L] and [F.t/L]
I_r	Non-dimensional radial impedance [-]
I_θ	Non-dimensional tangential impedance [-]
$\boldsymbol{j}$	$\sqrt{-1}$ [-]
k	Cross-coupled stiffness coefficient [F/L]
$\bar{k}$	Non-dimensional cross-coupled stiffness coefficient [-]
k^*	Non-dimensional cross-coupled stiffness coefficient [-]
K	Direct stiffness coefficient [F/L]
K^*	Non-dimensional direct stiffness coefficient [-]
$\bar{K}$	Non-dimensional direct stiffness coefficient [-]
K_{eff}	$K_{eff} = K(\Omega) + c(\Omega)\Omega$ effective stiffness [F/L]
K_{ij}	Direct and cross-coupled stiffness coefficients [F/L]
$K(\Omega)_{ij}$	Direct and cross-coupled frequency dependent stiffness coefficients [F/L]
K^*_{eff}	Non-dimensional effective stiffness [-]
K_{ij}^*	Non-dimensional direct and cross-coupled stiffness coefficients [-]
L	Seal length [L]
m	Cross-coupled added-mass coefficients [M]
M	Direct added-mass coefficients [M]
$\bar{M}$	Non-dimensional direct added-mass coefficient [-]

M_{ij}	Direct and cross-coupled added-mass coefficients [M]
M_s	Stator mass [M]
$\dot{m}$	Mass flow rate [M/ t]
m_s	Blasius coefficient [-]
n	Number of complex dynamic stiffness matrices produced [-]
n_s	Blasius coefficient [-]
$p_0(0)$	Non-dimensional zeroth order entrance pressure [-]
$p_0(1)$	Non-dimensional zeroth order exit pressure [-]
p_e	Non-dimensional zeroth order exit pressure [-]
P_{exit}	Pressure at exit [F/L^2]
P'_{exit}	Pressure at exit of seal [F/L^2]
P_{in}	Pressure at inlet [F/L^2]
P_{inlet}	Pressure at inlet [F/L^2]
P'_{inlet}	Pressure at inlet of seal [F/L^2]
Q	Volumetric flow rate [L^3/t]
R	Ideal gas constant [J.M/t]
R_e	Reynolds number [-]
s	Complex variable for Laplace transformation [1/t]
T_{in}	Temperature at inlet [T]
$u_0(0)$	Inlet preswirl ratio [-]
$V_{max\ clearance}$	Velocity through increased clearance side of a seal [L/t]
$V_{max\ clearance'}$	Velocity through increased clearance side of seal [L/t]
$V_{min\ clearance}$	Velocity through decreased clearance side of a seal [L/t]
$V_{min\ clearance'}$	Velocity through decreased clearance side of seal [L/t]
V_t	Inlet preswirl velocity [L/t]
w_0	Non-dimensional zeroth order axial velocity [-]
x,**y**	Fourier transformation relative motion between the stator and rotor [L]

γ	$\frac{Hole-pattern\ surface\ area}{Seal\ \ inner\ surface\ area}$ gamma ratio [-]
$\frac{\partial F_i}{\partial x_j}$	Definition of stiffness [F/L]
$\frac{\partial F_i}{\partial \dot{x}_j}$	Definition of damping [F.t/L]
$\frac{\partial F_i}{\partial \ddot{x}_j}$	Definition of added mass [M]
ΔH_{ij}	Dynamic uncertainty [F/L] or [F.t/L]
ΔP	Pressure difference [F/L^2]
$\Delta P_{\substack{entrance \\ loss}}$	Entrance loss pressure difference [F/L^2]
$\Delta P'_{\substack{entrance \\ loss}}$	Entrance loss pressure difference of seal [F/L^2]
Δx, Δy	Relative motion between the rotor and the stator [L]
Φ	Leakage coefficient [-]
Γ	Non-dimensional mass-flow-rate
ρ	Density [M/ L^3]
σ	Standard deviation [-]
ω	Running speed of rotor [1/t]
Ω	Excitation frequency [1/t]
Ω_ω	$\frac{k}{C\omega}$ whirl-frequency ratio [1/t]
$\mathbf{\mathfrak{F}}$	Fourier Transformation [-]

Subscripts

i,j	*x*,*y*
k	Individual complex dynamic stiffness matrices
x,*y*	*x* and *y* orthogonal directions

Abbreviations

ACFM	Actual cubic feet per minute
FFT	Fast Fourier Transformation
HC	Honeycomb
HP	Hole-pattern
HPFTP	High pressure fuel turbopump
HPOTP	High pressure oxygen turbopump
[K][C]	Dynamic seal model with stiffness and damping matrices
[K][C][M]	Dynamic seal model with stiffness, damping, and added-mass matrices
PSD	Power spectral densities
PR	Pressure ratio
RPM	Revolutions per minute
SSME	Space shuttle main engine
SQFD	Squeeze film damper
TPJB	Tilting-pad journal bearings

TABLE OF CONTENTS

Page

Page

LIST OF FIGURES

Page

Page

Page

Page

Page

LIST OF TABLES

Page

Page

1. INTRODUCTION

Turbomachines either extract (turbines) or increase (pumps and compressors) fluid energy via mechanical rotation. In 1884, Sir Charles Parsons built a steam turbine that extracted energy from steam in 15 gradual steps instead of all in one step, which was customary for a steam engine. The development of this steam turbine, in the latter half of the 19th century, gave rise to the study of rotordynamics as it relates to turbomachinery. From this time on, engineers have struggled to identify the characteristics of turbomachinery and ways to increase their efficiency and performance.

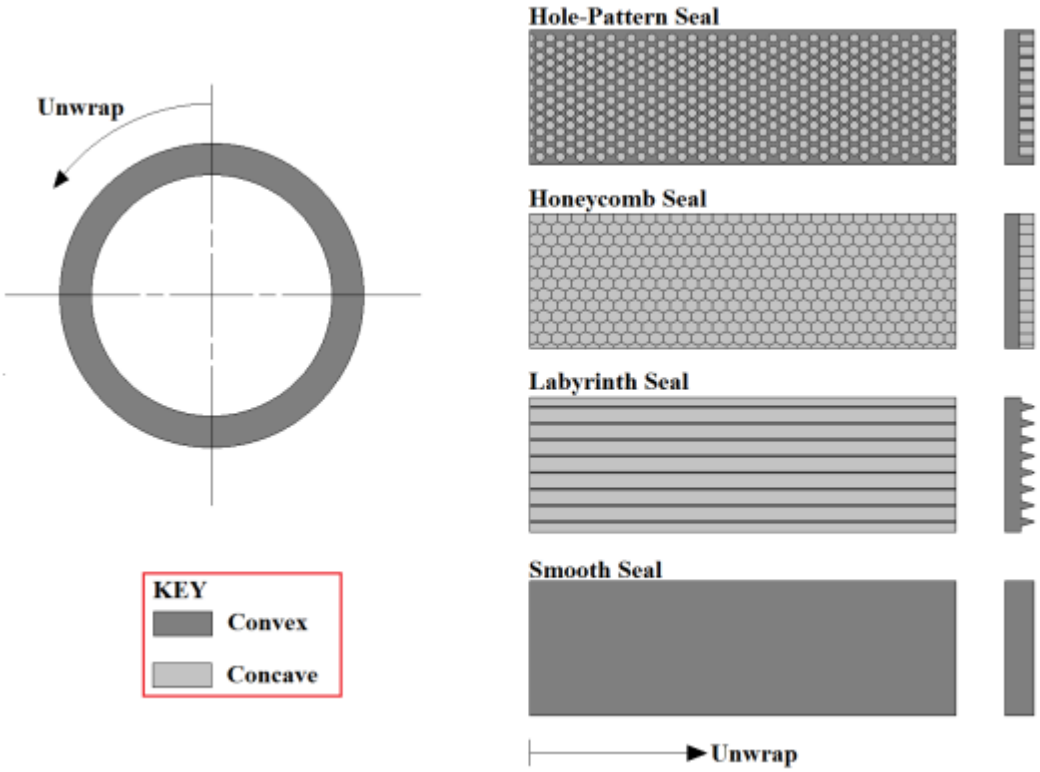

Figure 1. Hole-pattern, honeycomb, labyrinth, and smooth seal geometry

Necessary components for functional turbines and compressors are non-contacting annular gas seals. At their basic definition annular seals serve to impede axial flow and

---

This thesis follows the style of ASME Journal of Tribology.

provide a restriction to maintain pressure differences. Four typical annular seals: labyrinth, honeycomb (HC), hole-pattern (HP), and smooth, are shown in Figure 1. Figure 2 displays the seal locations and flow path for a four-stage back-to-back and series or straight through compressors.

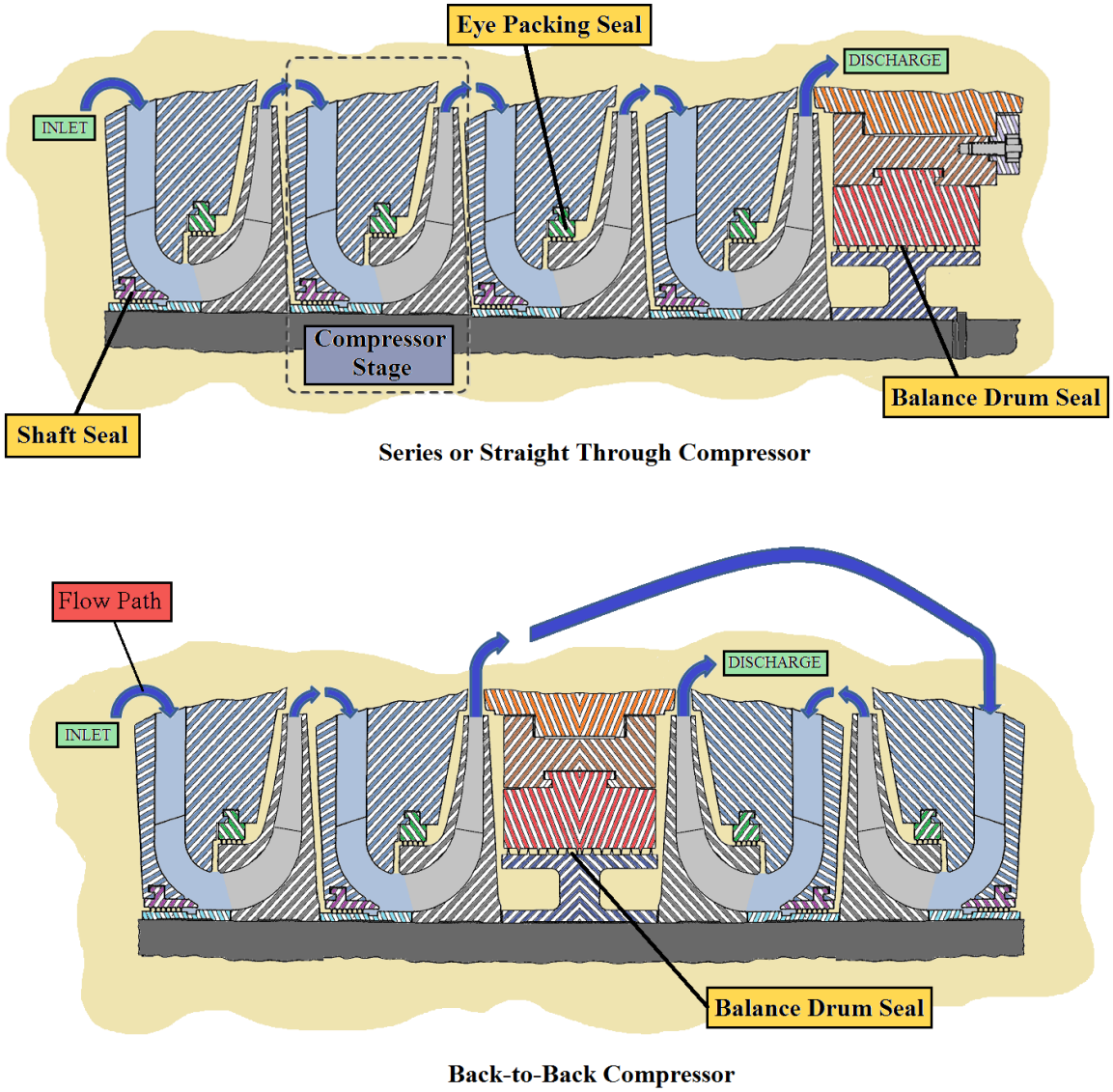

Figure 2. Series and back-to-back compressor configuration (adapted from [1])

Before 1974, it was widely thought that the sole function of gas seals was to limit leakage, and no additional rotordynamic characteristics could be expected from them [2]. This was not, necessarily, an unwarranted assumption or a careless oversight by the

engineers of the time. Instead, due to the continuing push to increase economic margins, the inclusion of gas seals became a necessity in rotordynamic analysis of high performance machines. Before delving into the developments that led to the inclusion of gas seals, a model for bearings and seals, reaction forces will be provided to clarify the discussion to follow.

1.1 Force-Displacement Model

Often, the fluid film forces ($f_{bearings\ or\ liquid\ seal_x}$, $f_{bearings\ or\ liquid\ seal_y}$) that act on the rotor due to bearings or liquid seals are modeled via the mechanical parameters of stiffness, damping and fluid inertia or added mass coefficients. For small motion, about an equilibrium position, the linearized force-displacement model is shown in Figure 3.

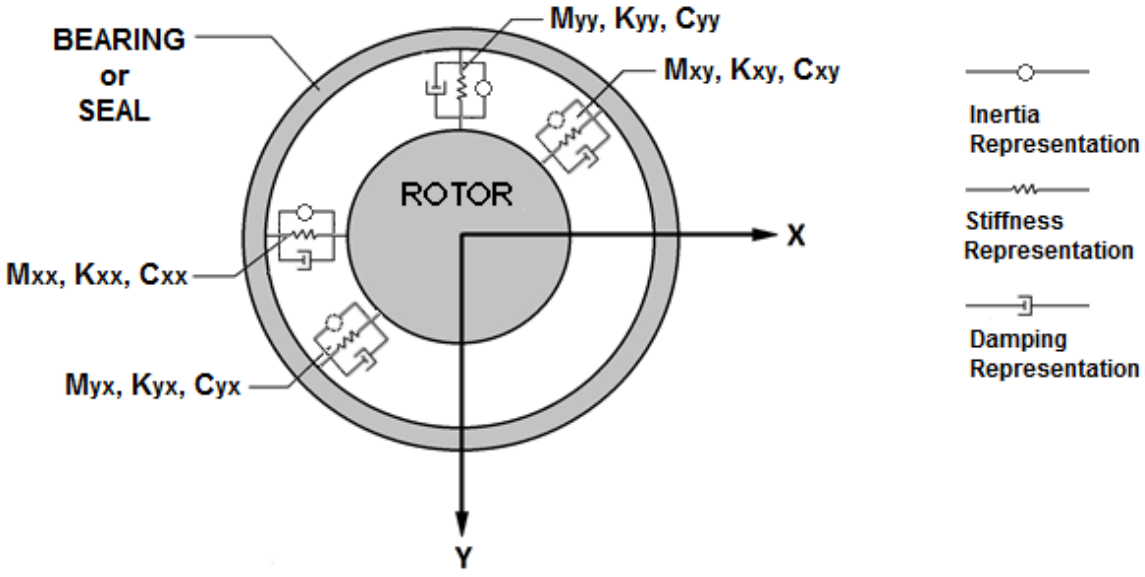

Figure 3. Linearized force-displacement model for fluid annuli (adapted from [3])

In equation form, the model of Figure 3 is represented as

$$-\begin{Bmatrix} f_{bearings\ or\ liquid\ seal_x} \\ f_{bearings\ or\ liquid\ seal_y} \end{Bmatrix} = \begin{bmatrix} K_{xx} & K_{xy} \\ K_{yx} & K_{yy} \end{bmatrix} \begin{Bmatrix} \Delta x \\ \Delta y \end{Bmatrix} + \begin{bmatrix} C_{xx} & C_{xy} \\ C_{yx} & C_{yy} \end{bmatrix} \begin{Bmatrix} \Delta \dot{x} \\ \Delta \dot{y} \end{Bmatrix} + \begin{bmatrix} M_{xx} & M_{xy} \\ M_{yx} & M_{yy} \end{bmatrix} \begin{Bmatrix} \Delta \ddot{x} \\ \Delta \ddot{y} \end{Bmatrix} \quad (1)$$

In the above equation, $(\Delta x, \Delta y)$ defines the relative motion between the bearing or liquid seal and rotor. Stiffness, damping, and added-mass are designated as K_{ij} , C_{ij} and M_{ij} respectively, and are defined as follows

$$K_{ij} \equiv -\frac{\partial F_i}{\partial x_j};\ C_{ij} \equiv -\frac{\partial F_i}{\partial \dot{x}_j};\ M_{ij} \equiv -\frac{\partial F_i}{\partial \ddot{x}_j} \tag{2}$$

where $i, j = x, y$ [4].

Eq. (1) is often implemented in the analysis of bearings and *liquid* seals[1]. When modeling *labyrinth* gas seals the added mass terms are found to be negligible. This fact leads to Eq. (3):

$$-\begin{Bmatrix} f_{seal_x} \\ f_{seal_y} \end{Bmatrix} = \begin{bmatrix} K_{xx} & K_{xy} \\ K_{yx} & K_{yy} \end{bmatrix} \begin{Bmatrix} \Delta x \\ \Delta y \end{Bmatrix} + \begin{bmatrix} C_{xx} & C_{xy} \\ C_{yx} & C_{yy} \end{bmatrix} \begin{Bmatrix} \Delta \dot{x} \\ \Delta \dot{y} \end{Bmatrix}. \tag{3}$$

In addition, HC and HP gas seal, which will be discussed at great detail later, are found to develop rotordynamic coefficients that are functions of the excitation frequency (Ω). In modifying Eq. (3) to demonstrate this fact, Eq. (4) results,

$$-\begin{Bmatrix} f_{seal_x} \\ f_{seal_y} \end{Bmatrix} = \begin{bmatrix} K(\Omega)_{xx} & K(\Omega)_{xy} \\ K(\Omega)_{yx} & K(\Omega)_{yy} \end{bmatrix} \begin{Bmatrix} \Delta x \\ \Delta y \end{Bmatrix} + \begin{bmatrix} C(\Omega)_{xx} & C(\Omega)_{xy} \\ C(\Omega)_{yx} & C(\Omega)_{yy} \end{bmatrix} \begin{Bmatrix} \Delta \dot{x} \\ \Delta \dot{y} \end{Bmatrix}. \tag{4}$$

Referring back to Eq. (2), when $i=j$ ($K(\Omega)_{xx}$, $K(\Omega)_{yy}$, $C(\Omega)_{xx}$, etc.) the coefficients are called direct, while when $i \neq j$ ($K(\Omega)_{yx}$, $K(\Omega)_{xy}$, $C(\Omega)_{yx}$, etc.) the coefficients are labeled cross-coupled. The direct and cross-coupled coefficients are defined in the nonrotating coordinate system.

[1] In rare cases Eq. (1) is used to model gas seals.

Eqs. (1), (3), and (4) provide the most complete force-displacement models. As Adams [4] shows, assuming rotational symmetry, for small motion about a centered position, the [K], [C] and [M] matrix of Eq. (1) and [K] and [C] matrix of Eqs. (3) and (4) must be skew-symmetric. Therefore, in its isotropic model, Eq. (1) and (4) can be restated as

$$-\begin{Bmatrix} f_{seal_x} \\ f_{sealy} \end{Bmatrix} = \begin{bmatrix} K & k \\ -k & K \end{bmatrix} \begin{Bmatrix} \Delta x \\ \Delta y \end{Bmatrix} + \begin{bmatrix} C & c \\ -c & C \end{bmatrix} \begin{Bmatrix} \Delta \dot{x} \\ \Delta \dot{y} \end{Bmatrix}. \tag{5}$$

and

$$-\begin{Bmatrix} f_{seal_x} \\ f_{seal_y} \end{Bmatrix} = \begin{bmatrix} K(\Omega) & k(\Omega) \\ -k(\Omega) & K(\Omega) \end{bmatrix} \begin{Bmatrix} \Delta x \\ \Delta y \end{Bmatrix} + \begin{bmatrix} C(\Omega) & c(\Omega) \\ -c(\Omega) & C(\Omega) \end{bmatrix} \begin{Bmatrix} \Delta \dot{x} \\ \Delta \dot{y} \end{Bmatrix}. \tag{6}$$

This simplification aids greatly in providing insight into just how direct and cross-coupled coefficients impact rotordynamics. The isotropic model does not apply for rotor motion that is not about a center equilibrium position. Therefore, Eq. (5) cannot be used to model bearings or seals operating at an eccentricity.

Direct coefficients are not surprising for engineers in that the kinematic quantities of displacement, velocity and acceleration cause a proportional force in the same axis of movement. The cross-coupling coefficients do not share this property. Taking cross-coupled stiffness (k) for instance, a rotor displacement along the x-axis produces a reaction force in the y-axis, hence the terminology cross-coupling.

The cross-coupling action is due to an oil wedge effect. The following statement taken from Palazzolo and von Pragenau gives additional insight into the cross-coupling coefficients. "One way to understand the origin of the cross-coupled coefficients is to assume that certain forces originate in some rotating coordinate system. The corresponding coefficients will occur in the cross-coupled positions after transformation to the non-rotating frame [5]." The cross-coupling coefficients are of great importance; in particular k affects the stability of a machine.

Figure 4 shows the vector forces resulting from gas-seal forces acting on a rotor that is precessing in a circular centered orbit at a rate of Ω. For Figure 4, *r* is the amplitude of the whirl, and ω is the rotational velocity of the rotor. The rotordynamic coefficients are treated as positive for this display.

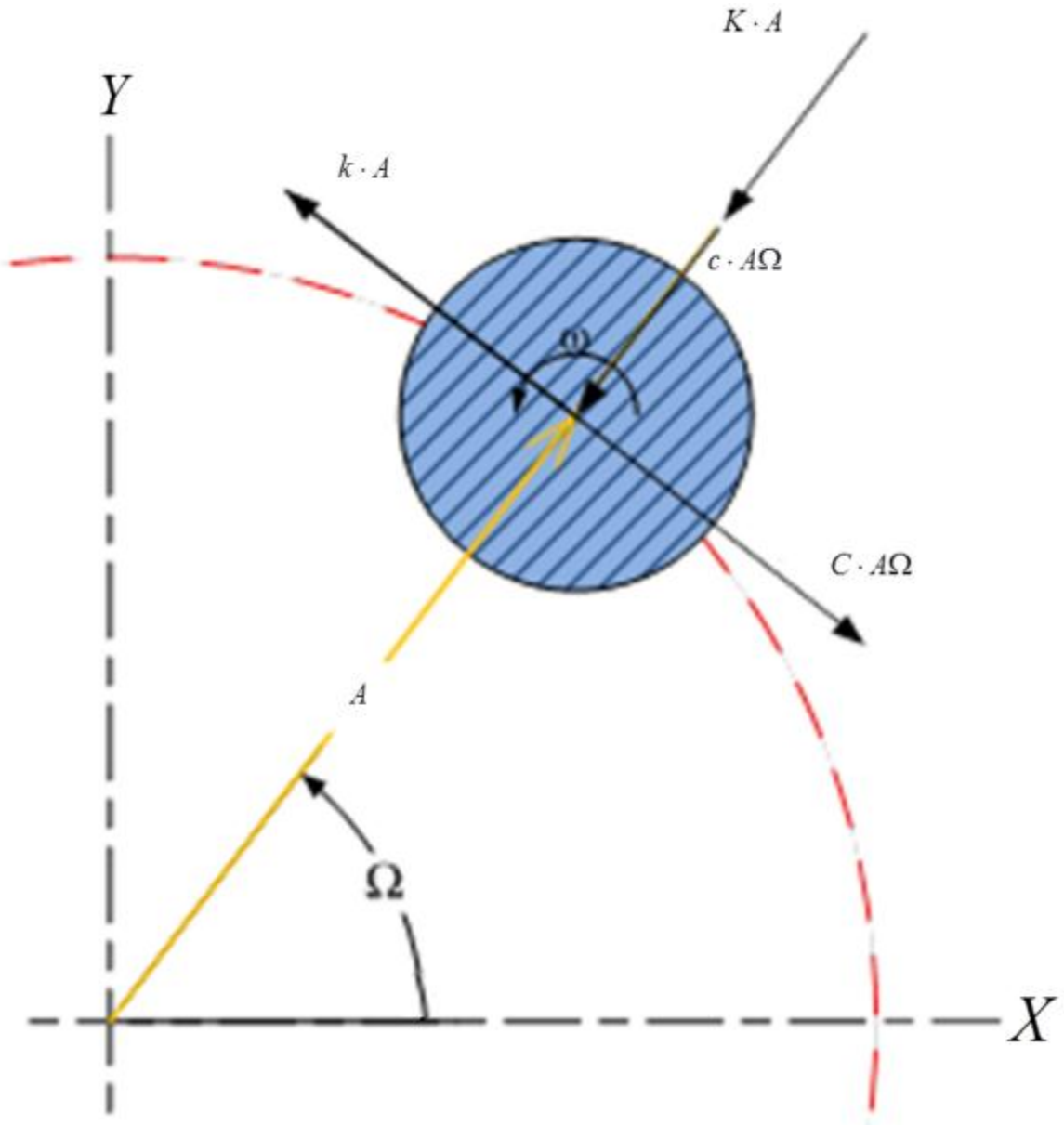

Figure 4. Vector forces acting on a whirling rotor

The jump from Eq. (5) to Figure 4 can be explained by separating the coefficient matrix into their skew-symmetric and symmetric forms. Next, the incremental work (*dw*)

performed on the rotor by each of the decomposed coefficient matrix is calculated. Conserved energy, dw=0, implies the reaction forces generated must act perpendicular to the instantaneous velocity. For non-conserved energy, $dw \neq 0$, the associated coefficients matrix will produce force vectors that act parallel to the instantaneous velocity. Adams [4] provides an excellent, and more detailed, explanation of the link between Eq. (5) and Figure 4.

The important facts to take away from Figure 4 are:

1) When direct stiffness (K) is positive it acts to center the rotor. For $K < 0$ an outward force is generated.
2) For, $k > 0$, a force is produced that is collinear with the instantaneous velocity vector and in the direction of the whirl. This increases the total energy of the system and promotes instability.
3) Positive direct damping (C) develops a drag force that is in an exactly opposite direction to the instantaneous velocity. For $C < 0$, just as with k, energy is added to the system and therefore destabilizing.
4) Positive cross-coupled damping (c) is stiffening.

Classical theory of vibration dictates that instability is the result of negative damping. While negative C, can lead to instability almost all rotordynamic instabilities encountered in turbomachinery result when the magnitude of k is greater than $C\Omega$.

To provide insight into the net result from the collinear force effective damping and stiffness are introduced and defined as:

$$C_{eff} = C(\Omega) - \frac{k(\Omega)}{\Omega} \tag{7}$$

$$K_{eff} = K(\Omega) + c(\Omega)\Omega \tag{8}$$

for frequency-dependent coefficients. Note, the above equations apply for a forward precession rotor about a centered equilibrium position. At some precession frequencies, seals develop negative C_{eff} . For seals that develop frequency dependent coefficients, the frequency at which C_{eff} goes from negative to positive is called the *cross-over frequency*.

Although the above discussion gives increased insight into the forces generated in fluid annuli, rotordynamic analysis did not begin with these models.

1.2 A Brief History: From Parsons to the 1950's

The first true attempts at rotordynamic analysis mainly focused on the rotor itself. Although elementary, these models did an adequate job of predicting natural frequencies and the response due to mass imbalance. Encouraged by these early findings, engineers began to push the envelope of turbomachinery performance further by increasing speeds and making the rotor lighter and more flexible. This increase in speed and flexibility made operational speeds greater than a critical speed[2] common place which in turn increased the likelihood of an instability occurring [6].

Until the 1920's instability in turbomachinery had not been seen. This circumstance changed in 1923 when GE researches encountered a subsynchronous[3] vibration that was later attributed to internal friction [7, 8]. Two years later, GE researchers Newkirk and Taylor encountered an instability attributed to the bearings that they labeled oil whip [9]. Oil whip is due to an asymmetrical pressure profile that produces a destabilizing tangential force component [10]. Both of these instabilities are found to be speed dependent. For the next 25 years or so the cause of most subsynchronous vibration was identified as oil whip or internal friction [11].

In the time between the 1920's and into the 1950's, advancements in rotordynamics continued. Some of these advancements included the inclusion of gyroscopic effects, increased investigation into the effects of bearings, development of transfer-matrix for calculation of mode shapes and natural frequencies.

1.3 The Inclusion of Seals

In 1958, Lomakin [12] provided the first investigation of the centering effects of smooth liquid seals on turbomachinery. Figure 5 illustrates the Lomakin effect. The axial pressure drop across a seal is accomplished through two mechanisms: (1) entrance losses due to fluid inertia acceleration and (2) the wall friction of the seal [13]. Lomakin recognized

[2] Critical speeds are defined as the speeds at which vibrational amplitude, due to an imbalance; reach a local maximum [6].
[3] Subsynchronous vibration resonates at a frequency lower than the running speed.

that as a shaft moves within a seal the changes in clearance lead to a proportional change in axial flow velocity and Reynolds number. Since entrance losses are proportional to axial velocity, as a shaft moves from the center, the side of decreasing clearance will experience a smaller pressure drop to entrance loss. Coupled with this, friction factor (f_f) (most of the time) decreases with increasing Reynolds number. Thus for the relatively smaller clearance side, the pressure absorbed by the wall will be greater and the accompanying entrance loss less than the opposing side. These two factors lead to a larger relative pressure profile on the side of decreasing clearance. This relatively larger pressure profile causes a "restoring" or positive *K* and has been coined as the Lomakin effect [4]. The Lomakin effect occurs if there is a pressure difference across the seal and is a purely hydrostatic effect.

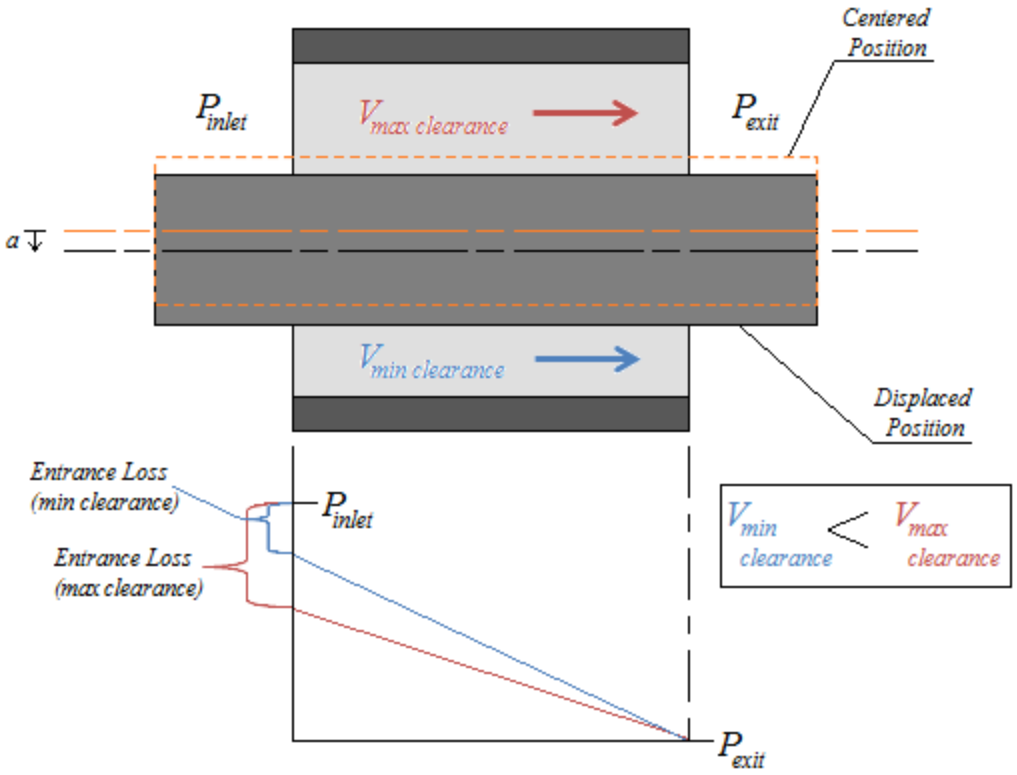

Figure 5. Lomakin effect delineated

For a given clearance, fluid and rotor the portion of pressure absorbed within a seal can be altered by changing the seal's length and/or roughness. Figure 6 show how increases in a seal's length can correlate with a greater proportion of pressure absorbed by the friction

of the wall and thus a decrease in entrance loss. As the length of the seal increases, the accompanying reduction in entrance loss causes the difference in the pressure profile between the seal sides to be lessened and thus leads to a reduction in *K*. In fact, as Childs [14] shows, some models predict negative stiffness or a "reverse" Lomakin effect as the ratio of length to diameter continues to increase.

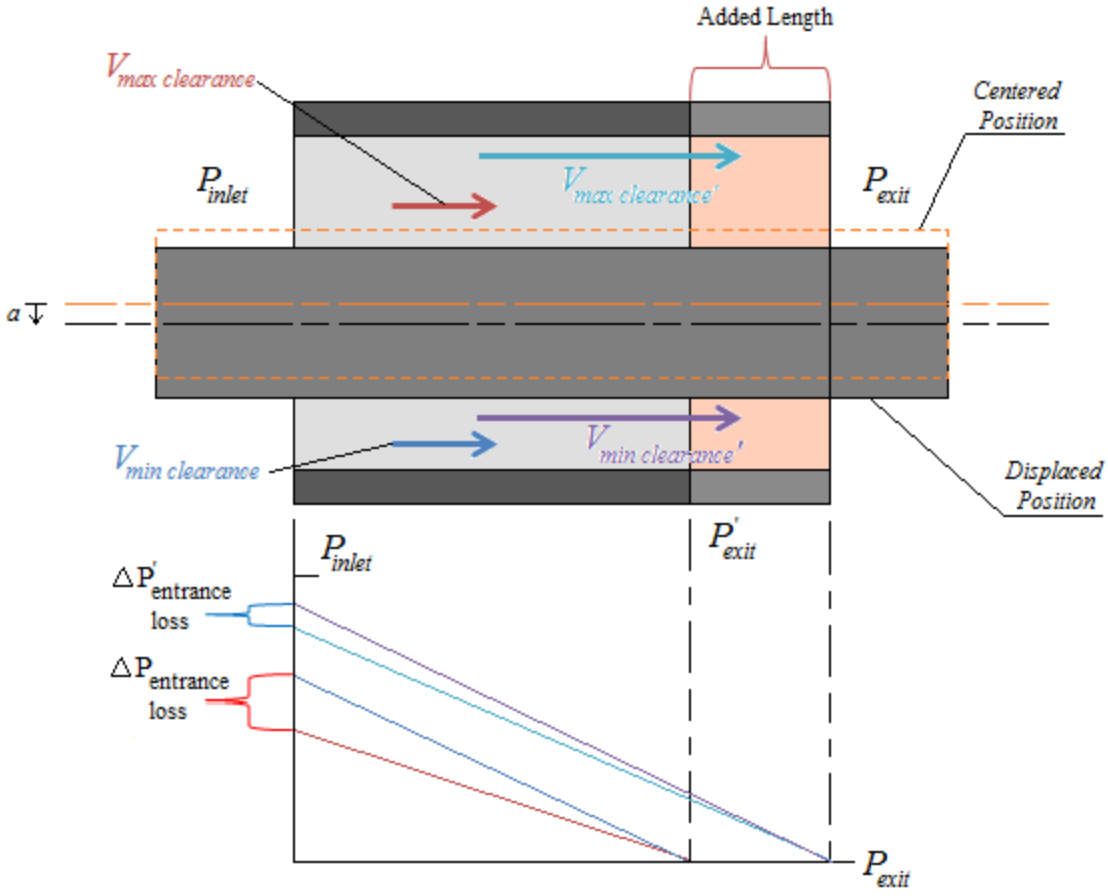

Figure 6. Effect of increase seal length on the Lomakin effect

In addition to Lomakin's paper, 1958 also marked the year that Thomas [15] identified an instability caused by variation in the clearance between the blades and housing of axial flow steam turbine [14]. Unlike, oil-whip and internal-friction instabilities, this instability was found to be load dependent not speed dependent. As with oil whip the destabilizing forces are modeled via *k*. Thomas', paper was written in German and went largely unnoticed in the US.

Seven years following Thomas' paper, while working with jet turbo compressors and turbines for GE, Alford [16] identified the same instability mechanism for compressors. After publishing his paper, the destabilizing k generated due to clearance variation at the blades largely became known as Alford forces in the US. Although Alford's paper is widely known for introducing Alford forces to the vocabulary of a rotordynamist, it also provided one of the first significant investigations of gas seals [17].

In addition to variation of blade-tip clearance, Alford suggested that variation in circumferential pressure within the glands of labyrinth seals could lead to instability. Alford modeled a convergent and divergent labyrinth seal consisting of only one gland and assumed axial flow only. He concluded that converging labyrinth seals were destabilizing [16]. Research following Alford's paper contradicted [18] and disproved [19] much of Alford's theory for labyrinth seals. The deficiency in Alford's model was the neglect of circumferential flow, which must be present if circumferential pressure variation is to exist within the glands of a labyrinth seal [6].

1.4 Mechanisms to Increase Stability

The 1960's saw a sharp increase in interest in squeeze film dampers (SQFD) and tilting pad journal bearings (TPJB). SQFDs provide viscous damping via a squeeze film between the bearings journal and housing [14]. TPJB's consist of pads that can rotate allowing them to "redirect" the fluid film forces towards the center of the journal thereby eliminating cross-coupling coefficients and oil whip. Both SQFD's and TPJB's, when applied correctly, lead to increased stability and reduced vibration amplitudes. While the application of SQFD's and TPJB's are positive, their use provided additional reasons to neglect gas seals in rotordynamic analysis.

1.5 Extension of Lomakin's Theory

As discussed earlier, Lomakin provided the first investigation into the effects of liquid seals. Lomakin's work provided valuable insight into liquid seals, it was solely theoretical and completely neglected rotational effects. According to Black and Jenssen [20], Marcinkowskij and Karinev [21] provided experimental results that, in part, proved Lomakin's theory but also showed that liquid seals exhibit hydrodynamic effects. With this knowledge, Henry Black set out to extend Lomakin's work and include rotational effects.

Through the course of four, or so, papers [20, 22-24] Black et al. provided the foundation for future analysis, and developments related to liquid seals. Some important outcomes from his work are:

1) In addition to *K*, liquid seals also generated *k*, *C*, *M*, and *c* [6, 23].
2) Couette flow (shear driven flow) causes destabilizing *k* [22, 25].
3) As fluid moves axially along the seal, for equal rotor and stator roughness, its circumferential bulk flow velocity asymptotically approaches ½ the rotor surface speed. Previously, it was assumed that the circumferential velocity reached its "terminal" velocity of ½ the rotor surface speed immediately. This insight lead to a reduction in *k* predicted [24, 26].

1.6 The Genesis of the Damper Seal

Using Black's work as his basis, von Pragenau [25] predicted that the asymptotic tangential bulk-flow velocity, and thus *k*, could be lowered by using a seal surface that had been roughened. In addition to the lower *k*, a reduction in leakage was also predicted. Figure 7 shows the iso-grid configuration that von Pragenau proposed and dubbed the "damper seal" [25].

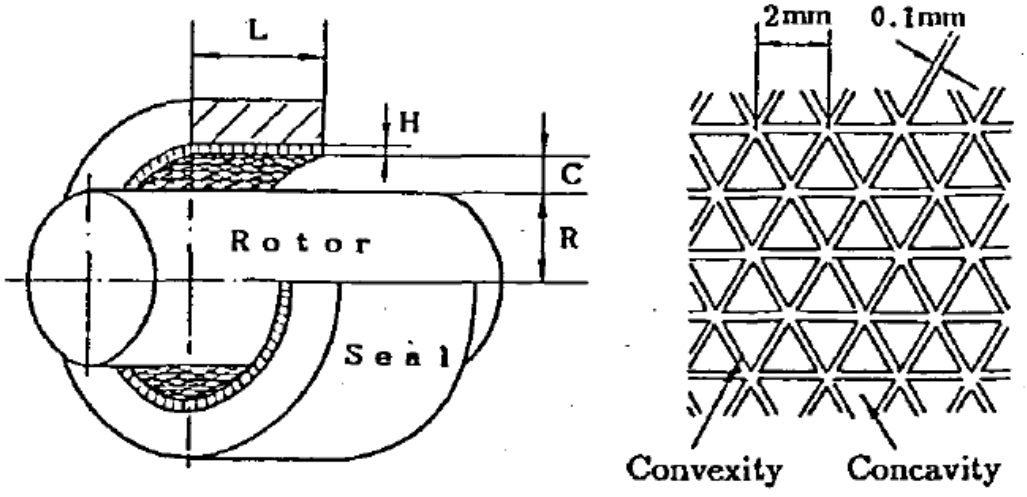

Figure 7. von Pragenau's iso-grid configuration [27]

von Pragenau's analysis showed that a roughened surface doesn't merely increase the axial distance it takes for the circumferential velocity to reach a speed of ½ the surface speed. It additionally predicts that the asymptotic or "terminal" tangential bulk-flow velocity is lowered by introducing a roughened surface.

von Pragenau, a NASA employee, proposed the roughened seal as a means to increase the stability of the Space Shuttle Main Engine (SSME). With funding from NASA, Childs and Kim [28] tested one smooth seal and three roughed seal configurations to experimentally verify the analytical results. Figure 8 shows the roughened surfaces tested.

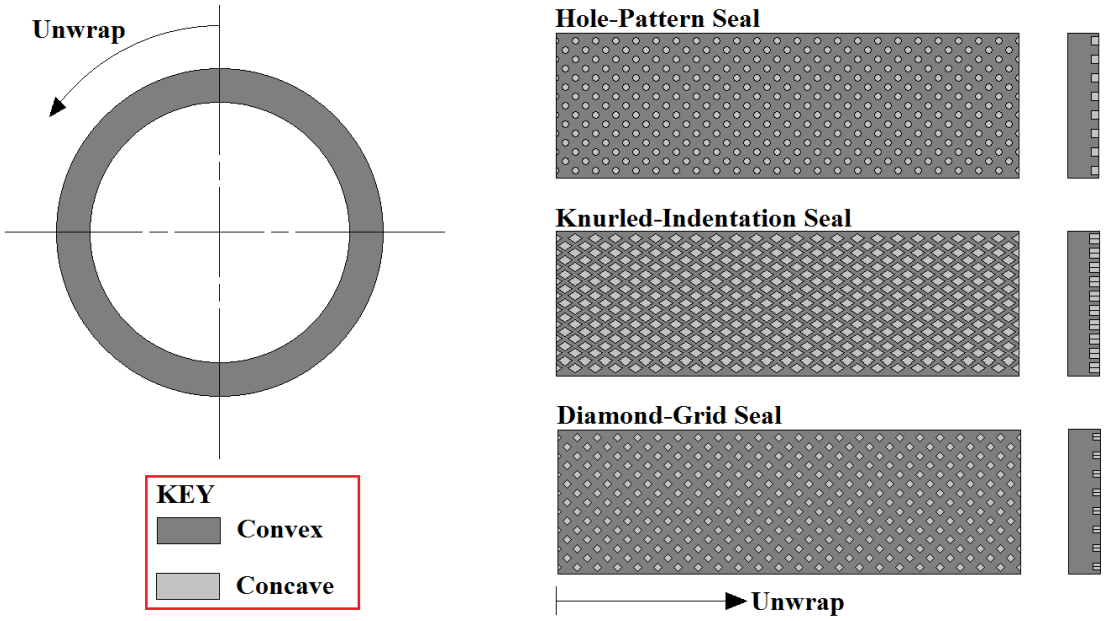

Figure 8. Hole-pattern, knurled-indentation, and diamond-grid seal geometry (not drawn to scale)

The experiments demonstrated that of the three roughened surfaces, the HP seal showed the most promise, providing the most effective damping and lowest leakage. The diamond grid developed the smallest effective stiffness and net damping values of the four seals [28]. Although the damper seals concept was proving to be very beneficial, Childs and Kim [28] demonstrated that not every configuration implemented to roughen the stator would always produce positive effects.

Encouraged by the HP results, Childs and Kim [29] tested 9 new HP seals to investigate how hole depth and gamma ratio affected leakage and rotordynamic characteristics. Here gamma ratio is defined as

$$\gamma = \frac{Hole - pattern\ surface\ area}{Seal\ inner\ surface\ area} \tag{9}$$

Of the nine hole-patterns, the best configuration was found to have a hole depth to radial clearance of 2.89 and a gamma ratio of 34 percent. For this configuration when compared to a smooth seal, the HP seal had a 37 percent increase in effective damping and a 23 and 46 percent decrease in K and leakage respectively [29]. By the time Childs and Kim's [29] paper was published (October 1986) the manufacture of the SSME had already replaced some of the labyrinth seals found in the High Pressure Oxygen Turbopump (HPOTP) with knurled-indentation damper seals to eliminate whirling [30].

Childs et al. [31] tested six additional HP damper seals at a smaller clearance and found no conclusive evidence of an optimum damper seal configuration as shown previously. In addition, contrary to Child and Kim [29], the effective damping was approximately equal to that developed by a smooth seal. The smooth seal had effective stiffness values 50 to 60 percent greater than the six HP [31].

Childs et al. [28, 29, 31] were the first to publish experimental results for liquid damper seals, but their test rig was limited by the fact that it did not control inlet tangential velocity (preswirl). Also, C and k could not be separated; hence, only effective damping was reported. As Childs [14] points out, "The central virtue of a damper seal is the reduction in tangential velocity and k coefficient, and this virtue can only be conclusively demonstrated by introducing a significant inlet tangential velocity and measuring a reduction in k."

Using the iso-grid configuration that von Pragenau suggested, Iwatsubo and Sheng [27] separately measured C and k for their damper seals. They were also able to control preswirl. Their results showed, for preswirl flow greater than zero (inlet flow in the direction of rotation), the iso-grid damper seal reduces k. With preswirl equal to zero, the seal also exhibited increased C and decreased K when compared to a smooth seal. Leakage for the

damper seal was found to be significantly smaller than that of a smooth seal [27]. The results verified the predictions von Pragenau had made eight years earlier.

Again, as with Childs et al. [29, 31], the iso-grid seal developed reduced K when compared to smooth seals. This result is not totally unexpected as the discussion of the Lomakin effect found above dictates; i.e., increases in roughness correlate with a smaller inlet loss and thus at some point a lessening of K. Although there is a reduction in K associated with many damper seal configurations, the decrease in k and leakage can justify the use of a damper seal.

As shown above, Black's work provided a sound foundation for the analysis of liquid seals and eventually the development of the damper seal. In the interest of continuity, the studies detailed above were focused on liquid seals. Fortunately, the evolution of rotordynamics does not proceed solely along one line. Instead, as Black was expanding on his model for liquid seals, increasing interest in gas seals was occurring. Now we will take a step back and look at the state of rotordynamics analysis in 1974 shortly after Black's initial developments for liquid seal analysis.

1.7 The Mid 1970's: A Call to Action

With the exception of Alford's incorrect analysis, as of 1974 no attention had been paid to gas seals. Childs and Vance [2] summarizes the views of gas seals at this time as:

> • "Bearing carry loads.
> • Squeeze-film dampers provide damping if needed.
> • Annular [gas] seals restrict leakage flow and are not important in rotordynamic. Proper seals "know their role" and certainly cannot be relied on for damping or stiffness.
> • Labyrinth-seal force coefficients are much smaller than bearing coefficients and have a negligible influence on rotordynamics".

Two well-known back-to-back centrifugal compressor instabilities (Kaybob and Ekofisk compressors discussed in Fowlie and Miles [32] and Geary et al. [33], respectively) helped lead to the questioning of the above views. These instabilities are very similar, and Vance et al. [6] provides an excellent overview of these instabilities. With this in mind, only a short summary of the Kaybob compressor will be given here.

Upon its initial onsite start-up, one of the Kaybob compressors developed a subsynchronous vibration frequency following between 40 and 60 percent of the running speed [34]. The unit had no known source of internal friction and was supported on tilting pad bearings [2, 32]. In addition, the manufacturer had performed partial-load tests of the unit at their factory with the unit meeting the API vibration specifications. These results suggested that the instability were load dependent, not speed dependent and therefore not due to a classic instability mechanism. The compressor was finally made operational through several modifications. Namely, the rotor was shortened and increased in diameter [32]. Although the instability was alleviated, later analysis would show that the root cause of the instabilities, i.e., the balance drum labyrinth seal, was missed [6].

In addition to the instabilities experienced with high-pressure compressors, some steam turbines began to exhibit subsynchronous vibrations. Greathead and Bostow [35] detail one such turbine that developed a load dependent instability. To remedy the instability, the bearings were switched to TPJB. Obviously, with the instability being load dependent and related to a turbine, the destabilizing forces Thomas [15] first proposed where considered. To combat this effect the blade tip clearances were increased. With these modifications the turbine did act "normally" but the operation was precarious. Eventually, Greathead and Bostow concluded that the instability was the result of the labyrinth seals.

From the summary above Childs states "Labyrinth-seal force coefficients are much smaller than bearing coefficients….." This is true, so how can it be justified that gas labyrinth seal can lead to instability? One reason, as stated earlier, is the ever continuing push to increase economical margins. Some of the typical methods engineers have employed to achieve higher efficiencies are as follows.

1) Decreasing the seal clearance thereby reducing leakage. This in turn increases the force generated in the seal.
2) Increasing the operational speed of turbomachinery. In addition to raising the operational speed above the first critical frequency increases in speed lead to increased circumferential flow velocity.
3) Increasing the working pressure of the machine and thereby the fluid density. Seal forces are proportional to ΔP and density. Consequently, high-pressure

compressors and steam turbines are more likely to experience instabilities than gas-turbines where the fluid densities are smaller.

4) Adding stages to the machine thereby increasing the bearing span length and modal amplitudes.

While all of the above factors do yield a machine of high energy density they also promote instabilities.

In addition to these factors, back-to-back compressors are designed such that the balance-piston seal naturally sees greater rotor motion. Figure 9 shows the first mode shape for a back-to-back and series compressor. As can be inferred, the back-to-back compressor is more subject to instabilities.

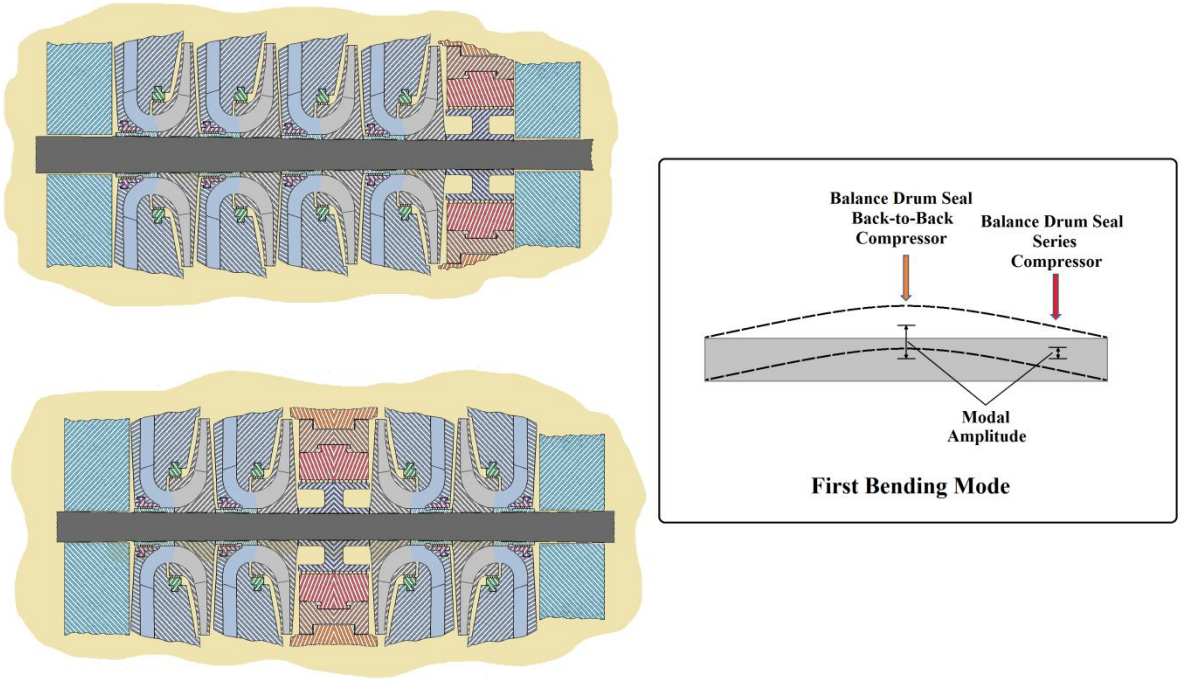

Figure 9. Series and back-to-back compressor configuration and first bending moment (adapted from [1])

The Kaybob and Greathed instabilities with others lead to increased awareness of the effects of gas seals. The first theoretical and experimental investigations dedicated solely to gas seals were soon to follow.

1.8 The Introduction of Gas Seals Analysis

One of the first, entirely gas seal focused theoretical analysis was performed by Fleming [36]. Two smooth-rotor, smooth-stator seal configurations (straight and converging), were studied. Fleming's study is analogous to Lomakin's [12] development for liquid seals. Again, rotational effects were neglected. Although the study was not complete, it did show that gas seals can develop significant *K*, and converging seals generate higher stiffness values.

Benckert and Wachter [37] provided some of the first data for labyrinth gas seals consisting of more than 3 glands. Their results showed that labyrinth seals could produce destabilizing tangential forces [6]. By pre-rotating the inlet air they also showed that swirl webs, the predecessor to swirl brakes, could be used to decrease *k*.

In addition to testing labyrinth seals, two honeycomb (HC) seals were tested. This marked the first time that HC seals were tested. When comparing the HC seal to a labyrinth seal its *k* was significantly higher. The effective damping could not be obtained as the test rig did not allow for *C* measurements [2, 37].

HC seals have been used since the 1960's. In some cases, aluminum labyrinth seals, that were deteriorating in caustic process fluid, were replaced with HC seals that were more resilient to the fluid [38].

Looking at the HC seal shown in Figure 1, it is easy to draw a parallel between it and the iso-grid seal. Although Benckert and Wachter [37] suggested that HC seals were not favorable for rotordynamic characteristics, research continued to investigate if HC seals could enhance stability.

Building off Fleming [36], Childs [39], and his own work [40], Nelson [41] analyzed HC and smooth tapered annular gas seals. Nelson's calculations showed that the HC seal had less leakage and a 9 percent reduction in *k* when compared to the smooth seal. Confusing the matter, his analysis predicted the HC seal would develop 2 and 10 percent less *C* and *K*, respectively. As Nelson [41] states, "In terms of the HC stator enhancing rotor stability, the results appear mixed……Thus, general statements concerning the problems of instability and critical speeds can only be addressed by considering the entire rotordynamic system…."

1.9 Honeycomb Seals: A Stabilizing Mechanism

With the obvious exclusion of Parson's first turbine, rocket engine turbopumps have spurred more growth in rotordynamics than any other machines. In the early 1980's, persistent instability delayed the development of the HPOTP at a cost of 1 million dollars a day. Based on the positive results from the use of liquid damper seals on the High Pressure Fuel Turbopump (HPFTP), gas HC seals where proposed to improve stability for the HPOTP. Specifically, the converging teeth-on-rotor labyrinth interstage seal was replaced with a straight HC seal. The switch proved beneficial, and the stability was improved. After adding swirl brakes, the subsynchronous response was completely eliminated [42].

This result contradicted Benckert and Wachter [37] conclusions that labyrinth seals were inherently more stable that HC seals. Childs et al. [43] set out to resolve this discrepancy. For their tests, seven HC configurations were tested. As with Childs et al. [31] tests for liquid HP seals, no optimal configuration was found. Results from the best performing HC seal were compared to a smooth and labyrinth seal. As with liquid damper seals, HC seals had decreased leakage and k when compared to the smooth seal. When comparing the HC and labyrinth seal, Benckert and Wachter [37] measurements were confirmed, i.e. the k for the labyrinth was significantly less. Unlike Benckert and Wachter [37] tests, C could be determined. The results demonstrated that C was greater than that of the labyrinth seal by a factor of six. This increase in damping outweighed the increase in k, and experiments showed that HC seals could be more stable that labyrinth seals. As an added bonus, the HC seal also had smaller leakage than the labyrinth seal.

For Childs et al. [43], the seals had an axial length over diameter (L/D) value of 1/3. Kleynhans [44] tested HC seal with L/D equal to 1/6. He found no justification to use HC instead of labyrinth seals. This led to the conclusion that HC or any roughened surface seal are only beneficial for long seals. As will be discussed later, typically the comparatively long balance piston seal is modified to enhance stability.

1.10 Improving Predictions

While HC seals can be superior to labyrinth seals, their behavior was erratic and hard to predict. In general, the predictions for HC seals were poor predictors of experimental findings. Elrod et al. [45, 46] provided marginal improvements to theoretical models. Ha

and Childs [47] performed flat-plate tests on several configurations to expand on the knowledge of HC seals. During their tests, some configurations experienced an unpredictable increase in f_f with increasing Reynolds number. This phenomena was labeled a "friction-factor-jump" and attributed to "an excitation of acoustic resonance frequencies within honeycomb seal" [48]. A friction-factor-jump can cause a losses of the Lomakin effect and in some cases cause negative K [47].

Ha and Childs [49] incorporated the flat-plate work into a model to predict rotordynamic coefficients for the HC. The derivation of the governing equations followed Nelson [50] with their new empirical friction-factor model (found through flat-plate test) replacing the Blasius friction-factor model for the HC seal. In addition, Moody's friction-factor was used to model the smooth rotor. Unfortunately, the theoretical results were still unsatisfactory. Although the prediction were not as favorable as hoped, in the authors' response to the Ha and Childs [49] paper, a two-control-volume model was proposed [51].

Kleynhans and Childs [52] undertook the job of developing this two-control-volume model. Their analysis showed "that the cells of honeycomb act to reduce the effective acoustic velocity of flow through the seal, which can drop seal acoustic natural frequency into the frequency range of interest for rotordynamics. In these circumstances, the conventional (frequency-independent) rotordynamic-coefficient model is invalid…." [52]. To address this, a Laplace transform model was proposed. The model used the Blasius friction model for both the stator and rotor.

Kleynhans and Childs [52] model would provide vast improvements to predictions and serve as the basics for ISOTSEAL a code developed at Texas A&M Turbomachinery Laboratory to predict seal rotordynamic coefficients.

1.11 Industry Experience with Honeycomb Seals

With the positive results of the HPOTP modification, industry would begin to implement HC seals into their machines. Zeidan et al. [53], Memmott [54], Gelin et al. [55] detail how subsynchronous vibrations experienced by four back-to-back, and one series (Gelin), compressor were eliminated by replacing the labyrinth balance drum seals with HC seals. Memmot and Gelin et al. also showed how re-injecting discharge gas at the inlet can improve stability. This process of re-injecting gas is known as shunt injection and serves the

same purposes as swirl brakes: reducing preswirl. Armstrong and Perricone [56] details a case in which an instability experienced by a steam turbine was eliminated by replacing a labyrinth seal with a HC seal.

The above outcomes cite positive results from implementing HC seals, but in some cases HC seals can lead to instability. Camatti et al. [57] and Kocur and Hayles [58] detail cases in which the HC seals became divergent. This divergence led to negative stiffness which dropped the critical speeds thereby making the machine more prone to instabilities. Note in [58] that if the HC seals had remained in their original, i.e. constant clearance state, the instabilities would not have occurred.

1.12 Gas Hole-Pattern Seals, an Alternative to Honeycomb Seals

Although the use of HC seals had largely been positive, they are manufacturing intensive. A HC seal is normally made by brazing a HC pattern onto the seal's steel base. Using the experience gained from liquid HP seals, HP gas seals were proposed as a direct replacement for HC seals. HP seals are much simpler and typically cheaper to manufacture and cause less damage in the event of a rub.

Yu and Childs [59] performed the first experiments to compare HP and HC seals. Their results showed that an HP seal with round holes and γ=69% had the least leakage. Also, effective damping was greater for this HP seal. The experimental findings were compared to theoretical results from Kleynhens and Childs [52]. The two did not show a strong correlation but due to the limited shake frequency (30-70Hz) of the test rig a conclusive evaluation of the model could not be made. Based on their finding Yu and Childs stated, "HP damper seals can be attractive alternatives to honeycomb seal," [59].

Using a different test rig, Holt and Childs [60] provided experimental and theoretical results for two HP seals using an excitation-frequency range of 40 to 230 Hz, low preswirl (no preswirl was imparted) and inlet pressures out to 17.2 bar (250 psi). For their tests, the two HP seals had similar configurations, i.e. γ=43% and hole diameter of 1.5875 mm (0.0625 inches), and differed only in their hole depth [2.032 mm (0.08 inches) and 3.175 mm (0.125 inches)]. Compared to an HC seal tested by Dawson [38], the HP seals showed higher leakage and higher effective damping at higher frequencies. When comparing the two HP seals, the hole depth of 3.175 mm (0.125 inches) had lower leakage, C and k while it had

higher *K*. The test also showed good agreement between predictions (ISOTSEAL) and experimental results.

Childs and Wade [61] tested HP seals with inlet pressures out to 70 bar (1015 psi) and three preswirl ratios. For their seal, γ=69%, and the hole pattern was comprised of holes of depth and diameter of 3.302 mm (0.130 inches) and 3.175 mm (0.125 inches) respectively. Tests at two radial clearances (0.1 and 0.2mm) showed that preswirl had little influence on *k* for the smaller clearance but a great impact on *k* for the larger clearance. For the 0.2 mm (8 mils) clearance *k* was found to increase as preswirl flow increased. Thus, for larger clearances a swirl brake was suggested. Predictions, generated by ISOTSEAL, were in good agreement with experimental results.

1.13 A New Design for Hole-Pattern Seals/Objectives

As Holt and Childs [60] and Childs and Wade [61] showed, HP seals are traditionally comprised of holes of small diameters with several thousand needed to produce one HP seal. To reduce manufacturing costs and time, the idea of increasing these hole diameters arose. Recent tests performed at the Texas A&M Turbomachinery Lab Flat-plate Test Facility showed that patterns incorporating larger holes can have similar friction factors and leakage to those of patterns found in traditional HP seals [62]. In particular, a pattern comprised of holes of 12.15 mm (0.48 inches) diameter and 1.8796 mm (0.074 inches) depth showed favorable leakage performance. Figure 10 compares of the seal configuration tested by Childs and Wade [61] and one that incorporates holes of 12.15 mm (0.48 inches) inches in diameter.

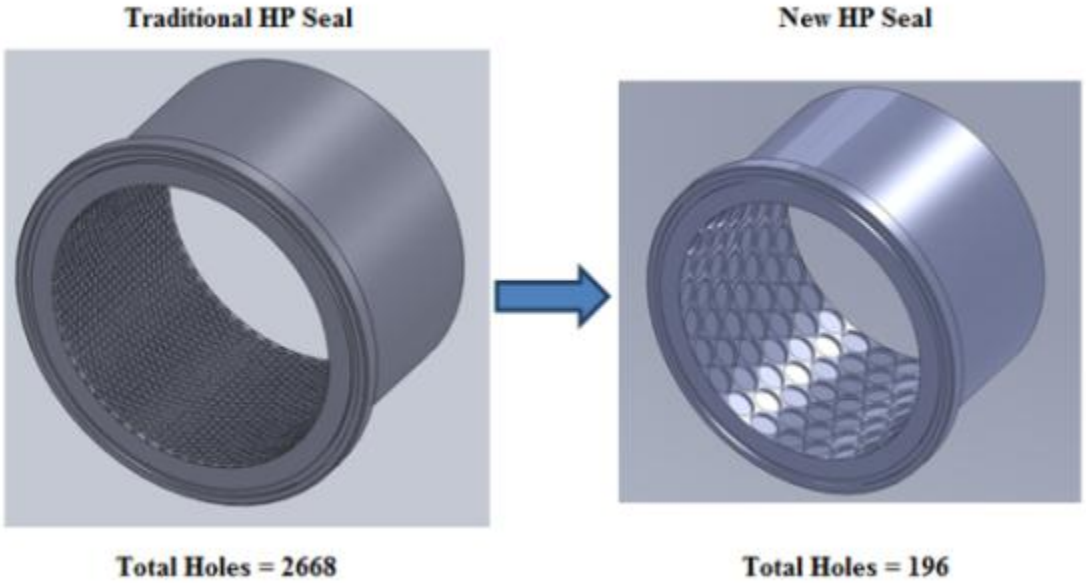

Figure 10. Comparison of traditional and new hole-pattern seals

This project will build from the flat-plate test results to accomplish three goals:

1) Provide experimental rotordynamic coefficients and leakage data for an HP seal comprised of larger holes, diameter of 12.15 mm (0.48 inches).
2) These results will be compared to the predicted rotordynamic coefficients generated by ISOTSEAL.
3) Finally, the results of the new HP seal will be compared to that of an HP seal previously tested by Childs and Wade [61].

2. TEST RIG DESCRIPTION

2.1 History of the Test Rig

The basic design and major hardware components of the test rig have proven to be durable, and effective at gathering rotordynamic coefficients. The test rig was initially designed to test high-speed hydrostatic bearings, as described in Childs and Hale [63]. Lindsey [64] described a later modification of the test rig to test liquid seals. Dawson [38] performed the first gas seal experiments using the test rig. The alterations, detailed in Dawson [38], allowed for testing out to an inlet pressure of 17.2bar (250 psi). Additional modifications [65], described by Weatherwax, allowed for testing to an inlet pressure of 70bar (1015psi). This configuration would be used almost continuously until the end of 2006 upon which time no further funding was provided.

Beginning in June 2009, funding was received that would allow for additional gas seal testing. For the next year and a half, the test rig was reassessed with substandard or obsolete components being refurbished or replaced. The upgrades to the test rig included but were not limited to:

1) Complete replacement of data acquisition system including data acquisition unit, signal conditioners, wiring, etc.
2) Refurbishment of support bearing pedestal.
3) Replacement of pump soft-start and motor variable frequency drive.
4) Design and implementation of a new safety logic system for automatic shutdown in the event of a malfunction.
5) Addition of new monitoring sensors.

2.2 Testing Apparatus

2.2.1 Auxiliary Components

Figure 11 shows a side view of the test rig with the coupling guards shown partially transparent for display purposes. A 125HP (93 kW) variable frequency drive electric motor is coupled to a 7:1 Lufkin gearbox to provide rotational speeds up to 29,000 RPM's. The output of the gearbox is connected to the test shaft via a flexible disc coupling.

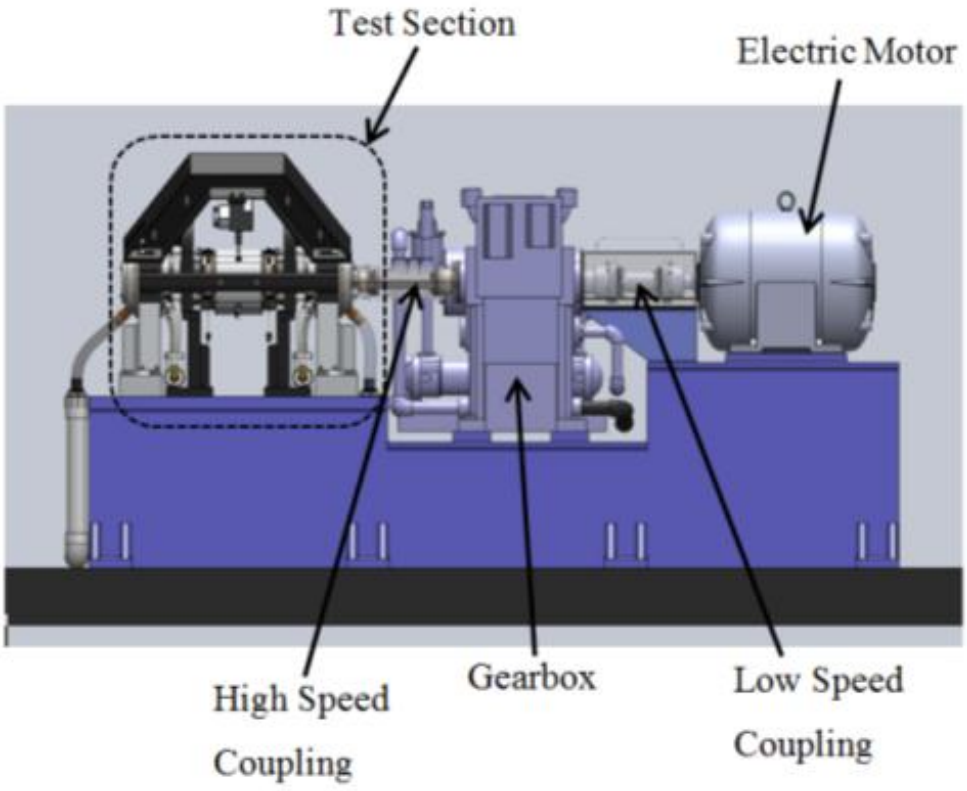

Figure 11. Complete test rig

Figure 12 provides front, side, and top views of the test section.

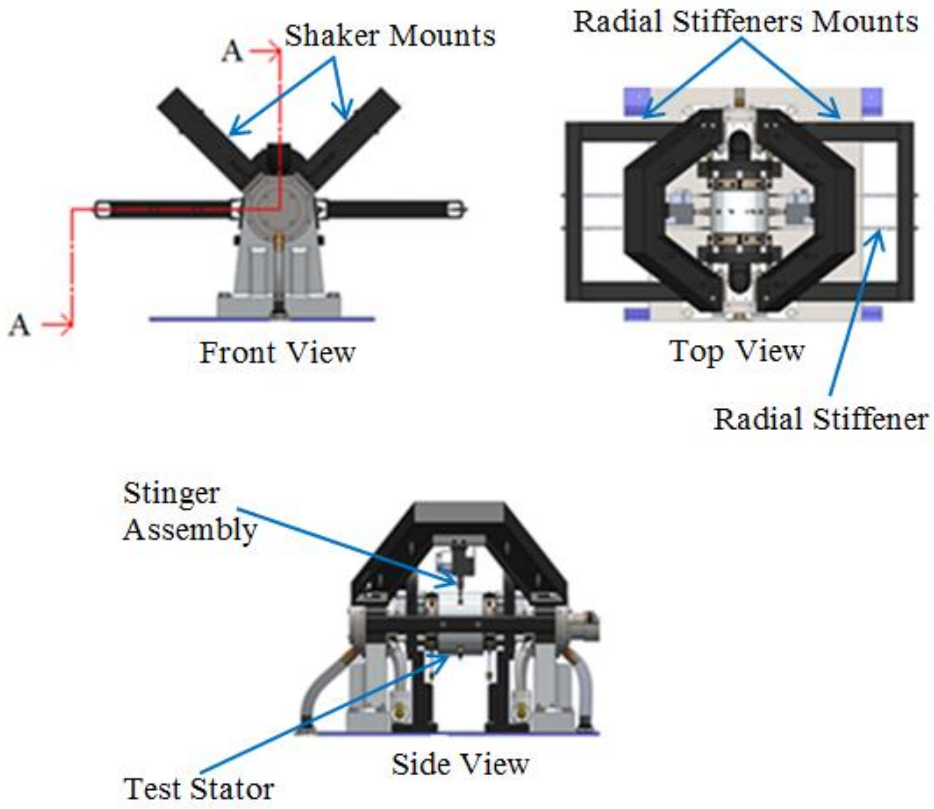

Figure 12. Front, side, and top view of the test rig

The test shaft shown in Figure 13 is supported by two hydrostatic bearings that use water, at a supply pressure of 70 bar (1015 psi) as their lubricant. Collars on the shaft impinge the axial flow of water out of the bearings, and air buffer seals help to trap water in the containment boots.

A sectional view followed by a detail view of the test rig is shown in Figures 13 and 14, respectively.

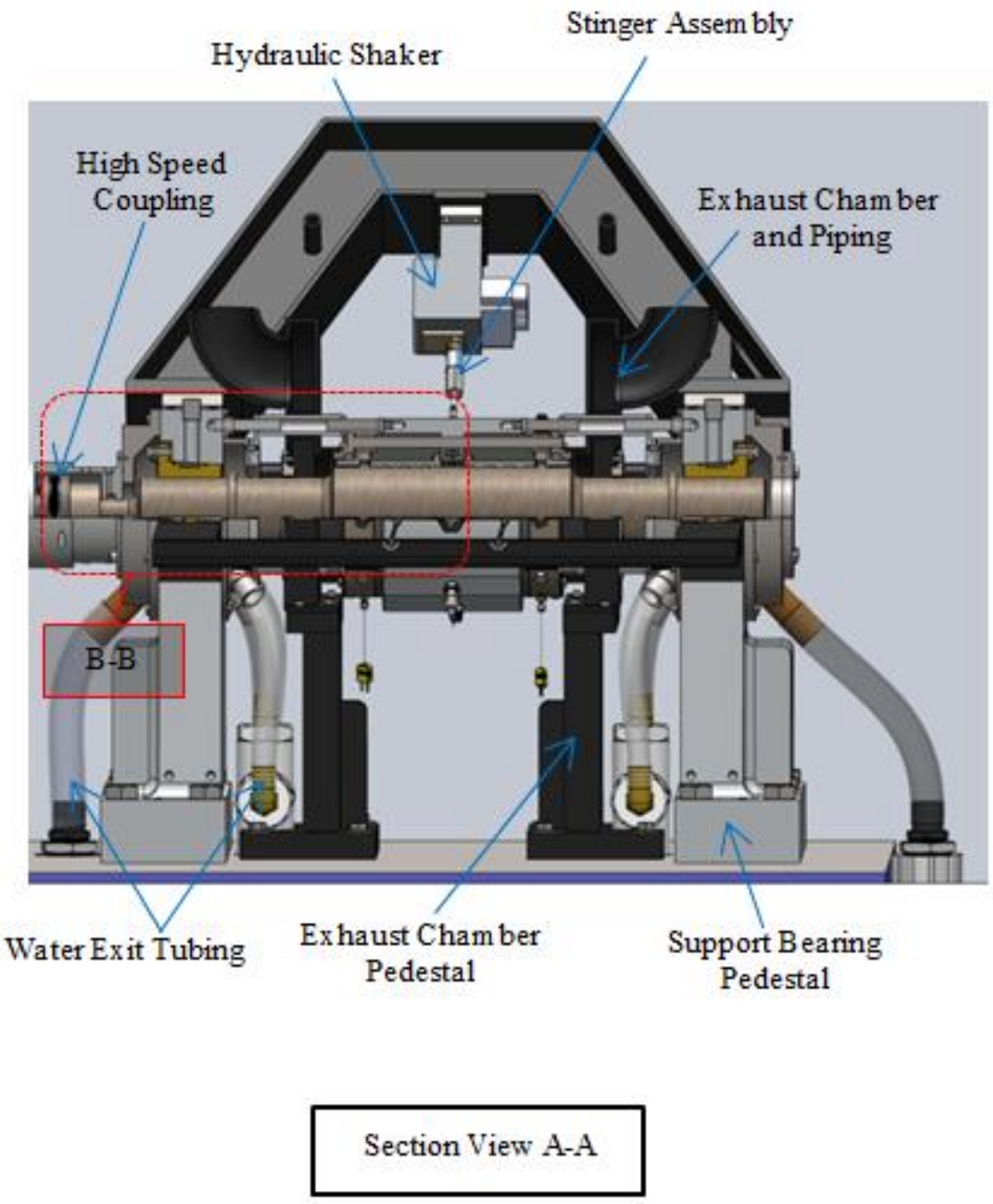

Figure 13. Sectional view A-A of the test section

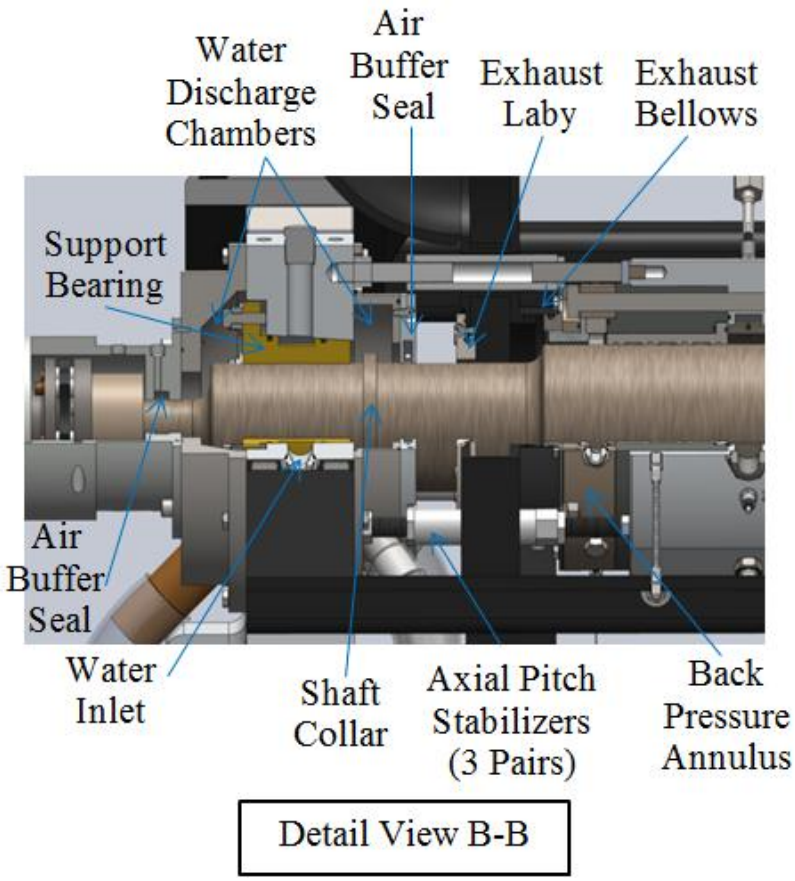

Figure 14. Sectional and detail view of the test rig

Unlike a machine application, the test stator is softly supported, allowing the stator itself to be excited. This "floating" design was originally used by Glienicke [66] and has many advantages as described by Rouvas [67]. Excitation is imparted on the stator, via stingers, by two orthogonally-mounted hydraulic shakers (shown in Figures 12 and 13) that can apply dynamic loads up to 4.5 kN (1000lbs) at a maximum frequency of 1000 Hz. The shakers are positioned above the stator and 45 degrees from vertical.

Pitch stabilizers shown in Figure 14 are used to eliminate pitch and yaw, thereby aligning the stator with the rotor. They also ensure the stator moves along a single plane during excitation and prevent the development of a pitch-mode. A pitch-mode occurs when the two sides of the stator (the two back pressure annulus shown in Figure 15) do not move in phase with each other.

The stator can develop unstable whirling motion. For this type of instability, as air is introduced into the stator, the stator will move in an orbital path. Note: The stator itself goes

unstable, not the rotor. The stator instability can occur without rotation of the test shaft. Radial stiffeners shown in Figure 12 are used to improve the stability of the stator. The radial stiffeners introduce support-stiffness orthotropy and are analogous to multilobe bearings that improve stability by developing orthotropic bearing stiffness. Radial stiffeners have previously been used in the testing of labyrinth seals [68] and smooth seals [69], to improve stability.

2.2.2 Test Stator

The test stator, shown in Figure 15, houses two back-to-back seals to limit axial thrust. Air enters the center plenum chamber and subsequently passes through a swirl ring which determines the preswirl flow.

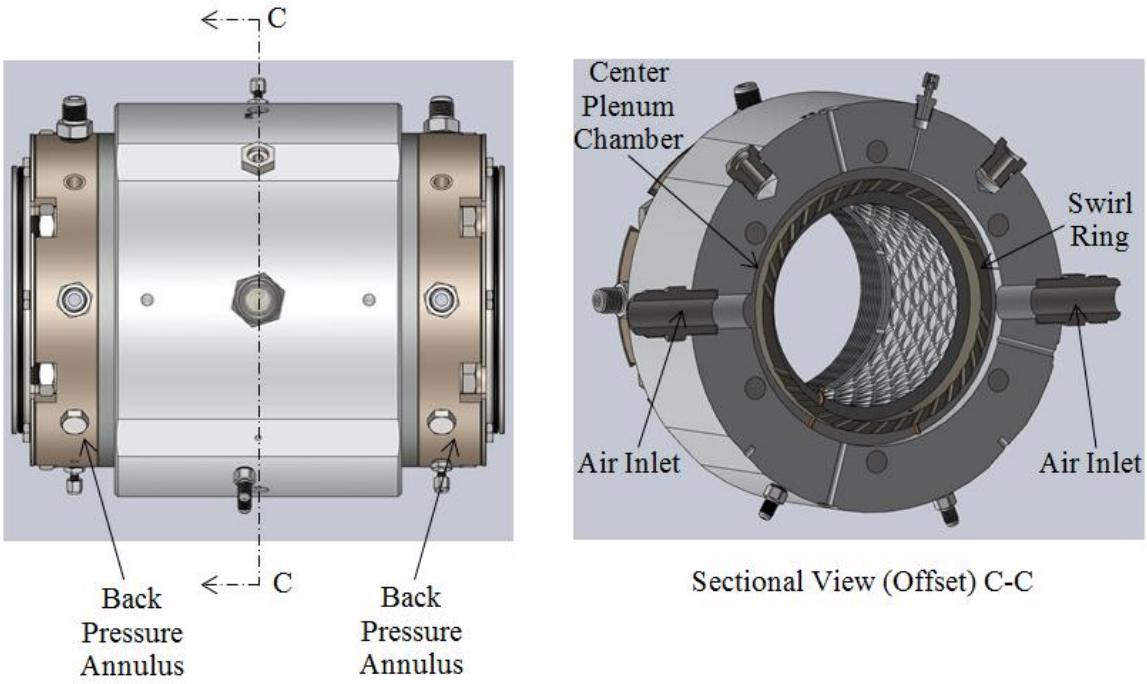

Figure 15. Test stator and sectional view C-C

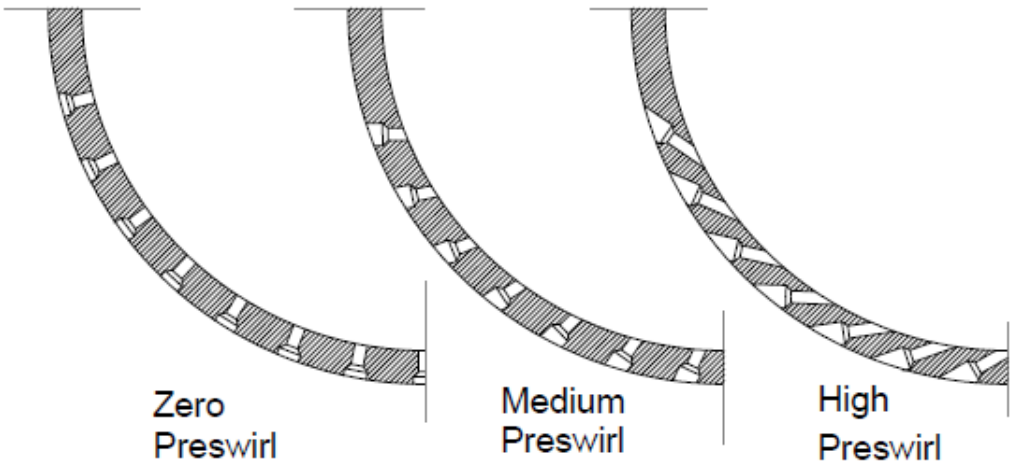

Figure 16. Cross section of swirl rings: zero, medium, and high [69]

Three swirl rings shown in Figure 16 impart varying degrees of preswirl and are designated as zero, medium, and high. The zero swirl ring directs the incoming air normal to the rotor. The medium and high swirl rings inject air with normal and tangential velocity components. After passing through the swirl ring, the air flow, ideally, divides in two with half the flow passing through one seal and half through the other seal.

The back pressure annuli, shown in Figure 17, are found at the exit of the test seals. A back pressure annulus houses a labyrinth seal, swirl brake, and three bleed-off ports. The flow through the bleed-off ports is metered by a global valve (not shown) that sets the exit pressure for the test seals. The flow that does not pass through the bleed-off ports passes past the swirl brake and continues on through the exit labyrinth shown in Figure 17. After flow exits the stator, it is vented to atmosphere.

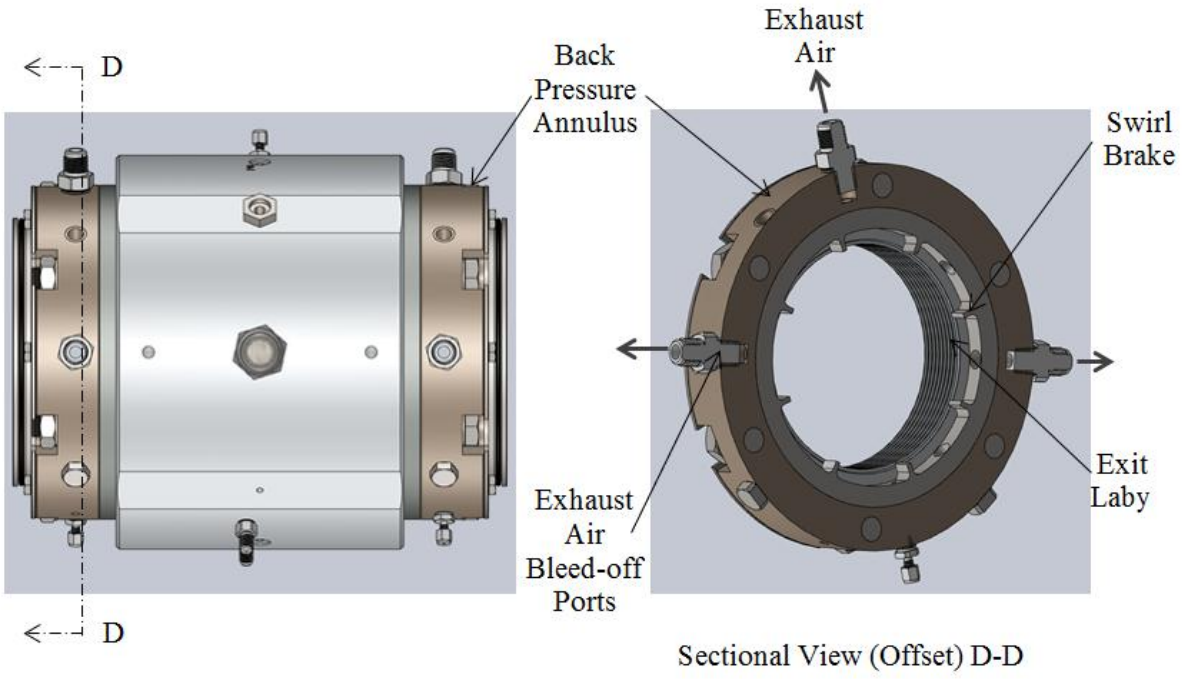

Figure 17. Test stator and sectional view D-D

The back pressure annuli are used to set the pressure ratio (*PR*) defined by Eq. (10).

$$PR = \frac{Back\ Pressure}{Inlet\ Pressure} \tag{10}$$

2.3 Test Seal

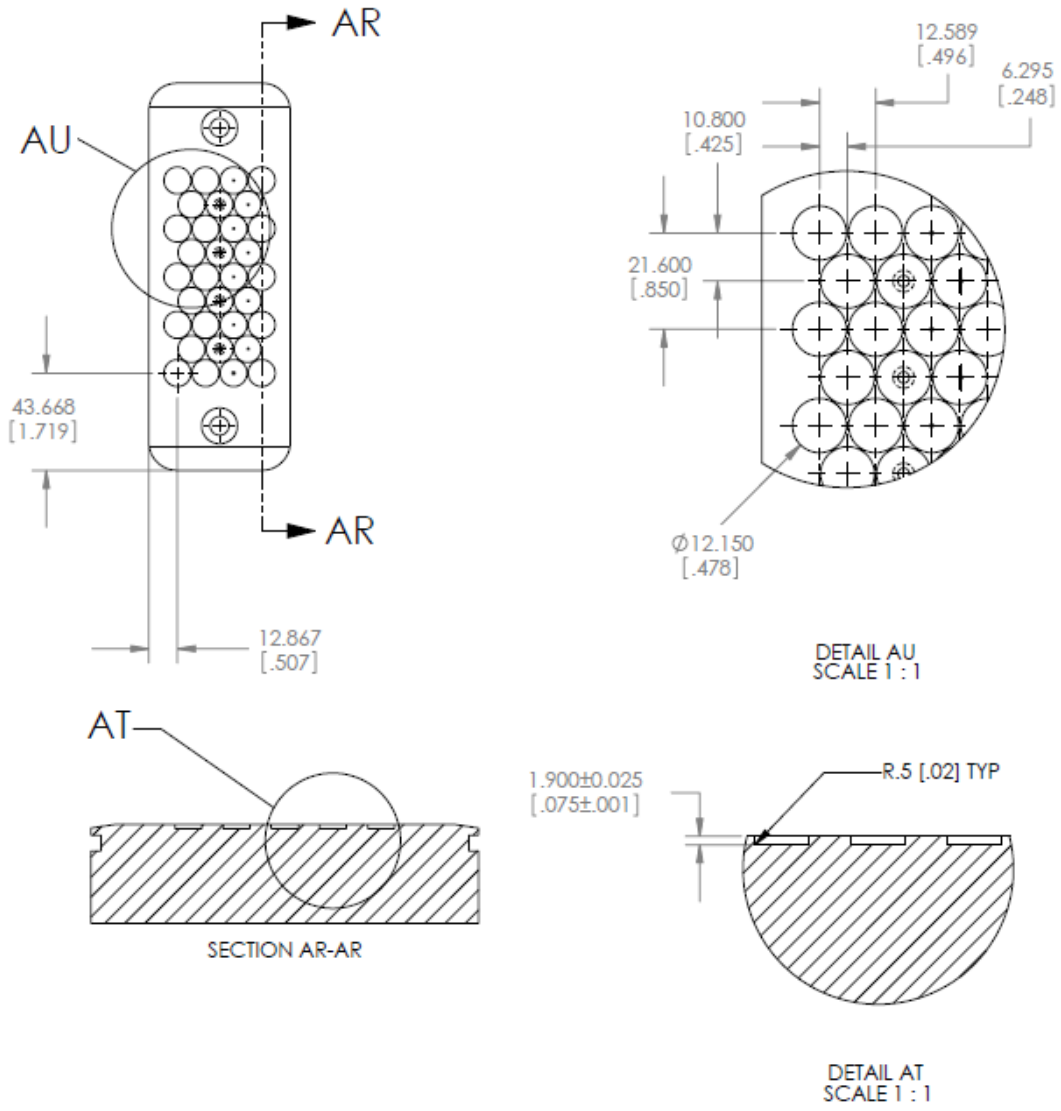

Figure 18. Flat plate hole pattern configuration [62]

The HP seal design tested for this thesis is based on the flat plate pattern shown in Figure 18. This hole-pattern configuration had to be modified to accommodate the dimensions of the test seal. Figure 19 shows the seal configuration that was arrived at, to mimic the pattern of the flat plate.

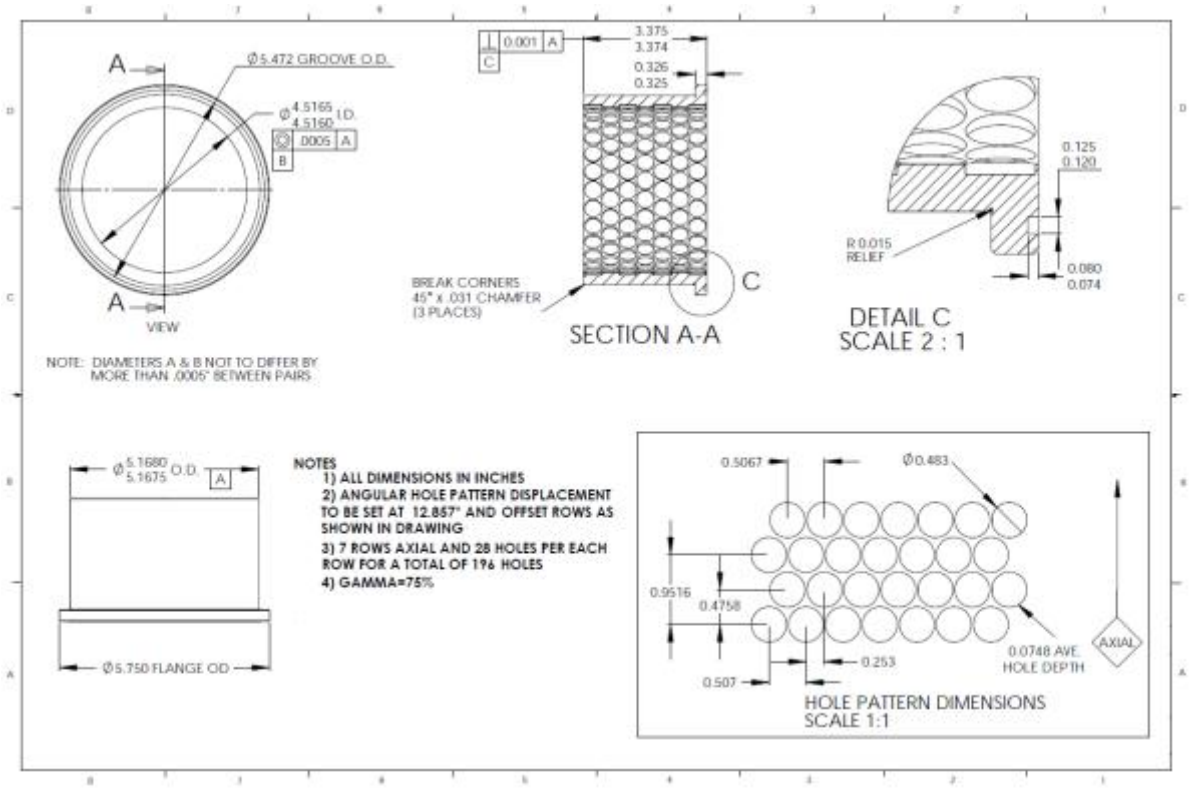

Figure 19. Test seal dimensions

Table 1 gives the percent difference between the flat plate and seal hole-pattern configurations.

Table 1. Percent difference between flat plate and seal hole-pattern configuration

Dimensions	Flat Plate		HP Seal		Percent Difference
Axial Spacing	10.8 mm	(0.425 in)	12.09 mm	(0.4758 in)	(2.29%)
Transverse Spacing	12.589 mm	(0.496 in)	12.870 mm	(0.507 in)	(0.55%)
Hole Diameter	12.15 mm	(0.478 in)	12.2682 mm	(0.483 in)	(0.24%)
Hole Depth (average)	1.9 mm	(0.075 in)	1.9 mm	(0.075 in)	(0.00%)
Gamma Ratio	75%		75%		(0.00%)

Both test seals, are manufactured as identical as possible, thus justifying the assumption that the mass flow rate through each seal is equal. Each seal was measured with a three-point gauge that can measure to within 0.00254 mm (0.0001 in). Table 2 displays the results of these measurements before testing. The seals were also measured after completion of testing, with no difference in measurements being found.

Table 2. Seals inter-diameter dimensions

Seal 1				
Angle	Inlet		Exit	
0	114.732 mm	(4.5170 in)	114.727 mm	(4.5168 in)
30	114.732 mm	(4.5170 in)	114.729 mm	(4.5169 in)
60	114.722 mm	(4.5166 in)	114.722 mm	(4.5166 in)
90	114.727 mm	(4.5168 in)	114.717 mm	(4.5164 in)
Average:	**114.728 mm**	**(4.5169 in)**	**114.724 mm**	**(4.5167 in)**

Seal 2				
Angle	Inlet		Exit	
0	114.722 mm	(4.5166 in)	114.717 mm	(4.5164 in)
30	114.717 mm	(4.5164 in)	114.727 mm	(4.5168 in)
60	114.714 mm	(4.5163 in)	114.711 mm	(4.5162 in)
90	114.722 mm	(4.5166 in)	114.711 mm	(4.5162 in)
Average:	**114.719 mm**	**(4.5165 in)**	**114.717 mm**	**(4.5164 in)**

Two shafts of diameter 114.3 mm (4.5 in) and 114.5032 mm (4.508) are used to provide the targeted clearances of 0.1 mm (4 mils) and 0.2 mm (8 mils).

2.4 Instrumentation

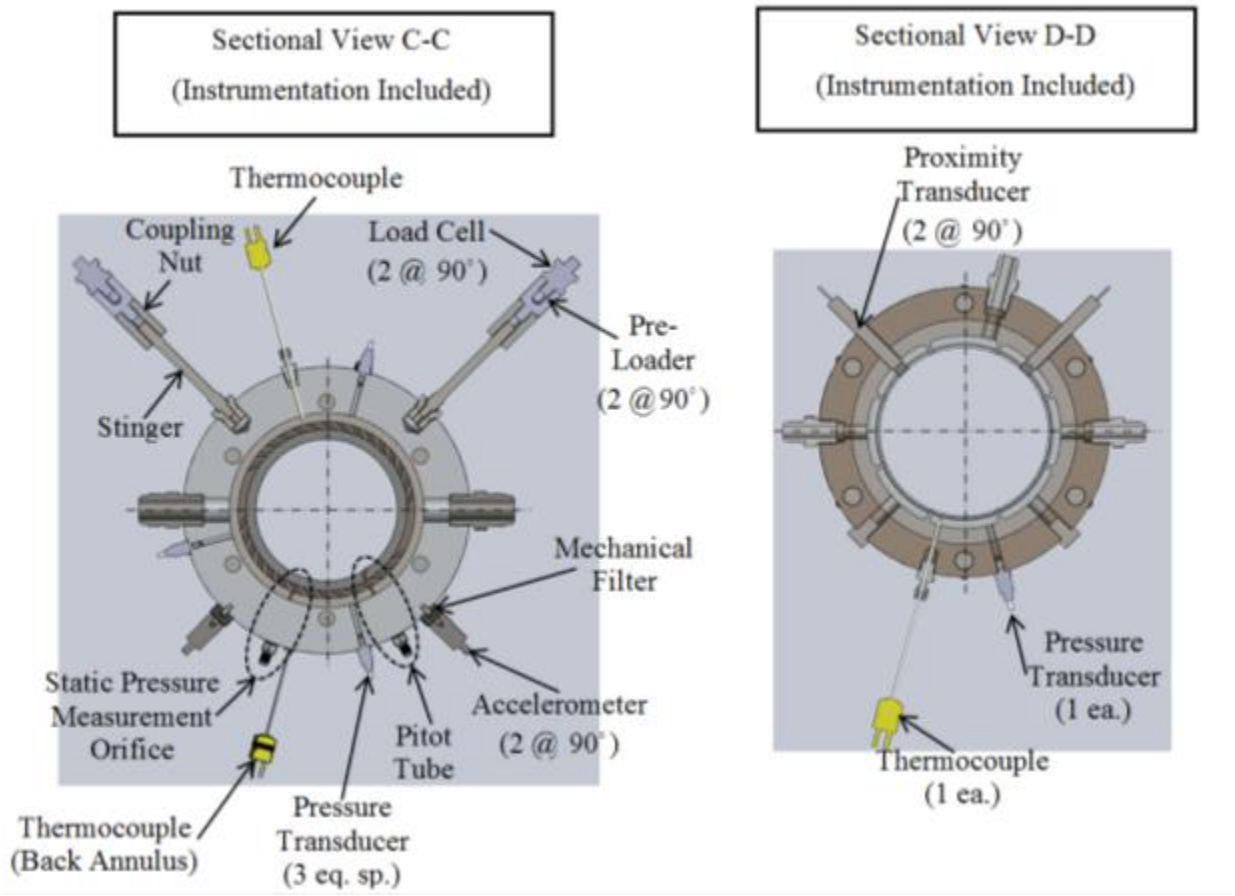

Figure 20. Sectional views including instrumentation

Figure 20 provides sectional views of the stator with all the instrumentation included. Two load cells measure the force applied to the stator by the hydraulic shakers. Pre-loaders are used to ensure the load cells are torqued properly and to reduce the risk of damage when installing or removing the stingers.

Piezoelectric accelerometers, found 180 degrees from the stinger attachments, record the absolute acceleration of the stator along the *x*-axis and *y*-axis. The accelerometers are mounted on mechanical filters to protect them from vibrational frequencies greater than the accelerometers' range.

Four eddy current proximity probes measure the relative motion between the stator and rotor in the *x* and *y* directions. The proximity probes are installed on top of the stator, as

experience detailed in Kulhanek [3] encourages. Two proximity probes are found on each of the back pressure annuli. The probes on either end of the stator are used to align the stator with the rotor, and monitor possible of pitch-mode motion.

Three pressure transducers, shown in the right picture of Figure 20, measure the center plenum chamber (reservoir pressure) for the seals. One pressure transducer is found at each of the back pressure annuli. The two probes found at the back pressure annuli are used to set the *PR* and ensure the pressure difference between the two sides of the stator are minimal.

Thermocouples are used to record the stagnation temperature of the air at each test seal's exit, and the center plenum.

The Pitot tube and static pressure orifice (shown circled in Figure 20 and again in Figure 21), are used to measure the stagnation and static pressure of the inlet air, respectively. The difference in static and stagnation pressure is evaluated via a differential pressure transmitter. Since changes in elevation are negligible, dynamic pressure is the difference in stagnation and static pressure. The dynamic pressure is then used to calculate the *inlet circumferential velocity* (V_t) as detailed in Picardo [68]. Preswirl ratio [$u_o(0)$] is defined as V_t divided by the rotor's surface speed.

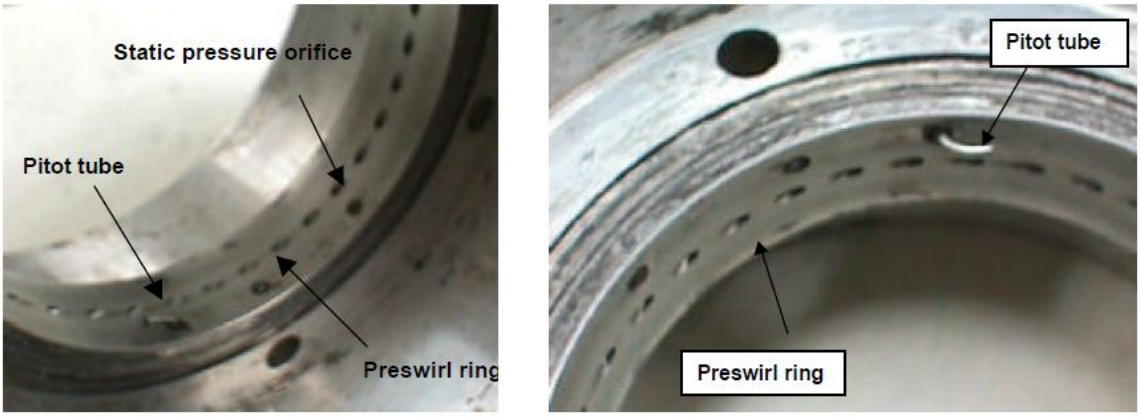

Figure 21. Preswirl ring [68]

The volumetric flow rate (leakage) of the air is measured upstream of the stator via a turbine flow meter (not shown). Pressure and temperature measurements are recorded before and after the flow meter.

3. PARAMETER IDENTIFICATION

3.1 Static Characteristics Identification

The turbine flow meter displays the total volumetric flow rate through both seals in Actual Cubic Feet per Minute (ACFM). The ACFM [Q] is converted to the mass flow rate [kg/sec] through each seal,

$$\dot{m}_{uncorrected} = \frac{Q/2 \cdot \rho}{(35.31466) \cdot 60} \quad (11)$$

The terms in the denominator are conversions factors. Since flow through the two test seals is assumed equal, the measured ACFM [Q] is divided by two. Using the temperature and pressure measurements at the time of testing, the ideal gas law is employed to determine the density of air (ρ).

3.2 Dynamic Characteristics Identification

The test rig was initially used to test hydrostatic bearings with the calculation of rotordynamic coefficients following the procedure detailed in Childs and Hale [63] and Rouvas [67]. The calculation of seal rotordynamic coefficients is based on this procedure.

3.2.1 Extraction of the System Complete Complex Dynamic Stiffness

When testing, the effects of the test seals and the test rig itself cannot be initially separated. The stiffness and damping contributed by the test rig is due to the pitch stabilizers, axial stiffeners, inlet and exit air hoses, etc. A baseline, discussed later is used to extract the effects of the test seal from the total system.

By applying Newton's Second Law the equation of motion for the stator mass M_s is:

$$M_s \begin{bmatrix} \ddot{x}_s \\ \ddot{y}_s \end{bmatrix} = \begin{bmatrix} f_x \\ f_y \end{bmatrix} - \begin{bmatrix} f_{seal_x} \\ f_{seal_y} \end{bmatrix} \tag{12}$$

where $\ddot{x}_s$, $\ddot{y}_s$ and f_x , f_y are the measured absolute stator acceleration (measured via accelerometers) and forces (measured via load cells), respectively. The test seal-reaction forces (f_{seal_x} , f_{seal_y}) are unknown. Substituting Eqs. (4) into Eq. (12), Eq. (13) is arrived at:

$$M_s \begin{bmatrix} \ddot{x}_s \\ \ddot{y}_s \end{bmatrix} = \begin{bmatrix} f_x \\ f_y \end{bmatrix} - \begin{bmatrix} K(\Omega)_{xx} & K(\Omega)_{xy} \\ K(\Omega)_{yx} & K(\Omega)_{yy} \end{bmatrix} \begin{Bmatrix} \Delta x \\ \Delta y \end{Bmatrix} - \begin{bmatrix} C(\Omega)_{xx} & C(\Omega)_{xy} \\ C(\Omega)_{yx} & C(\Omega)_{yy} \end{bmatrix} \begin{Bmatrix} \Delta \dot{x} \\ \Delta \dot{y} \end{Bmatrix} \tag{13}$$

By assuming harmonic motion and performing a Fourier transform ($\mathbf{F}$) on the measureable quantities,

$$\begin{bmatrix} \boldsymbol{F}_x - M_s \boldsymbol{A}_x \\ \boldsymbol{F}_y - M_y \boldsymbol{A}_t \end{bmatrix} = \begin{bmatrix} \tilde{\boldsymbol{H}}_{xx} & \tilde{\boldsymbol{H}}_{xy} \\ \tilde{\boldsymbol{H}}_{yx} & \tilde{\boldsymbol{H}}_{yy} \end{bmatrix} \begin{bmatrix} \boldsymbol{D}_x \\ \boldsymbol{D}_y \end{bmatrix}. \tag{14}$$

$\boldsymbol{F_i}$, $\boldsymbol{A_i}$, and $\boldsymbol{D_i}$ are the Fourier transformation of the external forces, stator acceleration, and relative motion respectively. $\tilde{\boldsymbol{H}}_{ij}$ is the complete complex dynamic stiffness of a test and defined as:

$$\tilde{\boldsymbol{H}}_{ij} = K(\Omega)_{ij} + \boldsymbol{j}\Omega C(\Omega)_{ij} \tag{15}$$

where $\boldsymbol{j}=\sqrt{-1}$.

To develop four independent equations for the four unknowns two multi-frequency dynamic loads are sequentially applied to the stator in the *x* and *y* directions. While a dynamic load is being applied (along one axis) to the stator, measurements are simultaneously recorded for both axes. Adding the two load cases together provides

$$\begin{bmatrix} \boldsymbol{F}_{xx} - M_s \boldsymbol{A}_x & \boldsymbol{F}_{xy} - M_s \boldsymbol{A}_{xy} \\ \boldsymbol{F}_{yx} - M_y \boldsymbol{A}_t & \boldsymbol{F}_{yy} - M_s \boldsymbol{A}_{yy} \end{bmatrix} = \begin{bmatrix} \tilde{\boldsymbol{H}}_{xx} & \tilde{\boldsymbol{H}}_{xy} \\ \tilde{\boldsymbol{H}}_{yx} & \tilde{\boldsymbol{H}}_{yy} \end{bmatrix} \begin{bmatrix} \boldsymbol{D}_{xx} & \boldsymbol{D}_{xy} \\ \boldsymbol{D}_{yx} & \boldsymbol{D}_{yy} \end{bmatrix}, \tag{16}$$

where the first subscript signifies the axis of excitation and the second the axis along which the responses was measured. With two independent excitations the displacement matrix can be inverted to solve for the complex dynamic stiffness.

3.2.2 Extraction of the Test Seals Complex Dynamic Stiffness

To identify the complex dynamic stiffness due solely to the test seal, a "baseline" test was performed. For baseline test, the stator is assembled without the test seals. Next, the stator is pressurized such that the pressures seen at the back pressures annuli are similar to those seen during testing. Finally, the rotor is spun to test speed, and dynamic data is recorded. This baseline data is subtracted from the complex dynamic stiffness measure during testing:

$$\boldsymbol{H}_{ij,TEST\ SEAL} = \tilde{\boldsymbol{H}}_{ij} - \boldsymbol{H}_{ij,BASELINE} \quad (17)$$

3.2.3 Estimation of Test Seals Stiffness and Damping Coefficients

Seal dynamic coefficients are found by separating the real and imaginary part of the complex dynamic stiffness coefficients and performing the necessary algebra:

$$K_{ij}(\Omega) = \mathrm{Re}(\boldsymbol{H}_{ii}(\Omega)) \quad (18)$$

and

$$C_{ij}(\Omega) = \frac{\mathrm{Im}(\boldsymbol{H}_{ii}(\Omega))}{\Omega} \quad (19)$$

4. UNCERTAINTIES, REPEATABILITY, AND DATA ACQUISITION

4.1 Static Uncertainties

Static uncertainties are calculated using the procedures detailed in Coleman and Steele [70] and Wheeler and Ganji [71]. Uncertainties were based on the calibration curve standard error of regression and the analog-to-digital converter (A/C) resolution. Table 3 displays the static uncertainty results.

Table 3. Static uncertainties

Shaft Speed	Pressure Flow Meter	Pressure Stator	Inlet Pressure Difference	Temperature	Flow Rate
2.807 RPM	5.00 psi	0.838 psi	1.28 in H_2O	5.61 F	0.069 gal/s
2.807 RPM	0.34 bar	0.058 bar	0.0323 m H_2O	14.7 C	0.26 liter/s

4.2 Data Acquisition and Dynamic Coefficients Repeatability

As discussed above, the stator is excited via a multi-frequency waveform. This waveform is comprised of nominal frequencies from 10 Hz to 360 Hz in 10 Hz increments. In fact, the nominal frequencies are multiplied by a factor of 1,000/1,024 to offset the excitation frequencies from electrical power noise.

Transducer signals are recorded simultaneously by LabVEIW dynamic cards at a sampling rate of 10,000 Hz. These time domain signals are converted into the frequency domain via a Fast Fourier Transformation (FFT). To ensure that the FFT is computed for a periodic signal a single excitation waveform is applied over a 0.1024 second interval. Therefore, the sample size and frequency resolution are found to be 1024 and 1000/1024 Hz respectively. Since the excitation incremental frequency and sampling frequency resolution are the same, leakage and the need for windowing is eliminated.

To minimize the effect of measured noise and provide repeatability, the excitation waveform is sequentially applied 320 times along both axes. These 320 excitations are then broken into groups of 64 excitations that will be referred to as sets of data. A total of 10 sets

of data (5 for the *x*-axis and 5 for the *y*-axis) are produced. Next, the sets of data from the *x*-axis and *y*-axis are combined to develop 25 complex dynamic stiffness matrices. Dynamic uncertainties are based on the dispersion of these 25 matrices.

For a given excitation frequency, the average complex dynamic stiffness ($\boldsymbol{H}_{ij}$) is:

$$\boldsymbol{H}_{ij} = \frac{1}{n}\sum_{k=1}^{n}(\boldsymbol{h}_{ij})_k \quad , \tag{20}$$

where ($\boldsymbol{h}_{ij}$) is the complex dynamic stiffness of each combination case, and *n* is the number of complex dynamic stiffness matrices produced (25 in this case). Repeatability of these 25 sets of data is defined:

$$\Delta\boldsymbol{H}_{ij} = 2\sigma_{\boldsymbol{H}_{ij}} = 2\sqrt{\frac{\sum_{k=1}^{n}((\boldsymbol{h}_{ij})_k - \boldsymbol{H}_{ij})^2}{n-1}} \quad . \tag{21}$$

Graphically, the repeatability is represented by error bars.

This is the first time the method described above has been employed for data analysis of gas seals. Previous tests have used the method described by Rouvas [67] for estimating uncertainties and minimizing noise. The current method was developed by Jason Wilkes and has been shown to produce data with significantly less uncertainty.

5. TEST CONDITIONS

For a radial clearance of 0.2 mm (8 mils), data were collected at 10,200, 15350, and 20200 rpm's, three pressure ratios (0.4, 0.5, and 0.6), and three swirl rings (zero, medium and high). Additional data for a radial clearance of 0.1 mm (4 mils), were collected using only the zero swirl ring. The test matrix summarizing these test cases and the absolute reservoir pressures is shown in Table 4. Table 7 in Appendix A list the exact absolute pressures at the time of testing.

Table 4. Test matrix

			Preswirl (-)		
Radial Seal Clearance	**Rotor Speed**	**Pressure Ratio**	**Zero**	**Medium**	**High**
(mm)	(RPM)	(-)	Reservoir Pressure [bar]		
0.2	10,200	0.4	*29*	*18*	*41*
		0.5	*42*	*18*	*41*
		0.6	*42*	*18*	*41*
	15,350	0.4	*30*	*18*	*41*
		0.5	*37*	*18*	*41*
		0.6	*42*	*18*	*41*
	20,200	0.4	*29*	*18*	*41*
		0.5	*42*	*18*	*41*
		0.6	*42*	*18*	*41*
0.1	10,200	0.4	*21*	*Not Tested*	
		0.5	*21*		
		0.6	*22*		
	15,350	0.4	*22*		
		0.5	*22*		
		0.6	*22*		
	20,200	0.4	*21*		
		0.5	*21*		
		0.6	*22*		

Typically, test preformed on the current test rig use an inlet pressure of 70 bar (1015 psi). Unfortunately, due to the factors described in Section 5.1, testing had to be performed at much lower, and various inlet pressures. In previous tests, the medium rotational speed

was 15,200 rpms. Due to excessive noise seen at approximately 253 Hz the medium speed was adjusted to 15,350 RPM.

5.1 Difficulties in Testing

5.1.1 Stator Dynamic Instability

The stator developed dynamic instability when the medium and high swirl rings were used. Without rotation of the shaft, and starting from a centered position, as the inlet pressure was increased, the stator would become unstable at some "onset pressure level of instability". The instability would cause the stator to "dance." The orbit would continue to grow in amplitude until the stator and rotor made contact. Next, the stator would follow the radius of the shaft producing a circular orbit. Instead of the rotor, the softly supported stator becomes unstable. Strangely, the high swirl ring had a higher onset pressure level of instability. The stator dynamic instability limited the inlet pressure at which the medium and high preswirl stator could be tested at.

Labyrinth [68] and smooth seals [69] tested developed this form of instability. This is the first time an HP seal tested at the Texas A&M Turbomachinery Laboratory had developed this type of instability.

5.1.2 Stator Static Instability

The test HP seal also exhibited an apparent "static instability". The position of the stator relative to the rotor can be controlled by the hydraulic shakers. Without rotation, no excitation, and the stator initially centered, as the inlet pressure was increased it became increasingly difficult to keep the stator centered for the zero preswirl stator. In some instances, the stator would be "sucked" against the rotor. When the rotor and stator made contact, a great deal of force was needed to separate the two.

6. RESULTS

The various test cases allow for inspection of how changes in PR, inlet preswirl, running speed, and radial clearance influence rotordynamic and leakage characteristics. Due to the varying inlet pressures, some data is presented in non-dimensionalized or normalized form:

$$K_{ij}^{*} = K_{ij} \frac{C_r}{2 \cdot L \cdot R \cdot \Delta P} \tag{22}$$

$$C_{ij}^{*} = C_{ij} \frac{C_r}{2 \cdot L \cdot R \cdot \Delta P} \tag{23}$$

where L, R, C_r, and ΔP are the seal length, seal radius, radial clearance and pressure differential, respectively. The asterisk signifies that the stiffness coefficient is non-dimensionalized or that the damping coefficient is normalized.

Leakage is non-dimensionalized via the flow coefficient

$$\Phi = \frac{\dot{m}}{\pi \cdot D \cdot C_r} \left(\sqrt{\frac{R \cdot T_{in}}{2 \cdot \Delta P \cdot P_{in}}} \right) \tag{24}$$

where $\dot{m}$, D, P_{in}, T_{in}, and R are the mass flow rate, seal diameter, inlet pressure, and ideal gas constant, respectively.

6.1 General Comments about Data

Figures 22 and 23 provide typical plots of direct and cross-coupled dynamic coefficients for test cases using high and medium preswirl stators, respectively. Note, that $K_{xx} \cong K_{yy}$ and $C_{xx} \cong C_{yy}$. Further, $K_{xy} \cong -K_{yx}$ and $C_{xy} \cong -C_{yx}$. Dynamic coefficients presented for the high and medium preswirl stators are the average of their x and y magnitudes.

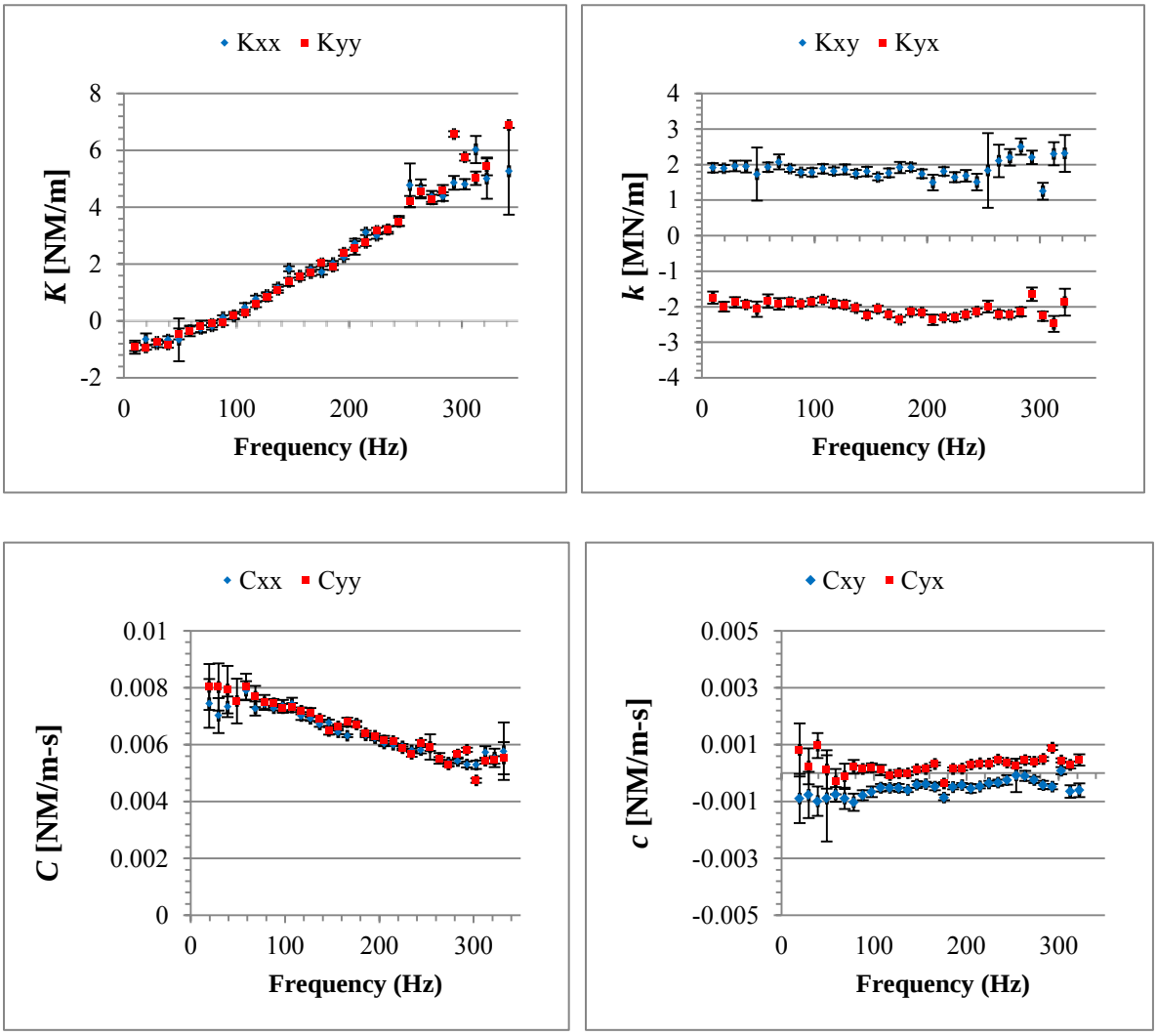

Figure 22. Complex stiffness for 0.2 mm (8 mils), PR=0.6, medium preswirl, and ω=20,200 RPM

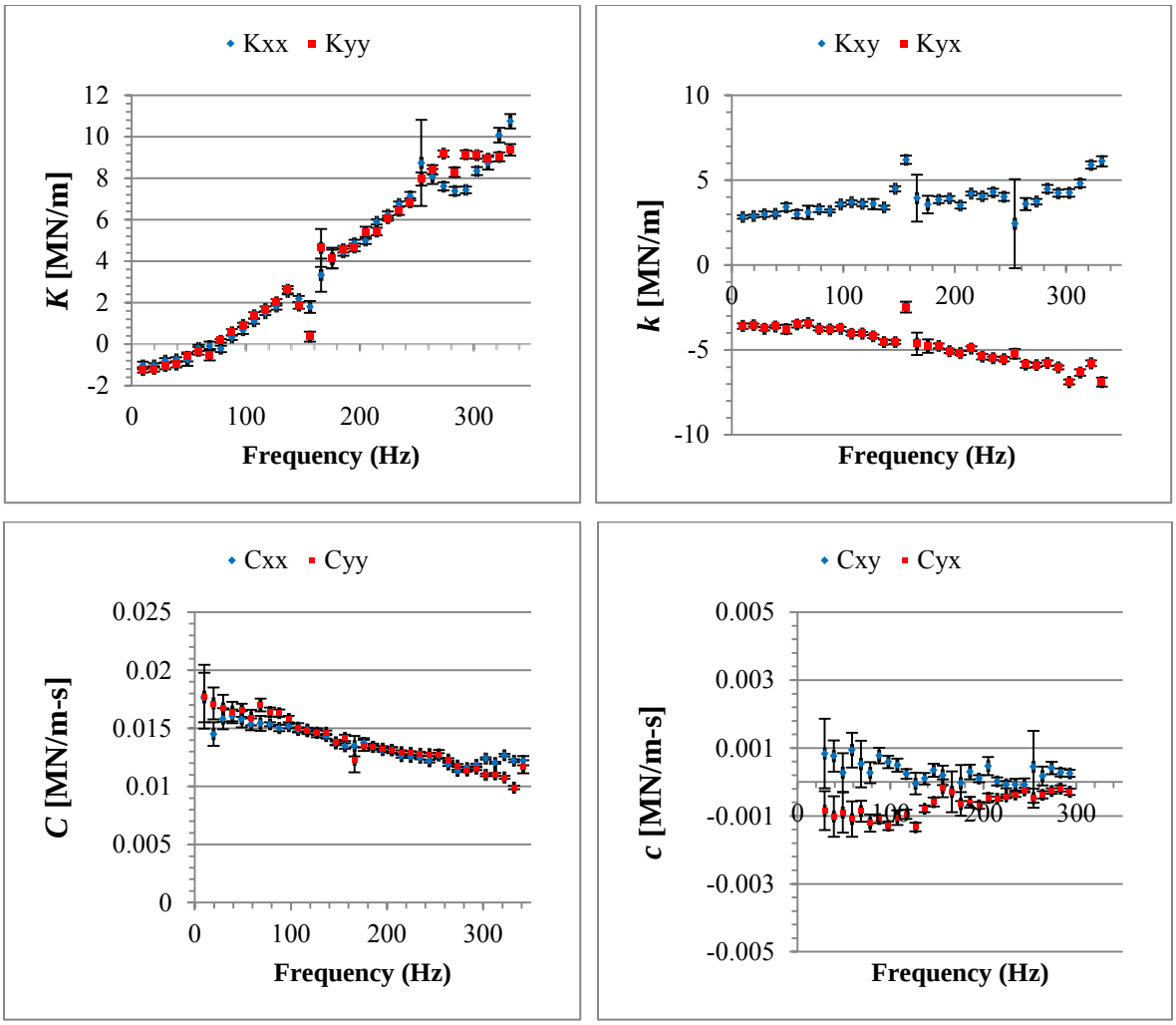

Figure 23. Complex dynamic stiffness for 0.2 mm (8 mils), PR=0.5, high preswirl, and ω= 10,200 RPM

Figure 24 provides typical plots of dynamic coefficients for zero preswirl, and 0.2 mm (8 mils) radial clearance. Note, direct complex dynamic stiffness coefficients are approximately equal, and *c* is very small in magnitude. Both K_{xy} and K_{yx}, exhibit a downward curve. For a clearance of 0.2 mm (8 mils) and zero preswirl, only K_{xy} is presented. Picardo [68] measured K_{xy} and K_{yx} that exhibit a downward curve for a labyrinth seal. At this time there is no explanation for this behavior.

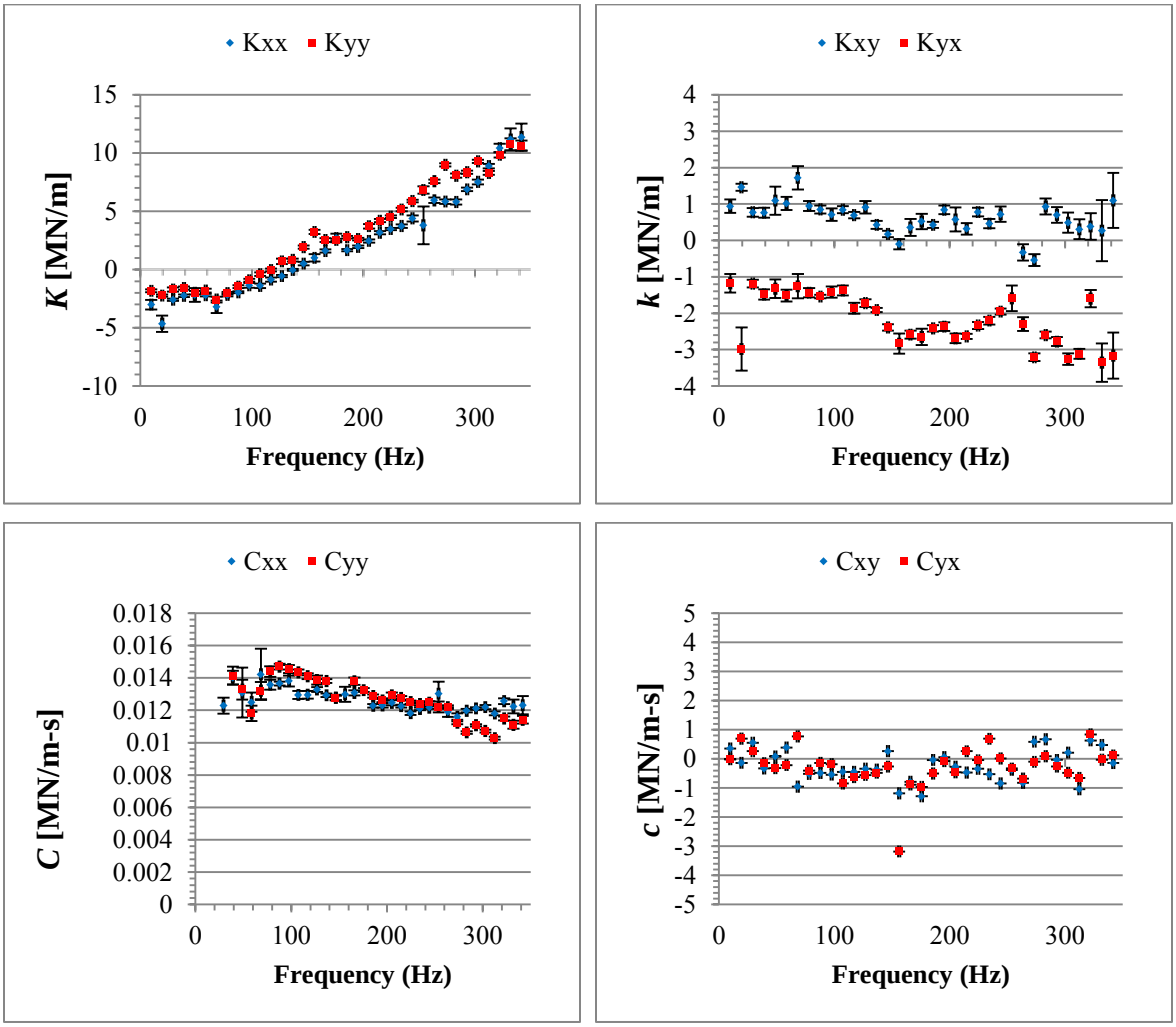

Figure 24. Complex dynamic stiffness for 0.2 mm (8 mils), PR=0.6, zero preswirl, and ω= 20,200 RPM

Figure 25 shows typical plots of direct and cross-coupling coefficients for zero preswirl, and 0.1 mm (4 mils) radial clearance. Note, direct complex dynamic stiffness coefficients are similar, and *c* is very small in magnitude. Also, $K_{xy} \cong - K_{yx}$ for frequencies below 220 Hz. The direct coefficients and *c* presented for zero preswirl and 0.1 mm (4 mils) radial clearance are the average of their *x* and *y* magnitudes. For *k*, data is presented up to a frequency of 220 Hz.

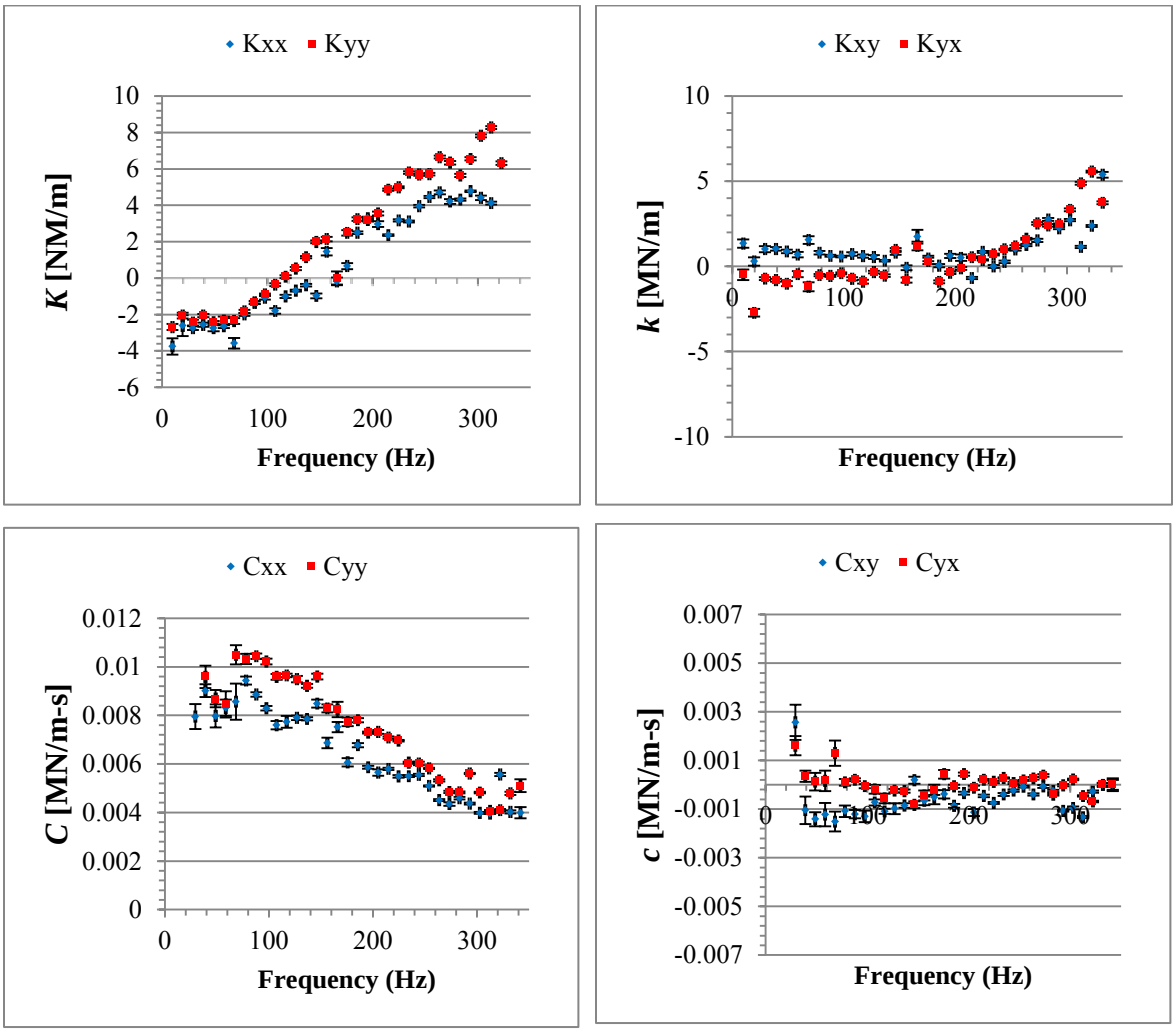

Figure 25. Complex dynamic stiffness for 0.1 mm (4 mils), PR=0.6, zero preswirl, and ω= 10,200 RPM

Figures 22 through 25, show negative K is exhibited for low excitation frequencies (approximately 80 Hz and less). In fact, K is negative for all test cases. The test rig can "overcome" some level of negative K, and keep the stator centered around the rotor. Ertas [72] modified the test rig by incorporating squirrel cages to stiffen the test section. Unfortunately, these squirrel cages failed, and time did not permit for the redesign, and manufacturing of new ones.

Negative stiffness can occur if a seal is diverging or a friction-factor jump occurs. Table 2 shows, the test seal are not divergent and flat-plate test for this hole-pattern configuration did not demonstrate a friction-factor jump [62]. In addition, recent flat-plate tests produced a friction-factor jump for flow between two roughened surfaces but not for flow between a roughened surface opposed to a smooth surface [62].

Figure 26 shows K^*, k^*, and C^* for a smooth seal tested by Kerr [69], and a HP seal tested by Wade [74]. Note, the smooth seal develops frequency-independent K^*, k^*, and C^*, while the HP seal produces frequency-dependent coefficients.

For the test seal here, K is proportional to frequency and C is inversely proportional to frequency. HP seals previously tested [60, 74] exhibit similar trends. Note, for the seal tested here, k is generally a weak functions of frequency. Similar to Kerr [69], c is relatively small. A comparison between the test seal and the seal test by Wade [74] is provided in section 6.4.

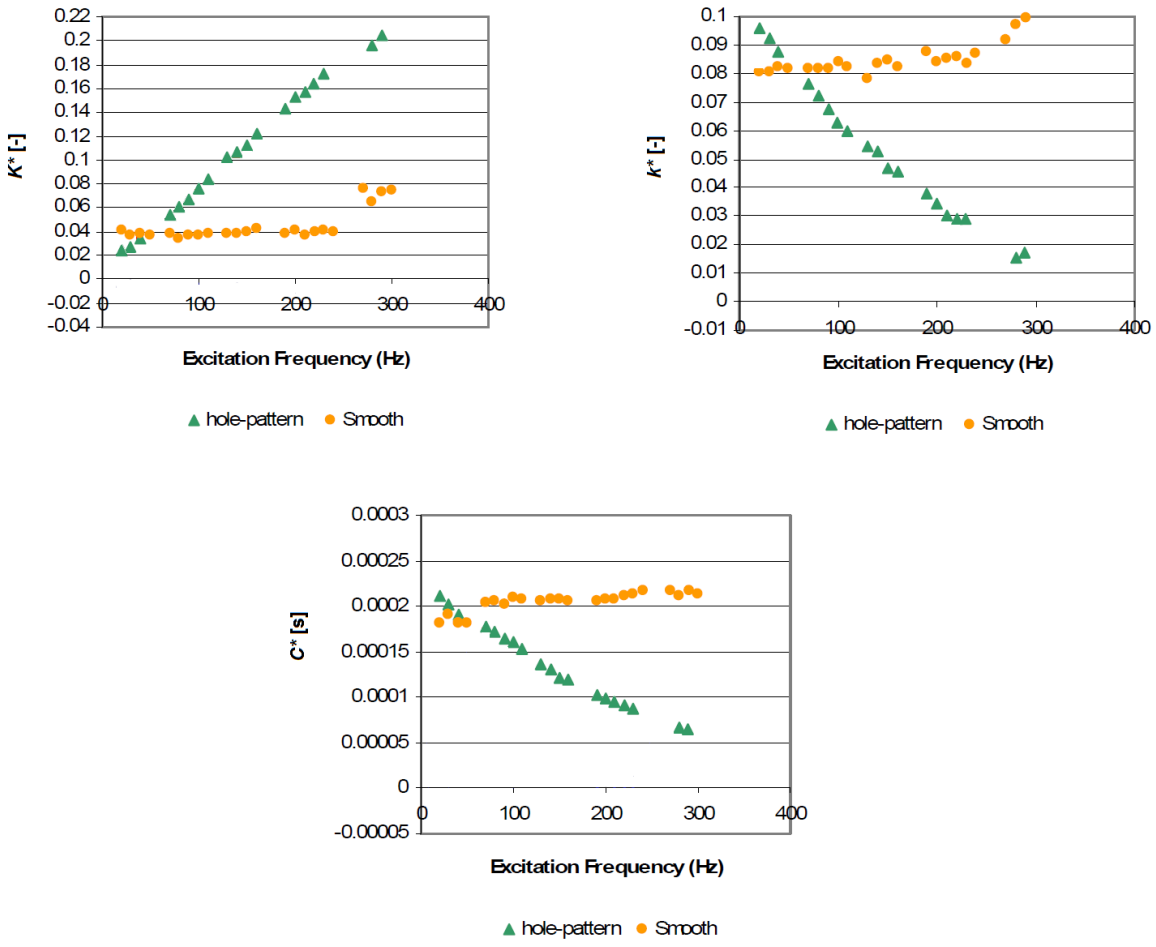

Figure 26. Non-dimensionalized stiffness and normalized direct damping for a smooth and hole-pattern seal (adapted from [2])

Reynolds numbers are greater than 40,000 and 17,000 for clearances of 0.2 mm (8 mils) and 0.1 mm (4 mils), respectively. Additionally flow is compressible. For a clearance of 0.2 mm (8 mils), all exit Mach numbers are greater than 0.3 with values, generally exceeding 0.5 for a PR=0.4. For a clearance of 0.1 mm (4 mils), all exit Mach numbers are greater than 0.27 with values greater than 0.45 for a PR=0.4.

6.2 Experimental Results

6.2.1 Static Results

To avoid redundancy, a discussion of leakage results is not given here. Instead, leakage results are found in sections 6.3.4 and 6.4.1.

6.2.2 Dynamic Results

Note, to examine the effect of preswirl and radial clearance the dynamic coefficients are non-dimensionalized or normalized.

6.2.2.1 Direct and Cross-Coupled Stiffness

6.2.2.1.1 Pressure Ratio

Figure 27 demonstrates that for the range considered PR has limited to no effect on *K* and *k*.

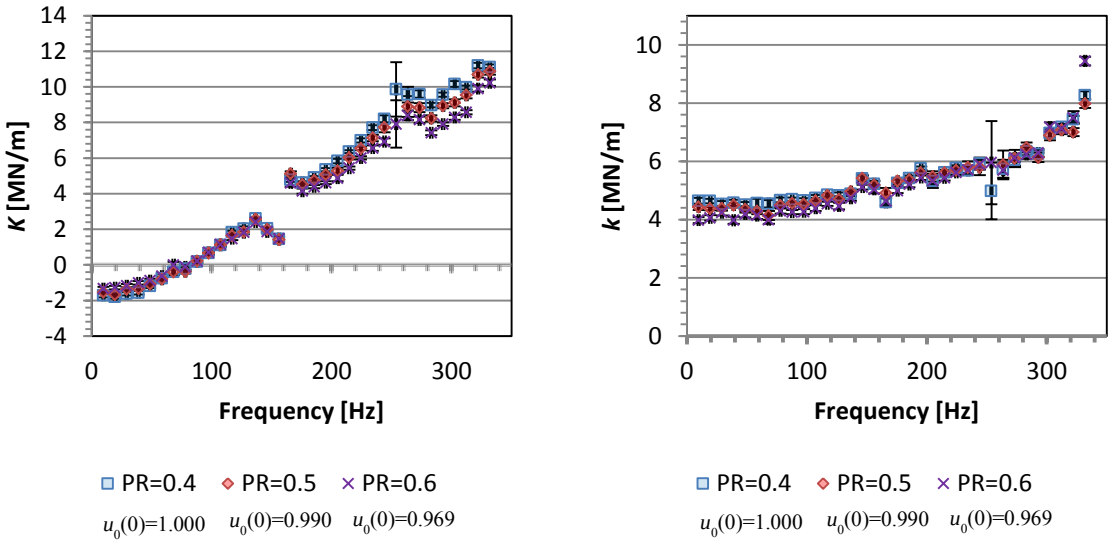

Figure 27. Direct and cross-coupled stiffness coefficients for 0.2 mm (8 mils), three pressure ratios, high inlet preswirl, and ω= 15,350 RPM

6.2.2.1.2 Preswirl

Figure 28 shows the influence of preswirl on K^* and k^*. K^* is approximately equal for high and medium preswirl cases and slightly smaller for the zero preswirl case. As expected the destabilizing k^* coefficient increases as inlet preswirl increases. The increase in k^* from zero to medium preswirl is greater than from medium to high preswirl. On average, k^* is 30% greater for high preswirl than medium preswirl.

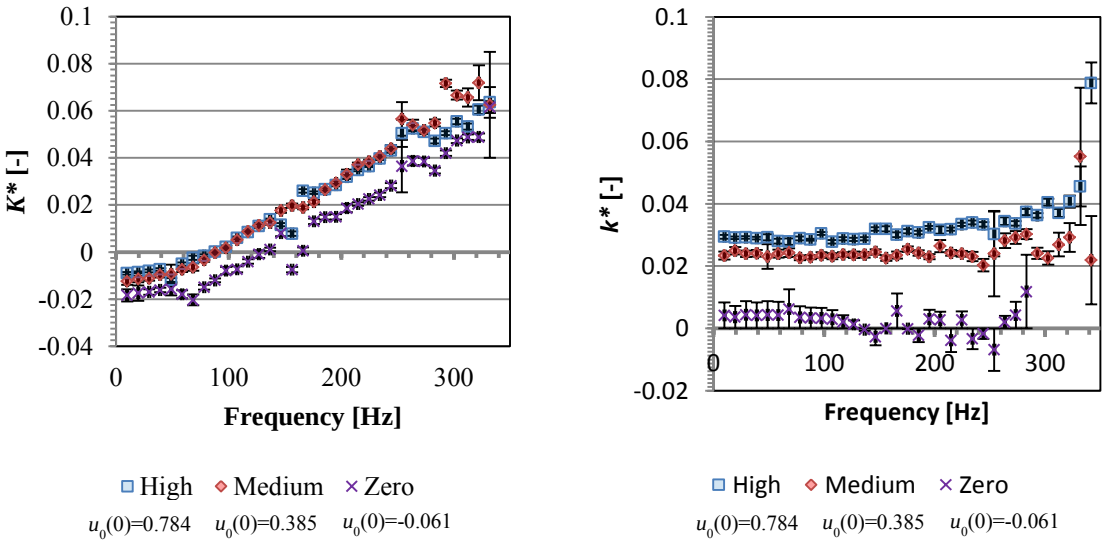

Figure 28. Normalized direct and cross-coupled stiffness coefficients for 0.2 mm (8 mils), PR=0.5, three inlet preswirl, and ω= 20,200 RPM

6.2.2.1.3 Running Speed

Figure 29 illustrates how running speed affects *K* and *k*. Note, running speed has limited influence on *K*. *k* increases with increasing running speed. As frequency increases, *k* values begin to merge for speeds of 20,200 and 15,350 RPM's.

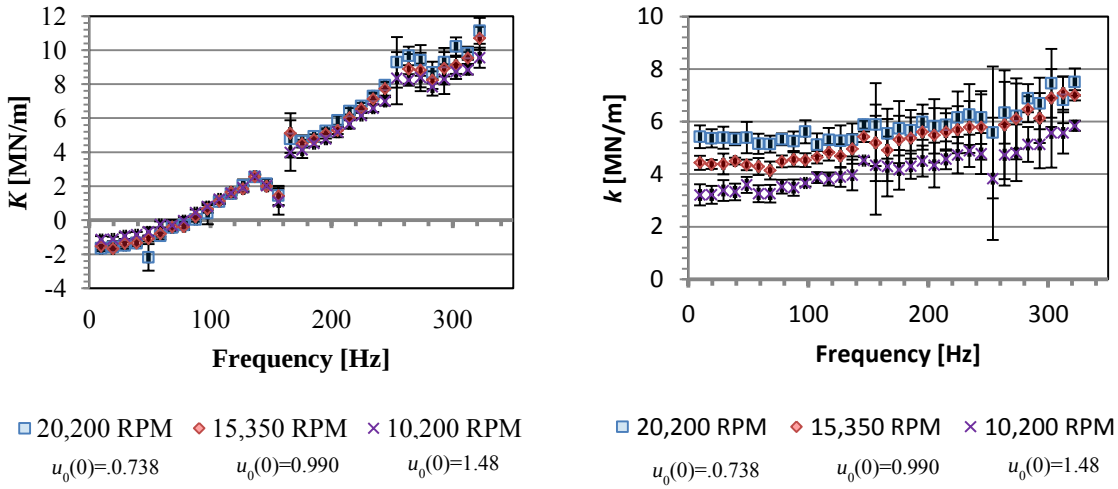

Figure 29. Direct and cross-coupled stiffness coefficients for 0.2 mm (8 mils), PR=0.5, high inlet preswirl, and three speeds

6.2.2.1.4 Radial Clearance

Figure 30 demonstrates that K^* is generally greater for the small clearance. Due to poor repeatability k^* is not presented for frequencies greater than 220 Hz. For a clearance of 0.1 mm (4 mils), k^* decreases with increasing frequency, while, generally, k^* is relatively constant for the larger clearance.

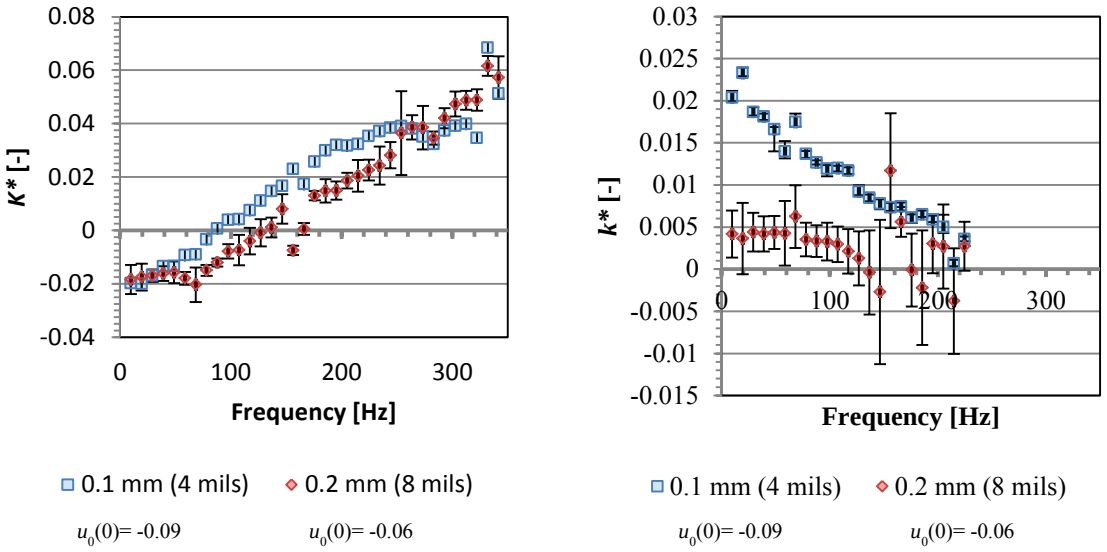

Figure 30. Normalized direct and cross-coupled stiffness coefficients for 0.2 mm (8 mils) and 0.1 mm (4 mils), PR=0.5, zero inlet preswirl, and 20,200 RPM

6.2.2.2 Direct and Cross-Coupled Damping

6.2.2.2.1 Pressure Ratio

Figure 31 demonstrates that PR has limited influence on C and c. Due to high uncertainties, c will not be presented for frequencies below 90 Hz. For frequencies greater than 300 Hz, c increases with increasing frequency. For frequencies below 300 Hz, c decreases with increasing frequency.

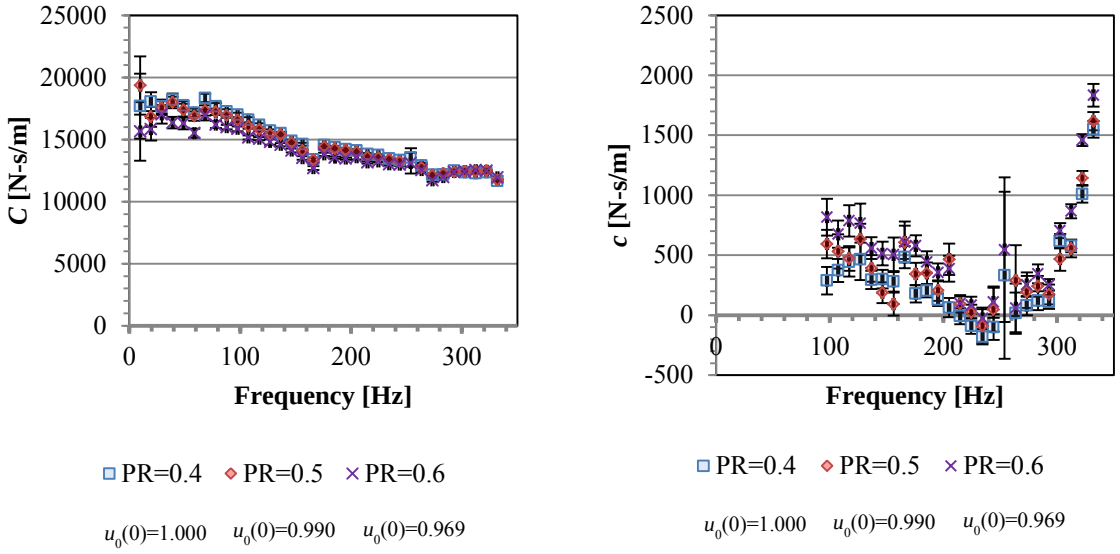

Figure 31. Direct and cross-coupled damping coefficients for 0.2 mm (8 mils), three pressure ratios, high inlet preswirl, and ω= 15,350 RPM

6.2.2.2.2 Preswirl

Figure 32 illustrates that *C** is greatest for medium preswirl and least for zero preswirl. Additionally, *c** is relatively low for the three preswirl ratios.

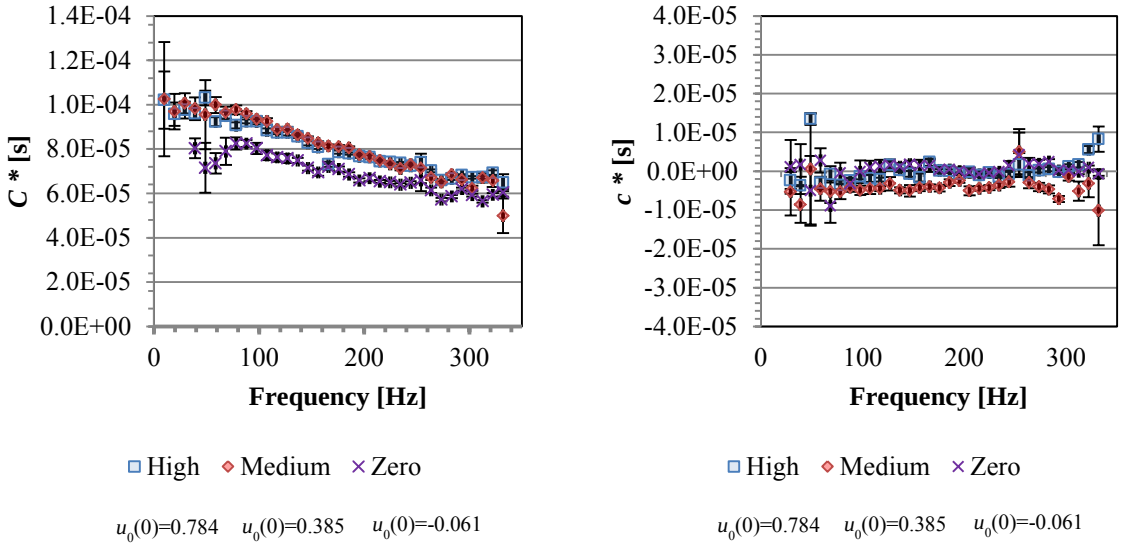

Figure 32. Normalized direct and cross-coupled damping coefficients for 0.2 mm (8 mils), PR=0.5, three inlet preswirl, and ω= 20,200 RPM

6.2.2.2.3 Running Speed

Figure 33 shows the effect ω has on *C*. *C* for a running speed of 20,200 is on average 1.8% greater than that for a running speed of 15,350 RPM. *C* is 9.6% greater for a running speed of 15,350 RPM than a running speed of 10,200. *c* is greatest for the running speeds 10,200 and 15,350 RPM. For the three speed *c* is relatively small.

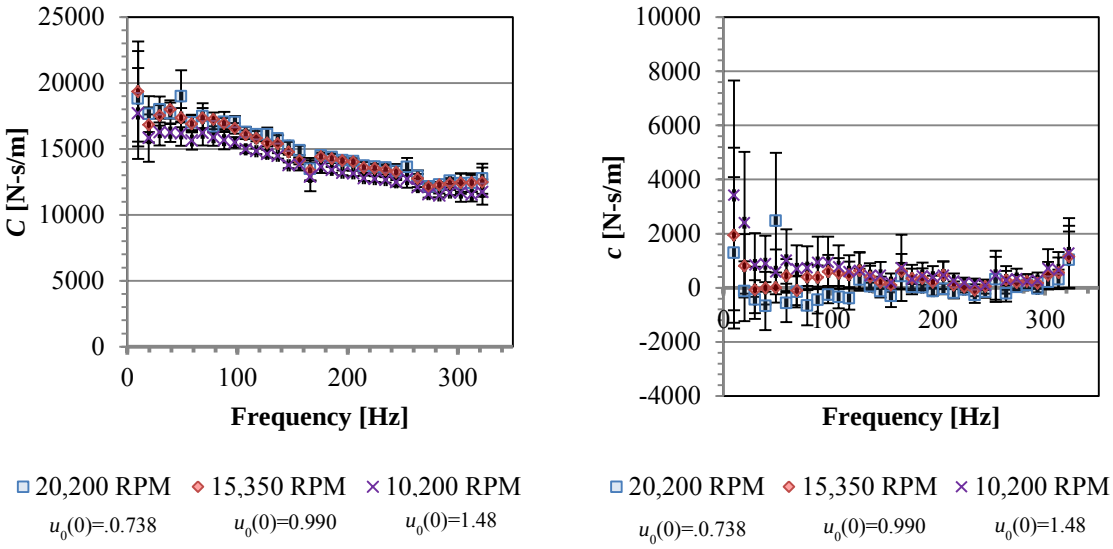

Figure 33. Direct and cross-coupled damping coefficients for 0.2 mm (8 mils), PR=0.5, high inlet preswirl, and three speeds

6.2.2.2.4 Radial Clearance

Figure 34 demonstrates that C^* is greatest for the largest clearance; a trend that increases in magnitude as frequency increases. c^* is greatest for the smallest clearance; a trend that decreases in magnitude as frequency increases.

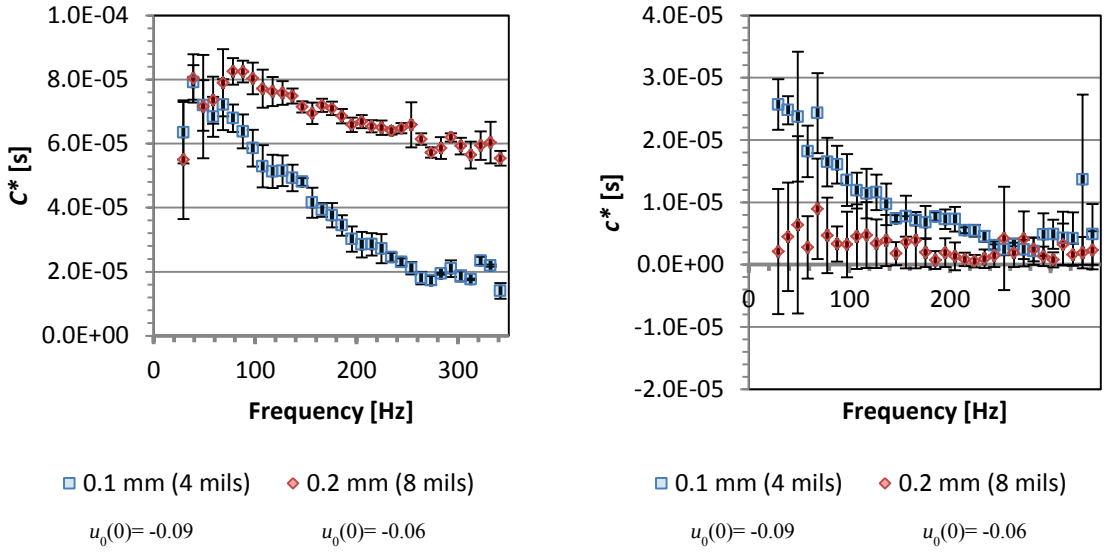

Figure 34. Normalized direct and cross-coupled damping coefficients for 0.2 mm (8 mils) and 0.1 mm (4 mils), PR=0.5, zero inlet preswirl, and 20,200 RPM

6.2.2.3 Effective Stiffness

6.2.2.3.1 Pressure Ratio

Figure 35 shows that for the range considered, PR has limited effect on K_{eff} .

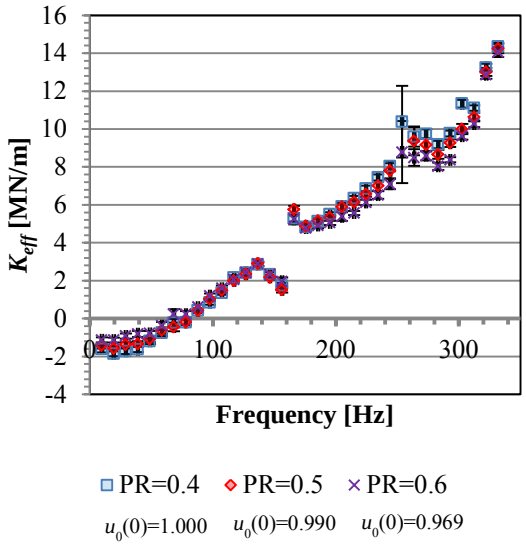

Figure 35. Effective stiffness for 0.2 mm (8 mils), three pressure ratios, high inlet preswirl, and ω= 15,350 RPM

6.2.2.3.2 Preswirl

Figure 36 illustrates K^*_{eff} is lowest for the zero preswirl case.

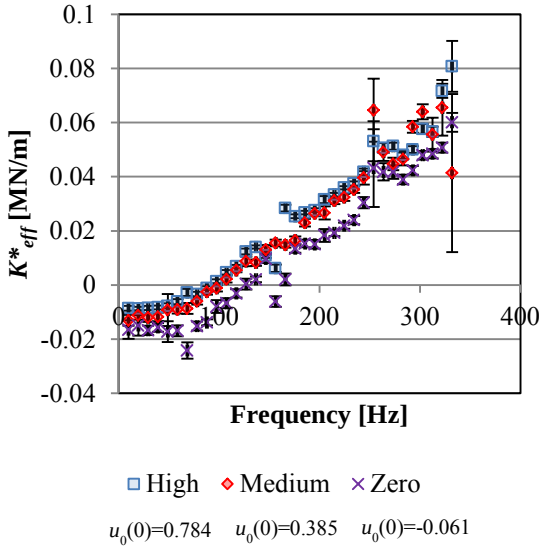

Figure 36. Normalized effective stiffness for 0.2 mm (8 mils), PR=0.5, three inlet preswirl, and ω= 20,200 RPM

6.2.2.3.3 Running Speed

As Figure 37 shows, running speed has minimal effect on K_{eff}.

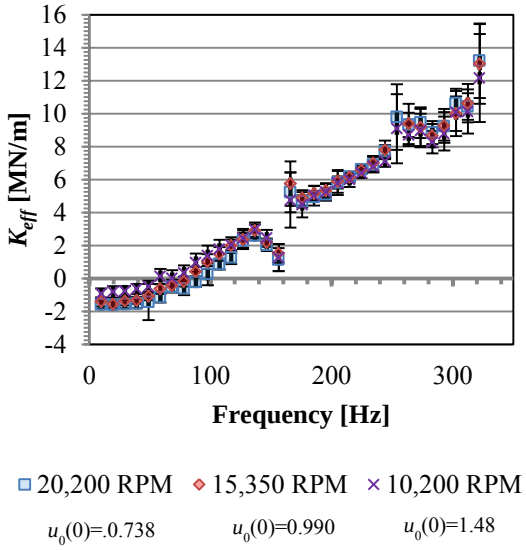

Figure 37. Effective stiffness for 0.2 mm (8 mils), PR=0.5, high inlet preswirl, and three speeds

6.2.2.3.4 Radial Clearance

Figure 38 provides plots of K^*_{eff} for two clearances. Excluding five data points, between 300 and 330 Hz, radial clearance has limited effect on K^*_{eff}.

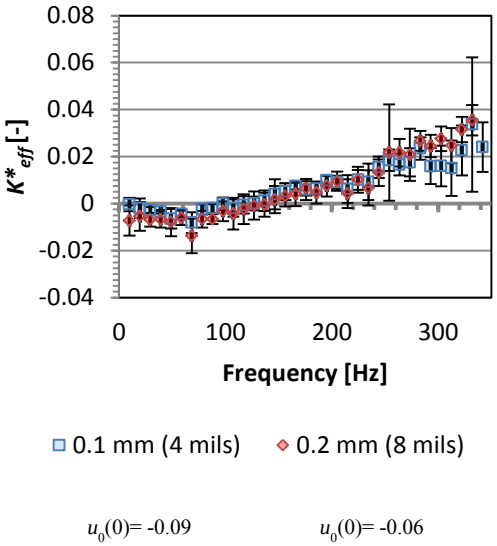

Figure 38. Normalized effective stiffness for 0.2 mm (8 mils) and 0.1 mm (4 mils), PR=0.5, zero inlet preswirl, and 20,200 RPM

6.2.2.4 Effective Damping

6.2.2.4.1 Pressure Ratio

Figure 39 demonstrates that for the range considered, PR has limit effect on C_{eff}.

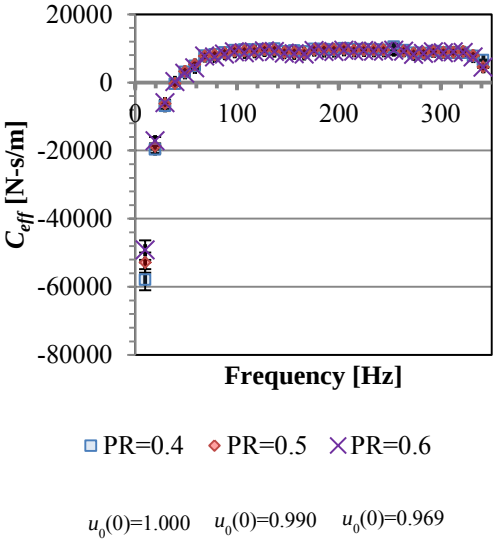

Figure 39. Effective damping for 0.2 mm (8 mils), three pressure ratios, high inlet preswirl, and ω= 15,350 RPM

6.2.2.4.2 Preswirl

Figure 40 shows C^*_{eff} for high, medium, and zero preswirl. Preswirl does not have a drastic effect on C^*_{eff} for frequencies greater than 100 Hz. For frequencies below 20 Hz, the high preswirl stator followed by the medium preswirl stator, exhibit the lowest values of C^*_{eff}. *Cross-over frequency* (frequency that C^*_{eff} goes from negative to positive) for the medium and high preswirl stators is approximately 40 Hz, while it is approximately 20 Hz for the zero preswirl stator. Thus, as expected the seal is more stable at zero preswirl.

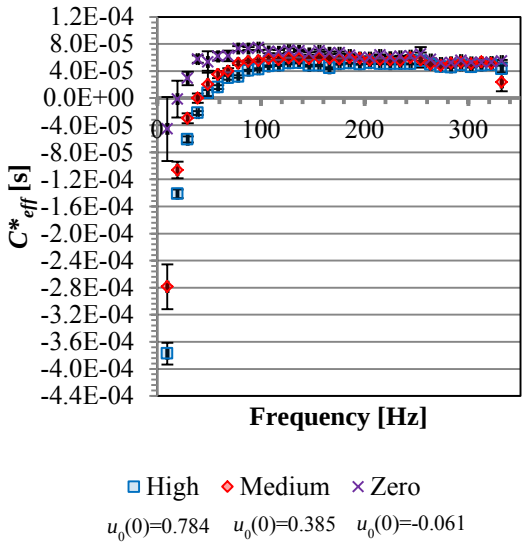

Figure 40. Normalized effective damping for 0.2 mm (8 mils), PR=0.5, three inlet preswirl, and ω= 20,200 RPM

6.2.2.4.3 Running Speed

Figure 41 demonstrates the influence of ω on C_{eff}. For frequencies below 20 Hz, C^*_{eff} is lowest for the 20,200 RPM case, followed by the 15,350 RPM case. For frequencies greater than 20 Hz, running speed has limited effect.

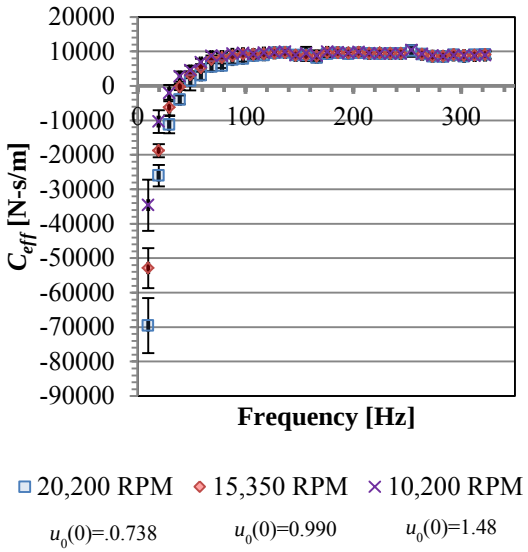

Figure 41. Effective damping for 0.2 mm (8 mils), PR=0.5, high inlet preswirl, and three speeds

6.2.2.4.4 Radial Clearance

Figure 42 shows C^*_{eff} is greatest for a clearance of 0.2 mm (8 mils). The 0.2mm (8 mils) clearance has a *cross-over frequency* of approximately 20 Hz, while the 0.1 mm (4 mil) clearance has a *cross-over frequency* of approximately 30 Hz. Thus, stability increases with the increase in clearance.

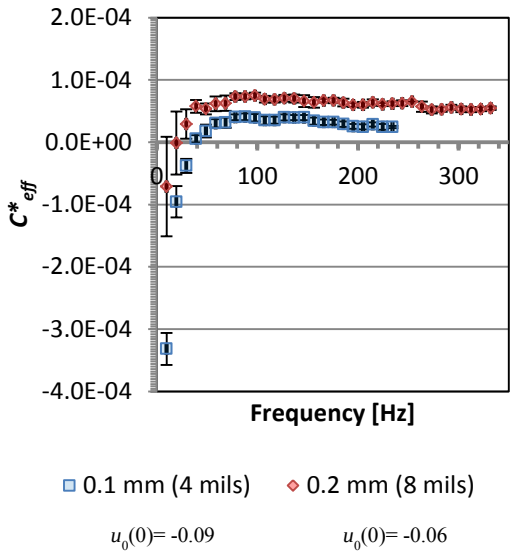

Figure 42. Normalized effective damping for 0.2 mm (8 mils) and 0.1 mm (4 mils), PR=0.5, zero inlet preswirl, and 20,200 RPM

6.3 Experimental Results versus Predictions

ISOTSEAL provides theoretical results. ISOTSEAL is based on Kleynhans and Childs [52] analysis. A summary of Kleynhans [52, 75] work will be given followed by a comparison of experimental and theoretical data.

6.3.1 Summary of Two-Control-Volume Bulk Flow Analysis

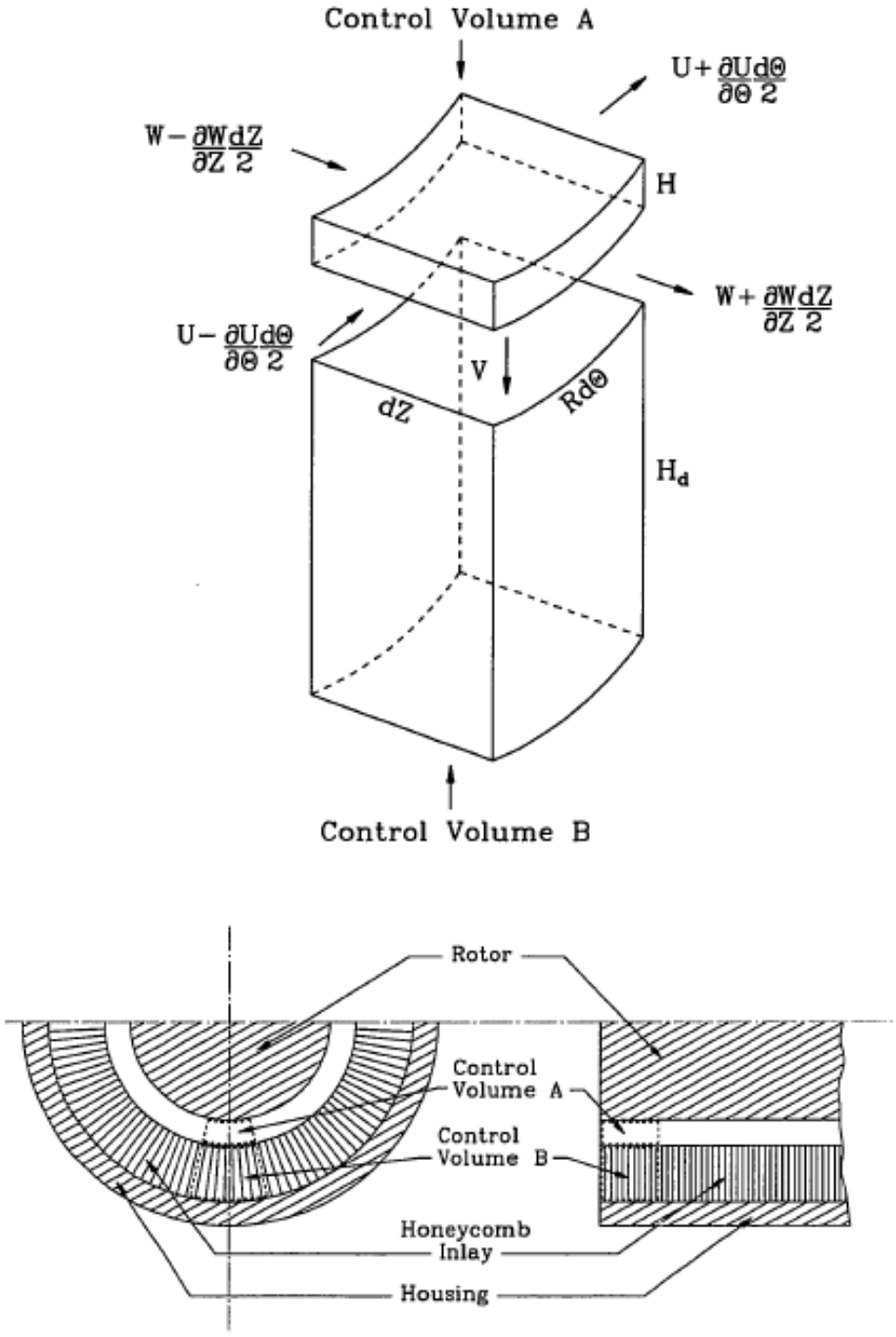

Figure 43. Two control volume model [75]

Figure 43 shows the two control-volume for Kleynhans and Childs [52] analysis.

The governing control-volume equations (continuity, axial-momentum, and circumferential-momentum equations) are simplified and non-dimensionalized as detailed in Kleynhan. For the momentum equations, the viscous shear stresses are modeled via a Hirs [73] type model. Hirs' model assumes friction-factor is directionally homogenous, and defined by the Blasius-type model.

Perturbation analysis is applied to develop the zeroth- and first-order equations. The zeroth-order equation is solved to determine leakage while the first-order equation is solved to provide, among other things, the perturbation pressures. By integrating the perturbation pressures for a range of discrete frequencies and curve fitting, the non-dimensional radial (I_r) and tangential impedances (I_θ) are found.

Kleynhans calculated I_r and I_θ for different honeycomb cell depths while holding all other parameters constant. Figure 44 shows the results of these calculations versus non-dimensional frequency (f). Non-dimensional frequency is defined as the ratio of precession frequency (Ω) to rotational velocity (ω). The parameter h_d is the non-dimensional honeycomb cell-depth and is equal to the effective cell depth (H_d) over the inlet radial clearance (C_r). H_d is defined as the total honeycomb cell volume divided by the surface area of the seal.

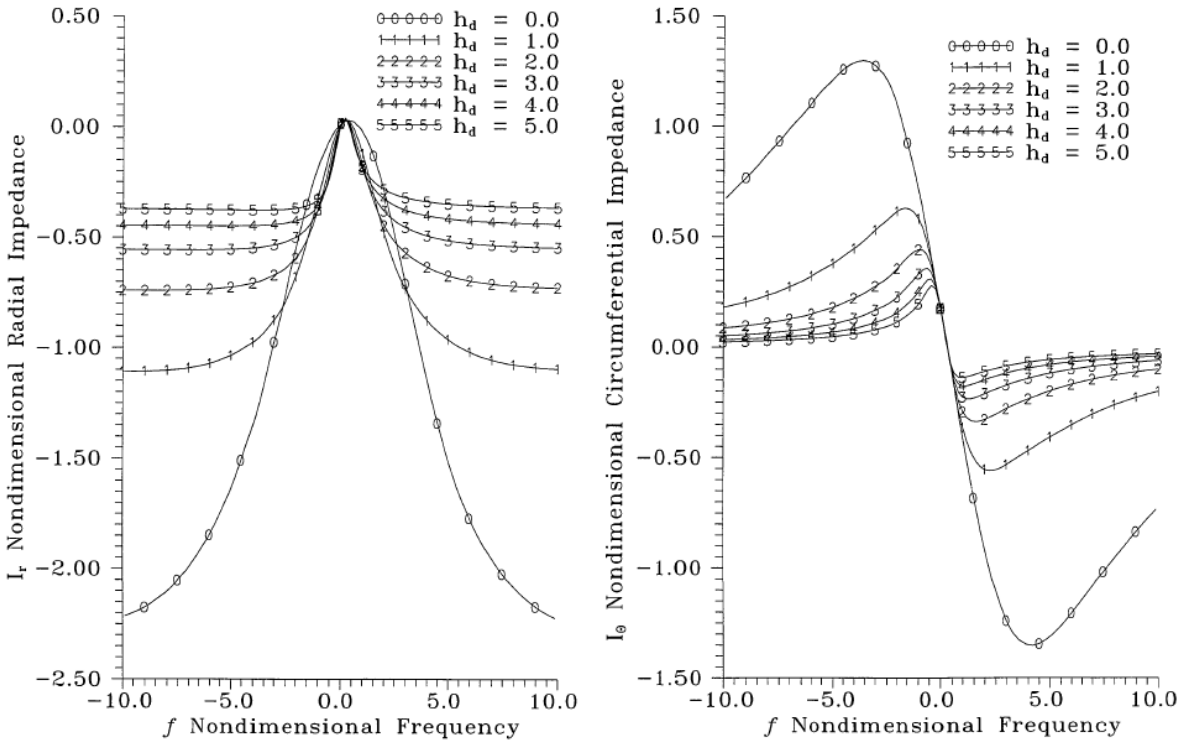

Figure 44. Non-dimensional radial and tangential impedances

Figure 4 and the related discussion, details how tangential and radial forces are related to Eq. (5). Similarly, for h_d=0 (smooth seal) the non-dimensional radial and tangential impedances can be related to Eq. (1) (for frequency plus or minus four times the running speed) via Eqs. (25) and (26):

$$I_r(f) = -(\overline{K} - \overline{M}f^2) + \overline{c}f \tag{25}$$

$$I_\theta(f) = \overline{k} - \overline{C}f \tag{26}$$

where,

$$\overline{K}_{ij} = K_{ij}\frac{C_r}{P_{in}RL} \tag{27}$$

$$\bar{C}_{ij} = C_{ij}\frac{C_r\omega}{P_{in}RL} \tag{28}$$

$$\bar{M}_{ij} = M_{ij}\frac{C_r\omega^2}{P_{in}RL} \tag{29}$$

Although Eq. (1) is used for modeling liquid seal and bearings, Kleynhans noted that for the given seal, input condition, and h_d=0 a negative added mass term is needed to capture the parabolic form of the I_r graph. The added mass term is not due to fluid inertia, but rather results from the compressibility of gas, and acts as a stiffening mechanism.

As h_d increases, the range of f, over which Eqs. (25) and (26) and in turn Eq. (1) can adequately model I_r and I_θ decreases. For I_θ a local minima or maxima, signify the occurrence of resonances. The frequency-independent model of Eq. (1) cannot account for these resonances.

Kleynhans showed that the increase in effective volume, due to the HC cells, cause a reduction in effective acoustic velocity. He also found that the depths of the HC cells are inversely proportional to the effective acoustic velocity. Thus, as HC cell depth increases, the effective acoustic velocity, and acoustic natural frequencies decrease. This drop in acoustic natural frequencies correlates with the decrease in resonant frequency seen in Figure 44. To account for the resonances the Laplace transform of Eq. (30) was introduced.

$$-\begin{Bmatrix}\mathbf{F}_x(s)\\ \mathbf{F}_y(s)\end{Bmatrix} = \begin{bmatrix}\mathbf{D} & \mathbf{E}\\ \mathbf{-E} & \mathbf{D}\end{bmatrix}\begin{Bmatrix}\mathbf{x}(s)\\ \mathbf{y}(s)\end{Bmatrix} \tag{30}$$

For a forward circular precession, I_r and I_θ are found from the two-control-volume analysis, and related to Eq. (30) by Eqs. (31) and (32). $I_r^+ = -\mathrm{Re}(\boldsymbol{D}) - \mathrm{Im}(\boldsymbol{E})$

$$I_r^+ = -\mathrm{Re}(\boldsymbol{D}) - \mathrm{Im}(\boldsymbol{E}) \tag{31}$$

$$I_{\vartheta}^{+} = \mathrm{Re}(\boldsymbol{D}) + \mathrm{Im}(\boldsymbol{E}) \tag{32}$$

By curve fitting the magnitude and phase of *D* and *E*, an approximate transfer function is found. Kleynhans goes on, to convert these transfer functions into frequency-dependent effective stiffness and damping terms, and subsequently frequency-dependent *K*, *k*, *C*, and *c*.

In the end, for frequency-dependent seals Eq. (30) is related to Eq. (6) by Eqs. (33) and (34).

$$\boldsymbol{D}(\boldsymbol{j}\Omega) = K(\Omega) + \boldsymbol{j}C(\Omega) \tag{33}$$

$$\boldsymbol{E}(\boldsymbol{j}\Omega) = k(\Omega) + \boldsymbol{j}c(\Omega) \tag{34}$$

6.3.2 Input Variables for ISOTSEAL

Table 5. Input variables for ISOTSEAL

No.	Name	Value	Unit	No.	Name	Value	Unit
1	Reservoir Pressure	21.44	bar	12	Exit Recovery	1	-
2	Sump Pressure	8.4491	bar	13	Absolute Viscosity	1.88E-05	Ns/m^2
3	Reservoir Temperature	11.8	C	14	Molecular Weight	28.96	-
4	Rotational Speed	15350	RPM	15	Specific Heat Ratio	1.4	-
5	Seal Diameter	114.722	mm	16	Compressibility Factor	1	-
6	Seal Length	85.7123	mm	17	Tolerance Rercentage	1.00E-02	-
7	Inlet Clearance	0.110014	mm	18	# Integration Steps	100	-
8	Exit Clearance	0.108426	mm	19	NRZ	0.0586	-
9	Cell Volume/Area	1.425	-	20	MRZ	-0.217	-
10	Inlet Preswirl Ratio	0	-	21	NSZ	0.0301	-
11	Entrance Loss Coefficient	0	-	22	MSZ	-0.124	-

Table 5 shows sample input parameters for ISOTSEAL. Input variables 1-4 and 10 are operating conditions recorded at the time of testing. Parameters 5-9 are the seal geometry. Cell volume/area (number 9) is the effective cell depth defined as the total volume of the hole-pattern cells divided by the surface area of the seal or, equivalently, γ multiplied by the actual hole depth. The entrance loss (ξ) and exit recovery (ξ_e) coefficient are used in Eqs. (35) and (36) to model the sudden contraction or expansion of flow at the inlet and exit of the seal, respectively.

$$p_0(0) = \frac{1 + \sqrt{1 - \dfrac{2(1+\xi)\Gamma^2}{h_0^2(0)}}}{2} \tag{35}$$

$$p_0(1) = \frac{p_e + \sqrt{p_e^2 - \dfrac{2(1+\xi_e)\Gamma^2}{h_0^2(0)}}}{2} \tag{36}$$

Here $p_0(0)$, Γ, h_0, $p_0(1)$, p_e are the zeroth order entrance pressure, non-dimensional mass-flow-rate, non-dimensional zeroth order clearance, zeroth order exit pressure, and zeroth order exit to entrance pressure ratio, respectively. Non-dimensional mass-flow-rate is defined as,

$$\Gamma = p_0 w_0 h_0 \tag{37}$$

where w_0 is the zeroth order axial velocity. Note, non-dimensional mass-flow-rate (Γ) and flow coefficient (Φ) are not the same.

Parameters 13-16 are air properties.

When solving the zeroth order equation, the axial momentum equation is nonlinear. Thus, an iterative procedure is used, with input 17 defining the percent tolerance for convergence. Parameter 18 defines the size of the control-volume.

For ISOTSEAL, friction factor (f_f) is defined by the Blasius model:

$$f_f = n_s R_e^{m_s} \tag{38}$$

where n and m values are found from the curve fitting of f_f versus Reynold number (R_e). Input variables 19 and 20 are the Blasius rotor friction coefficients found experimental by Yamada [76] for smooth seals. The empirical Blasius seal friction coefficients (parameters 21 and 22) are from flat-plate test performed by Asirvatham [62]. Three observations of Asirvatham tests are:

1) f_f was found for flow between the hole-pattern configuration of Figure 19, and a smooth plate. Hence, the coefficients are for a combination stator plus rotor.
2) Tested were performed for three clearances, and three inlet pressures. Friction factors for a clearance of 0.254 mm (10 mil) and 56 bar (812 psi) are closest to the application here.
3) The Blasius coefficient chosen here has a curve fit value (R^2) of 0.7661.

6.3.3 Validity of Code for This Seal

Past research [60, 74, 77] at the Turbomachinery Laboratory, has shown ISOTSEAL to be a good predictor of rotordynamic coefficients and leakage rates for gas HP seals. The HP seal tested here incorporates holes that are at least 3.84 times larger in diameter than previously tested HP seals. In addition, previously tested seal HP seals had hole diameter to hole depth ratios less than one. For the seal tested here, the hole diameter to hole depth ratio is 6.5.

ISOTSEAL treats the "cells" of a HP or HC seal as "pockets" with flow moving radial in or out. Observing Figure 10, it seems intuitive that this model can capture the flow behavior of the seal tested by Wade [74], but not the seal tested here. Namely, flow will not move purely radially with in a larger hole.

6.3.4 Static Results

Both experimental and theoretical leakages have been normalized using Eq. (24). Figure 45 provides an example of how well ISOTSEAL predicts leakage coefficients for changes in PR and preswirl. In general, ISOTSEAL does a fair job in predicting leakage. The largest discrepancy in predictions and experiments are seen for low preswirl ratio values. For these preswirl ratios, the percent difference between code and experiments is 17%, 17%, and 13% for PR of 0.4, 0.5, and 0.6, respectively. Leakage coefficients are predicted best for the medium preswirl value producing a percent difference of no more that 5%. At higher preswirl ratio the percent difference between code and experiment are 0.2%, 8%, and 6% for PR of 0.4, 0.5, and 0.6, respectively.

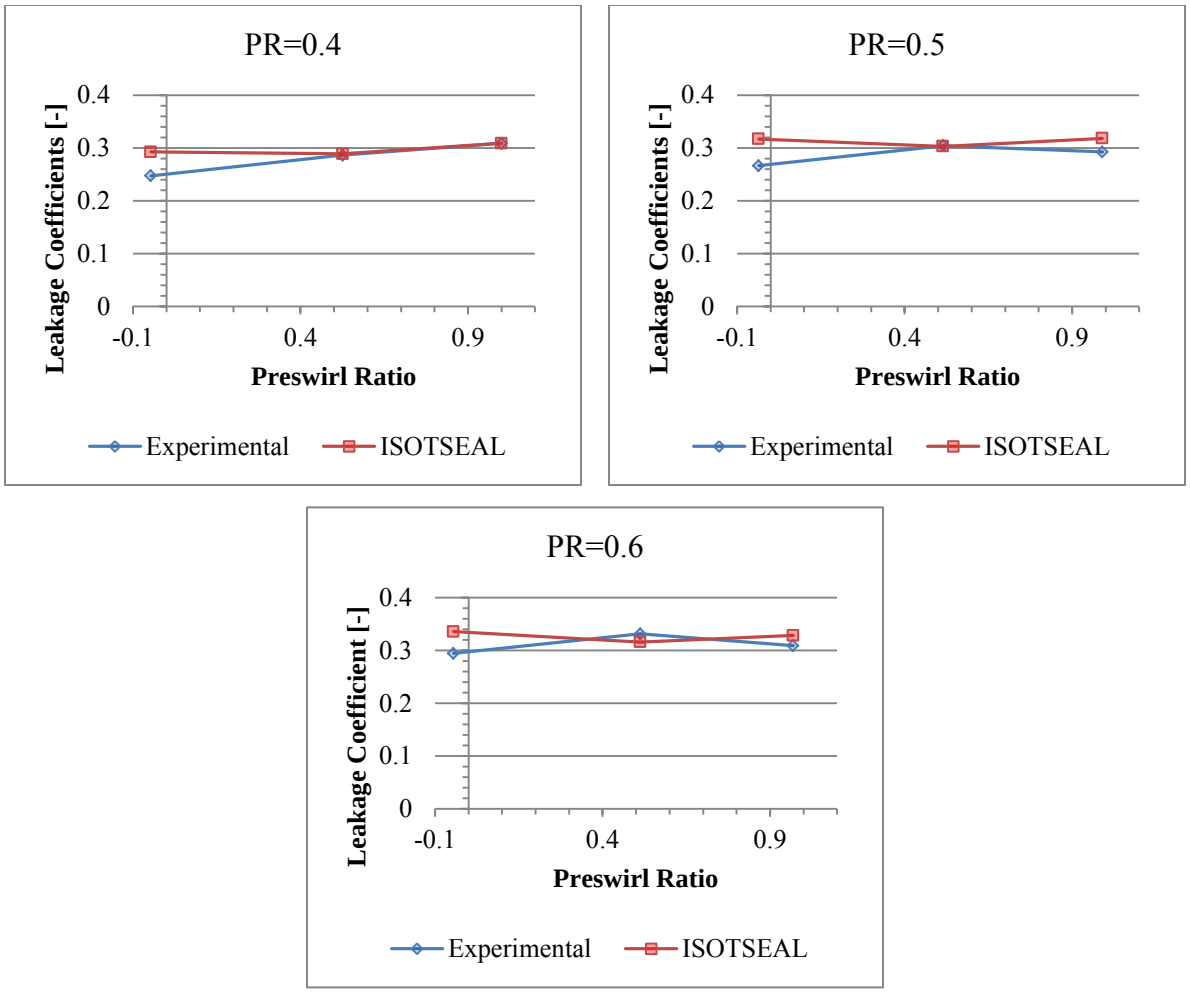

Figure 45. Leakage coefficient (Eq. (24)) versus preswirl ratio for 0.2 mm (8 mils), three PR, all preswirl ratios, and 15,350 RPM

As stated in section 6.3.2, the Blasius coefficients used here are for a combination smooth plus rough surface. Subtracting out the effect of the smooth surface would result in lower friction factors and an increase in predicted leakage; hence leakage predictions would worsen.

Conditions for the flat-plate test that most closely resemble those of the application here were chosen. Figure 46 shows f_f versus Reynolds number for combination smooth and hole-pattern plate of Figure 19. Note, f_f is proportional to clearance and relatively unaffected by inlet pressure. Since, f_f is proportional to clearance adjusting f_f for a clearance of 0.2 mm (8 mils) would result in poor leakage predictions.

Figure 46. Friction factor versus Reynolds number for flat-plate test using 12.15 mm and 1.9mm hole diameter and hole depth, respectively [62]

6.3.5 Dynamic Results

Note, to examine how predictions are affected by preswirl the dynamic coefficients will be non-dimensionalized or normalized.

6.3.5.1 Direct and Cross-Coupled Stiffness

The following figures demonstrate how well ISOTSEAL compensates for changes in rotation (Figure 47), preswirl (Figure 48), and rotational speed (Figure 49), when predicting *K* and *k*. Figure 50 and Figure 51 are plots of *K* and *k* for a radial clearance of 0.1 mm (4 mils). Thus allowing inspection of how well ISOTSEAL performs at a smaller clearance. Since only one preswirl ring (zero) was used for the 0.1 mm (4 mils) clearance, plots that demonstrate the effect of changes in pressure ratios and rotational speeds will be displayed.

Regarding the validity of ISOTSEAL in predicting *K* and *k* the following observations are made:

1) Negative *K* is not predicted for any test case. As mentioned earlier all test cases demonstrated negative *K* for low frequencies.
2) *K* is over-predicted for all cases by approximately 5 MN/m.
3) Predictions for *K* do not substantially improve or worsen by varying running speed, preswirl, or PR.
4) For a clearance of 0.2 mm (8 mils), experiments show that *k* increases slightly with frequency. ISOTSEAL predicts *k* will decrease with increasing frequency. Predicted and experimental values of *k* converge at higher frequencies. With the exception of the limit range surrounding this convergent frequency, ISOTSEAL does a poor job predicting *k*.
5) ISOTSEAL over-predicts *k* for the smaller clearance. Both experiments and predictions show *k* decreases with increasing frequency.

6.3.5.1.1 Pressure Ratio

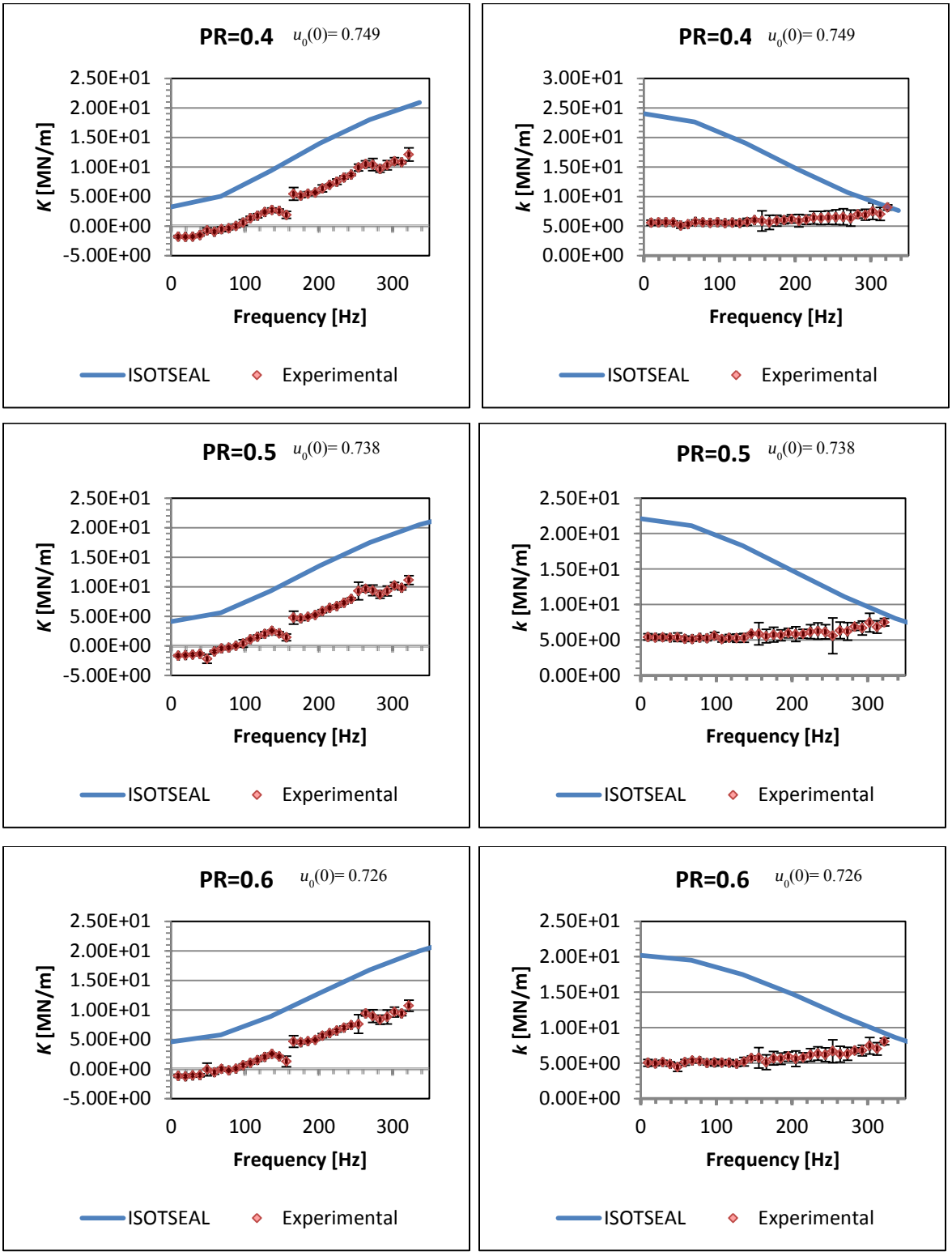

Figure 47. Direct and cross-coupling stiffness for 0.2 mm (8 mils), three PR, high inlet preswirl, and 20,200 RPM

6.3.5.1.2 Preswirl

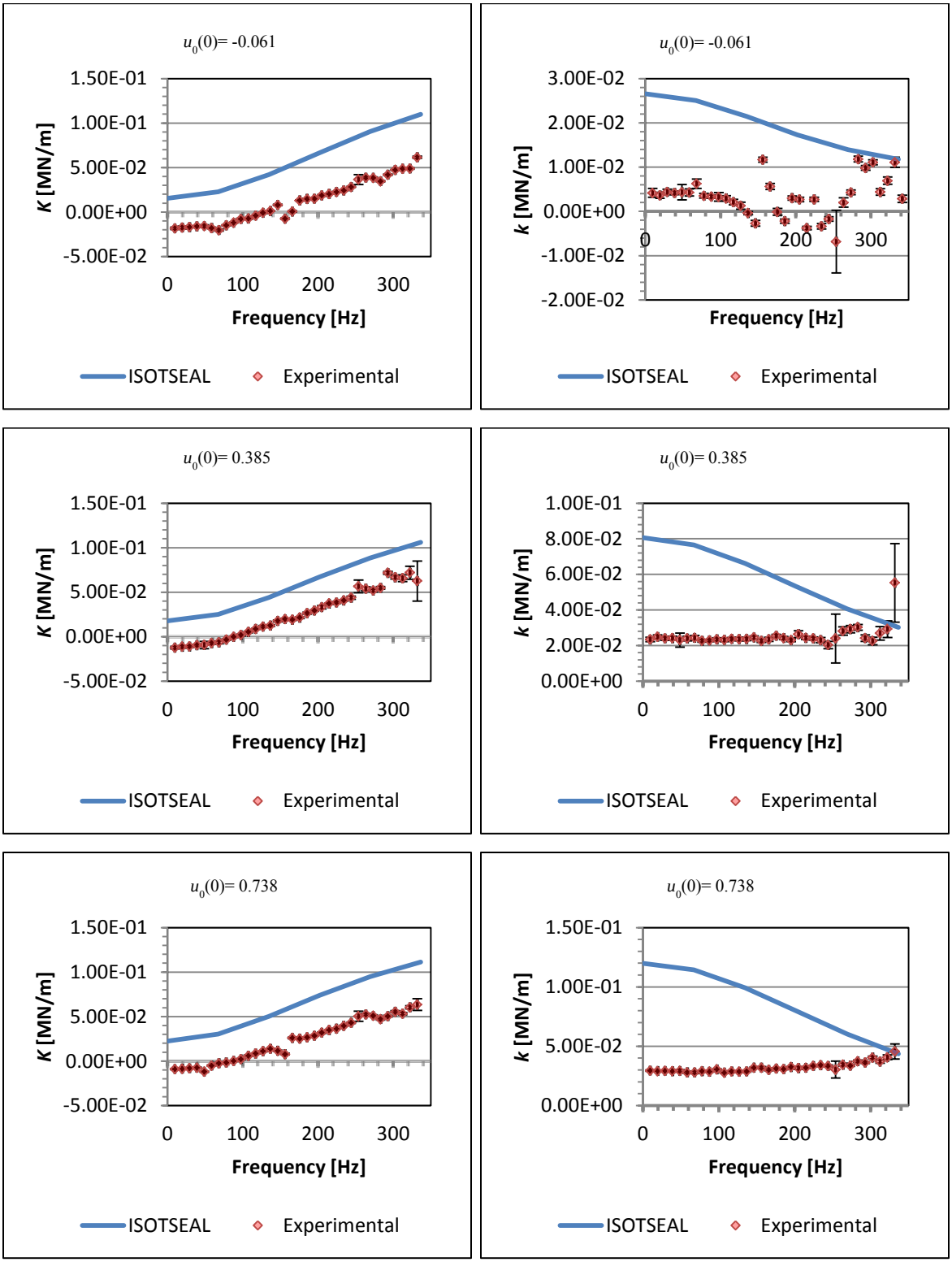

Figure 48. Direct and cross-coupled stiffness for 0.2 mm (8 mils), PR=0.5, three inlet preswirl, and 20,200 RPM

6.3.5.1.3 Running Speed

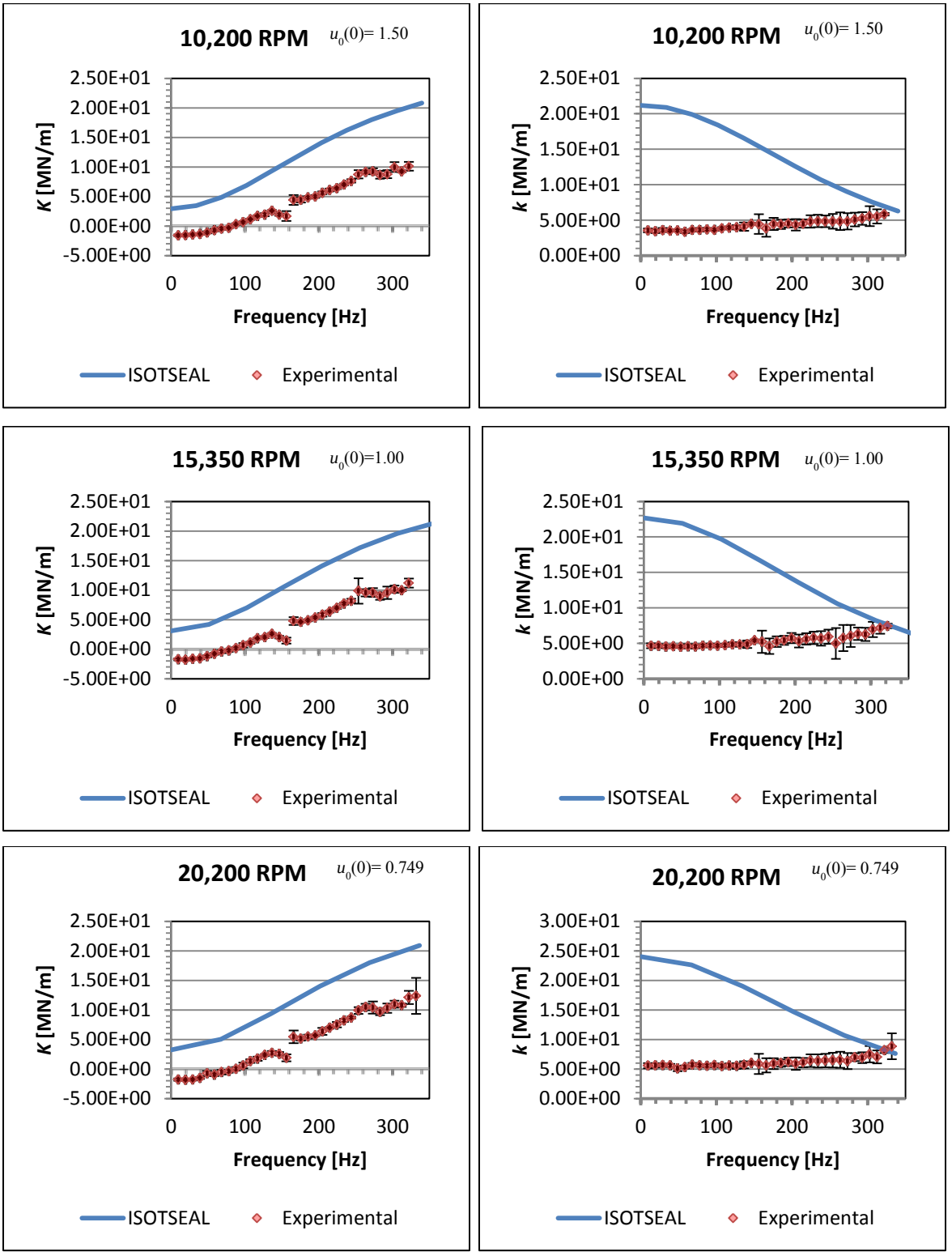

Figure 49. Direct and cross-coupling stiffness for 0.2 mm (8 mils), PR=0.4, high inlet preswirl, and three speeds

6.3.5.1.4 0.1 mm (4 mils) Radial Clearance (PR)

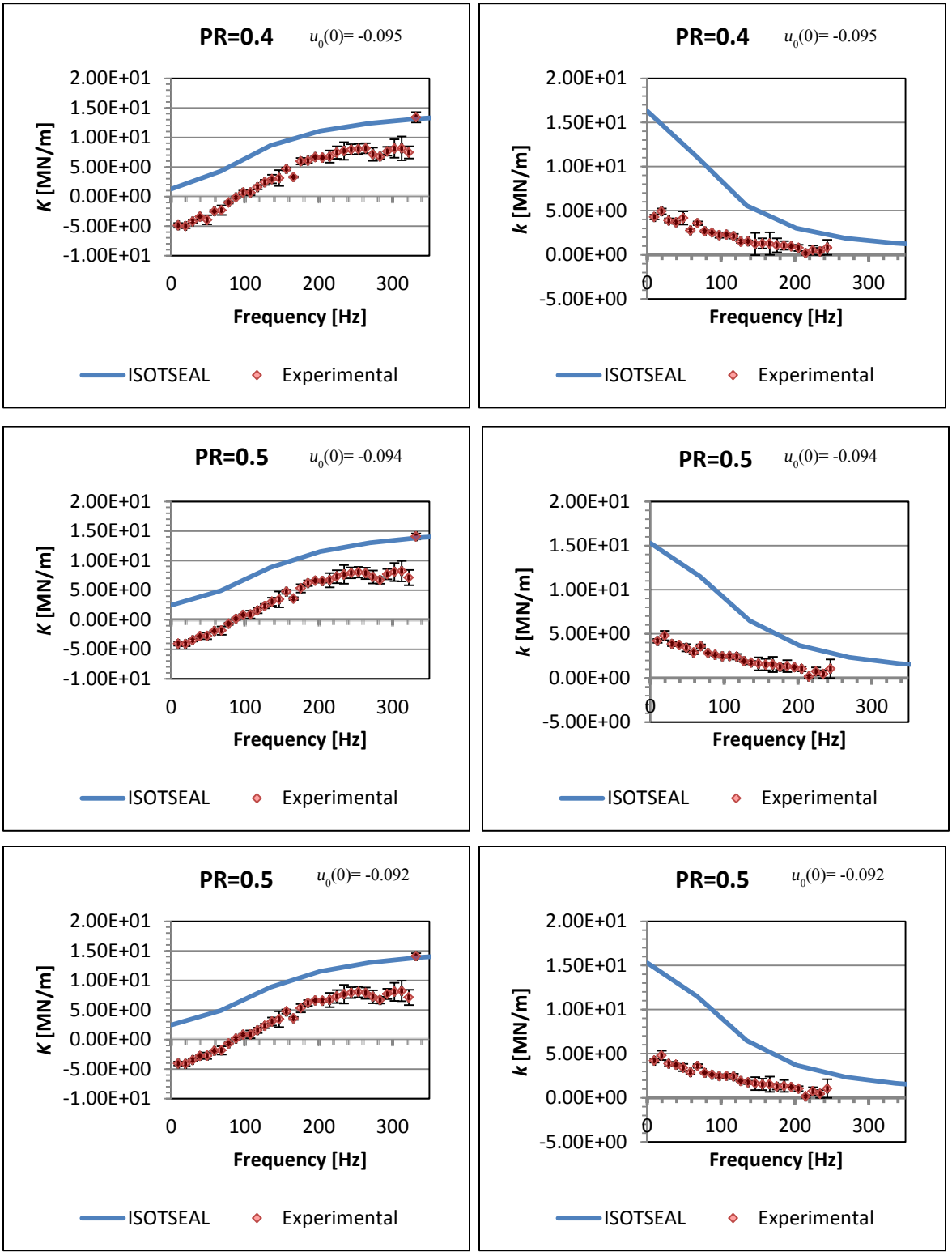

Figure 50. Direct and cross-coupling stiffness for 0.1 mm (4 mils), three PR, zero inlet preswirl, and 20,200 RPM

6.3.5.1.5 0.1 mm (4 mils) Radial Clearance (Running Speed)

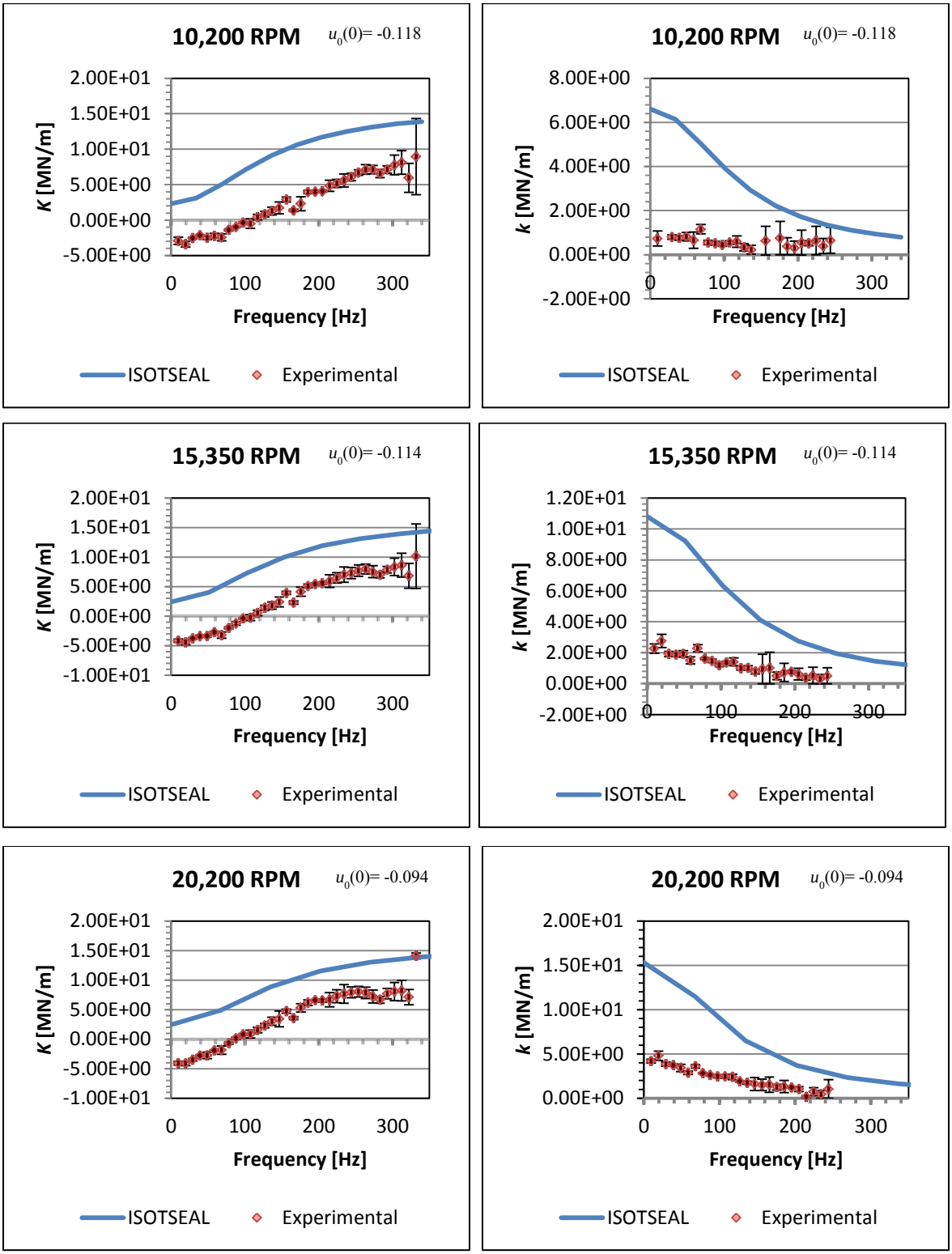

Figure 51. Direct and cross-coupling stiffness for 0.1 mm (4 mils), PR=0.5, zero inlet preswirl, and three speeds

6.3.5.2 Direct and Cross-Coupled Damping

Figure 52, Figure 53, and Figure 54 show how well ISOTSEAL compensates for changes in rotation, preswirl, and rotational speed, when predicting *C* and *c*, respectively. *C* and *c* for a radial clearance of 0.1 mm (4 mils) are demonstrated in Figure 55 and Figure 56.

Conclusions from Figures 51 through 53 are:

1) ISOTSEAL does a fair job at predicting *C* for the larger clearance cases. In general, predictions and experimental data show strong agreement for frequencies below 150 Hz. For frequencies of approximately 150 Hz and above, the disparity between theory and experiments increase with increasing frequency. In general, *C* is under-predicted for all frequencies.
2) As with *K*, predictions do not substantially improve or worsen for *C* by varying rotational speed, preswirl, or PR.
3) ISOTSEAL does an excellent job of predicting *C* for the 0.1 mm (4 mils) clearance cases.
4) For the 0.2 mm (8 mils) clearance cases, *c* is very small and relatively frequency-independent, while ISOTSEAL predicts *c* will be frequency-dependent. ISOTSEAL over-predicts the magnitude of *c*. Thus, ISOTSEAL does a poor job at predicting *c*. Predictions of *c* are best of the 0.2 mm clearance, medium preswirl case.
5) For frequencies above 200 Hz, ISOTSEAL does a good job of predicting *c* for the smaller clearance.
6) Considering a clearance of 0.1 mm (4 mils) and frequencies below 200 Hz, the disparity between predictions and experimental data increase with increasing running speed. For these same conditions, the difference between predictions and experimental data decrease with increasing PR.

6.3.5.2.1 Pressure Ratio

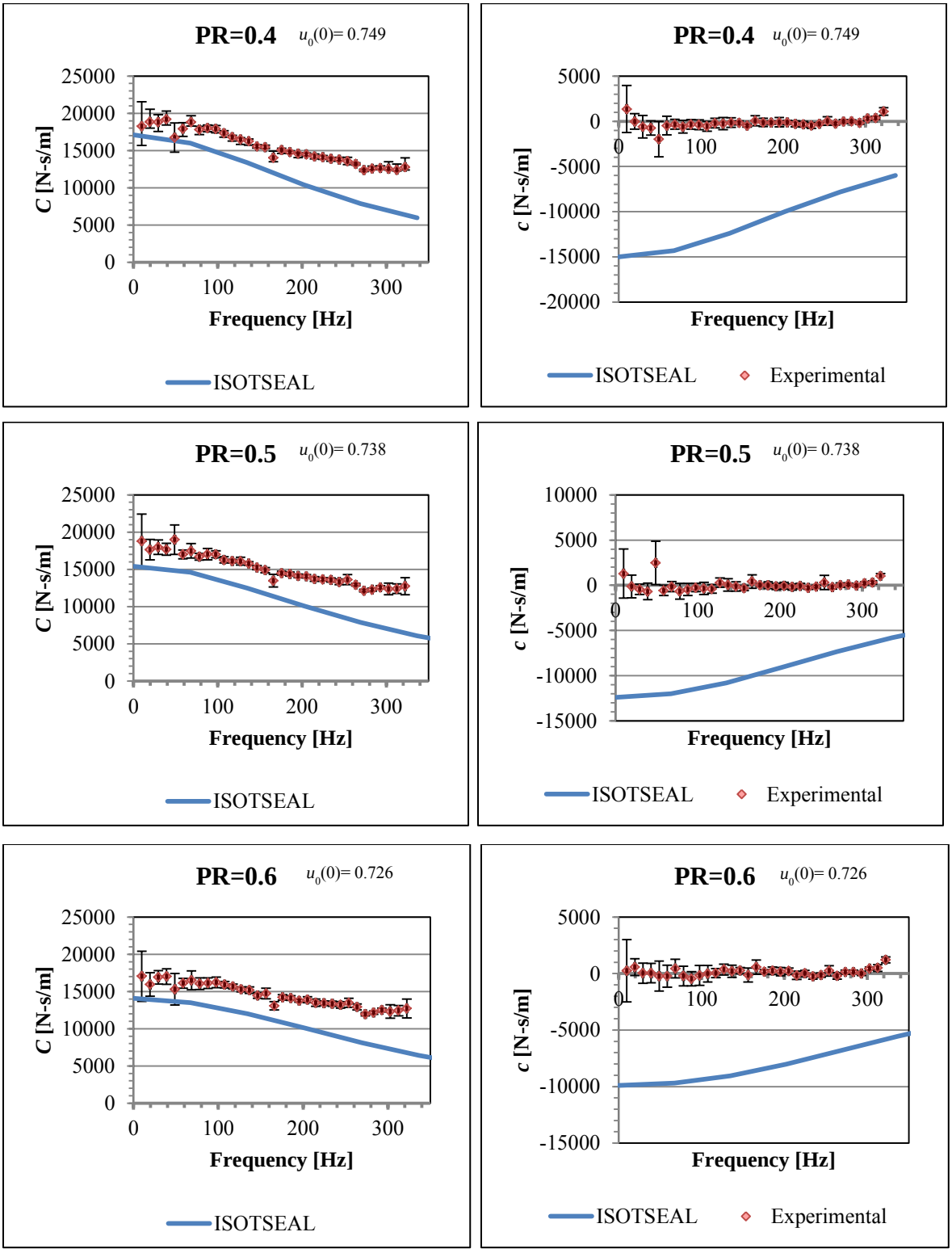

Figure 52. Direct and cross-coupled damping for 0.2 mm (8 mils), three PR, high inlet preswirl, and 20,200 RPM

6.3.5.2.2 Preswirl

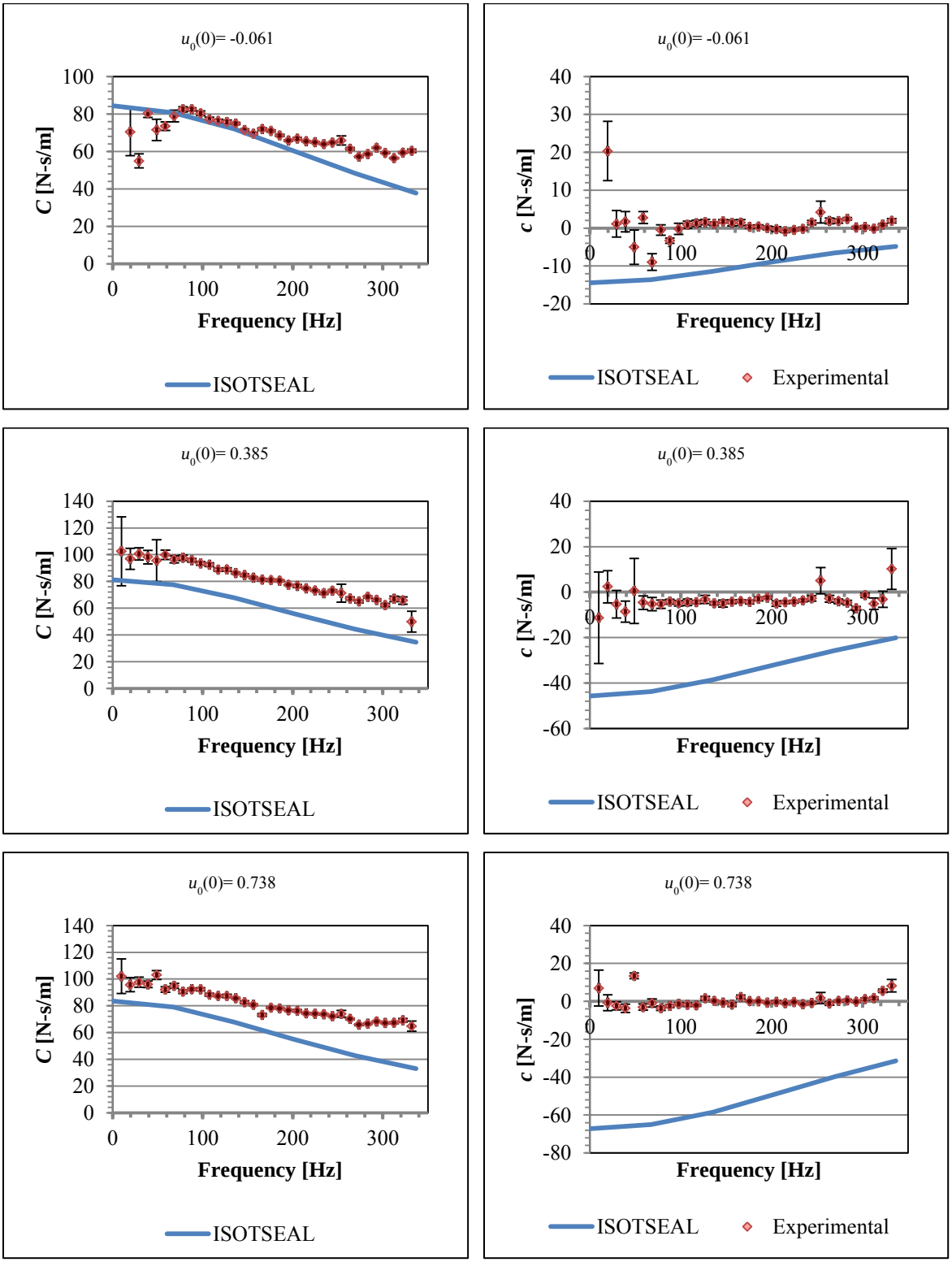

Figure 53. Direct and cross-coupled damping for 0.2 mm (8 mils), PR=0.4, three inlet preswirl, and 20,200 RPM

6.3.5.2.3 Running Speed

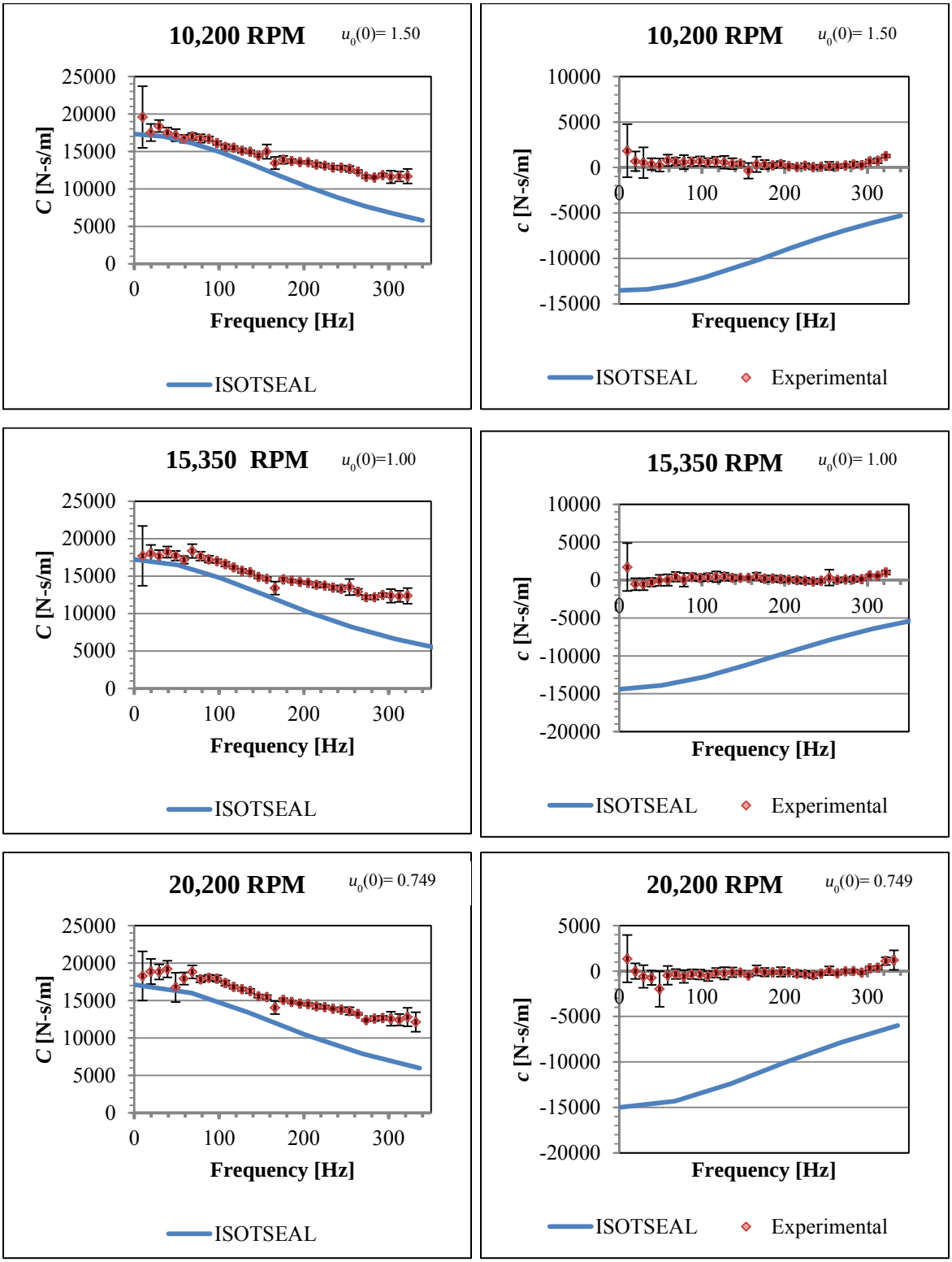

Figure 54. Direct and cross-coupling damping for 0.2 mm (8 mils), PR=0.4, high inlet preswirl, and three speeds

6.3.5.2.4 0.1 mm (4 mils) Radial Clearance (PR)

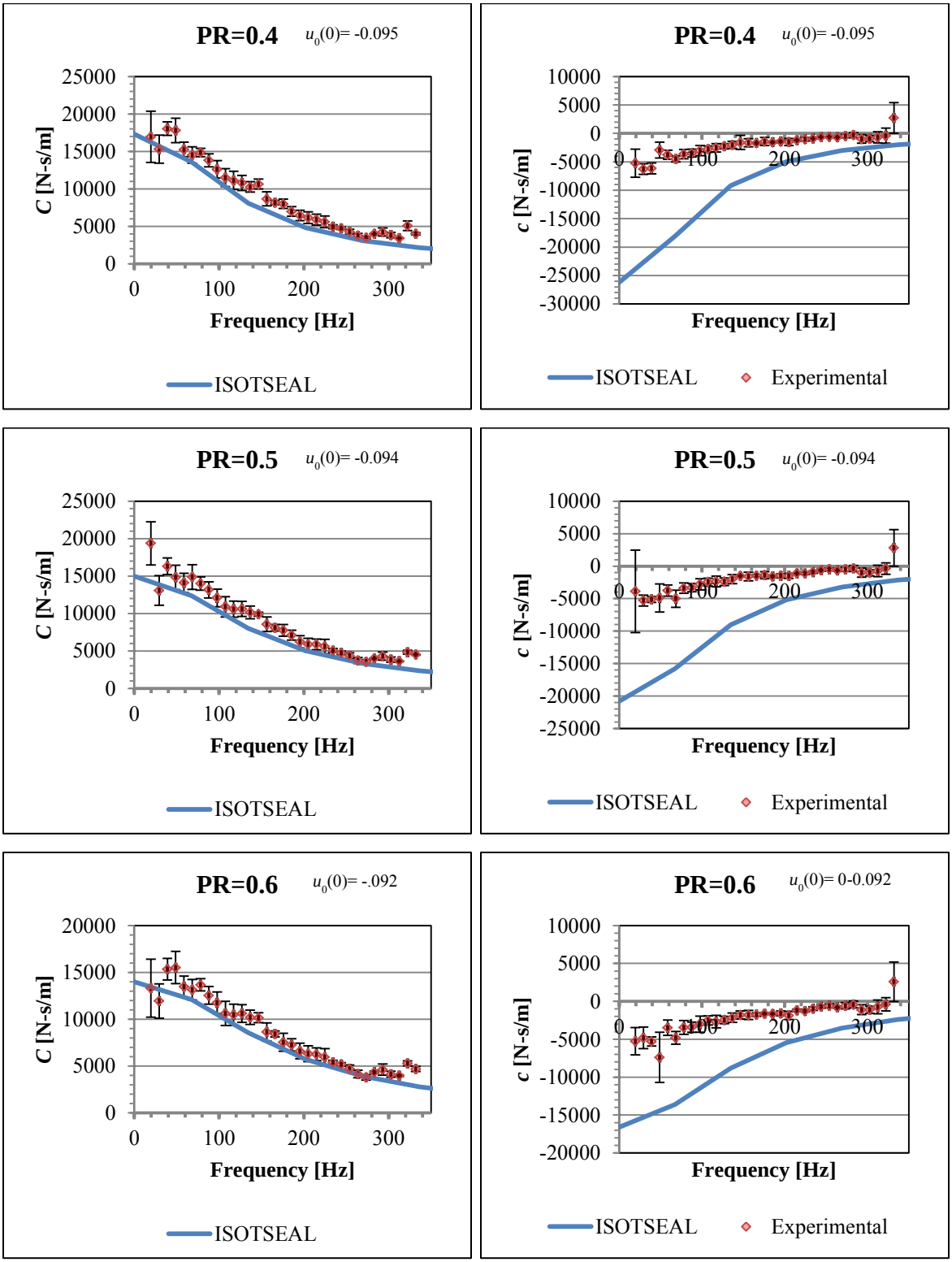

Figure 55. Direct and cross-coupling damping for 0.1 mm (4 mils), three PR, zero inlet preswirl, and 20,200 RPM

6.3.5.2.5 0.1 mm (4 mils) Radial Clearance (Running Speed)

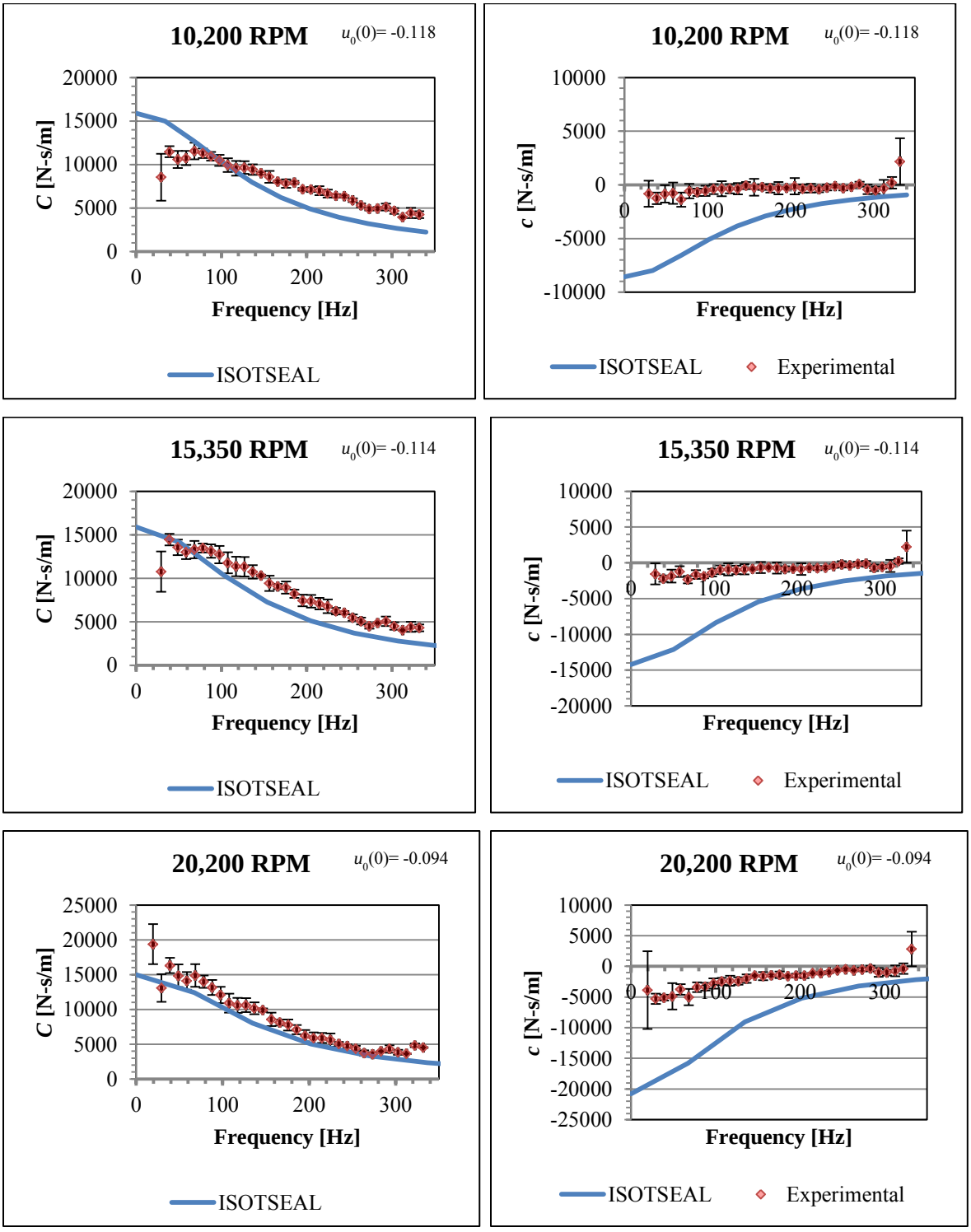

Figure 56. Direct and cross-coupling damping for 0.1 mm (4 mils), PR=0.5, zero inlet preswirl, and three speeds

6.3.5.3 Effective Stiffness

Predictions and experimental data are plotted for K_{eff} to demonstrate the influence of PR (Figure 57), preswirl (Figure 58), and rotational speed (Figure 59) on predictions. Figure 60 and Figure 61 are plots for a radial clearance of 0.1 mm (4 mils).

Regarding the validity of ISOTSEAL predictions, the following observations are made:

1) For a clearance of 0.2 mm (8 mils), predictions do not substantially improve or worsen by varying PR or rotational speed.
2) For frequencies above 60 Hz and a radial clearance of 0.2 mm (8mils), K_{eff} is over-predicted for a preswirl of zero and under-predicted for a preswirl of high. Considering these same conditions, ISOTSEAL and experimental data are in strong agreement for medium preswirl values.
3) Considering a clearance of 0.1 mm (4 mils), PR does not improve or worsen predication.
4) Predictions for the smaller clearance improve with running speed. Section 6.3.5.1.3 show that running speed does not improve K predictions. Also, section 6.3.5.2.5 demonstrates that prediction worsens with increasing speed. Thus, the improved predictions at high running speeds are not the result of improved accuracy. Rather, at higher speeds the amount K is over-predicted is offset by the difference in c between code and experimental data.
5) For a clearance of 0.1 mm (4 mils), PR does not affect the accuracy of ISOTSEAL.

6.3.5.3.1 Pressure Ratio

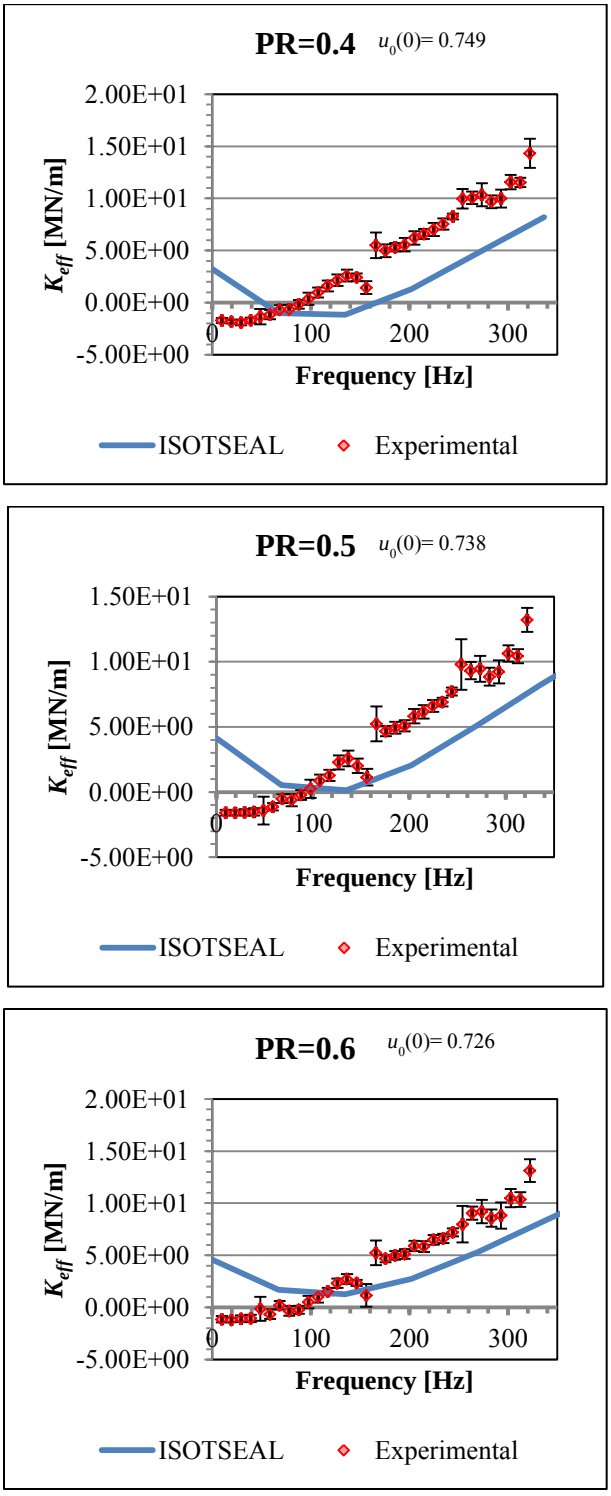

Figure 57. Effective stiffness for 0.2 mm (8 mils), three PR, high inlet preswirl, and 20,200 RPM

6.3.5.3.2 Preswirl

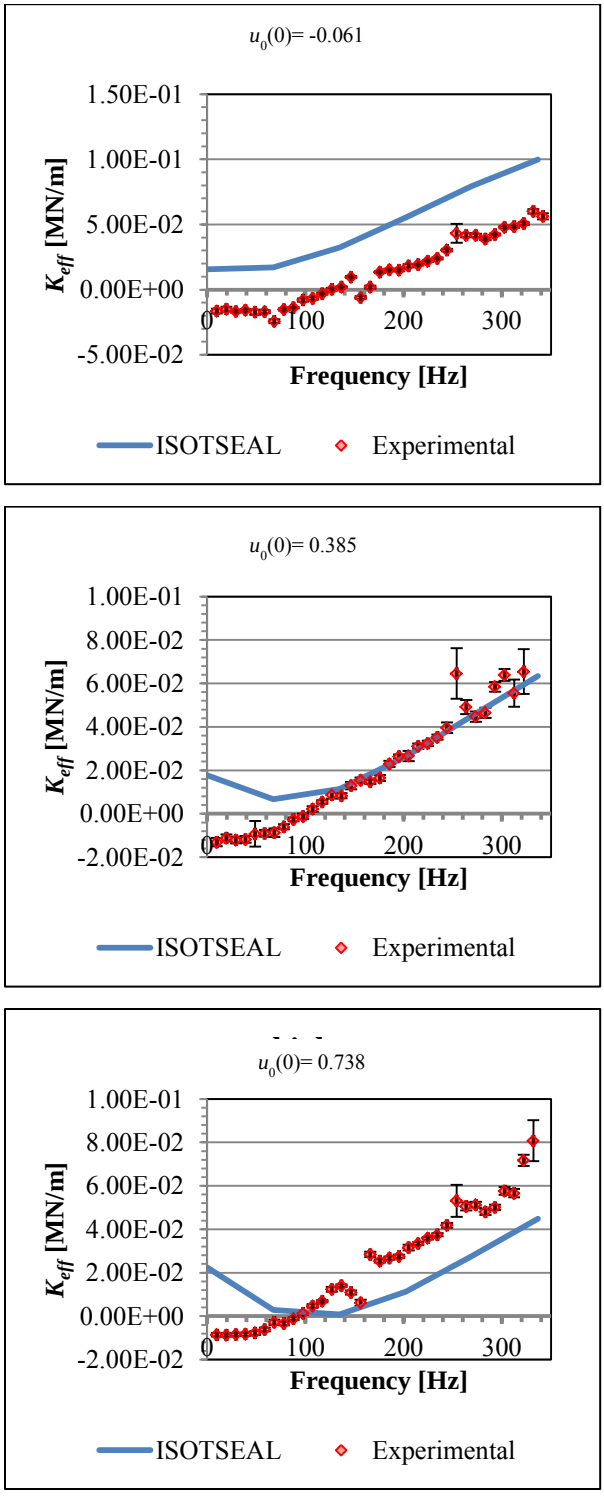

Figure 58. Effective stiffness for 0.2 mm (8 mils), PR=0.4, three inlet preswirl, and 20,200 RPM

6.3.5.3.3 Running Speed

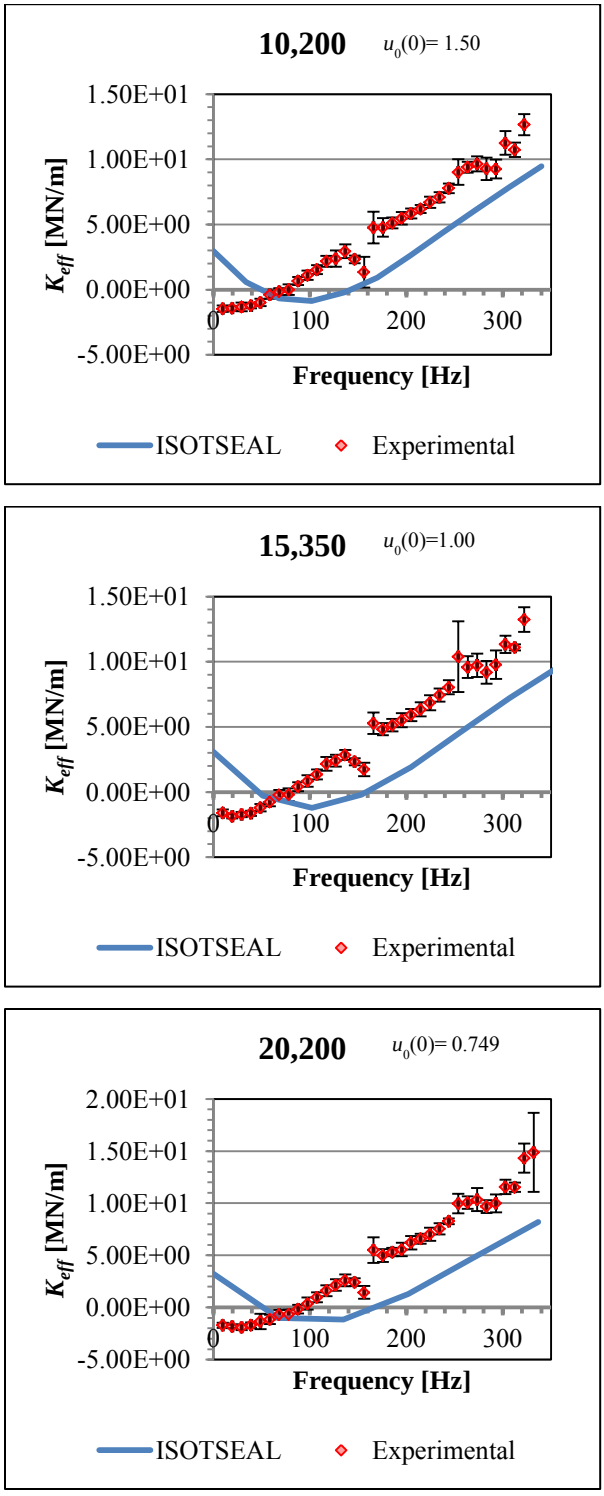

Figure 59. Effective stiffness for 0.2 mm (8 mils), PR=0.4, high inlet preswirl, and three speeds

6.3.5.3.4 0.1 mm (4 mils) Radial Clearance (PR)

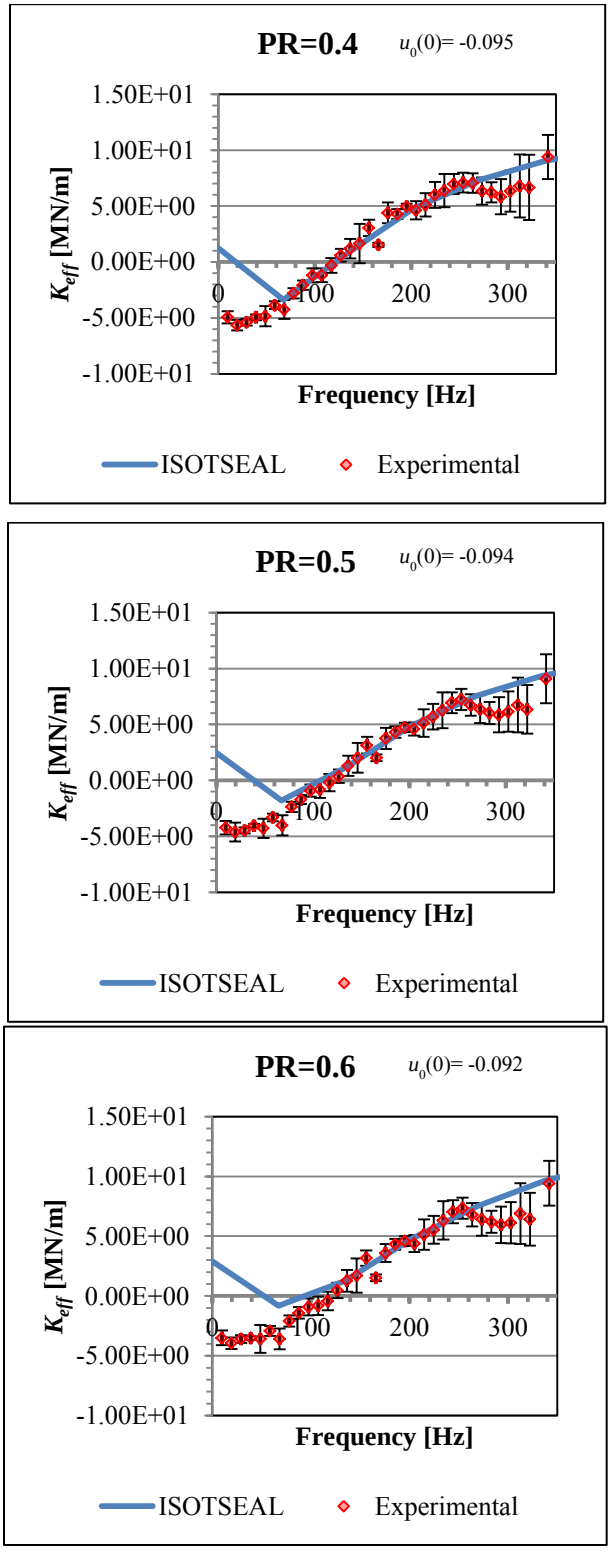

Figure 60. Effective stiffness for 0.1 mm (4 mils), three PR, zero inlet preswirl, and 20,200 RPM

6.3.5.3.5 0.1 mm (4 mils) Radial Clearance (Running Speed)

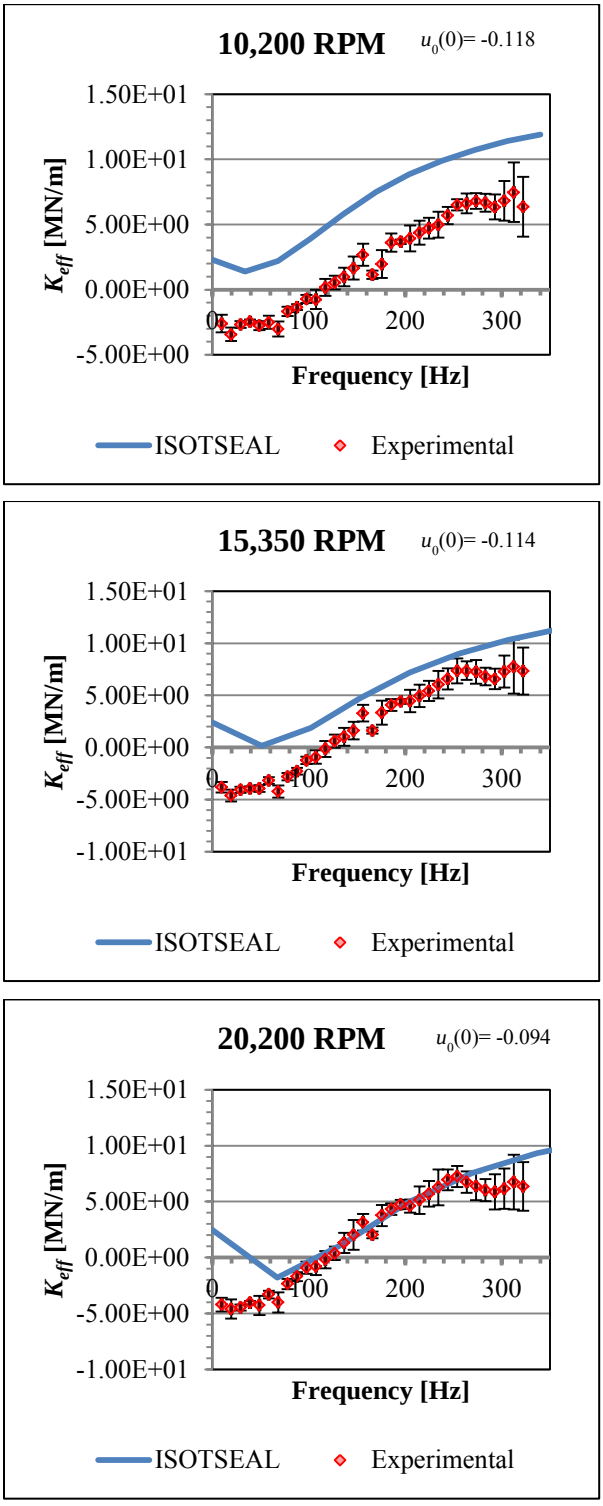

Figure 61. Effective stiffness for 0.1 mm (4 mils), PR=0.5, zero inlet preswirl, and three speeds

6.3.5.4 Effective Damping

Experimental and theoretical C_{eff} data is plotted to investigate the influence of the parameters PR (Figure 62), preswirl (Figure 63), and running speed (Figure 64) on predictions. Figure 65 and Figure 66 are plots of C_{eff} for a radial clearance of 0.1 mm (4 mils).

Conclusions drawn from Figures 62-66 are:

1) In all cases theory predicts a higher cross-over frequency and lower C_{eff} than experimental data demonstrates.
2) Predictions improve slightly for a clearance of 0.1 mm (4 mils). Specifically, the crossover frequency predicted is closer to test results.

6.3.5.4.1 Pressure Ratio

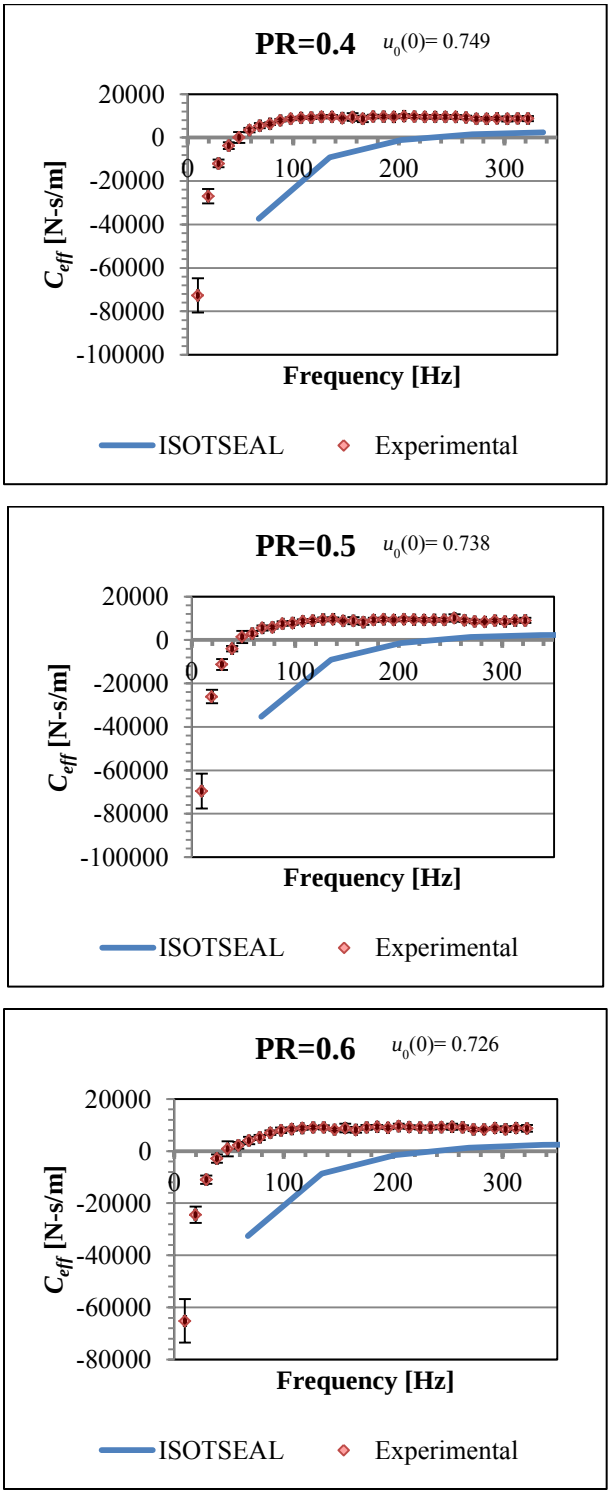

Figure 62. Effective damping for 0.2 mm (8 mils), three PR, high inlet preswirl, and 20,200 RPM

6.3.5.4.2 Preswirl

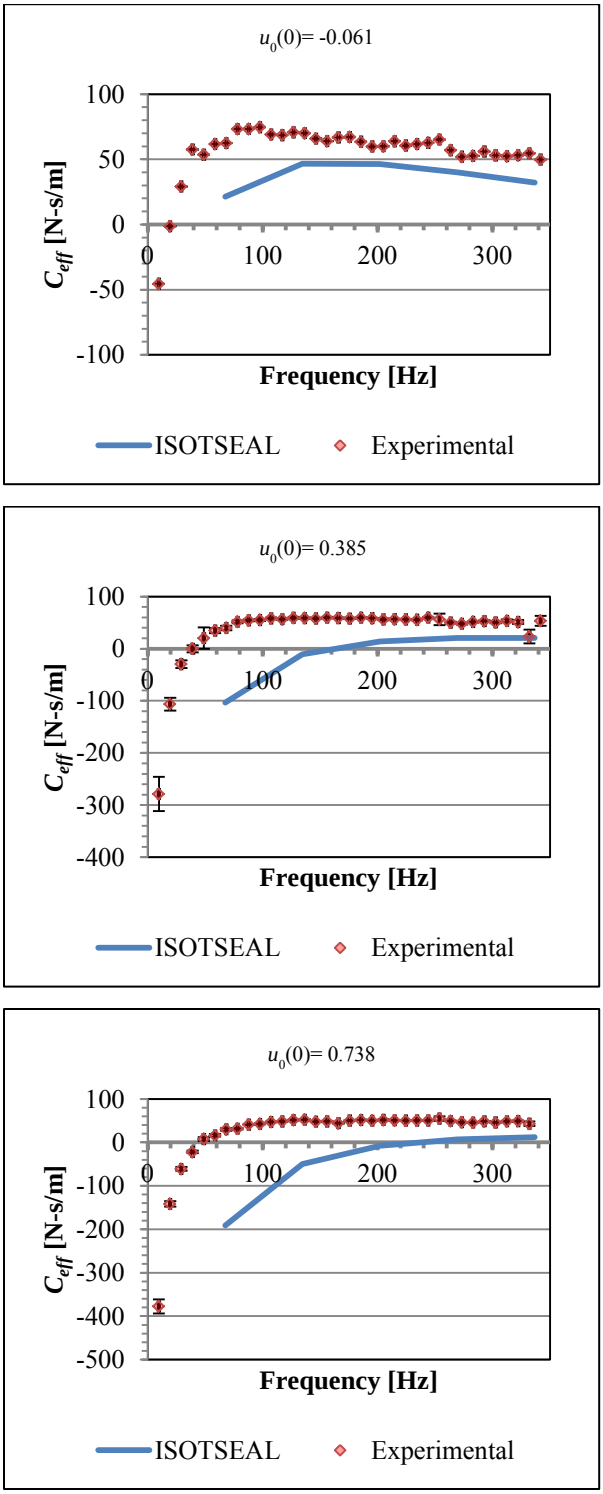

Figure 63. Effective damping for 0.2 mm (8 mils), PR=0.4, three inlet preswirl, and 20,200 RPM

6.3.5.4.3 Running Speed

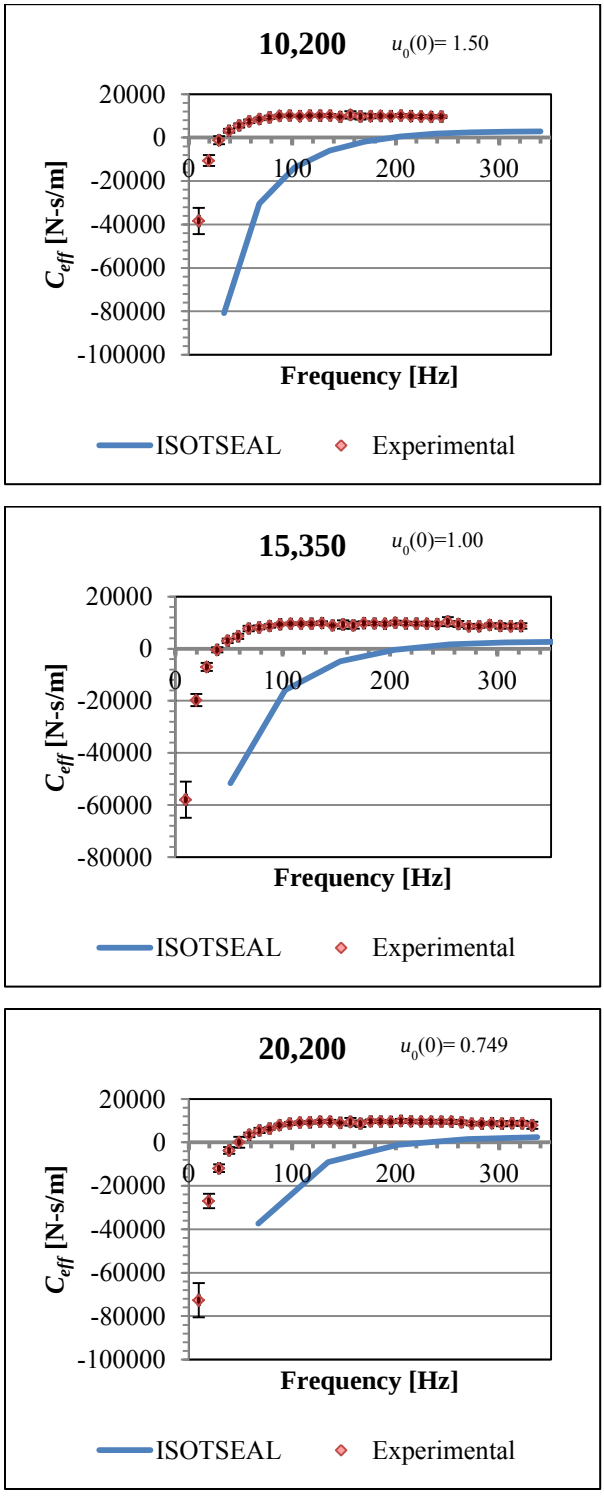

Figure 64. Effective damping for 0.2 mm (8 mils), PR=0.4, high inlet preswirl, and three speeds

6.3.5.4.4 0.1 mm (4 mils) Radial Clearance (PR)

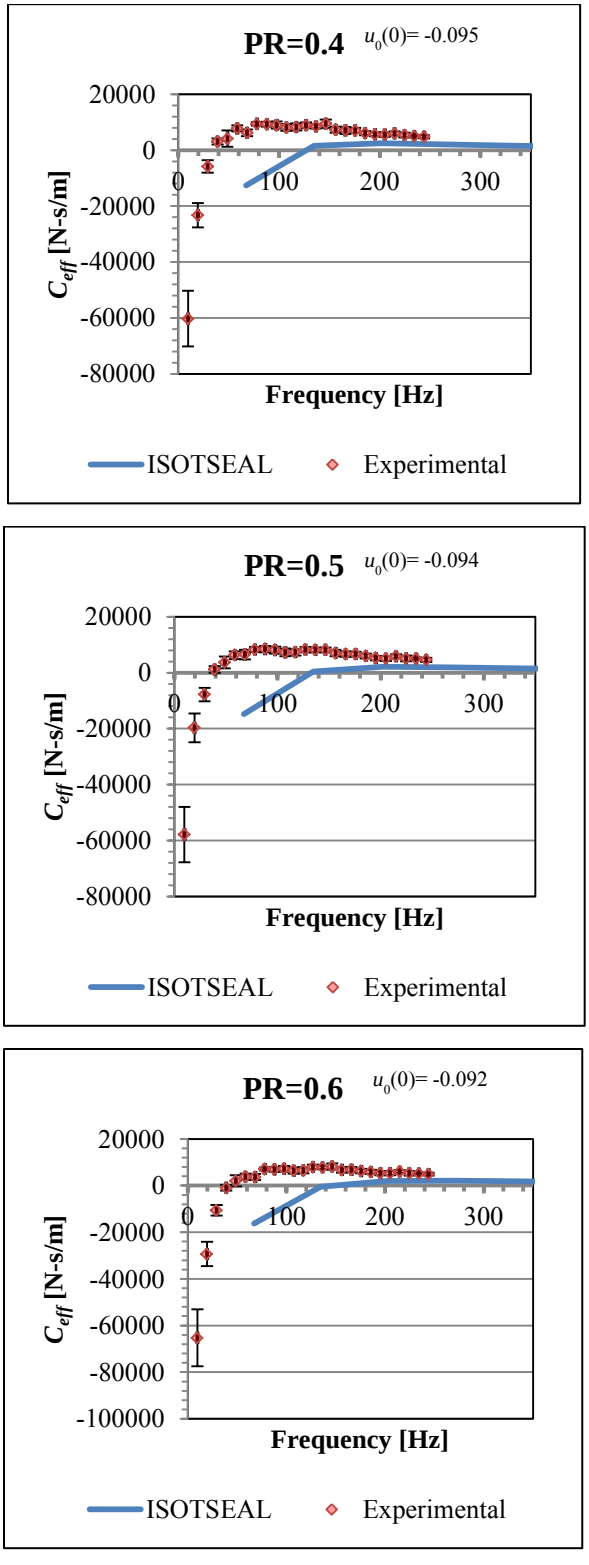

Figure 65. Effective damping for 0.1 mm (4 mils), three PR, zero inlet preswirl, and 20,200 RPM

6.3.5.4.5 0.1 mm (4 mils) Radial Clearance (Running Speed)

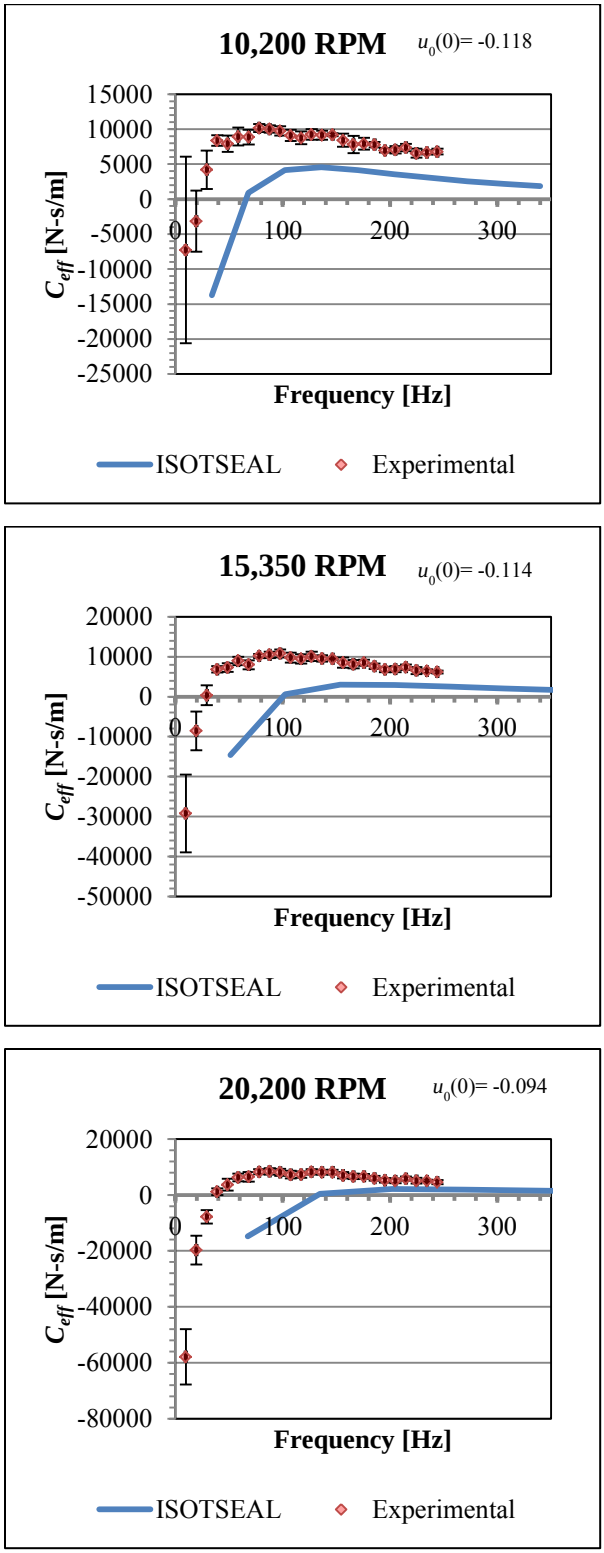

Figure 66. Effective damping for 0.1 mm (4 mils), PR=0.5, zero inlet preswirl, and three speeds

6.4 Comparison of Test Seal to Traditional Hole-Pattern Seals

The HP seal tested by Wade provides a point of comparison for the HP seal tested here. Wade's seal is comprised of 2668 holes that are individually 3.175mm (0.125 in) and 3.302 mm (0.130 in) in diameter and depth, respectively. Figure 10 shows the seal tested by Wade and the current test seal. To avoid confusion for the remainder of this thesis HPT (hole-pattern traditional) will refer to the seal tested by Wade and HPLD (hole-pattern larger diameter hole) will refer to the HP seal tested for this thesis.

For comparisons, all data will be normalized or non-dimensionalized using Eqs. (22), (23), or (24).

6.4.1 Static Results

Figure 67 shows leakage coefficients are on average 23% greater for the HPLD seal than the HPT seal. Asirvatham [62] measured mass flow rate for the plate shown in Figure 18 and a plate incorporating the same hole-pattern configuration as the HPT seal. At a clearance of 0.254 mm (10 mils), mass flow rate was greatest of the plate displayed in Figure 18. From a leakage performance view, the HPLD seal is not recommended for use over the HPT seal.

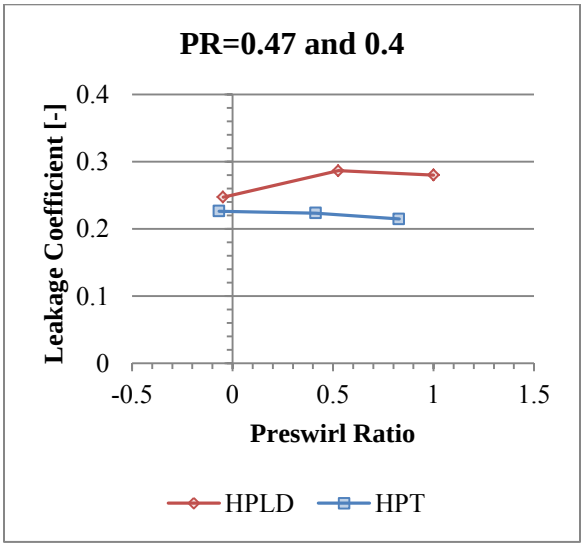

Figure 67. HPT and HPLD leakage coefficient versus preswirl ratio for 0.2 mm (8 mils), PR=0.40 (HPLD) and PR=0.47 (HPT), all preswirl ratios, and 15,350 RPM

6.4.2 Dynamic Results

Table 6 summarizes the test cases chosen to compare the dynamic characteristics of the HPLD and HPT seals.

Table 6. Test cases of seals for comparison

Seal	Rotor Speed [rpms]	Inlet Pressure [24]	Pressure Ratio [-]	Radial Clearance [54]	Preswirl [-]
HPT	20,200	70	0.47	0.2	Zero
HPLD	20,200	40	0.5	0.2	Zero

Eqs. (22) and (23) will be used to non-dimensionalize or normalize data obtained from both seals.

6.4.2.1 Direct and Cross-Coupled Stiffness

Figure 68 shows the HPT seal generates greater K^* that the HPLD seal. Note, the HPLD seal exhibits negative K^* while the HPT seal does not. k^* is greatest for the HPT seal

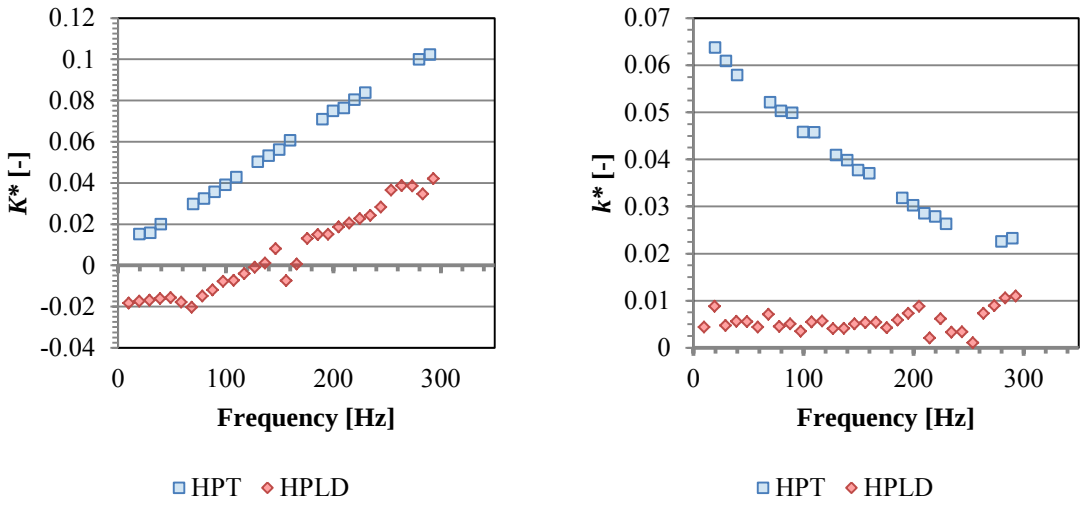

Figure 68. Direct and cross-coupled stiffness for 0.2 mm (8 mils), PR=0.47 and 0.5, high inlet preswirl, and 20,200 RPM

6.4.2.2 Direct and Cross-Coupled Damping

Figure 69 shows C^* and c^* for the HPLD and HPT seals. For frequencies above 100 Hz, C^* is larger for the HPLD. Note, c^* is negative for all frequencies for the HPT seal. c^* is relatively low for the HPLD seal and, generally, frequency-independent.

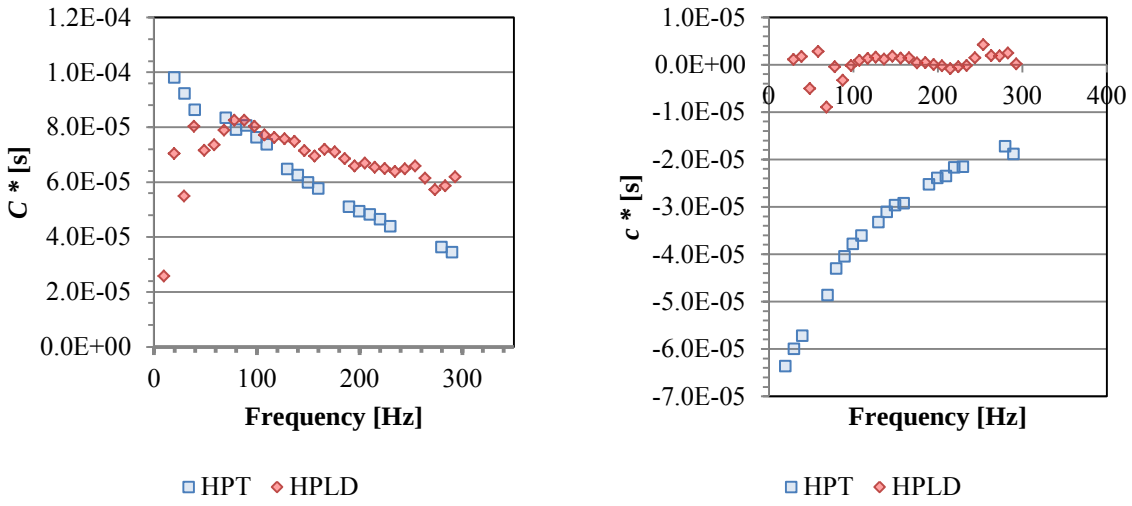

Figure 69. Direct and cross-coupled damping for 0.2 mm (8 mils), PR=0.47 and 0.5, high inlet preswirl, and 20,200 RPM

6.4.2.3 Effective Stiffness

Figure 70 demonstrates that K^*_{eff} is greatest for the HPT seal. As frequency increases, the disparity between the HPLD seal and the HPT seal increases. Note, the HPLD seal develop negative K^*_{eff} at low frequencies. Thus even though the HPT seal develops negative c^* it generates K^* of a great enough magnitude to produce positive K^*_{eff}.

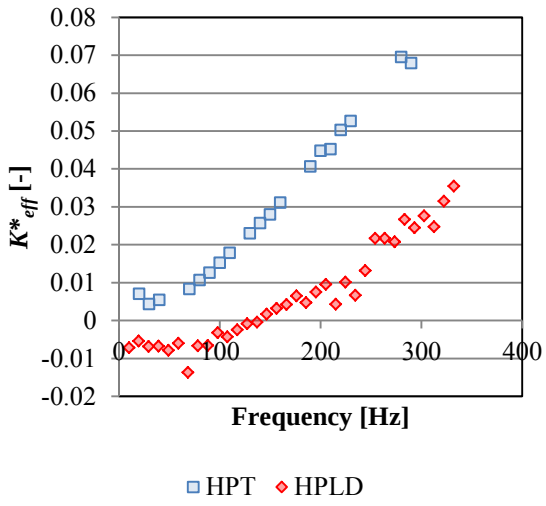

Figure 70. Effective stiffness for 0.2 mm (8 mils) and 0.1 mm (4 mils), PR=0.47 and 0.5, high inlet preswirl, and 20,200 RPM

6.4.2.4 Effective Damping

Figure 71 shows that the HPLD has a lower crossover frequency implying it is more stable. C^*_{eff} is larger for the HPLD seal.

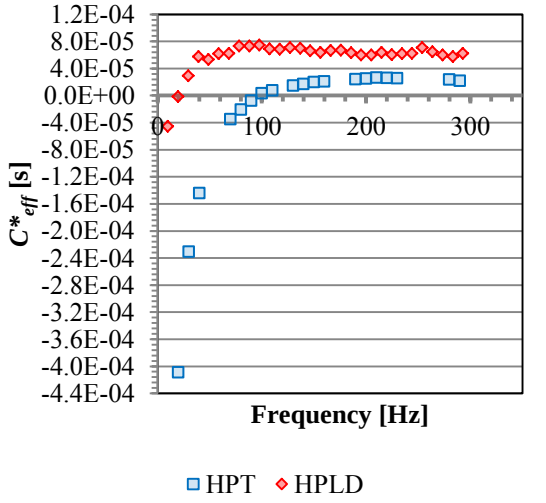

Figure 71. Effective damping for 0.2 mm (8 mils) and 0.1 mm (4 mils), PR=0.47 and 0.5, high inlet preswirl, and 20,200 RPM

7. SUMMARY AND CONCLUSIONS

Data presented accomplishes the following objectives:

1) Provide experimental rotordynamic coefficients for an HP seal comprised of larger holes (diameter of 0.48 inches).
2) Compare experimental results to predictions generated by ISOTSEAL.
3) Finally, compare experimental results of this "new" HP seal to an HP seals tested by Wade [74].

Regarding objective 1, testing of this new seal was extremely difficult and puzzling. Stator dynamic and static instabilities that cannot be explained at this time, forced testing at lower inlet pressure than typical. Unexpectedly, the medium preswirl stator was more susceptible to stator dynamic instability than the high preswirl stator. Although, testing was challenging, results gathered allowed for the inspection of the seals characteristics and how PR, preswirl, rotor speed, and clearance influence rotordynamic coefficients.

Like previously tested HP seals [60, 74] , K and C are frequency-dependent. Similar to a smooth seal tested by Kerr [69], c is relatively small. For a clearance of 0.1 mm (4 mils), k decreased with increasing frequency a trend indicative of HP seals. Note, that compared to the HP seal tested by Wade [74], k for the small clearance is a weak function of excitation frequency.

PR had no effect on rotordynamic coefficients.

To evaluate the influence of preswirl on rotordynamic coefficients the results had to be non-dimensionalized or normalized. K^* and K^*_{eff} are lowest for the zero preswirl stator. There is not a drastic difference in values of K^* and K^*_{eff} for the high and medium preswirl cases. As expected, k^* increases with preswirl. Compared to medium and high preswirl, k^* is approximately an order of magnitude smaller for zero preswirl case. In general, preswirl has limited impact on c^* and it remains relatively small for all preswirl ratios. C^* is smallest for the zero preswirl stator. Although, C^* is smallest for zero preswirl, the low k^* values lead to a cross-over frequency approximately 50% less than the high and medium preswirl ratios. Thus, swirl brakes or shut injection would be beneficial, assuming they drop the preswirl ratio to approximately 0.

Running speed changes have limited influence on K, K_{eff}, and C_{eff}. k increases with increasing speed. C also increases with increasing running speed. In the end, the effects of running speed on stability practical cancel each other out, i.e. cross-over frequency and C_{eff} are approximately equal for all running speeds. For frequencies of 150 Hz and greater, c is approximately equal for all speeds. For frequencies below 150 Hz, c is greatest for the lower speeds: 10,200 and 15,350 RPM.

For comparisons between clearances, the rotordynamic coefficients were non-dimensionalized or normalized. Changes in clearances have limited influence on K^* and K_{eff}. k^* is inversely proportional to frequency for the 0.1 mm (4 mils) clearance. C^* and C^*_{eff} are greater for the larger clearances. The seal becomes more stable at increased clearance.

Leakage coefficient was smallest for a preswirl ratio of approximately 0. This coupled with the increased stability for a preswirl ratio of 0 suggested this seal should be used with swirl brakes or shunt injection.

For the larger clearance, the cross coupled terms show limited frequency dependence and as such, ISOTSEAL is poor in predicting trends in the cross-coupled coefficients. ISOTSEAL does slightly better at predicting cross-coupled coefficients for the 0.1 mm (4 mil) clearance. That being said, correlation between code and experimental data for cross-coupled coefficient is poor. For all test cases, K is negative at low frequencies, a fact that is not predicted by ISOTSEAL. C is reasonably well predicted, with an increase in accuracy seen for a clearance of 0.1 mm (4 mils). ISOTSEAL assumes flow only moves radial within the cell control-volume. Due to the large hole-diameters flow is not constrained to move purely radial and ISOTEALS cannot accurately model the seal tested for this thesis.

ISOTSEAL does a fair job of predicting leakage.

The seal characteristics for this thesis (HPLD) were compared to a HP seal (HPT) tested by Wade. K^* and K^*_{eff} are greater for the HPT seal. The HPLD seal develops negative stiffness at low frequencies, while the HPT seal does not. k^* is larger for the HPT seal while C^* and C^*_{eff} are larger for the HPLD seal. Also, the HPLD exhibit a *cross-over frequency* at approximately 40 Hz or 33% less than the HPT. These results imply that the HPLD seal is more stable. On average, the HPLD seal leakage coefficient is 23% greater that the HPT.

This seal was proposed to reduce cost. Unfortunately, the fabrication was more challenging than the supplier originally thought. In the end, the HPLD did not reduce manufacturing cost or time.

REFERENCES

[1] Kirk, R. G., 1990, "A Method for Calculating Labyrinth Seal Inlet Swirl Velocity," ASME J. of Vibration and Acoustics, **112**, pp. 380-383.

[2] Childs, D. W., and Vance, J., 2007, "Gas Annular Seals and Their Influence on Rotordynamics of Turbomachinery," Presented at the Thirty Sixth Turbomachinery Symposium, Houston, TX.

[3] Kulhanek, C. D., 2010, "Dynamic and Static Characteristics of a Rocker-Pivot, Tilting-Pad Bearing with 50% and 60% Offsets," M.S. thesis, Texas A&M University, College Station, TX.

[4] Adams, M. L., 2010, *Rotating Machinery Vibration: From Analysis to Troubleshooting*, CRC Press, Boca Raton, FL.

[5] Palazzolo, A., and von Pragenau, G. L., 1991, "A Theoretical Manual for G. L. von Pragenou's Liquid Seal Simulation Program," Paper presented at the Texas A&M University, College Station, TX.

[6] Vance, J. M., Murphy, B., and Zeidan, F., 2010, *Machinery Vibration and Rotordynamics*, John Wiley & Sons, Inc., Hoboken, NJ.

[7] Newkirk, B. L., 1924, "Shaft Whipping," General Electric Review, **27**, pp. 169-178.

[8] Kimball, A. L., 1924, "Internal Friction Theory of Shaft Whirling," General Electric Review, **27**, pp. 244-251.

[9] Newkirk, B. L., and Taylor, H. D., 1925, "Shaft Whipping Due to Oil Action in Journal Bearings," General Electric Review, **28**, pp. 559-568.

[10] Enrich, F., and Childs, D. W., 1984, "Self-Excited Vibrations in High-Performance Turbomachinery," J. of Mechanical Engineering, **106**, pp. 33-79.

[11] Vance, J. M., 1988, *Rotordynamics of Turbomachinery*, John Wiley & Sons, Inc., New York, NY.

[12] Lomakin, A. A., 1958, "Calculation of Critical Speed and Securing of Dynamic Stability of the Rotor of Hydraulic High Pressure Machines with Reference to Forces Arising in the Seal Gaps," Energomashinostroenie, **4**, pp. 1-5.

[13] San Andres, L., 2010, "Annular Pressure Seals," Modern Lubrication Theory, Notes 12, Texas A&M University Digital Libraries, https://repository.tamu.edu/handle/1969.1/93197. 01/02/2011

[14] Childs, D. W., 1993, *Turbomachinery Rotordynamics: Phenomena Modeling and Analysis*, John Wiley & Sons, Inc., New York, NY.

[15] Thomas, H., 1958, "Instabile Eigenschwingungen von Turbinenlaufern angefacht durch die Spaltstromungen Stopfbuschen und Beschauflungen," Bull de L'AIM, **71**, pp. 1039-1063.

[16] Alford, J. S., 1965, "Protecting Turbomachinery from Self-Excited Rotor Whirl," J. of Engineering for Power, **87**, pp. 333-344.

[17] Leong, Y. M. M. S., and Brown, R.D., 1982, "Circumferential Pressure Distributions in a Model Labyrinth Seal," NASA CP2250, Proceedings from a Workshop on Rotordynamic Instability Problems in High-Performance Turbomachinery - 1982, held at Texas A&M University, College Station, TX, pp. 223-241.

[18] Spürk, S. H., and Keiper, R., 1974, "Self-Excited Rotor Whirl," C. E. Trans. 6785. Translated from Ingenieur Archiv. **43**, pp. 127-135.

[19] Vance, J. M., Zierer, J. J., and Conway, E. M., 1993, "Effect of Straight-Though Labyrinth Seals on Rotordynamics," Proceedings of the 14th Vibration and Noise Conference, Albuquerque, NM, pp. 159-171.

[20] Black, H. F., and Jenssen, D. N., 1971, "Effects of High Pressure Ring Seals on Pump Rotor Vibrations," ASME Paper No. 71-WA/ff-38.

[21] Marcinkowskij, W. A., and Karincev, J. B., 1961, "Influence of Seal Gaps on the Critical Speeds of Feed Pump Rotors," Energomashinostroenie, **7**(4), p. 33.

[22] Black, H. F., 1969, "Effects of Hydraulic Forces in Annular Pressure Seals on the Vibrations of Centrifugal Pump Rotors," J. of Mechanical Engineering Science, **11**(2), pp. 206-213.

[23] Black, H. F., and Jenssen, D. N., 1970, 1970, "Dynamic Hybrid Bearing Characteristics of Annular Controlled Leakage Seals," Proceedings of the Institution of Mechanical Engineers, London, England, **184**(3N), pp. 92-100.

[24] Black, H. F., Allaire, P. E., and Barrett, L. E., 1981, 1981, "Inlet Flow Swirl in Short Turbulent Annular Seal Dynamics," Proceeding of the Ninth International Conferences on Fluid Sealing, Noordwijkerhout, Netherlands, pp. 141-152.

[25] von Progenau, G. L., 1982, "Damping Seals for Turbomachinery," Marshall Space Flight Center, Huntsville, AL, NASA TP-1987.

[26] Childs, D. W., 1983, "Dynamic Analysis of Turbulent Annular Seals Based On Hirs' Lubrication Equation," ASME J. of Lubrication Technology, **105**, pp. 429-436.

[27] Iwatsubo, T., and Sheng, B. C., 1990, 1990, "An Experimental Study on the Static and Dynamic Characteristics of Damper Seals," Proceedings of the Third IFToMN International Conference on Rotordynamics, Lyon, France, pp. 307-312.

[28] Childs, D. W., and Kim, C-H., 1985, "Analysis and Testing of Turbulent Annular Seals with Different, Directionally Homogeneous Surface Roughness Treatments for Rotor and Stator Elements," ASME J. of Tribology, **107**, pp. 296-306.

[29] Childs, D. W., and Kim, C-H., 1986, "Test Results for Round-Hole-Pattern Damper Seals; Optimum Configurations and Dimensions for Maximum Net Damping," ASME J. of Tribology, **108**, pp. 605-611.

[30] von Progenau, G., 1986, discussion of the paper, "Test Results for Round-Hole-Pattern Damper Seals; Optimum Configurations and Dimensions for Maximum Net Damping," by Childs, D.W. and Kim, C-H ASME J. of Tribology, **108**, pp. 605-611.

[31] Childs, D. W., Nolan, S. A., and Kilgore, J. J., 1990, "Additional Test Results for Round-Hole-Pattern Damper Seals: Leakage, Friction Factors, and Rotordynamic Force Coefficients," ASME J. of Tribology, **112**, pp. 365-371.

[32] Fowlie, D. W., and Miles, D. D., 1975, "Vibration Problems with High Pressure Centrifugal Compressors," ASME Paper No. 75-PET-28.

[33] Geary, J., C. H., Damratowski, L. P., and Seyer, C., 1976, "Design and Operation of the World's Highest Pressure Gas Injection Centrifugal Compressors," Proceedings of the Eighth Annual Offshore Technology Conference, Houston, TX, pp. 3-6.

[34] Smith, K. J., 1975, "An Operation History of Fractional Frequency Whirl," Proc. Fourth Turbomachinery Symposium, Texas A&M University, pp. 115-125.

[35] Greathead, S. H., and Bostow, P., 1976, "Investigations into Load Dependent Vibrations of the High Pressure Rotor on Large Turbo-Generators," Proceeding of the IMechE. Conference on Vibrations in Rotating Machinery, Cambridge, England, pp. 279-286.

[36] Fleming, D. P., 1979, "Stiffness of Straight and Tapered Annular Gas Path Seals," ASME J. of Lubrication Technology, **101**, pp. 349-355.

[37] Benckert, H., and Wachter, J., 1980, "Flow Induced Spring Coefficients of Labyrinth Seals for Applications in Turbomachinery," NASA CP 2133, Proceedings from a Workshop on Rotordynamic Instability Problems in High-Performance Turbomachinery - 1980, held at Texas A&M University, College Station, TX, pp. 189-212.

[38] Dawson, P. M., 2000, "A Comparison of the Static and Dynamic Characteristics of Straight-Bore and Convergent Tapered-Bore Honeycomb Annular Gas Seals," M.S. thesis, Texas A&M University, College Station, TX.

[39] Childs, D. W., 1983, "Finite-Length Solutions for Rotordynamic Coefficients of Turbulent Annular Seals," ASME J. of Lubrication Technology, **105**, pp. 437-445.

[40] Nelson, C. C., 1983, "Rotordynamic Coefficients for Compressible Flow in Tapered Annular Seals," ASME J. of Tribology, **107**, pp. 318-325.

[41] Nelson, C., 1984, "Analysis for Leakage and Rotordynamic Coefficients of Surface-Roughened Tapered Annular Gas Seals," ASME J. of Engineering for Gas Turbine and Power, **106**, pp. 927-934.

[42] Scharrer, J., 1989, discussion of the paper, "Annular Honeycomb Seals: Test Results for Leakage and Rotordynamic Coefficients; Comparisons to Labyrinth and Smooth Configurations," by Childs et al. ASME J. of Tribology, **111**, pp. 293-301.

[43] Childs, D. W., Elrod, D., and Hale, K., 1989, "Annular Honeycomb Seals: Test Results for Leakage and Rotordynamic Coefficients; Comparisons to Labyrinth and Smooth Configurations," ASME J. of Tribology, **111**, pp. 293-301.

[44] Kleynhans, G. F., 1991, "A Comparison of Experimental Results and Theoretical Predictions for the Rotordynamic and Leakage Characteristics of Short (L/D = 1/6) Honeycomb and Smooth Annular Seals," Texas A&M University, Turbomachinery Laboratory Report, TL-SEAL-91.

[45] Elrod, D. A., Nelson, C. C., and Childs, D. W., 1989, "An Entrance Region Friction Factor Model Applies to Annular Seal Analysis Theory vs. Experiment for Smooth and Honeycomb Seals," ASME J. of Tribology, **111**, pp. 337-343.

[46] Elrod, D. A., Childs, D. W., and Nelson, C. C., 1990, "An Annular Gas Seal Analysis Using Empirical Entrance and Exit Region Friction Factors," ASME J. of Tribology, **112**, pp. 196-204.

[47] Ha, T.-W., and Childs, D. W., 1992, "Friction-Factor Data for Flat-Plate Tests of Smooth and Honeycomb Surfaces," ASME J. of Tribology, **114**, pp. 722-730.

[48] Ha, T. W., and Childs, D. W., 1991, "Friction-Factor Data for Flat Plate Tests of Smooth and Honeycomb Surfaces (Including Extended Test Data)," Texas A&M University, Turbomachinery Laboratories Report, TL-SEAL-1-91, Jan.

[49] Ha, T. W., and Childs, D. W., 1994, "Annular Honeycomb-Stator Turbulent Gas Seal Analysis Using a New Friction-Factor Model Based on Flat Plate Tests," ASME J. of Tribology, **116**(2), pp. 352-360.

[50] Nelson, C., 1985, "Rotordynamic Coefficients for Compressible-Flow in Tapered Annular Seals," ASME J. of Tribology, **107**, pp. 318-325.

[51] Childs, D. W., 1994, discussion of the paper, "Annular Honeycomb Stator Turbulent Gas Seal Analysis Using a New Friction Factor Model Based on Flat Plate Tests," by Childs et al. ASME J. of Tribology, **116**, pp. 352-360.

[52] Kleynhans, G., and Childs, D., 1997, "The Acoustic Influence of Cell Depth on the Rotordynamic Characteristics of Smooth-Rotor/Honeycomb-Stator Annular Gas Seals," ASME J. of Engineering for Gas Turbines and Power, **119**, pp. 949-957.

[53] Zeidan, F., Perez, R., and Stephenson, E., 1993, "The Use of Honeycomb Seals in Stabilizing Two Centrifugal Compressors," Proceedings of the Twenty-Second Turbomachinery Symposium, College Station, TX, pp. 3-15.

[54] Memmott, E. A., 1994, "Stability of a High Pressure Centrifugal Compressor Through Application of Shunt Holes and a Honeycomb Labyrinth," Proceedings of the Thirtieth Machinery Dynamics Seminar, CMVA, Toronto, Canada, pp. 211-233.

[55] Gelin, A., Pugnet, J. -M., Bolusset, D., and Friez, P., 1997, "Experience in Full-Load Testing of Natural Gas Centrifugal Compressors for Rotordynamics Improvements," ASME J. of Engineering for Gas Turbines and Power, **119**, pp. 934-941.

[56] Armstrong, J., and Perricone, F., 1996, 1996, "Turbine Instability Solution-Honeycomb Seals," Proceedings of the Twenty-Second Turbomachinery Symposium, College Station, TX, pp. 47-56.

[57] Camatti, M., Vannini, G., Fulton, J., and Hopenwasser, F., 2003, 2003, "Instability of a High-Pressure Compressor Equipped with Honeycomb Seals," Proceedings of the Thirty-Second Turbomachinery Symposium, Houston, TX, pp. 39-48.

[58] Kocur, J., and Hayles, G., 2004, "Low Frequency Instability in a Process Compressor," Proceedings of the Thirty-Third Turbomachinery Symposium, Houston, TX, pp. 25-32.

[59] Yu, Z., and Childs, D. W., 1998, "A Comparison of Experimental Rotordynamic Coefficients and Leakage Characteristics Between Hole-Pattern Gas Damper Seals and a Honeycomb Seal," ASME J. of Engineering for Gas Turbines and Power, **120**, pp. 778-783.

[60] Holt, C., and Childs, D. W., 2002, "Theory Versus Experiment Results for the Dynamic Impedances of Two Hole-Pattern Annular Gas Seals," ASME J. of Tribology, **124**, pp. 137-143.

[61] Childs, D. W., and Wade, J., 2004, "Rotordynamic-Coefficient and Leakage Characteristics for Hole-Pattern-Stator Annular Gas Seals-Measurements Versus Predictions," ASME J. of Tribology, **126**, pp. 326-333.

[62] Asirvatham, T., 2010, "Friction Factor Measurement, Analysis, and Modeling for Flat-Plates with 12.15 mm Diameter Hole-Pattern, Tested with Air at Different Clearances, Inlet Pressures, and Pressure Ratios," M.S. thesis, Texas A&M University, College Station, TX.

[63] Childs, D. W., and Hale, K., 1994, "A Test Apparatus and Facility to Identify the Rotordynamic Coefficients of High-Speed Hydrostatic Bearings," ASME J. of Tribology, **116**, pp. 337-343.

[64] Lindsey, W. T., 1993, "Experimental versus Theoretical Comparison of the Effects of Taper and Static Eccentricity of the Rotordynamic Coefficients of Short, Smooth, High-Speed, Liquid Annular Seals," M.S. thesis, Texas A&M University, College Station, TX.

[65] Weatherwax, M., 2001, "A Study of the Effects of Eccentricity on Honeycomb annular Gas Seals," M.S. thesis, Texas A&M University, College Station, TX.

[66] Glienicke, J., 1966, "Experimental Investigation of Stiffness and Damping Coefficients of Turbine Bearings and Their Application to Instability Predictions," Proceedings of the IMechE., **181**, pp. 116-129.

[67] Rouvas, C., 1993, "Parameter Identification of the Rotordynamic Coefficients of High-Reynolds-Number Hydrostatic Bearings," Ph. D. dissertation, Texas A&M University, College Station, TX.

[68] Picardo, A., 2003, "High Pressure Testing of Labyrinth Seals," M.S. thesis, Texas A&M University, College Station, TX.

[69] Kerr, B. G., 2004, "Experimental and Theoretical Rotordynamic Coefficients and Leakage of Straight Smooth Annular Gas Seals," M.S. thesis, Texas A&M University, College Station, TX.

[70] Coleman, H. W., and Steele, W. G., 1999, *Experimentation and Uncertainty Analysis for Engineers*, John Wiley & Sons, Inc., New York.

[71] Wheeler, A. J., and Ganji, A. R., 1996, *Introduction to Engineering Experimentation*, Prentice Hall, Englewood Cliffs, NJ.

[72] Ertas, B. H., 2005, "Rotordynamic Force Coefficients of Pocket Damper Seals," Ph.D. dissertation, Texas A&M University, College Station, TX.

[73] Hirs, G. G., 1973, "A Bulk-Flow Theory for Turbulence in Lubricant Films," ASME J. of Lubrication Technology, **95**, pp. 137-146.

[74] Wade, J. L., 2004, "Test Versus Predictions for Rotordynamic Coefficients and Leakage Rates of Hole-Pattern Gas Seals at Two Clearances in Choked and Unchoked Conditions," M.S. thesis, Texas A&M University, College Station, TX.

[75] Kleynhans, G. F., 1997, "A Two-Control-Volume Bulk-Flow Rotordynamic Analysis for Smooth-Rotor/Honeycomb-Stator Gas Annular Seals," Ph.D. dissertation, Texas A&M University, College Station, TX.

[76] Yamada, Y., 1962, "Resistance of Flow through an Annulus with an Inner Rotating Cylinder," Bull J.S.M.E., **5**(1), pp. 302-310.

[77] Carter, J. J., 2001, "The Static and Dynamic Characteristics of Divergent Tapered-Bore Hole-Pattern Gas Seals," M.S. thesis, Texas A&M, College Station, TX.

APPENDIX A

EXACT TEST CONDITIONS

Table 7. Exact test conditions (absolute pressures)

Inlet Preswirl Condition	Radial Clearance [54]	Rotor Speed [RPM]	P_{in} [24]	P_{out} [24]
Zero	*0.1*	10,200	21.44	9.46
			20.91	11.44
			22.26	13.92
		15,350	21. 90	9.38
			21.67	11.74
			21.70	14.17
		20,200	20.88	8.53
			21.41	10.94
			22.37	13.80
	0.2	10,200	27.98	10.80
			41.30	21.13
			41.39	25.04
		15,350	29.31	11.03
			36.12	18.11
			41.72	25.35
		20,200	28.33	10.82
			41.07	21.26
			40.89	25.10
Medium	*0.2*	10,200	18.11	7.88
			18.18	9.52
			18.20	11.26
		15,350	18.11	7.76
			18.14	9.40
			18.01	11.10
		20,200	18.31	7.74
			18.40	9.54
			18.27	11.28
High	*0.2*	10,200	41.29	19.10
			41.43	21.49
			41.28	24.31
		15,350	41.28	19.21
			41.57	21.60
			41.25	24.18
		20,200	41.87	19.65
			41.51	21.72
			41.45	24.36

APPENDIX B

RAW DATA

Table 8. 0.1 mm (4 mils), PR=0.4, zero inlet preswirl, and 10,200 RPM

	Test Data								Uncertainties							
Freq Hz	Re H_{xx}	Re H_{xy}	Re H_{yx}	Re H_{yy}	Im H_{xx}	Im H_{xy}	Im H_{yx}	Im H_{yy}	Re H_{xx}	Re H_{xy}	Re H_{yx}	Re H_{yy}	Im H_{xx}	Im H_{xy}	Im H_{yx}	Im H_{yy}
9.77	-4.45	0.88	-0.47	-3.67	-0.78	0.02	-0.33	0.64	-0.45	-0.14	-0.33	-0.09	-0.38	-0.25	-0.42	-0.18
19.53	-4.35	1.10	-1.92	-4.02	1.89	-0.53	-0.79	1.23	-0.54	-0.08	-0.22	-0.09	-0.44	-0.08	-0.20	-0.07
29.30	-3.75	1.02	-0.52	-3.66	1.61	0.14	0.41	0.85	-0.10	-0.11	-0.11	-0.05	-0.08	-0.14	-0.09	-0.15
39.06	-3.77	1.07	-0.41	-3.43	2.46	-0.40	0.31	2.86	-0.13	-0.07	-0.11	-0.09	-0.14	-0.08	-0.07	-0.06
48.83	-3.76	1.03	-0.52	-3.61	2.81	-0.76	0.01	3.54	-0.17	-0.09	-0.15	-0.09	-0.15	-0.08	-0.12	-0.09
58.59	-3.31	0.29	-0.16	-3.09	3.53	-0.58	-0.12	4.05	-0.10	-0.20	-0.19	-0.19	-0.12	-0.27	-0.13	-0.25
68.36	-4.14	1.03	-1.02	-3.08	4.20	-0.86	0.44	5.24	-0.30	-0.29	-0.20	-0.29	-0.38	-0.22	-0.26	-0.19
78.13	-2.49	0.80	-0.12	-2.67	5.42	-0.67	-0.13	5.77	-0.09	-0.09	-0.06	-0.06	-0.08	-0.10	-0.07	-0.09
87.89	-1.62	0.58	-0.26	-1.97	5.47	-0.78	-0.07	6.36	-0.07	-0.06	-0.05	-0.08	-0.05	-0.08	-0.03	-0.07
97.66	-1.37	0.44	-0.16	-1.35	5.61	-0.83	-0.29	6.78	-0.10	-0.10	-0.08	-0.08	-0.12	-0.08	-0.07	-0.06
107.42	-2.17	0.55	-0.59	-0.85	5.52	-0.60	-0.30	7.17	-0.18	-0.07	-0.09	-0.06	-0.19	-0.07	-0.16	-0.08
117.19	-1.07	0.35	-0.80	-0.18	6.01	-0.79	-0.39	7.66	-0.09	-0.06	-0.10	-0.06	-0.17	-0.09	-0.16	-0.07
126.95	-0.65	0.25	-0.24	0.44	6.67	-0.81	-0.38	8.41	-0.07	-0.08	-0.07	-0.08	-0.07	-0.13	-0.08	-0.18
136.72	-0.37	0.14	-0.37	1.02	7.15	-0.80	-0.33	8.44	-0.10	-0.08	-0.09	-0.06	-0.10	-0.08	-0.06	-0.08
146.48	1.32	0.11	-1.25	2.78	9.39	-2.66	-1.77	10.44	-0.09	-0.15	-0.10	-0.13	-0.16	-0.08	-0.11	-0.08
156.25	1.43	-0.22	-0.36	1.89	7.15	-0.70	-0.57	8.60	-0.26	-0.14	-0.23	-0.14	-0.35	-0.19	-0.28	-0.18
166.02	-0.14	1.70	1.33	0.33	7.73	-0.06	0.21	8.31	-0.33	-0.61	-0.25	-0.54	-0.36	-0.74	-0.24	-0.49
175.78	1.96	0.06	-0.33	3.00	7.57	-0.48	-0.15	8.81	-0.30	-0.31	-0.24	-0.23	-0.38	-0.37	-0.28	-0.30
185.55	2.56	-0.17	-0.49	3.44	7.36	-0.50	0.13	8.80	-0.11	-0.09	-0.08	-0.10	-0.15	-0.12	-0.11	-0.10
195.31	3.54	0.31	-0.18	3.48	7.14	-0.44	0.47	8.96	-0.09	-0.07	-0.05	-0.06	-0.16	-0.07	-0.09	-0.09
205.08	3.25	0.73	0.27	3.60	6.96	-1.06	-0.08	8.99	-0.16	-0.17	-0.12	-0.14	-0.18	-0.26	-0.13	-0.17
214.84	2.75	-0.75	1.10	5.19	7.39	-0.47	0.27	9.26	-0.05	-0.05	-0.06	-0.06	-0.05	-0.07	-0.04	-0.06
224.61	3.48	0.42	0.72	5.88	7.12	-0.70	-0.05	9.36	-0.06	-0.06	-0.05	-0.06	-0.07	-0.07	-0.04	-0.06
234.38	3.34	-0.12	0.92	6.27	7.49	-0.15	0.31	8.12	-0.05	-0.07	-0.07	-0.06	-0.03	-0.07	-0.04	-0.06
244.14	4.16	0.54	1.25	5.85	7.73	-0.08	0.08	8.29	-0.06	-0.06	-0.06	-0.09	-0.10	-0.07	-0.08	-0.06

Table 9. 0.1 mm (4 mils), PR=0.4, zero inlet preswirl, and 15,350 RPM

	Test Data								Uncertainties							
Freq Hz	Re H_{xx}	Re H_{xy}	Re H_{yx}	Re H_{yy}	Im H_{xx}	Im H_{xy}	Im H_{yx}	Im H_{yy}	Re H_{xx}	Re H_{xy}	Re H_{yx}	Re H_{yy}	Im H_{xx}	Im H_{xy}	Im H_{yx}	Im H_{yy}
9.77	-4.91	2.31	-2.19	-5.05	-0.14	-0.10	-0.38	0.98	-0.38	-0.18	-0.25	-0.13	-0.35	-0.13	-0.36	-0.08
19.53	-5.45	2.72	-3.11	-5.63	2.19	-0.74	-0.16	1.75	-0.52	-0.15	-0.22	-0.06	-0.49	-0.15	-0.25	-0.08
29.30	-4.57	2.20	-1.67	-4.79	2.67	-0.30	0.62	1.77	-0.09	-0.10	-0.08	-0.09	-0.08	-0.13	-0.09	-0.15
39.06	-4.34	2.06	-1.58	-4.23	3.79	-0.79	0.50	4.04	-0.13	-0.07	-0.11	-0.07	-0.13	-0.09	-0.11	-0.05
48.83	-4.01	2.19	-1.67	-4.14	4.22	-0.85	0.32	4.64	-0.19	-0.07	-0.14	-0.06	-0.13	-0.12	-0.08	-0.09
58.59	-3.41	1.54	-1.33	-3.57	4.79	-0.59	0.44	5.32	-0.08	-0.15	-0.18	-0.23	-0.14	-0.18	-0.16	-0.14
68.36	-4.26	2.38	-2.04	-3.21	5.82	-1.36	0.95	6.80	-0.28	-0.16	-0.25	-0.15	-0.35	-0.21	-0.24	-0.22
78.13	-2.03	1.71	-1.16	-2.66	6.79	-1.38	0.36	7.27	-0.09	-0.06	-0.06	-0.10	-0.11	-0.10	-0.08	-0.11
87.89	-1.33	1.46	-1.11	-2.03	6.97	-1.44	0.69	7.91	-0.08	-0.10	-0.05	-0.06	-0.07	-0.10	-0.06	-0.10
97.66	-0.58	0.99	-1.03	-0.99	7.16	-1.45	0.20	8.52	-0.09	-0.05	-0.06	-0.07	-0.09	-0.08	-0.08	-0.07
107.42	-1.28	1.36	-1.31	-0.20	6.98	-1.08	0.19	8.89	-0.12	-0.12	-0.10	-0.09	-0.15	-0.12	-0.11	-0.11
117.19	-0.19	1.03	-1.37	0.52	7.41	-1.33	0.04	9.34	-0.10	-0.07	-0.10	-0.06	-0.14	-0.07	-0.13	-0.08
126.95	0.58	0.64	-0.85	1.46	8.01	-1.60	0.25	10.01	-0.10	-0.13	-0.07	-0.08	-0.10	-0.22	-0.07	-0.11
136.72	0.72	0.77	-1.12	2.18	8.43	-1.39	0.21	9.86	-0.07	-0.06	-0.04	-0.08	-0.05	-0.07	-0.09	-0.05
146.48	2.67	-0.26	-1.90	4.90	10.31	-2.77	-0.82	11.21	-0.11	-0.08	-0.06	-0.13	-0.13	-0.14	-0.09	-0.12
156.25	3.04	0.26	-1.16	3.15	8.26	-1.28	-0.08	9.97	-0.20	-0.09	-0.15	-0.11	-0.23	-0.08	-0.20	-0.11
166.02	1.84	2.03	0.55	1.63	8.98	-0.97	0.60	9.64	-0.09	-0.09	-0.07	-0.11	-0.09	-0.09	-0.05	-0.10
175.78	3.79	0.18	-1.11	4.37	8.44	-1.24	0.29	10.27	-0.06	-0.09	-0.08	-0.08	-0.09	-0.10	-0.11	-0.11
185.55	4.37	0.10	-1.01	5.15	8.10	-1.10	1.06	9.84	-0.07	-0.08	-0.08	-0.08	-0.14	-0.09	-0.07	-0.09
195.31	5.53	0.76	-0.72	5.33	7.77	-0.94	1.27	10.01	-0.10	-0.09	-0.07	-0.05	-0.09	-0.06	-0.07	-0.06
205.08	5.28	0.68	-0.31	5.78	7.63	-1.84	0.45	10.19	-0.15	-0.17	-0.10	-0.11	-0.17	-0.18	-0.12	-0.09
214.84	4.67	-0.47	0.46	7.08	7.92	-0.89	1.00	10.14	-0.09	-0.05	-0.06	-0.07	-0.08	-0.12	-0.06	-0.08
224.61	5.44	0.62	0.41	7.79	7.57	-0.87	0.64	9.72	-0.08	-0.07	-0.06	-0.07	-0.09	-0.08	-0.04	-0.05
234.38	5.22	0.16	0.82	8.29	7.56	-0.50	0.83	8.60	-0.09	-0.08	-0.07	-0.09	-0.07	-0.10	-0.05	-0.09
244.14	5.89	0.74	0.91	7.89	7.79	-0.64	0.46	8.54	-0.13	-0.18	-0.07	-0.11	-0.15	-0.20	-0.08	-0.13

Table 10. 0.1 mm (4 mils), PR=0.4, zero inlet preswirl, and 20,200 RPM

	Test Data								Uncertainties							
Freq Hz	Re H_{xx}	Re H_{xy}	Re H_{yx}	Re H_{yy}	Im H_{xx}	Im H_{xy}	Im H_{yx}	Im H_{yy}	Re H_{xx}	Re H_{xy}	Re H_{yx}	Re H_{yy}	Im H_{xx}	Im H_{xy}	Im H_{yx}	Im H_{yy}
9.77	-5.01	4.37	-4.19	-4.73	0.11	-0.28	-0.16	1.06	-0.49	-0.13	-0.32	-0.12	-0.39	-0.13	-0.43	-0.08
19.53	-4.94	4.64	-5.22	-5.05	2.35	-0.90	0.39	1.81	-0.51	-0.09	-0.20	-0.09	-0.44	-0.11	-0.20	-0.12
29.30	-4.00	4.07	-3.71	-4.43	3.13	-1.03	1.29	2.51	-0.11	-0.20	-0.10	-0.10	-0.08	-0.12	-0.10	-0.19
39.06	-3.40	3.80	-3.54	-3.43	4.22	-1.73	1.30	4.64	-0.11	-0.09	-0.09	-0.10	-0.07	-0.10	-0.07	-0.07
48.83	-4.50	4.80	-3.57	-3.36	5.51	-0.79	1.01	5.41	-0.73	-0.55	-0.23	-0.23	-0.70	-0.55	-0.19	-0.12
58.59	-2.39	2.75	-2.77	-2.55	5.29	-1.64	1.13	5.94	-0.08	-0.13	-0.18	-0.20	-0.13	-0.14	-0.17	-0.15
68.36	-3.07	3.63	-3.52	-1.53	5.88	-1.86	2.00	6.59	-0.30	-0.19	-0.22	-0.19	-0.39	-0.16	-0.25	-0.18
78.13	-0.81	2.77	-2.56	-1.19	7.04	-2.18	1.38	7.54	-0.07	-0.04	-0.06	-0.04	-0.10	-0.08	-0.08	-0.13
87.89	0.00	2.55	-2.50	-0.30	7.16	-2.28	1.55	8.10	-0.05	-0.06	-0.06	-0.10	-0.05	-0.08	-0.03	-0.06
97.66	0.72	2.19	-2.27	0.63	7.10	-2.33	1.41	8.39	-0.42	-0.42	-0.11	-0.13	-0.42	-0.42	-0.11	-0.14
107.42	0.20	2.23	-2.36	1.18	6.96	-2.22	1.51	8.57	-0.16	-0.07	-0.10	-0.06	-0.11	-0.07	-0.14	-0.06
117.19	1.23	1.86	-2.35	1.90	7.31	-2.41	1.33	9.07	-0.09	-0.08	-0.09	-0.10	-0.18	-0.06	-0.10	-0.11
126.95	1.99	1.38	-1.64	2.83	7.81	-2.16	1.46	9.42	-0.08	-0.09	-0.09	-0.13	-0.09	-0.12	-0.09	-0.12
136.72	2.23	1.45	-1.59	3.65	8.22	-2.26	1.23	9.42	-0.07	-0.10	-0.07	-0.06	-0.07	-0.09	-0.07	-0.08
146.48	1.84	2.34	0.14	4.42	9.31	-2.56	0.37	10.29	-0.17	-0.27	-0.24	-0.39	-0.24	-0.27	-0.41	-0.45
156.25	4.46	0.75	-1.87	4.88	7.60	-2.28	0.95	9.41	-0.16	-0.12	-0.12	-0.07	-0.22	-0.14	-0.22	-0.12
166.02	3.30	2.42	0.13	3.29	8.25	-1.89	1.63	8.80	-0.11	-0.13	-0.08	-0.09	-0.09	-0.13	-0.06	-0.12
175.78	5.44	0.30	-1.86	6.49	8.16	-2.33	0.81	9.54	-0.11	-0.09	-0.10	-0.08	-0.16	-0.15	-0.12	-0.13
185.55	5.68	0.58	-1.54	6.48	7.40	-1.97	1.63	8.90	-0.06	-0.08	-0.06	-0.07	-0.09	-0.07	-0.06	-0.06
195.31	6.75	0.93	-1.00	6.64	7.06	-1.57	1.89	8.78	-0.15	-0.10	-0.08	-0.08	-0.17	-0.14	-0.09	-0.11
205.08	6.54	1.10	-0.47	6.60	6.93	-2.73	1.16	8.92	-0.11	-0.21	-0.10	-0.14	-0.22	-0.15	-0.13	-0.15
214.84	5.72	0.04	0.29	7.79	6.98	-1.78	1.50	8.95	-0.07	-0.07	-0.05	-0.05	-0.05	-0.08	-0.05	-0.07
224.61	6.38	0.89	0.16	8.52	6.82	-1.89	1.00	8.98	-0.06	-0.08	-0.05	-0.05	-0.08	-0.06	-0.06	-0.07
234.38	6.22	0.26	0.52	9.20	6.91	-1.27	1.39	7.67	-0.06	-0.08	-0.05	-0.07	-0.05	-0.06	-0.04	-0.09
244.14	7.08	0.78	0.89	8.85	7.01	-1.07	0.92	7.52	-0.06	-0.08	-0.07	-0.07	-0.10	-0.08	-0.05	-0.10

Table 11. 0.1 mm (4 mils), PR=0.5, zero inlet preswirl, and 10,200 RPM

	Test Data								Uncertainties							
Freq Hz	Re H_{xx}	Re H_{xy}	Re H_{yx}	Re H_{yy}	Im H_{xx}	Im H_{xy}	Im H_{yx}	Im H_{yy}	Re H_{xx}	Re H_{xy}	Re H_{yx}	Re H_{yy}	Im H_{xx}	Im H_{xy}	Im H_{yx}	Im H_{yy}
9.77	-3.24	0.58	-0.89	-2.60	-0.35	0.10	-0.52	0.93	-0.50	-0.28	-0.33	-0.20	-0.50	-0.31	-0.48	-0.20
19.53	-3.50	1.42	-1.97	-3.30	1.54	-0.30	-0.24	1.07	-0.54	-0.13	-0.19	-0.07	-0.50	-0.11	-0.25	-0.10
29.30	-2.46	0.81	-0.79	-2.60	2.04	0.01	0.31	1.10	-0.09	-0.11	-0.09	-0.11	-0.14	-0.19	-0.11	-0.18
39.06	-2.12	0.72	-0.80	-2.18	2.71	-0.33	0.29	2.92	-0.10	-0.12	-0.06	-0.09	-0.13	-0.15	-0.11	-0.10
48.83	-2.48	0.83	-0.81	-2.50	2.98	-0.50	0.02	3.52	-0.32	-0.15	-0.22	-0.10	-0.18	-0.06	-0.08	-0.09
58.59	-1.98	0.87	-0.46	-2.47	3.71	-0.63	-0.06	4.20	-0.11	-0.40	-0.17	-0.33	-0.13	-0.13	-0.12	-0.21
68.36	-2.86	1.05	-1.27	-1.98	4.64	-0.80	0.38	5.29	-0.26	-0.15	-0.20	-0.20	-0.32	-0.19	-0.20	-0.13
78.13	-1.28	0.56	-0.55	-1.50	5.30	-0.59	-0.03	5.80	-0.07	-0.12	-0.07	-0.08	-0.09	-0.13	-0.07	-0.10
87.89	-0.89	0.46	-0.57	-1.03	5.77	-0.53	0.23	6.30	-0.05	-0.08	-0.05	-0.09	-0.07	-0.16	-0.04	-0.10
97.66	-0.42	0.44	-0.47	-0.31	6.05	-0.62	0.06	6.82	-0.10	-0.08	-0.06	-0.07	-0.09	-0.11	-0.06	-0.08
107.42	-1.15	0.57	-0.54	0.18	6.19	-0.56	-0.03	7.22	-0.13	-0.07	-0.09	-0.05	-0.14	-0.09	-0.14	-0.08
117.19	0.07	0.35	-0.84	0.80	6.43	-0.77	-0.25	7.67	-0.16	-0.08	-0.09	-0.06	-0.16	-0.10	-0.12	-0.08
126.95	0.44	0.41	-0.27	1.21	7.12	-0.62	-0.04	8.27	-0.08	-0.19	-0.07	-0.15	-0.11	-0.12	-0.07	-0.07
136.72	0.75	0.05	-0.41	1.82	7.58	-0.76	-0.14	8.60	-0.10	-0.10	-0.07	-0.06	-0.06	-0.09	-0.06	-0.07
146.48	0.90	-0.11	0.24	2.54	8.37	0.22	0.35	8.19	-0.09	-0.10	-0.08	-0.10	-0.14	-0.12	-0.10	-0.07
156.25	2.57	-0.48	-0.79	3.22	7.79	-0.97	-0.52	9.06	-0.16	-0.11	-0.13	-0.14	-0.25	-0.12	-0.22	-0.08
166.02	1.48	1.51	1.04	1.23	8.38	0.04	0.46	8.37	-0.09	-0.14	-0.07	-0.12	-0.13	-0.12	-0.08	-0.12
175.78	1.33	0.64	0.87	3.28	8.12	-0.77	-0.08	9.16	-0.10	-0.07	-0.09	-0.09	-0.09	-0.11	-0.08	-0.13
185.55	3.76	-0.22	-0.54	4.18	9.05	-1.03	-0.30	9.44	-0.08	-0.10	-0.06	-0.09	-0.08	-0.08	-0.06	-0.07
195.31	4.13	0.55	0.07	3.90	8.58	-0.42	0.27	8.99	-0.06	-0.06	-0.05	-0.07	-0.07	-0.09	-0.07	-0.08
205.08	4.12	0.63	0.46	4.06	8.85	-1.14	-0.81	9.52	-0.13	-0.17	-0.10	-0.12	-0.21	-0.18	-0.13	-0.12
214.84	4.06	-0.62	0.42	5.63	8.74	-0.95	-0.01	10.14	-0.04	-0.07	-0.05	-0.05	-0.07	-0.07	-0.05	-0.07
224.61	4.62	0.79	0.49	5.72	8.77	-1.01	-0.13	10.05	-0.06	-0.07	-0.04	-0.05	-0.08	-0.06	-0.05	-0.05
234.38	4.68	-0.06	0.73	6.51	9.16	-0.99	0.23	9.70	-0.05	-0.07	-0.05	-0.07	-0.06	-0.08	-0.05	-0.06
244.14	5.56	-0.07	1.23	6.60	9.57	-0.80	-0.02	9.94	-0.06	-0.06	-0.05	-0.09	-0.07	-0.08	-0.04	-0.09

Table 12. 0.1 mm (4 mils), PR=0.5, zero inlet preswirl, and 15,350 RPM

	Test Data								Uncertainties							
Freq Hz	Re H_{xx}	Re H_{xy}	Re H_{yx}	Re H_{yy}	Im H_{xx}	Im H_{xy}	Im H_{yx}	Im H_{yy}	Re H_{xx}	Re H_{xy}	Re H_{yx}	Re H_{yy}	Im H_{xx}	Im H_{xy}	Im H_{yx}	Im H_{yy}
9.77	-4.13	2.41	-2.12	-4.20	0.04	0.13	-0.58	0.90	-0.38	-0.17	-0.32	-0.15	-0.38	-0.23	-0.41	-0.14
19.53	-4.46	2.38	-3.14	-4.41	1.96	-0.57	-0.21	1.46	-0.53	-0.14	-0.21	-0.07	-0.47	-0.13	-0.22	-0.08
29.30	-3.69	2.05	-1.79	-3.85	2.39	-0.03	0.54	1.57	-0.09	-0.11	-0.10	-0.11	-0.10	-0.10	-0.10	-0.11
39.06	-3.55	1.96	-1.79	-3.24	3.42	-0.62	0.46	3.67	-0.08	-0.07	-0.08	-0.08	-0.11	-0.09	-0.07	-0.09
48.83	-3.34	2.10	-1.75	-3.38	3.92	-0.82	0.31	4.39	-0.21	-0.06	-0.13	-0.08	-0.16	-0.10	-0.11	-0.10
58.59	-2.61	1.44	-1.56	-2.81	4.54	-0.70	0.21	5.05	-0.09	-0.24	-0.18	-0.18	-0.15	-0.14	-0.12	-0.17
68.36	-3.70	2.36	-2.22	-2.72	5.39	-1.13	0.88	6.04	-0.32	-0.20	-0.24	-0.10	-0.34	-0.14	-0.22	-0.21
78.13	-1.84	1.61	-1.63	-2.16	6.38	-1.09	0.52	6.85	-0.07	-0.07	-0.06	-0.07	-0.10	-0.09	-0.08	-0.07
87.89	-0.94	1.37	-1.58	-1.52	6.82	-1.18	0.91	7.67	-0.04	-0.05	-0.04	-0.05	-0.07	-0.07	-0.04	-0.07
97.66	-0.30	1.24	-1.14	-0.47	7.20	-1.15	0.52	8.42	-0.11	-0.09	-0.08	-0.07	-0.10	-0.10	-0.06	-0.07
107.42	-0.72	1.37	-1.36	0.22	7.13	-1.06	0.27	8.77	-0.17	-0.06	-0.09	-0.06	-0.11	-0.07	-0.13	-0.09
117.19	0.11	1.17	-1.65	0.97	7.55	-1.29	0.06	9.18	-0.13	-0.08	-0.10	-0.05	-0.14	-0.06	-0.14	-0.08
126.95	0.98	0.95	-1.04	1.82	8.15	-1.25	0.33	9.94	-0.08	-0.15	-0.06	-0.12	-0.11	-0.10	-0.07	-0.07
136.72	1.19	0.90	-1.14	2.40	8.55	-1.38	0.16	9.88	-0.09	-0.08	-0.04	-0.06	-0.09	-0.08	-0.07	-0.07
146.48	1.58	0.66	-0.89	3.24	9.46	-0.74	0.84	9.51	-0.09	-0.10	-0.10	-0.09	-0.10	-0.10	-0.09	-0.11
156.25	3.70	-0.06	-1.84	4.14	8.42	-1.37	-0.09	10.09	-0.19	-0.11	-0.14	-0.07	-0.26	-0.13	-0.23	-0.09
166.02	2.51	2.00	0.03	2.06	9.15	-0.75	0.58	9.74	-0.08	-0.09	-0.12	-0.19	-0.09	-0.12	-0.09	-0.15
175.78	3.37	0.29	-0.72	4.90	9.10	-1.65	-0.06	10.64	-0.12	-0.08	-0.12	-0.13	-0.13	-0.12	-0.09	-0.07
185.55	4.78	0.14	-1.31	5.42	9.06	-1.47	0.57	10.13	-0.10	-0.09	-0.07	-0.07	-0.10	-0.07	-0.07	-0.06
195.31	5.57	0.76	-0.76	5.29	8.33	-0.89	1.13	9.94	-0.10	-0.09	-0.09	-0.07	-0.12	-0.09	-0.11	-0.07
205.08	5.66	0.92	-0.31	5.51	8.57	-2.16	0.10	10.40	-0.16	-0.29	-0.11	-0.18	-0.23	-0.26	-0.16	-0.13
214.84	4.87	-0.52	0.24	7.00	8.67	-1.18	0.78	10.45	-0.04	-0.08	-0.05	-0.06	-0.08	-0.08	-0.05	-0.07
224.61	5.61	0.85	0.22	7.33	8.45	-1.45	0.63	10.67	-0.07	-0.06	-0.06	-0.05	-0.10	-0.06	-0.04	-0.06
234.38	5.72	0.02	0.57	8.32	8.60	-1.22	0.76	9.71	-0.06	-0.09	-0.06	-0.11	-0.03	-0.14	-0.04	-0.10
244.14	6.37	0.31	0.70	8.23	9.02	-1.07	0.36	9.53	-0.12	-0.15	-0.08	-0.08	-0.10	-0.16	-0.06	-0.12

Table 13. 0.1 mm (4 mils), PR=0.5, zero inlet preswirl, and 20,200 RPM

	Test Data								Uncertainties							
Freq Hz	Re H_{xx}	Re H_{xy}	Re H_{yx}	Re H_{yy}	Im H_{xx}	Im H_{xy}	Im H_{yx}	Im H_{yy}	Re H_{xx}	Re H_{xy}	Re H_{yx}	Re H_{yy}	Im H_{xx}	Im H_{xy}	Im H_{yx}	Im H_{yy}
9.77	-4.21	4.31	-4.08	-3.95	0.14	-0.55	-0.29	1.16	-0.41	-0.09	-0.25	-0.08	-0.32	-0.13	-0.37	-0.11
19.53	-4.14	4.29	-5.30	-4.12	2.55	-1.23	-0.28	2.21	-0.49	-0.07	-0.23	-0.10	-0.43	-0.15	-0.20	-0.10
29.30	-3.28	4.08	-3.62	-3.69	2.75	-0.89	1.06	2.06	-0.08	-0.08	-0.06	-0.07	-0.11	-0.15	-0.10	-0.13
39.06	-2.72	3.79	-3.67	-2.85	3.74	-1.34	1.17	4.26	-0.12	-0.08	-0.11	-0.07	-0.07	-0.10	-0.04	-0.08
48.83	-3.01	3.35	-3.49	-2.52	4.37	-1.99	1.02	4.72	-0.63	-0.53	-0.24	-0.29	-0.64	-0.60	-0.21	-0.18
58.59	-1.86	2.82	-2.94	-1.98	4.75	-1.65	1.11	5.63	-0.09	-0.17	-0.19	-0.15	-0.14	-0.16	-0.15	-0.19
68.36	-2.52	3.49	-3.71	-1.18	5.75	-2.67	1.63	7.03	-0.29	-0.11	-0.21	-0.09	-0.38	-0.19	-0.26	-0.14
78.13	-0.50	2.82	-2.81	-0.89	6.45	-2.05	1.28	7.30	-0.07	-0.10	-0.05	-0.09	-0.09	-0.11	-0.08	-0.11
87.89	0.31	2.52	-2.70	-0.05	6.66	-2.17	1.49	7.86	-0.05	-0.04	-0.07	-0.08	-0.04	-0.09	-0.04	-0.08
97.66	0.87	2.54	-2.37	0.75	6.70	-2.21	1.22	8.12	-0.18	-0.18	-0.08	-0.06	-0.20	-0.25	-0.05	-0.08
107.42	0.22	2.30	-2.64	1.50	6.46	-2.05	1.26	8.27	-0.11	-0.08	-0.08	-0.05	-0.14	-0.06	-0.10	-0.07
117.19	1.10	2.13	-2.70	1.99	7.01	-2.33	1.13	8.57	-0.11	-0.09	-0.11	-0.07	-0.13	-0.05	-0.12	-0.08
126.95	1.90	1.94	-1.85	2.67	7.68	-2.37	1.45	9.25	-0.06	-0.08	-0.06	-0.05	-0.10	-0.12	-0.07	-0.07
136.72	2.35	1.58	-1.91	3.70	8.00	-2.30	1.13	9.45	-0.08	-0.08	-0.08	-0.09	-0.05	-0.10	-0.08	-0.08
146.48	2.11	2.33	-0.89	4.75	8.91	-1.45	1.35	9.32	-0.08	-0.14	-0.11	-0.06	-0.10	-0.08	-0.10	-0.12
156.25	4.41	0.87	-2.15	5.04	7.47	-2.22	0.93	9.35	-0.13	-0.08	-0.10	-0.10	-0.19	-0.09	-0.19	-0.11
166.02	3.76	2.38	-0.68	3.36	8.01	-1.38	1.70	8.91	-0.09	-0.10	-0.10	-0.14	-0.11	-0.08	-0.08	-0.10
175.78	4.59	0.95	-1.56	6.01	7.71	-2.13	0.95	9.42	-0.08	-0.13	-0.08	-0.10	-0.15	-0.11	-0.09	-0.08
185.55	5.69	0.66	-2.02	6.66	7.52	-1.99	1.71	9.05	-0.09	-0.06	-0.09	-0.07	-0.11	-0.07	-0.08	-0.07
195.31	6.53	1.22	-1.21	6.64	6.64	-1.45	2.23	8.64	-0.08	-0.06	-0.06	-0.07	-0.09	-0.09	-0.09	-0.07
205.08	6.33	1.29	-0.77	6.72	6.51	-2.43	1.45	8.61	-0.14	-0.14	-0.11	-0.17	-0.18	-0.22	-0.14	-0.17
214.84	5.45	0.18	0.10	7.89	6.99	-1.42	1.65	8.91	-0.05	-0.07	-0.04	-0.05	-0.05	-0.06	-0.03	-0.07
224.61	6.16	1.19	-0.28	8.38	6.58	-1.85	1.31	9.23	-0.06	-0.05	-0.03	-0.06	-0.11	-0.07	-0.06	-0.05
234.38	6.07	0.49	0.38	9.23	7.03	-1.11	1.63	7.85	-0.05	-0.05	-0.05	-0.05	-0.03	-0.08	-0.03	-0.07
244.14	7.01	1.31	0.78	8.83	6.93	-0.78	1.17	7.64	-0.05	-0.10	-0.04	-0.06	-0.08	-0.07	-0.05	-0.09

Table 14. 0.1 mm (4 mils), PR=0.6, zero inlet preswirl, and 10,200 RPM

	Test Data								Uncertainties							
Freq Hz	Re H_{xx}	Re H_{xy}	Re H_{yx}	Re H_{yy}	Im H_{xx}	Im H_{xy}	Im H_{yx}	Im H_{yy}	Re H_{xx}	Re H_{xy}	Re H_{yx}	Re H_{yy}	Im H_{xx}	Im H_{xy}	Im H_{yx}	Im H_{yy}
9.77	-3.75	1.34	-0.49	-2.69	-0.06	-0.23	-0.89	0.82	-0.44	-0.25	-0.31	-0.17	-0.40	-0.19	-0.42	-0.14
19.53	-2.62	0.29	-2.73	-2.06	1.20	-0.36	-0.40	0.86	-0.57	-0.24	-0.23	-0.16	-0.49	-0.21	-0.23	-0.12
29.30	-2.75	1.02	-0.72	-2.45	1.46	0.47	0.30	0.34	-0.10	-0.18	-0.09	-0.16	-0.09	-0.13	-0.07	-0.12
39.06	-2.57	1.02	-0.81	-2.06	2.21	-0.26	0.09	2.35	-0.11	-0.10	-0.09	-0.09	-0.06	-0.14	-0.06	-0.11
48.83	-2.75	0.88	-1.01	-2.42	2.45	-0.43	0.04	2.67	-0.17	-0.10	-0.15	-0.07	-0.15	-0.09	-0.11	-0.11
58.59	-2.65	0.69	-0.45	-2.34	3.06	-0.45	0.06	3.11	-0.10	-0.17	-0.18	-0.24	-0.12	-0.18	-0.15	-0.20
68.36	-3.58	1.55	-1.20	-2.36	3.68	-0.65	0.56	4.51	-0.29	-0.23	-0.26	-0.16	-0.32	-0.18	-0.22	-0.17
78.13	-2.00	0.81	-0.52	-1.83	4.63	-0.53	0.05	5.07	-0.07	-0.10	-0.06	-0.08	-0.08	-0.11	-0.07	-0.11
87.89	-1.35	0.62	-0.56	-1.34	4.89	-0.67	0.12	5.77	-0.07	-0.05	-0.05	-0.08	-0.05	-0.09	-0.03	-0.06
97.66	-1.08	0.58	-0.40	-0.90	5.09	-0.80	-0.03	6.27	-0.10	-0.06	-0.06	-0.05	-0.06	-0.15	-0.05	-0.07
107.42	-1.80	0.73	-0.73	-0.37	5.13	-0.49	-0.13	6.47	-0.15	-0.10	-0.09	-0.08	-0.12	-0.09	-0.12	-0.08
117.19	-1.01	0.61	-0.90	0.08	5.70	-0.80	-0.41	7.10	-0.09	-0.09	-0.11	-0.08	-0.18	-0.08	-0.15	-0.06
126.95	-0.69	0.55	-0.33	0.52	6.30	-0.78	-0.19	7.57	-0.06	-0.11	-0.07	-0.09	-0.08	-0.18	-0.06	-0.10
136.72	-0.38	0.34	-0.54	1.15	6.75	-0.73	-0.22	7.92	-0.07	-0.05	-0.07	-0.06	-0.06	-0.08	-0.05	-0.07
146.48	-0.98	0.80	0.96	1.99	7.81	0.17	-0.76	8.84	-0.13	-0.12	-0.11	-0.08	-0.15	-0.14	-0.13	-0.11
156.25	1.45	-0.08	-0.80	2.15	6.74	-0.65	-0.43	8.14	-0.20	-0.14	-0.15	-0.12	-0.22	-0.17	-0.20	-0.16
166.02	-0.18	1.74	1.20	0.01	7.85	-0.53	-0.22	8.60	-0.21	-0.40	-0.25	-0.36	-0.22	-0.30	-0.22	-0.33
175.78	0.66	0.47	0.32	2.49	6.70	-0.43	0.48	8.54	-0.17	-0.16	-0.19	-0.15	-0.19	-0.19	-0.19	-0.19
185.55	2.49	0.05	-0.91	3.24	7.90	-1.00	-0.07	9.09	-0.07	-0.10	-0.09	-0.10	-0.10	-0.09	-0.07	-0.10
195.31	3.29	0.62	-0.38	3.20	7.20	-0.42	0.54	8.95	-0.09	-0.12	-0.07	-0.08	-0.08	-0.07	-0.08	-0.05
205.08	2.97	0.51	-0.12	3.55	7.28	-1.47	-0.16	9.43	-0.17	-0.19	-0.09	-0.11	-0.17	-0.19	-0.11	-0.10
214.84	2.37	-0.68	0.54	4.86	7.83	-0.62	0.28	9.57	-0.05	-0.07	-0.04	-0.07	-0.07	-0.07	-0.04	-0.07
224.61	3.17	0.85	0.38	4.99	7.74	-1.06	0.17	9.82	-0.06	-0.06	-0.04	-0.05	-0.08	-0.06	-0.07	-0.05
234.38	3.11	-0.01	0.70	5.80	8.09	-0.59	0.41	8.92	-0.05	-0.08	-0.06	-0.07	-0.06	-0.08	-0.04	-0.05
244.14	3.95	0.27	1.00	5.69	8.50	-0.37	0.12	9.24	-0.06	-0.07	-0.05	-0.06	-0.07	-0.06	-0.07	-0.11

Table 15. 0.1 mm (4 mils), PR=0.6, zero inlet preswirl, and 15,350 RPM

	Test Data								Uncertainties							
Freq Hz	Re H_{xx}	Re H_{xy}	Re H_{yx}	Re H_{yy}	Im H_{xx}	Im H_{xy}	Im H_{yx}	Im H_{yy}	Re H_{xx}	Re H_{xy}	Re H_{yx}	Re H_{yy}	Im H_{xx}	Im H_{xy}	Im H_{yx}	Im H_{yy}
9.77	-4.05	2.34	-1.87	-3.48	0.17	0.14	-0.74	0.75	-0.40	-0.20	-0.27	-0.13	-0.39	-0.13	-0.41	-0.10
19.53	-3.37	2.02	-3.81	-3.31	1.87	-0.33	-0.29	1.28	-0.52	-0.19	-0.19	-0.12	-0.54	-0.14	-0.27	-0.09
29.30	-3.00	2.08	-1.93	-3.22	2.19	-0.05	0.48	1.46	-0.11	-0.13	-0.11	-0.12	-0.12	-0.16	-0.09	-0.13
39.06	-2.73	1.97	-1.97	-2.74	3.16	-0.75	0.28	3.55	-0.10	-0.09	-0.09	-0.08	-0.11	-0.09	-0.05	-0.06
48.83	-2.79	2.05	-2.04	-2.72	3.58	-0.78	0.22	4.01	-0.21	-0.10	-0.13	-0.08	-0.14	-0.12	-0.08	-0.09
58.59	-2.35	2.02	-1.71	-2.59	4.07	-0.62	0.22	4.50	-0.10	-0.15	-0.18	-0.17	-0.13	-0.21	-0.14	-0.22
68.36	-3.49	2.68	-2.36	-2.30	4.84	-0.87	0.81	5.54	-0.27	-0.11	-0.24	-0.25	-0.37	-0.19	-0.24	-0.21
78.13	-1.62	1.85	-1.79	-1.95	5.82	-1.10	0.54	6.24	-0.07	-0.08	-0.05	-0.07	-0.10	-0.05	-0.07	-0.06
87.89	-0.95	1.53	-1.72	-1.50	6.32	-1.25	0.99	7.25	-0.08	-0.07	-0.08	-0.08	-0.06	-0.07	-0.03	-0.07
97.66	-0.36	1.32	-1.13	-0.47	6.64	-1.24	0.53	7.99	-0.09	-0.07	-0.08	-0.06	-0.05	-0.07	-0.05	-0.06
107.42	-0.96	1.60	-1.44	0.24	6.63	-1.01	0.30	8.30	-0.11	-0.08	-0.08	-0.08	-0.12	-0.11	-0.14	-0.08
117.19	0.10	1.39	-1.81	0.89	7.14	-1.25	0.08	8.81	-0.14	-0.05	-0.07	-0.06	-0.17	-0.09	-0.14	-0.08
126.95	0.76	1.26	-1.18	1.80	7.67	-1.12	0.32	9.23	-0.09	-0.11	-0.07	-0.09	-0.14	-0.23	-0.08	-0.19
136.72	1.08	1.08	-1.26	2.28	8.27	-1.39	0.31	9.49	-0.08	-0.07	-0.05	-0.07	-0.08	-0.09	-0.06	-0.06
146.48	1.38	0.85	-0.31	2.66	9.01	-0.43	0.61	9.89	-0.10	-0.06	-0.07	-0.07	-0.10	-0.08	-0.10	-0.10
156.25	3.31	0.33	-1.70	3.79	8.11	-1.59	0.21	9.95	-0.20	-0.09	-0.10	-0.15	-0.17	-0.12	-0.21	-0.08
166.02	1.76	2.08	0.37	1.90	8.93	-1.18	0.69	9.55	-0.09	-0.21	-0.10	-0.12	-0.13	-0.19	-0.08	-0.18
175.78	2.79	0.74	-0.54	4.46	7.85	-0.97	0.99	9.80	-0.12	-0.09	-0.11	-0.07	-0.10	-0.11	-0.09	-0.10
185.55	4.55	0.35	-1.66	5.09	8.80	-1.66	0.63	10.24	-0.08	-0.06	-0.05	-0.07	-0.12	-0.11	-0.08	-0.09
195.31	5.21	0.77	-0.92	5.11	8.18	-1.09	1.22	10.13	-0.09	-0.06	-0.08	-0.06	-0.09	-0.09	-0.07	-0.08
205.08	5.05	1.26	-0.58	5.15	8.46	-1.99	0.18	10.49	-0.10	-0.24	-0.10	-0.19	-0.21	-0.11	-0.14	-0.06
214.84	4.53	-0.39	0.01	6.85	8.49	-1.14	0.97	10.44	-0.06	-0.05	-0.08	-0.05	-0.08	-0.09	-0.05	-0.08
224.61	5.23	0.93	0.12	7.16	8.28	-1.34	0.82	10.72	-0.09	-0.07	-0.04	-0.05	-0.11	-0.07	-0.04	-0.07
234.38	5.20	0.10	0.37	8.10	8.53	-0.92	0.86	9.66	-0.06	-0.09	-0.04	-0.06	-0.05	-0.08	-0.04	-0.10
244.14	5.85	0.56	0.67	7.79	8.92	-0.89	0.47	9.48	-0.13	-0.11	-0.07	-0.11	-0.10	-0.18	-0.09	-0.13

Table 16. 0.1 mm (4 mils), PR=0.6, zero inlet preswirl, and 20,200 RPM

	Test Data								Uncertainties							
Freq Hz	Re H_{xx}	Re H_{xy}	Re H_{yx}	Re H_{yy}	Im H_{xx}	Im H_{xy}	Im H_{yx}	Im H_{yy}	Re H_{xx}	Re H_{xy}	Re H_{yx}	Re H_{yy}	Im H_{xx}	Im H_{xy}	Im H_{yx}	Im H_{yy}
9.77	-3.60	4.96	-4.32	-3.35	0.17	-0.40	-0.36	1.11	-0.45	-0.29	-0.26	-0.17	-0.55	-0.20	-0.42	-0.12
19.53	-3.11	4.75	-5.72	-3.49	1.82	-0.80	0.50	1.45	-0.54	-0.13	-0.21	-0.10	-0.46	-0.14	-0.18	-0.09
29.30	-2.57	4.36	-3.91	-2.86	2.52	-0.65	1.12	1.88	-0.10	-0.08	-0.10	-0.09	-0.10	-0.15	-0.09	-0.13
39.06	-2.26	4.08	-3.89	-2.18	3.50	-1.42	1.18	4.03	-0.07	-0.09	-0.10	-0.07	-0.12	-0.09	-0.07	-0.07
48.83	-0.88	4.37	-3.89	-1.75	4.93	-3.25	1.29	4.59	-0.53	-0.61	-0.21	-0.11	-0.70	-0.36	-0.14	-0.11
58.59	-1.50	3.69	-3.42	-1.77	4.59	-1.63	0.94	5.33	-0.08	-0.16	-0.15	-0.14	-0.13	-0.12	-0.14	-0.24
68.36	-2.27	4.29	-3.86	-0.77	5.27	-2.31	1.82	6.02	-0.30	-0.21	-0.27	-0.22	-0.35	-0.30	-0.23	-0.20
78.13	-0.26	3.26	-3.16	-0.52	6.41	-2.13	1.25	7.01	-0.07	-0.09	-0.07	-0.05	-0.11	-0.07	-0.09	-0.06
87.89	0.76	3.10	-3.08	0.17	6.40	-2.24	1.51	7.44	-0.08	-0.07	-0.04	-0.07	-0.06	-0.08	-0.04	-0.06
97.66	0.95	2.76	-2.80	0.91	6.55	-2.45	1.24	7.86	-0.35	-0.39	-0.08	-0.08	-0.36	-0.36	-0.07	-0.08
107.42	0.24	2.67	-3.02	1.52	6.30	-2.09	1.30	8.03	-0.12	-0.07	-0.10	-0.07	-0.11	-0.07	-0.10	-0.05
117.19	1.06	2.49	-3.23	2.04	6.87	-2.57	1.38	8.54	-0.12	-0.06	-0.11	-0.09	-0.19	-0.06	-0.15	-0.06
126.95	1.94	1.95	-2.26	2.91	7.72	-2.34	1.59	9.21	-0.09	-0.12	-0.07	-0.09	-0.10	-0.14	-0.07	-0.09
136.72	2.38	1.82	-2.26	3.87	8.10	-2.37	1.34	9.42	-0.06	-0.05	-0.07	-0.08	-0.06	-0.08	-0.05	-0.07
146.48	2.04	2.93	-0.66	4.68	8.97	-2.07	1.24	9.73	-0.12	-0.20	-0.28	-0.37	-0.17	-0.23	-0.27	-0.37
156.25	4.72	1.11	-2.56	5.13	7.53	-2.33	1.19	9.43	-0.19	-0.09	-0.11	-0.12	-0.23	-0.07	-0.25	-0.07
166.02	3.32	2.87	-0.55	3.37	8.49	-2.04	1.61	9.09	-0.10	-0.12	-0.10	-0.16	-0.14	-0.15	-0.09	-0.12
175.78	4.64	1.12	-1.70	6.12	7.27	-1.85	1.73	9.38	-0.08	-0.08	-0.11	-0.09	-0.12	-0.10	-0.09	-0.11
185.55	5.81	0.92	-2.34	6.70	7.72	-1.96	1.90	9.21	-0.05	-0.06	-0.05	-0.08	-0.09	-0.07	-0.07	-0.09
195.31	6.54	1.64	-1.57	6.55	7.07	-1.57	2.35	9.11	-0.10	-0.07	-0.06	-0.07	-0.12	-0.10	-0.10	-0.06
205.08	6.63	1.39	-1.14	6.92	7.05	-3.05	1.72	9.21	-0.12	-0.23	-0.10	-0.15	-0.20	-0.17	-0.15	-0.12
214.84	5.48	0.41	-0.23	8.00	7.54	-1.42	1.79	9.35	-0.06	-0.09	-0.04	-0.05	-0.08	-0.09	-0.06	-0.06
224.61	6.19	1.40	-0.44	8.48	7.11	-1.99	1.62	9.66	-0.05	-0.06	-0.05	-0.05	-0.08	-0.07	-0.05	-0.06
234.38	6.17	0.70	0.14	9.32	7.66	-1.08	1.76	8.26	-0.08	-0.07	-0.07	-0.08	-0.05	-0.09	-0.05	-0.10
244.14	7.21	1.37	0.53	9.04	7.65	-0.83	1.33	8.20	-0.05	-0.05	-0.04	-0.07	-0.08	-0.07	-0.07	-0.09

Table 17. 0.2 mm (8 mils), PR=0.4, zero inlet preswirl, and 10,200 RPM

	Test Data								Uncertainties							
Freq Hz	Re H_{xx}	Re H_{xy}	Re H_{yx}	Re H_{yy}	Im H_{xx}	Im H_{xy}	Im H_{yx}	Im H_{yy}	Re H_{xx}	Re H_{xy}	Re H_{yx}	Re H_{yy}	Im H_{xx}	Im H_{xy}	Im H_{yx}	Im H_{yy}
9.77	-3.44	-0.87	0.47	-2.54	0.17	0.22	-0.83	0.94	0.41	0.28	0.31	0.22	0.38	0.15	0.44	0.16
19.53	-3.56	-0.78	-0.81	-2.88	1.96	0.00	-0.84	1.37	0.57	0.15	0.31	0.15	0.54	0.26	0.32	0.21
29.30	-2.98	-0.95	0.57	-2.37	2.10	0.20	0.00	1.08	0.15	0.18	0.15	0.16	0.16	0.24	0.14	0.20
39.06	-2.70	-1.20	0.45	-2.16	3.20	-0.19	-0.01	3.21	0.16	0.10	0.09	0.17	0.14	0.17	0.09	0.12
48.83	-3.09	-0.83	0.53	-2.39	3.56	-0.06	-0.44	3.77	0.23	0.12	0.17	0.13	0.20	0.15	0.14	0.12
58.59	-2.67	-1.30	0.59	-2.31	4.43	0.02	-0.39	4.41	0.14	0.35	0.21	0.30	0.15	0.22	0.16	0.33
68.36	-3.41	-0.64	-0.09	-2.13	4.96	0.42	-0.09	5.75	0.37	0.23	0.29	0.22	0.36	0.36	0.32	0.27
78.13	-2.15	-0.93	0.55	-2.12	5.93	-0.12	-0.59	6.60	0.11	0.12	0.12	0.16	0.11	0.15	0.14	0.21
87.89	-1.66	-0.90	0.13	-1.23	6.77	-0.05	-0.48	7.57	0.07	0.12	0.10	0.13	0.06	0.13	0.05	0.14
97.66	-0.93	-0.97	0.29	-0.57	7.33	-0.11	-0.47	8.03	0.10	0.14	0.12	0.15	0.09	0.13	0.11	0.12
107.42	-1.57	-0.84	-0.01	-0.17	7.60	0.15	-0.60	8.65	0.19	0.08	0.13	0.13	0.25	0.20	0.19	0.13
117.19	-1.05	-0.97	-0.11	0.26	8.02	0.08	-0.81	9.27	0.15	0.12	0.14	0.10	0.15	0.14	0.16	0.16
126.95	-0.17	-1.28	0.10	0.62	8.82	-0.05	-0.70	9.93	0.15	0.21	0.11	0.26	0.16	0.18	0.16	0.18
136.72	-0.12	-1.55	-0.21	1.12	9.30	-0.07	-0.65	10.48	0.14	0.13	0.11	0.17	0.07	0.15	0.07	0.18
146.48	0.82	-1.97	-0.78	2.57	10.13	0.40	-0.31	10.15	0.14	0.19	0.11	0.23	0.17	0.19	0.13	0.19
156.25	-0.70	0.50	1.59	-1.05	9.82	0.14	-0.87	11.12	0.43	0.33	0.25	0.28	0.31	0.40	0.35	0.34
166.02	0.33	-2.30	0.97	0.07	11.00	-0.45	-0.68	13.81	0.87	2.69	0.78	1.79	0.87	2.21	0.62	2.21
175.78	1.41	-1.32	0.34	2.91	12.32	0.75	-1.25	12.15	0.79	1.03	0.65	0.82	0.81	1.05	0.67	0.93
185.55	2.34	-1.82	-0.75	3.25	12.11	-0.31	-0.71	12.84	0.28	0.34	0.22	0.28	0.30	0.34	0.21	0.30
195.31	2.09	-1.00	-0.37	3.04	11.91	0.73	0.32	12.69	0.21	0.17	0.12	0.11	0.21	0.24	0.14	0.20
205.08	2.96	-0.22	-0.39	3.22	13.38	0.02	-0.45	13.89	0.18	0.27	0.18	0.30	0.30	0.30	0.15	0.34
214.84	2.81	-1.90	-0.08	4.43	12.87	0.08	0.15	13.97	0.10	0.16	0.12	0.14	0.13	0.21	0.10	0.12
224.61	3.37	-0.77	-0.17	4.11	13.49	-0.03	-0.09	14.45	0.14	0.13	0.09	0.11	0.13	0.18	0.13	0.10
234.38	3.51	-1.96	-0.25	5.29	14.28	0.38	-0.04	14.58	0.12	0.21	0.09	0.17	0.13	0.24	0.10	0.15
244.14	4.50	-1.79	-0.03	5.47	14.78	0.95	-0.38	14.87	0.17	0.28	0.07	0.12	0.19	0.29	0.13	0.16
253.91	5.83	-1.07	-0.04	5.75	15.26	1.33	-0.60	15.42	0.80	1.11	0.12	0.20	0.72	1.00	0.14	0.17
263.67	5.80	-1.05	-0.39	6.46	14.72	1.27	-0.31	15.33	0.30	0.35	0.10	0.13	0.32	0.27	0.11	0.16
273.44	5.45	-0.95	-0.67	7.25	14.95	1.98	-0.11	15.17	0.18	0.20	0.14	0.13	0.19	0.20	0.14	0.17
283.20	5.32	0.65	-0.32	6.89	16.19	1.46	-0.33	15.00	0.12	0.19	0.11	0.24	0.13	0.25	0.12	0.16
292.97	6.53	-0.18	-0.42	7.29	17.16	0.10	-0.35	16.41	0.16	0.14	0.10	0.13	0.13	0.22	0.10	0.12
302.73	7.28	-0.24	-0.36	8.61	17.60	0.58	-0.62	16.17	0.15	0.19	0.09	0.15	0.20	0.22	0.12	0.18
312.50	8.73	-0.89	-0.15	8.24	16.28	0.13	-0.82	14.67	0.18	0.18	0.12	0.13	0.14	0.21	0.09	0.16
322.27	8.89	0.19	-1.38	7.19	17.52	1.04	-0.95	16.08	0.18	0.17	0.13	0.14	0.18	0.18	0.15	0.18
332.03	8.91	-0.25	-2.12	7.66	17.77	0.69	0.29	18.86	0.33	0.19	0.23	0.28	0.19	0.29	0.18	0.29
341.80	9.94	-1.66	-1.77	7.41	17.76	0.44	0.82	17.29	1.25	0.42	1.07	0.44	0.49	1.34	0.52	1.21

Table 18. 0.2 mm (8 mils), PR=0.4, zero inlet preswirl, and 15,350 RPM

	Test Data								Uncertainties							
Freq Hz	Re H_{xx}	Re H_{xy}	Re H_{yx}	Re H_{yy}	Im H_{xx}	Im H_{xy}	Im H_{yx}	Im H_{yy}	Re H_{xx}	Re H_{xy}	Re H_{yx}	Re H_{yy}	Im H_{xx}	Im H_{xy}	Im H_{yx}	Im H_{yy}
9.77	-2.66	0.01	-0.19	-1.53	0.17	0.40	-0.49	0.89	0.52	0.23	0.29	0.19	0.38	0.26	0.40	0.17
19.53	-1.96	0.22	-1.50	-1.75	2.11	-0.06	-0.03	1.12	0.52	0.13	0.26	0.10	0.50	0.18	0.26	0.14
29.30	-1.07	-0.45	0.06	-1.01	2.72	0.14	0.43	1.28	0.16	0.17	0.09	0.14	0.20	0.26	0.15	0.20
39.06	-1.11	-0.13	-0.22	-0.95	3.52	-0.08	-0.07	3.26	0.14	0.12	0.11	0.09	0.13	0.13	0.11	0.20
48.83	-1.30	0.03	-0.30	-1.09	4.00	-0.01	-0.21	3.89	0.27	0.14	0.20	0.15	0.19	0.18	0.15	0.16
58.59	-0.85	-0.36	0.05	-0.95	4.85	-0.03	0.03	4.60	0.23	0.19	0.20	0.20	0.19	0.16	0.18	0.18
68.36	-1.36	0.35	-0.34	-0.56	5.57	-0.20	0.17	5.92	0.37	0.33	0.28	0.21	0.36	0.30	0.28	0.20
78.13	0.24	-0.04	0.16	-0.35	6.37	-0.24	-0.46	6.35	0.14	0.09	0.15	0.12	0.11	0.17	0.11	0.14
87.89	0.41	-0.03	-0.24	0.13	6.71	-0.26	-0.20	7.10	0.10	0.17	0.08	0.12	0.08	0.10	0.08	0.11
97.66	0.71	-0.32	-0.14	0.72	7.56	-0.34	-0.42	7.54	0.11	0.11	0.14	0.12	0.10	0.13	0.08	0.12
107.42	0.46	-0.09	-0.42	0.93	8.25	-0.34	-0.48	8.18	0.17	0.15	0.15	0.08	0.14	0.12	0.19	0.15
117.19	1.24	-0.37	-0.75	1.45	8.51	-0.41	-0.49	8.76	0.15	0.09	0.12	0.08	0.22	0.11	0.14	0.12
126.95	1.78	-0.37	-0.46	2.10	8.66	-0.28	-0.54	9.16	0.11	0.22	0.08	0.19	0.10	0.19	0.11	0.13
136.72	2.16	-0.84	-0.87	2.45	9.40	-0.03	-0.37	9.64	0.05	0.08	0.06	0.07	0.07	0.15	0.08	0.10
146.48	2.81	-1.18	-1.51	4.18	9.98	0.34	0.01	9.59	0.09	0.16	0.09	0.10	0.12	0.15	0.11	0.15
156.25	1.48	0.91	0.87	0.89	9.72	0.49	-0.35	10.25	0.23	0.13	0.10	0.09	0.19	0.13	0.18	0.12
166.02	2.05	0.98	0.53	1.49	11.09	-0.08	-0.14	10.91	0.13	0.26	0.09	0.16	0.12	0.25	0.09	0.22
175.78	2.88	-0.26	-0.10	4.15	12.01	0.27	-0.45	11.55	0.13	0.12	0.13	0.14	0.16	0.15	0.14	0.15
185.55	3.54	-0.37	-0.25	4.05	13.37	-0.69	-0.84	12.25	0.09	0.12	0.13	0.10	0.13	0.13	0.09	0.17
195.31	4.00	-0.27	-0.67	4.29	13.12	0.08	-0.40	12.09	0.18	0.14	0.12	0.14	0.14	0.09	0.12	0.12
205.08	4.37	-0.12	-0.59	4.73	13.94	0.02	-0.57	12.81	0.18	0.27	0.10	0.24	0.24	0.20	0.14	0.18
214.84	5.51	-0.28	-0.71	4.82	14.09	-0.39	-0.32	13.25	0.10	0.14	0.10	0.12	0.11	0.13	0.09	0.10
224.61	5.99	-0.08	-0.53	5.35	14.15	-0.42	-0.08	13.93	0.16	0.10	0.09	0.11	0.08	0.13	0.07	0.09
234.38	6.11	-0.60	-0.39	5.93	14.52	-1.20	-0.18	14.73	0.10	0.20	0.07	0.16	0.13	0.16	0.05	0.13
244.14	6.62	-1.31	-0.10	6.67	15.36	-1.27	-0.61	15.36	0.15	0.18	0.07	0.13	0.17	0.25	0.08	0.11
253.91	6.11	-1.44	0.88	8.78	17.02	1.03	0.16	14.52	1.27	1.87	0.76	0.96	1.55	1.90	0.43	0.60
263.67	8.18	-2.46	-0.67	8.69	16.32	-0.57	-1.10	15.86	0.29	0.36	0.14	0.13	0.29	0.22	0.12	0.13
273.44	8.47	-2.70	-1.26	9.47	16.34	0.18	-0.89	15.35	0.19	0.16	0.09	0.18	0.16	0.20	0.14	0.12
283.20	8.27	-1.64	-1.27	9.31	16.42	1.68	-0.18	14.49	0.11	0.18	0.11	0.14	0.17	0.19	0.10	0.16
292.97	8.77	-0.25	-0.97	9.02	17.58	1.04	-0.29	14.68	0.15	0.12	0.09	0.13	0.15	0.19	0.09	0.12
302.73	9.78	-0.15	-1.18	9.71	18.42	0.30	-0.63	15.26	0.17	0.12	0.08	0.10	0.17	0.15	0.09	0.10
312.50	11.49	-0.50	-1.08	9.59	17.62	-0.23	-0.46	14.26	0.15	0.14	0.12	0.12	0.11	0.18	0.09	0.13
322.27	11.50	-0.72	-1.27	9.31	18.89	0.07	0.15	16.34	0.16	0.16	0.10	0.15	0.16	0.15	0.11	0.11
332.03	12.24	-1.64	-2.17	8.17	18.89	0.47	0.31	17.58	0.23	0.18	0.11	0.12	0.23	0.17	0.13	0.22
341.80	12.30	-1.43	-2.32	10.18	18.87	0.61	0.20	16.81	0.24	0.13	0.18	0.12	0.23	0.18	0.20	0.13

Table 19. 0.2 mm (8 mils), PR=0.4, zero inlet preswirl, and 20,200 RPM

	Test Data								Uncertainties							
Freq Hz	Re H_{xx}	Re H_{xy}	Re H_{yx}	Re H_{yy}	Im H_{xx}	Im H_{xy}	Im H_{yx}	Im H_{yy}	Re H_{xx}	Re H_{xy}	Re H_{yx}	Re H_{yy}	Im H_{xx}	Im H_{xy}	Im H_{yx}	Im H_{yy}
9.77	-2.77	0.58	-1.11	-2.19	-0.21	0.13	-0.63	0.90	0.47	0.11	0.26	0.09	0.33	0.16	0.38	0.12
19.53	-2.25	0.60	-2.59	-2.52	2.06	-0.29	-0.50	1.07	0.56	0.16	0.24	0.13	0.50	0.12	0.27	0.09
29.30	-2.05	0.54	-0.88	-2.32	2.12	0.26	0.13	0.94	0.16	0.15	0.14	0.15	0.12	0.21	0.07	0.14
39.06	-1.95	0.52	-1.05	-1.78	2.81	-0.03	0.23	2.77	0.16	0.13	0.08	0.13	0.11	0.17	0.07	0.13
48.83	-1.06	-0.33	-0.78	-2.09	3.09	-0.40	0.17	3.07	0.52	0.37	0.25	0.16	0.91	0.67	0.21	0.16
58.59	-2.03	0.42	-0.74	-2.02	3.97	-0.15	0.03	4.12	0.18	0.13	0.21	0.22	0.16	0.16	0.18	0.19
68.36	-2.86	1.23	-1.19	-1.84	4.66	-0.31	0.36	5.08	0.32	0.18	0.27	0.22	0.41	0.27	0.27	0.16
78.13	-1.32	0.78	-0.78	-1.72	5.45	-0.36	-0.49	5.76	0.12	0.13	0.10	0.15	0.11	0.13	0.13	0.13
87.89	-0.85	0.74	-0.93	-1.11	6.37	-0.71	-0.39	6.51	0.08	0.12	0.07	0.13	0.07	0.12	0.06	0.10
97.66	-0.28	0.50	-0.97	-0.55	6.80	-0.95	-0.43	6.96	0.37	0.35	0.32	0.34	0.33	0.40	0.31	0.29
107.42	-0.81	0.53	-1.43	-0.15	6.83	-0.66	-0.50	7.53	0.15	0.17	0.15	0.10	0.20	0.10	0.16	0.14
117.19	-0.05	0.22	-1.54	0.16	7.27	-0.60	-0.53	8.13	0.15	0.10	0.13	0.10	0.22	0.10	0.14	0.10
126.95	0.37	0.06	-1.42	1.00	7.74	-0.58	-0.49	8.54	0.12	0.13	0.11	0.18	0.10	0.16	0.11	0.15
136.72	0.67	-0.17	-1.75	1.17	8.46	-0.48	-0.45	8.95	0.06	0.08	0.12	0.11	0.07	0.09	0.06	0.07
146.48	1.47	-0.62	-2.31	2.92	9.22	-0.15	-0.03	8.77	0.16	0.17	0.09	0.10	0.21	0.15	0.11	0.14
156.25	-0.19	1.79	0.20	-0.88	9.02	-0.30	-0.58	9.64	0.18	0.13	0.11	0.08	0.15	0.14	0.22	0.12
166.02	0.85	0.87	-0.33	0.28	9.71	-0.08	0.02	9.80	0.13	0.13	0.09	0.13	0.13	0.22	0.10	0.16
175.78	2.89	0.08	-1.04	3.00	11.42	-0.72	-0.38	10.59	0.19	0.13	0.15	0.08	0.14	0.21	0.12	0.12
185.55	2.82	-0.29	-1.74	3.17	11.02	-0.73	-0.05	10.92	0.09	0.10	0.11	0.12	0.13	0.14	0.11	0.10
195.31	2.91	-0.13	-1.36	2.94	10.62	0.01	0.36	10.75	0.10	0.10	0.09	0.08	0.15	0.08	0.07	0.11
205.08	3.33	0.12	-1.46	3.37	12.24	-0.26	-0.43	11.66	0.15	0.22	0.12	0.16	0.19	0.23	0.13	0.19
214.84	3.58	-0.68	-1.50	3.95	11.69	-0.76	0.19	12.05	0.11	0.07	0.08	0.10	0.10	0.10	0.07	0.10
224.61	4.09	0.14	-1.38	4.22	12.06	-0.51	0.16	12.41	0.11	0.13	0.05	0.09	0.14	0.11	0.07	0.08
234.38	4.07	-0.63	-1.42	4.85	12.59	-0.43	0.50	12.61	0.09	0.20	0.09	0.15	0.10	0.13	0.08	0.12
244.14	4.94	-0.43	-1.00	4.92	13.40	-0.15	0.04	13.17	0.14	0.22	0.10	0.11	0.17	0.25	0.08	0.12
253.91	6.19	-0.07	-1.04	5.55	13.46	-0.03	-0.31	13.50	0.75	1.03	0.13	0.20	0.71	1.01	0.11	0.20
263.67	5.91	-0.12	-1.28	6.22	13.29	-0.38	-0.35	13.37	0.30	0.43	0.11	0.13	0.35	0.24	0.13	0.16
273.44	5.66	-0.85	-1.93	6.98	13.82	0.23	-0.23	13.33	0.20	0.29	0.12	0.13	0.22	0.19	0.12	0.15
283.20	5.52	0.61	-1.48	6.49	14.65	0.14	-0.29	13.60	0.16	0.23	0.16	0.17	0.17	0.32	0.09	0.14
292.97	6.31	0.57	-1.58	7.00	15.54	-0.79	-0.09	14.39	0.23	0.14	0.09	0.12	0.18	0.29	0.10	0.13
302.73	7.15	-0.20	-1.60	8.50	16.51	-0.74	-0.35	14.46	0.22	0.21	0.12	0.16	0.30	0.34	0.09	0.16
312.50	9.04	-0.68	-1.96	8.52	16.01	-0.74	-0.67	12.63	0.28	0.25	0.16	0.18	0.29	0.43	0.17	0.17
322.27	9.06	-0.47	-2.29	7.15	17.48	-0.62	0.15	14.51	0.48	0.23	0.22	0.30	0.52	0.61	0.26	0.22
332.03	12.86	2.25	-1.01	9.82	17.66	0.15	0.03	13.80	1.93	1.28	0.73	0.98	1.42	2.11	1.05	0.89
341.80	10.93	-0.66	-3.28	7.99	15.13	-0.27	0.64	15.55	2.08	1.51	0.73	0.32	1.33	1.08	0.93	0.87

Table 20. 0.2 mm (8 mils), PR=0.5, zero inlet preswirl, and 10,200 RPM

	Test Data								Uncertainties							
Freq Hz	Re H_{xx}	Re H_{xy}	Re H_{yx}	Re H_{yy}	Im H_{xx}	Im H_{xy}	Im H_{yx}	Im H_{yy}	Re H_{xx}	Re H_{xy}	Re H_{yx}	Re H_{yy}	Im H_{xx}	Im H_{xy}	Im H_{yx}	Im H_{yy}
9.77	-3.84	-0.89	0.79	-3.01	-0.02	0.19	-1.08	0.57	0.36	0.18	0.30	0.29	0.30	0.18	0.63	0.20
19.53	-3.41	-0.55	-0.70	-2.19	2.55	-0.07	-0.58	2.12	0.52	0.11	0.40	0.14	0.45	0.15	0.23	0.12
29.30	-2.63	-1.28	0.30	-1.27	2.97	0.63	0.61	1.87	0.07	0.10	0.08	0.16	0.10	0.14	0.31	0.19
39.06	-2.63	-1.09	-0.26	-1.62	3.67	0.10	-0.24	3.84	0.13	0.11	0.41	0.17	0.09	0.15	0.11	0.17
48.83	-2.92	-0.91	0.28	-1.61	4.16	0.08	-0.48	4.51	0.20	0.11	0.28	0.13	0.21	0.11	0.27	0.12
58.59	-2.73	-1.02	0.20	-1.48	5.13	0.11	-0.14	5.45	0.12	0.13	0.24	0.15	0.15	0.14	0.28	0.14
68.36	-3.05	-0.61	-0.47	-1.49	6.23	-0.12	0.62	5.96	0.30	0.14	0.46	0.20	0.32	0.15	0.54	0.26
78.13	-1.79	-1.01	-0.21	-0.62	7.17	-0.11	-0.49	7.59	0.12	0.10	0.31	0.15	0.14	0.10	0.29	0.21
87.89	-1.41	-0.98	0.90	-0.15	7.58	-0.11	-0.41	7.96	0.10	0.09	0.53	0.19	0.06	0.11	0.08	0.15
97.66	-1.23	-1.08	0.44	0.22	8.21	0.00	-0.99	8.13	0.13	0.10	0.17	0.10	0.09	0.09	0.27	0.22
107.42	-1.86	-0.95	0.32	0.31	9.65	-0.35	-1.14	8.76	0.17	0.09	0.32	0.15	0.14	0.10	0.43	0.21
117.19	-0.92	-1.14	-0.19	0.33	9.92	-0.05	-0.46	9.77	0.12	0.08	0.16	0.12	0.13	0.11	0.21	0.17
126.95	-0.15	-1.20	0.42	1.20	10.37	0.04	-0.86	10.35	0.11	0.11	0.25	0.17	0.10	0.16	0.17	0.21
136.72	0.27	-1.43	-0.20	1.51	11.04	0.05	-0.65	11.39	0.11	0.08	0.19	0.12	0.08	0.10	0.06	0.12
146.48	0.59	-2.09	-1.23	3.03	11.78	0.39	-0.62	11.47	0.07	0.07	0.19	0.15	0.11	0.10	0.12	0.10
156.25	-0.14	0.14	1.46	-0.32	11.86	0.01	-0.42	12.37	0.16	0.07	0.27	0.14	0.17	0.11	0.40	0.11
166.02	0.03	0.47	1.12	0.35	13.82	-0.12	-1.10	14.21	0.10	0.19	0.20	0.12	0.11	0.18	0.06	0.17
175.78	-1.06	-1.04	1.23	3.08	15.16	0.88	-0.20	14.13	0.14	0.12	0.46	0.09	0.10	0.11	0.22	0.19
185.55	1.82	-1.59	-0.56	3.48	15.34	-0.37	-1.41	15.17	0.08	0.09	0.14	0.11	0.15	0.09	0.21	0.14
195.31	1.89	-0.84	-0.61	3.64	14.79	0.34	-0.64	14.85	0.11	0.08	0.06	0.11	0.12	0.10	0.21	0.12
205.08	2.55	-0.72	-0.32	4.12	15.90	0.11	-1.02	15.07	0.09	0.13	0.19	0.16	0.19	0.25	0.14	0.25
214.84	3.11	-1.06	-0.06	4.66	16.12	-0.24	-0.30	16.79	0.09	0.09	0.21	0.10	0.12	0.12	0.13	0.16
224.61	3.35	-0.99	-0.02	4.81	16.96	-0.16	-0.36	17.27	0.08	0.14	0.21	0.08	0.13	0.12	0.14	0.13
234.38	4.10	-1.42	0.20	5.66	17.59	-0.31	-0.72	17.88	0.11	0.12	0.26	0.13	0.10	0.16	0.21	0.18
244.14	4.52	-1.50	0.13	6.66	18.19	-0.39	-1.43	18.39	0.16	0.14	0.15	0.15	0.20	0.29	0.33	0.13
253.91	6.56	-3.57	0.22	7.80	20.05	0.50	-1.84	18.95	2.06	2.56	0.38	0.32	1.40	1.64	0.54	0.50
263.67	5.72	-2.76	-0.48	8.40	19.12	0.24	-1.56	18.70	0.34	0.31	0.29	0.12	0.33	0.40	0.32	0.18
273.44	6.24	-2.82	-0.71	9.55	19.44	1.34	-1.10	18.32	0.15	0.12	0.29	0.13	0.23	0.24	0.36	0.22
283.20	5.96	-0.98	-0.19	8.21	20.41	1.58	-1.15	17.95	0.17	0.16	0.23	0.21	0.18	0.20	0.34	0.21
292.97	7.21	-1.50	-0.78	9.54	21.51	0.98	-1.15	18.92	0.12	0.15	0.16	0.16	0.15	0.12	0.28	0.15
302.73	8.03	-1.17	-0.73	9.92	21.79	1.18	-1.87	18.26	0.19	0.14	0.17	0.30	0.21	0.14	0.77	0.18
312.50	9.54	-1.37	-0.44	9.13	21.29	0.40	-1.80	18.28	0.16	0.16	0.22	0.23	0.14	0.15	0.57	0.24
322.27	9.97	-1.46	-1.56	9.04	22.85	1.26	-1.64	20.13	0.20	0.14	0.17	0.12	0.22	0.14	0.34	0.18
332.03	10.32	-1.33	-1.94	10.06	22.66	0.82	-1.24	20.67	0.23	0.19	0.27	0.09	0.18	0.19	0.32	0.18
341.80	11.12	-0.85	-1.72	9.85	23.07	1.62	-1.18	20.75	0.26	0.14	0.34	0.24	0.31	0.20	0.86	0.33

Table 21. 0.2 mm (8 mils), PR=0.5, zero inlet preswirl, and 15,350 RPM

	Test Data								Uncertainties							
Freq Hz	Re H_{xx}	Re H_{xy}	Re H_{yx}	Re H_{yy}	Im H_{xx}	Im H_{xy}	Im H_{yx}	Im H_{yy}	Re H_{xx}	Re H_{xy}	Re H_{yx}	Re H_{yy}	Im H_{xx}	Im H_{xy}	Im H_{yx}	Im H_{yy}
9.77	-3.09	-0.22	-0.20	-2.05	-0.07	0.12	-0.54	0.84	0.39	0.17	0.28	0.11	0.35	0.24	0.39	0.17
19.53	-3.22	0.27	-1.41	-2.47	2.07	-0.26	-0.52	1.53	0.64	0.12	0.31	0.11	0.52	0.14	0.27	0.18
29.30	-2.36	-0.36	-0.09	-2.15	2.42	0.12	0.08	1.34	0.10	0.22	0.11	0.14	0.14	0.19	0.10	0.20
39.06	-2.47	-0.16	-0.34	-1.97	3.45	-0.21	0.04	3.21	0.14	0.15	0.12	0.14	0.10	0.13	0.09	0.13
48.83	-2.45	-0.07	-0.20	-2.09	3.95	0.03	-0.31	4.00	0.23	0.10	0.21	0.13	0.16	0.17	0.13	0.18
58.59	-2.07	-0.82	0.04	-2.10	4.94	0.33	-0.31	4.96	0.13	0.34	0.22	0.20	0.16	0.15	0.18	0.21
68.36	-3.03	0.38	-0.53	-1.88	5.49	0.09	0.07	5.89	0.39	0.39	0.29	0.17	0.38	0.57	0.30	0.27
78.13	-1.46	-0.38	-0.11	-1.56	6.56	-0.20	-0.51	6.95	0.13	0.10	0.15	0.14	0.12	0.16	0.13	0.15
87.89	-1.13	-0.28	-0.28	-0.92	7.35	-0.01	-0.30	7.72	0.08	0.09	0.07	0.10	0.07	0.15	0.05	0.17
97.66	-0.63	-0.35	-0.28	-0.36	8.03	-0.04	-0.39	8.48	0.09	0.12	0.11	0.17	0.11	0.19	0.08	0.15
107.42	-1.07	0.00	-0.49	0.10	8.46	-0.20	-0.66	9.20	0.17	0.12	0.16	0.11	0.23	0.16	0.18	0.18
117.19	-0.41	-0.26	-0.54	0.40	8.84	-0.04	-0.68	9.48	0.18	0.10	0.12	0.09	0.20	0.17	0.13	0.12
126.95	0.19	-0.44	-0.49	0.79	9.72	-0.06	-0.63	10.48	0.11	0.20	0.06	0.22	0.12	0.24	0.12	0.18
136.72	0.53	-0.95	-0.69	1.35	10.19	-0.13	-0.59	10.95	0.12	0.12	0.09	0.13	0.06	0.14	0.06	0.12
146.48	1.24	-1.48	-1.36	2.76	10.99	0.52	-0.42	10.81	0.10	0.13	0.09	0.18	0.13	0.23	0.12	0.15
156.25	-0.19	1.13	1.11	-0.57	10.52	0.26	-0.69	12.04	0.20	0.14	0.12	0.15	0.16	0.22	0.20	0.15
166.02	1.18	0.08	0.11	0.98	12.88	-0.23	-0.98	12.40	0.09	0.19	0.12	0.14	0.16	0.25	0.11	0.27
175.78	2.67	-1.35	0.06	3.00	13.75	2.04	-0.35	13.55	0.12	0.23	0.12	0.25	0.17	0.23	0.14	0.20
185.55	2.80	-1.05	-1.18	3.15	13.47	-0.27	-0.75	13.84	0.08	0.15	0.11	0.17	0.22	0.13	0.14	0.09
195.31	2.70	-0.33	-0.78	3.14	13.26	0.55	-0.09	13.64	0.12	0.14	0.07	0.13	0.16	0.12	0.14	0.10
205.08	3.22	0.00	-1.05	3.25	14.80	0.03	-1.02	14.73	0.22	0.49	0.14	0.44	0.30	0.30	0.26	0.28
214.84	3.47	-1.32	-0.69	4.35	14.57	-0.41	-0.18	15.46	0.15	0.21	0.11	0.20	0.14	0.21	0.10	0.16
224.61	3.78	-0.18	-0.66	4.22	15.27	-0.10	-0.41	15.89	0.21	0.14	0.13	0.18	0.12	0.27	0.10	0.14
234.38	3.95	-0.83	-0.66	5.29	15.99	-0.32	-0.37	16.27	0.28	0.22	0.15	0.32	0.21	0.48	0.14	0.26
244.14	4.76	-0.91	-0.73	5.56	16.86	-0.32	-0.94	16.89	0.42	0.40	0.26	0.48	0.44	0.82	0.20	0.30
253.91	5.07	-3.86	-0.61	5.68	17.81	-1.61	-0.36	19.45	2.31	4.81	1.65	1.63	2.96	2.87	1.00	2.49
263.67	6.52	-1.04	-1.28	6.74	17.60	0.44	-0.74	17.71	0.69	0.94	0.44	0.75	0.90	1.45	0.43	0.73
273.44	6.48	-1.30	-1.49	7.80	17.40	1.81	-0.38	17.13	0.37	0.37	0.19	0.42	0.45	0.79	0.30	0.28
283.20	5.70	0.79	-0.81	6.79	18.76	1.41	-0.51	17.26	0.26	0.52	0.13	0.18	0.27	0.31	0.18	0.26
292.97	7.29	-0.21	-1.37	7.95	20.03	0.18	-0.73	18.55	0.23	0.36	0.12	0.19	0.21	0.22	0.13	0.20
302.73	8.40	-0.29	-1.25	9.13	20.34	1.13	-0.64	18.12	0.27	0.36	0.12	0.20	0.21	0.20	0.13	0.18
312.50	9.49	0.05	-0.93	8.59	19.36	0.51	-1.00	16.92	0.19	0.27	0.13	0.16	0.22	0.27	0.12	0.15
322.27	10.34	0.97	-1.95	7.93	20.95	1.27	-0.92	18.98	0.19	0.22	0.15	0.18	0.25	0.23	0.12	0.13
332.03	10.80	0.80	-2.41	9.93	20.28	0.87	-0.18	20.54	0.23	0.20	0.16	0.31	0.27	0.30	0.15	0.16
341.80	12.10	-0.69	-2.69	8.96	21.73	0.60	-0.01	19.99	0.29	0.14	0.13	0.18	0.24	0.20	0.23	0.19

Table 22. 0.2 mm (8 mils), PR=0.5, zero inlet preswirl, and 20,200 RPM

	Test Data								Uncertainties							
Freq Hz	Re H_{xx}	Re H_{xy}	Re H_{yx}	Re H_{yy}	Im H_{xx}	Im H_{xy}	Im H_{yx}	Im H_{yy}	Re H_{xx}	Re H_{xy}	Re H_{yx}	Re H_{yy}	Im H_{xx}	Im H_{xy}	Im H_{yx}	Im H_{yy}
9.77	-4.14	0.77	-0.84	-2.64	-0.22	0.16	-0.54	0.80	0.46	0.23	0.29	0.15	0.36	0.21	0.38	0.17
19.53	-3.60	0.67	-2.58	-2.85	1.99	0.08	-0.84	1.20	0.59	0.12	0.22	0.14	0.52	0.23	0.27	0.23
29.30	-3.42	0.81	-0.94	-2.84	2.39	0.11	0.03	1.35	0.14	0.17	0.14	0.17	0.11	0.20	0.14	0.23
39.06	-3.41	0.77	-1.29	-2.53	3.45	-0.13	-0.28	3.83	0.14	0.10	0.11	0.11	0.11	0.21	0.13	0.17
48.83	-3.15	0.80	-1.23	-2.65	4.20	-0.65	-0.08	3.90	0.47	0.57	0.30	0.19	0.60	0.48	0.19	0.23
58.59	-3.39	0.79	-0.82	-3.24	4.76	0.04	-0.34	5.24	0.14	0.23	0.18	0.28	0.18	0.16	0.15	0.25
68.36	-4.79	1.15	-1.45	-2.72	5.79	-1.13	0.29	6.73	0.35	0.28	0.28	0.26	0.40	0.23	0.26	0.27
78.13	-3.02	0.65	-1.02	-2.50	7.36	-0.47	-0.38	7.59	0.13	0.11	0.15	0.13	0.15	0.14	0.20	0.20
87.89	-2.38	0.62	-1.25	-2.05	8.14	-0.55	0.13	8.67	0.09	0.11	0.08	0.12	0.11	0.12	0.07	0.12
97.66	-1.75	0.61	-0.68	-1.14	8.70	-0.39	-0.35	9.49	0.20	0.27	0.22	0.20	0.24	0.30	0.15	0.16
107.42	-2.35	0.55	-1.46	-0.36	8.97	-0.45	-0.67	10.25	0.21	0.12	0.17	0.13	0.21	0.17	0.15	0.17
117.19	-1.63	0.39	-1.71	0.14	9.85	-0.47	-0.82	10.87	0.13	0.14	0.17	0.13	0.19	0.12	0.19	0.18
126.95	-1.01	0.24	-1.25	0.67	10.80	-0.26	-0.73	11.50	0.11	0.26	0.11	0.28	0.13	0.18	0.12	0.27
136.72	-0.46	-0.07	-1.59	0.87	11.61	-0.43	-0.80	12.13	0.08	0.09	0.09	0.10	0.08	0.15	0.06	0.17
146.48	0.51	-0.50	-2.35	2.44	12.18	0.07	-0.53	12.08	0.13	0.22	0.09	0.20	0.14	0.12	0.10	0.15
156.25	-1.48	2.16	0.18	-1.28	12.11	-0.40	-0.90	13.05	0.19	0.15	0.14	0.10	0.17	0.13	0.25	0.21
166.02	-0.05	1.04	-0.94	0.25	13.72	-0.48	-1.03	13.97	0.13	0.21	0.12	0.24	0.12	0.30	0.10	0.24
175.78	2.27	-0.02	-1.58	2.55	14.19	-0.32	-0.46	14.74	0.13	0.23	0.16	0.16	0.14	0.11	0.14	0.18
185.55	1.97	-0.41	-2.56	3.50	14.39	-0.07	-0.24	15.10	0.13	0.15	0.11	0.12	0.14	0.14	0.13	0.18
195.31	2.20	0.56	-2.15	3.32	14.49	0.44	0.42	15.32	0.14	0.14	0.10	0.15	0.14	0.18	0.11	0.16
205.08	3.15	0.50	-2.73	3.73	15.70	-0.38	-0.25	16.10	0.13	0.16	0.09	0.29	0.24	0.23	0.20	0.20
214.84	2.69	-0.70	-1.46	4.84	15.87	-0.08	0.34	16.70	0.10	0.12	0.08	0.10	0.11	0.15	0.07	0.12
224.61	3.47	0.50	-1.76	4.87	16.39	-0.27	-0.02	17.44	0.10	0.15	0.09	0.10	0.11	0.14	0.08	0.14
234.38	3.18	-0.62	-1.82	5.77	17.31	0.21	0.30	17.43	0.13	0.20	0.11	0.12	0.13	0.22	0.05	0.16
244.14	4.35	-0.31	-1.55	6.05	18.68	0.65	-0.16	18.00	0.17	0.17	0.06	0.13	0.17	0.31	0.11	0.13
253.91	6.80	-1.26	-1.65	6.67	19.97	1.76	-0.71	18.81	2.04	2.60	0.25	0.32	1.34	1.66	0.36	0.49
263.67	6.46	0.37	-2.31	7.80	18.58	0.79	-0.37	18.96	0.34	0.34	0.17	0.11	0.31	0.45	0.15	0.19
273.44	5.67	0.79	-2.50	8.54	18.52	1.90	0.72	17.75	0.19	0.17	0.10	0.23	0.19	0.32	0.15	0.16
283.20	6.06	2.18	-1.72	6.70	20.30	1.33	-0.27	18.18	0.14	0.21	0.11	0.19	0.17	0.22	0.09	0.18
292.97	7.11	1.81	-2.24	8.39	21.36	-0.39	-0.51	20.72	0.13	0.17	0.08	0.16	0.17	0.16	0.13	0.14
302.73	7.91	2.05	-2.30	9.57	21.62	-0.16	-0.38	19.95	0.14	0.17	0.11	0.13	0.13	0.21	0.11	0.20
312.50	8.41	0.81	-2.11	9.58	21.93	-1.22	-1.12	18.96	0.16	0.23	0.14	0.14	0.19	0.16	0.18	0.13
322.27	9.65	1.28	-3.36	8.37	23.78	-0.25	-0.94	20.58	0.23	0.26	0.17	0.15	0.27	0.17	0.12	0.17
332.03	11.58	2.05	-2.35	11.15	25.54	-1.01	-0.46	20.92	0.41	0.32	0.28	0.23	0.63	0.32	0.31	0.25
341.80	11.73	0.53	-3.90	9.40	21.83	0.75	1.08	22.08	0.62	0.22	0.21	0.19	0.62	0.39	0.43	0.21

Table 23. 0.2 mm (8 mils), PR=0.6, zero inlet preswirl, and 10,200 RPM

	Test Data								Uncertainties							
Freq Hz	Re H_{xx}	Re H_{xy}	Re H_{yx}	Re H_{yy}	Im H_{xx}	Im H_{xy}	Im H_{yx}	Im H_{yy}	Re H_{xx}	Re H_{xy}	Re H_{yx}	Re H_{yy}	Im H_{xx}	Im H_{xy}	Im H_{yx}	Im H_{yy}
9.77	-2.34	-0.83	0.45	-1.30	0.61	-0.09	-0.22	1.45	0.53	0.16	0.41	0.19	0.43	0.25	0.48	0.17
19.53	-2.99	-0.34	0.99	-1.33	4.48	0.01	1.54	1.63	1.16	0.20	0.90	0.18	0.67	0.17	0.37	0.18
29.30	-1.68	-1.09	0.33	-0.30	2.94	0.53	0.29	2.63	0.10	0.19	0.10	0.23	0.12	0.18	0.14	0.23
39.06	-1.40	-1.07	0.38	-0.60	3.84	0.07	0.05	3.53	0.10	0.16	0.13	0.17	0.10	0.15	0.06	0.12
48.83	-1.31	-0.96	0.42	-0.82	4.67	-0.05	-0.11	4.75	0.31	0.22	0.25	0.12	0.31	0.29	0.13	0.25
58.59	-1.32	-0.96	0.45	-0.72	5.71	0.34	-0.20	5.27	0.17	0.17	0.18	0.23	0.15	0.21	0.19	0.16
68.36	-0.60	-0.65	0.51	-0.57	6.39	0.25	0.46	6.25	0.67	0.22	0.52	0.23	0.59	0.34	0.39	0.32
78.13	-0.04	-0.70	0.38	-0.07	7.46	-0.15	-0.58	7.25	0.18	0.13	0.13	0.13	0.19	0.14	0.14	0.14
87.89	0.04	-0.82	0.19	0.54	7.64	-0.08	-0.51	8.43	0.11	0.15	0.06	0.10	0.06	0.17	0.06	0.15
97.66	0.07	-1.01	0.12	1.03	8.59	0.02	-0.55	8.95	0.14	0.13	0.12	0.12	0.10	0.15	0.13	0.12
107.42	0.54	-0.90	0.60	1.23	9.91	-0.17	-0.46	9.47	0.36	0.13	0.17	0.16	0.31	0.14	0.30	0.14
117.19	0.93	-0.88	-0.19	1.48	10.34	-0.06	-0.11	10.19	0.17	0.09	0.20	0.13	0.25	0.11	0.13	0.14
126.95	1.17	-0.64	0.17	2.03	11.00	-0.04	-0.35	10.34	0.12	0.31	0.13	0.19	0.16	0.24	0.13	0.27
136.72	1.47	-1.05	-0.07	2.26	11.49	-0.05	-0.31	11.62	0.11	0.16	0.08	0.12	0.13	0.13	0.10	0.12
146.48	2.15	-1.47	-0.67	3.38	12.09	0.39	-0.05	11.58	0.20	0.20	0.15	0.18	0.33	0.26	0.16	0.20
156.25	2.69	-2.02	-1.37	4.52	15.25	-1.97	-4.34	16.36	1.21	0.46	0.91	0.42	0.96	0.50	0.93	0.40
166.02	2.80	-3.49	-1.39	6.26	15.43	-1.03	-2.08	16.13	1.01	2.40	0.98	2.42	1.23	3.02	0.91	2.09
175.78	-0.82	-0.89	0.20	4.00	14.32	-0.20	-0.55	14.62	0.70	0.79	0.67	0.65	0.88	0.85	0.81	0.73
185.55	3.38	-1.48	-0.62	4.16	15.93	-0.28	-0.85	15.25	0.23	0.33	0.24	0.23	0.26	0.29	0.17	0.29
195.31	2.84	-0.68	-0.23	3.93	16.05	0.06	-0.38	15.47	0.35	0.17	0.18	0.15	0.26	0.19	0.19	0.16
205.08	3.30	-0.93	-0.34	4.97	16.98	0.17	-0.73	16.36	0.21	0.43	0.26	0.29	0.37	0.37	0.22	0.28
214.84	4.37	-0.74	-0.34	4.77	17.68	-0.29	-0.56	17.17	0.12	0.19	0.15	0.18	0.12	0.20	0.09	0.17
224.61	4.91	-1.23	-0.12	5.76	18.52	-0.65	-0.74	17.97	0.13	0.15	0.07	0.12	0.13	0.15	0.12	0.13
234.38	5.72	-1.15	-0.36	5.58	19.13	-0.75	-0.44	18.47	0.19	0.13	0.09	0.18	0.13	0.23	0.13	0.17
244.14	6.12	-1.49	0.12	6.48	19.82	-0.90	-0.84	19.84	0.27	0.23	0.15	0.18	0.12	0.37	0.10	0.12
253.91	5.67	-0.88	0.30	7.68	22.10	-0.35	-1.14	20.43	1.64	2.25	0.40	0.36	1.19	0.90	0.37	0.54
263.67	7.54	-2.68	-0.55	8.78	20.69	-0.71	-1.63	20.85	0.21	0.27	0.19	0.13	0.45	0.48	0.14	0.19
273.44	7.86	-3.30	-1.52	10.40	21.17	0.50	-1.29	20.66	0.13	0.20	0.13	0.17	0.31	0.29	0.17	0.20
283.20	8.20	-2.58	-1.39	9.94	21.18	2.05	0.11	19.04	0.16	0.23	0.15	0.15	0.20	0.24	0.13	0.17
292.97	8.20	-1.68	-0.47	10.26	22.37	1.24	-0.53	20.46	0.16	0.25	0.11	0.20	0.19	0.15	0.16	0.14
302.73	9.07	-1.91	-1.32	10.06	24.03	1.23	-0.75	19.85	0.18	0.24	0.10	0.12	0.24	0.16	0.12	0.14
312.50	10.11	-1.56	-0.87	8.71	23.30	0.52	-0.65	20.18	0.16	0.21	0.12	0.13	0.15	0.20	0.11	0.17
322.27	10.75	-2.01	-0.14	9.95	26.33	1.80	1.88	24.29	0.16	0.26	0.18	0.19	0.27	0.17	0.16	0.18
332.03	11.67	-2.39	-0.65	10.76	25.13	0.89	-1.05	22.10	0.20	0.13	0.17	0.21	0.20	0.24	0.27	0.26
341.80	9.55	-0.41	-0.16	9.91	29.07	3.59	0.50	24.53	0.45	0.43	0.56	0.39	0.66	0.35	0.57	0.40

Table 24. 0.2 mm (8 mils), PR=0.6, zero inlet preswirl, and 15,350 RPM

	Test Data								Uncertainties							
Freq Hz	Re H_{xx}	Re H_{xy}	Re H_{yx}	Re H_{yy}	Im H_{xx}	Im H_{xy}	Im H_{yx}	Im H_{yy}	Re H_{xx}	Re H_{xy}	Re H_{yx}	Re H_{yy}	Im H_{xx}	Im H_{xy}	Im H_{yx}	Im H_{yy}
9.77	-3.27	-0.04	-0.22	-1.61	0.00	0.23	0.11	0.82	0.50	0.14	0.40	0.13	0.32	0.13	0.47	0.13
19.53	-3.46	0.36	-1.13	-2.20	3.80	-0.04	1.40	1.07	1.43	0.17	0.29	0.10	0.92	0.18	0.88	0.17
29.30	-2.50	-0.22	-0.40	-1.40	2.38	0.64	0.25	1.37	0.11	0.19	0.10	0.17	0.09	0.17	0.10	0.15
39.06	-2.49	-0.08	-0.29	-1.57	3.47	-0.11	-0.02	3.52	0.11	0.20	0.13	0.13	0.10	0.19	0.08	0.17
48.83	-2.33	0.03	-0.22	-1.74	4.31	-0.23	-0.07	4.24	0.23	0.10	0.21	0.10	0.22	0.13	0.12	0.15
58.59	-2.30	-0.02	-0.07	-1.79	4.91	-0.19	0.06	4.89	0.18	0.19	0.18	0.17	0.16	0.20	0.14	0.14
68.36	-2.97	0.29	-0.09	-1.36	6.18	-0.14	1.13	6.30	0.55	0.27	0.55	0.20	0.49	0.22	0.42	0.22
78.13	-1.78	-0.03	-0.17	-1.28	6.81	-0.16	-0.57	7.31	0.16	0.13	0.12	0.12	0.14	0.13	0.15	0.15
87.89	-1.91	-0.09	-0.46	-0.87	7.66	-0.24	-0.41	8.27	0.10	0.16	0.06	0.11	0.06	0.13	0.07	0.10
97.66	-1.39	-0.19	-0.39	-0.21	8.72	-0.11	-0.42	8.98	0.09	0.14	0.11	0.11	0.13	0.10	0.11	0.13
107.42	-1.17	0.01	-0.39	-0.02	8.94	-0.19	-0.50	9.64	0.25	0.10	0.11	0.13	0.34	0.12	0.25	0.14
117.19	-0.53	-0.18	-0.86	0.38	9.64	-0.26	-0.56	10.39	0.14	0.11	0.17	0.11	0.20	0.14	0.16	0.14
126.95	-0.36	-0.01	-0.63	0.83	10.86	-0.22	-0.75	11.09	0.12	0.16	0.12	0.22	0.13	0.20	0.12	0.23
136.72	0.05	-0.33	-0.80	1.09	11.36	-0.19	-0.64	11.84	0.08	0.10	0.08	0.10	0.08	0.13	0.06	0.12
146.48	0.82	-0.87	-1.44	2.19	12.01	0.43	-0.29	11.81	0.16	0.14	0.12	0.11	0.16	0.14	0.10	0.11
156.25	1.45	-1.27	-2.58	3.72	13.48	-1.14	-3.38	15.62	0.46	0.14	0.37	0.20	0.34	0.17	0.46	0.15
166.02	1.86	-0.86	-1.68	3.09	14.49	-0.59	-1.25	14.29	0.13	0.29	0.13	0.32	0.16	0.18	0.12	0.19
175.78	0.21	0.33	-0.97	2.65	19.47	0.77	-0.94	14.35	0.39	0.21	0.11	0.12	0.20	0.24	0.14	0.14
185.55	1.86	-0.64	-1.29	2.99	14.97	0.08	-0.74	15.12	0.07	0.14	0.10	0.17	0.14	0.13	0.09	0.15
195.31	2.05	0.12	-1.55	2.98	15.42	0.18	-0.54	15.63	0.19	0.13	0.14	0.13	0.17	0.18	0.18	0.14
205.08	2.51	-0.30	-1.41	3.55	16.61	0.09	-0.63	16.70	0.22	0.46	0.20	0.23	0.28	0.26	0.17	0.25
214.84	3.33	-0.41	-1.49	3.83	17.03	-0.39	-0.27	17.38	0.14	0.15	0.13	0.17	0.09	0.21	0.10	0.15
224.61	3.57	-0.41	-1.22	4.58	17.50	-0.34	-0.39	18.01	0.17	0.17	0.13	0.13	0.22	0.18	0.14	0.17
234.38	3.95	-0.56	-1.11	5.11	18.02	-0.54	0.02	18.78	0.25	0.30	0.12	0.19	0.20	0.28	0.14	0.22
244.14	4.19	-0.76	-0.87	5.76	18.88	-0.95	-0.73	19.60	0.46	0.48	0.22	0.31	0.38	0.56	0.28	0.32
253.91	3.41	-0.01	-0.66	6.85	21.31	0.00	-0.65	19.60	3.17	3.73	1.46	1.40	2.77	2.38	1.50	1.59
263.67	5.62	-1.83	-1.32	7.60	20.38	-0.28	-1.12	20.67	0.70	0.68	0.52	0.43	0.87	0.98	0.46	0.48
273.44	5.66	-1.95	-2.12	9.01	20.71	1.00	-1.06	20.04	0.35	0.41	0.26	0.28	0.54	0.51	0.30	0.34
283.20	5.89	-0.52	-1.86	7.82	21.57	1.57	-0.29	19.43	0.32	0.38	0.22	0.23	0.32	0.36	0.17	0.22
292.97	6.53	-0.42	-1.73	8.32	22.88	1.14	-0.38	20.40	0.20	0.30	0.20	0.15	0.26	0.23	0.16	0.14
302.73	7.53	-0.47	-2.14	8.83	24.06	0.82	-0.74	20.98	0.20	0.28	0.12	0.14	0.25	0.20	0.17	0.20
312.50	9.07	-0.45	-2.07	7.94	23.82	-0.18	-1.02	20.94	0.22	0.27	0.12	0.15	0.15	0.26	0.09	0.20
322.27	10.24	-0.51	-0.29	9.96	26.06	1.65	0.80	24.48	0.17	0.30	0.21	0.19	0.23	0.14	0.20	0.18
332.03	10.70	-0.85	-2.30	9.60	25.39	1.10	-0.35	24.38	0.21	0.21	0.16	0.23	0.22	0.22	0.20	0.21
341.80	11.01	0.68	-1.56	10.49	29.36	0.72	0.09	25.67	0.31	0.20	0.18	0.16	0.40	0.20	0.27	0.23

Table 25. 0.2 mm (8 mils), PR=0.6, zero inlet preswirl, and 20,200 RPM

	Test Data								Uncertainties							
Freq Hz	Re H_{xx}	Re H_{xy}	Re H_{yx}	Re H_{yy}	Im H_{xx}	Im H_{xy}	Im H_{yx}	Im H_{yy}	Re H_{xx}	Re H_{xy}	Re H_{yx}	Re H_{yy}	Im H_{xx}	Im H_{xy}	Im H_{yx}	Im H_{yy}
9.77	-3.01	0.94	-1.17	-1.82	-0.19	0.35	-0.01	0.56	0.41	0.19	0.25	0.13	0.28	0.22	0.38	0.16
19.53	-4.64	1.46	-2.98	-2.23	2.77	-0.14	0.69	1.05	0.70	0.10	0.59	0.10	0.79	0.12	0.46	0.10
29.30	-2.59	0.77	-1.19	-1.71	2.26	0.55	0.26	1.14	0.10	0.12	0.11	0.19	0.09	0.16	0.10	0.16
39.06	-2.25	0.76	-1.48	-1.59	3.44	-0.33	-0.14	3.47	0.12	0.14	0.14	0.14	0.11	0.15	0.08	0.14
48.83	-2.17	1.09	-1.32	-1.99	4.02	0.08	-0.32	4.07	0.58	0.39	0.25	0.15	0.48	0.43	0.16	0.19
58.59	-2.20	1.01	-1.52	-1.81	4.60	0.39	-0.21	4.35	0.11	0.18	0.17	0.17	0.22	0.19	0.20	0.17
68.36	-3.20	1.72	-1.26	-2.58	6.11	-0.95	0.77	5.68	0.54	0.32	0.33	0.25	0.68	0.20	0.49	0.23
78.13	-2.17	0.94	-1.43	-2.03	6.67	-0.52	-0.41	7.07	0.13	0.13	0.13	0.12	0.15	0.12	0.16	0.16
87.89	-1.95	0.85	-1.54	-1.47	7.54	-0.48	-0.14	8.12	0.09	0.11	0.05	0.12	0.07	0.14	0.08	0.10
97.66	-1.35	0.71	-1.42	-0.91	8.47	-0.54	-0.18	8.93	0.20	0.18	0.15	0.12	0.20	0.19	0.14	0.15
107.42	-1.39	0.84	-1.37	-0.39	8.74	-0.45	-0.85	9.68	0.19	0.10	0.14	0.15	0.17	0.11	0.25	0.12
117.19	-0.85	0.70	-1.86	-0.03	9.54	-0.45	-0.63	10.39	0.18	0.09	0.15	0.11	0.18	0.11	0.18	0.13
126.95	-0.55	0.91	-1.72	0.70	10.60	-0.34	-0.55	11.06	0.09	0.17	0.11	0.24	0.11	0.22	0.13	0.22
136.72	-0.03	0.43	-1.91	0.82	11.10	-0.37	-0.48	11.86	0.09	0.11	0.06	0.12	0.09	0.13	0.08	0.11
146.48	0.51	0.18	-2.39	1.92	11.77	0.26	-0.27	11.75	0.15	0.09	0.09	0.13	0.16	0.11	0.14	0.13
156.25	1.00	-0.10	-2.83	3.23	12.75	-1.19	-3.18	15.44	0.31	0.14	0.28	0.17	0.45	0.13	0.40	0.21
166.02	1.60	0.36	-2.59	2.54	13.64	-0.79	-0.88	14.40	0.13	0.24	0.11	0.16	0.16	0.18	0.13	0.24
175.78	2.71	0.52	-2.65	2.55	18.70	-1.29	-0.96	14.63	0.36	0.21	0.22	0.10	0.33	0.18	0.09	0.13
185.55	1.67	0.43	-2.42	2.77	14.31	-0.04	-0.50	15.01	0.10	0.09	0.09	0.12	0.12	0.10	0.14	0.11
195.31	1.95	0.84	-2.37	2.61	15.08	0.06	-0.07	15.48	0.12	0.12	0.12	0.11	0.16	0.11	0.10	0.12
205.08	2.46	0.58	-2.69	3.72	16.06	-0.27	-0.46	16.64	0.13	0.33	0.13	0.20	0.21	0.23	0.19	0.22
214.84	3.16	0.32	-2.63	4.20	16.54	-0.47	0.26	17.24	0.13	0.16	0.07	0.14	0.11	0.14	0.08	0.14
224.61	3.47	0.78	-2.34	4.54	16.68	-0.34	-0.05	17.64	0.10	0.12	0.10	0.11	0.15	0.12	0.07	0.13
234.38	3.73	0.46	-2.20	5.16	17.80	-0.53	0.69	18.24	0.16	0.12	0.10	0.15	0.13	0.15	0.13	0.16
244.14	4.39	0.72	-1.95	5.89	18.67	-0.84	0.01	19.14	0.26	0.21	0.09	0.12	0.13	0.35	0.08	0.13
253.91	3.80	1.47	-1.59	6.83	20.78	-0.38	-0.33	19.47	1.63	2.23	0.35	0.32	1.18	0.90	0.38	0.54
263.67	5.94	-0.33	-2.30	7.58	19.71	-0.82	-0.68	20.20	0.24	0.22	0.19	0.16	0.49	0.52	0.14	0.18
273.44	5.84	-0.54	-3.21	8.98	19.94	0.59	-0.10	19.29	0.19	0.17	0.11	0.14	0.34	0.24	0.15	0.16
283.20	5.80	0.93	-2.60	8.06	21.31	0.67	0.09	18.91	0.21	0.22	0.09	0.17	0.19	0.24	0.14	0.14
292.97	6.89	0.70	-2.78	8.35	22.30	-0.04	-0.26	20.39	0.15	0.22	0.13	0.13	0.15	0.19	0.14	0.13
302.73	7.52	0.49	-3.26	9.29	23.20	0.21	-0.48	20.39	0.21	0.28	0.16	0.13	0.24	0.19	0.12	0.17
312.50	8.88	0.31	-3.11	8.30	23.18	-1.04	-0.66	20.18	0.20	0.27	0.13	0.16	0.22	0.22	0.13	0.18
322.27	10.42	0.38	-1.60	9.85	25.44	0.63	0.84	23.27	0.36	0.36	0.24	0.24	0.36	0.24	0.25	0.24
332.03	11.17	0.27	-3.36	10.74	25.53	0.48	-0.03	23.16	0.95	0.84	0.53	0.53	0.89	0.88	0.57	0.52
341.80	11.37	1.10	-3.16	10.63	26.45	-0.14	0.12	24.50	1.15	0.76	0.63	0.43	1.22	0.73	0.70	0.50

Table 26. 0.2 mm (8 mils), PR=0.4, medium inlet preswirl, and 10,200 RPM

	Test Data								Uncertainties							
Freq Hz	Re H_{xx}	Re H_{xy}	Re H_{yx}	Re H_{yy}	Im H_{xx}	Im H_{xy}	Im H_{yx}	Im H_{yy}	Re H_{xx}	Re H_{xy}	Re H_{yx}	Re H_{yy}	Im H_{xx}	Im H_{xy}	Im H_{yx}	Im H_{yy}
9.77	-0.96	0.93	-1.18	-0.97	0.54	-0.11	0.03	0.55	-0.18	-0.13	-0.23	-0.16	-0.26	-0.12	-0.25	-0.12
19.53	-0.79	1.08	-1.19	-1.14	0.91	0.00	0.01	0.90	-0.17	-0.08	-0.14	-0.12	-0.11	-0.08	-0.10	-0.12
29.30	-0.96	0.88	-1.06	-0.91	1.26	-0.13	-0.04	1.56	-0.10	-0.13	-0.12	-0.18	-0.09	-0.12	-0.11	-0.14
39.06	-0.85	0.91	-1.12	-0.75	1.81	-0.06	0.13	1.77	-0.07	-0.15	-0.11	-0.17	-0.08	-0.12	-0.07	-0.08
48.83	-0.73	1.01	-1.07	-0.87	2.29	-0.03	-0.01	2.27	-0.17	-0.19	-0.16	-0.23	-0.19	-0.13	-0.23	-0.15
58.59	-0.59	1.13	-1.11	-0.77	2.74	-0.13	-0.23	2.93	-0.12	-0.11	-0.15	-0.19	-0.12	-0.13	-0.18	-0.22
68.36	-0.64	1.01	-1.12	-0.43	3.08	0.11	-0.26	3.09	-0.12	-0.26	-0.14	-0.19	-0.11	-0.27	-0.14	-0.20
78.13	-0.34	0.88	-1.11	-0.26	3.50	-0.11	-0.15	3.77	-0.09	-0.10	-0.14	-0.10	-0.08	-0.10	-0.12	-0.12
87.89	-0.19	1.13	-1.20	-0.09	3.88	-0.09	-0.18	4.15	-0.07	-0.11	-0.06	-0.11	-0.08	-0.08	-0.06	-0.13
97.66	-0.04	1.15	-1.23	-0.03	4.25	-0.01	-0.09	4.38	-0.12	-0.10	-0.09	-0.11	-0.08	-0.08	-0.11	-0.11
107.42	0.24	1.02	-1.29	0.40	4.57	-0.19	-0.10	4.72	-0.09	-0.12	-0.17	-0.14	-0.08	-0.10	-0.12	-0.11
117.19	0.44	1.02	-1.17	0.48	4.84	-0.12	-0.20	5.06	-0.11	-0.10	-0.08	-0.11	-0.07	-0.12	-0.06	-0.12
126.95	0.65	0.86	-1.41	1.00	5.16	-0.06	-0.22	5.39	-0.10	-0.17	-0.08	-0.11	-0.08	-0.15	-0.10	-0.15
136.72	0.66	1.16	-1.26	0.84	5.42	-0.24	-0.11	5.68	-0.06	-0.08	-0.08	-0.14	-0.05	-0.06	-0.08	-0.09
146.48	0.86	1.08	-1.40	1.17	5.94	-0.09	-0.07	5.57	-0.07	-0.13	-0.06	-0.10	-0.06	-0.11	-0.05	-0.13
156.25	1.25	1.04	-1.44	1.32	6.04	-0.15	-0.42	6.53	-0.06	-0.08	-0.08	-0.15	-0.10	-0.09	-0.12	-0.07
166.02	0.18	2.13	-0.73	0.65	7.71	-1.24	-1.41	7.57	-0.09	-0.19	-0.09	-0.20	-0.13	-0.22	-0.13	-0.12
175.78	1.13	1.65	-0.77	1.05	6.20	-0.10	-0.03	6.55	-0.06	-0.12	-0.08	-0.14	-0.08	-0.11	-0.08	-0.08
185.55	1.84	1.03	-1.56	2.04	6.83	-0.24	-0.04	6.96	-0.06	-0.10	-0.06	-0.12	-0.06	-0.06	-0.07	-0.08
195.31	1.81	1.01	-1.40	2.18	6.94	-0.12	0.02	7.24	-0.08	-0.13	-0.07	-0.12	-0.07	-0.09	-0.07	-0.11
205.08	2.22	0.82	-1.89	2.18	7.26	-0.10	0.05	7.38	-0.16	-0.24	-0.17	-0.21	-0.10	-0.23	-0.08	-0.23
214.84	2.60	0.98	-1.54	2.62	7.36	-0.09	0.30	7.72	-0.07	-0.10	-0.06	-0.08	-0.08	-0.09	-0.04	-0.12
224.61	2.50	0.93	-1.59	2.77	7.61	-0.03	0.24	7.69	-0.10	-0.14	-0.09	-0.11	-0.08	-0.11	-0.08	-0.08
234.38	2.75	0.93	-1.43	2.84	7.76	-0.02	0.35	7.95	-0.07	-0.11	-0.06	-0.14	-0.10	-0.20	-0.07	-0.09
244.14	2.99	1.03	-1.38	2.93	8.14	0.10	0.10	8.55	-0.15	-0.22	-0.05	-0.14	-0.15	-0.23	-0.05	-0.11
253.91	3.88	1.03	-1.38	3.75	8.16	1.84	0.14	8.73	-1.14	-2.20	-0.19	-0.18	-1.69	-1.49	-0.15	-0.23
263.67	3.60	1.30	-1.66	4.05	8.68	0.24	-0.03	8.60	-0.27	-0.29	-0.15	-0.22	-0.21	-0.28	-0.11	-0.21
273.44	3.56	1.40	-1.75	3.80	8.57	-0.04	0.15	8.50	-0.14	-0.23	-0.13	-0.16	-0.11	-0.16	-0.12	-0.22
283.20	3.78	1.62	-1.79	4.00	8.89	0.18	0.45	9.49	-0.12	-0.21	-0.07	-0.12	-0.16	-0.16	-0.07	-0.14
292.97	4.21	1.32	-1.51	4.50	8.86	-0.29	1.03	8.76	-0.18	-0.14	-0.11	-0.22	-0.14	-0.13	-0.11	-0.13
302.73	2.69	1.59	0.00	4.36	9.35	-0.51	-0.08	9.43	-0.28	-0.28	-0.27	-0.31	-0.17	-0.76	-0.14	-0.58
312.50	4.53	1.26	-1.65	4.33	9.05	-0.80	0.58	9.61	-0.13	-0.17	-0.12	-0.22	-0.12	-0.14	-0.13	-0.11
322.27	4.69	1.34	-1.48	4.80	9.05	-0.57	0.57	10.16	-0.16	-0.18	-0.13	-0.16	-0.19	-0.20	-0.13	-0.10
332.03	4.05	0.95	-1.17	5.35	9.90	-0.21	0.41	10.56	-0.18	-0.14	-0.15	-0.18	-0.15	-0.18	-0.15	-0.11
341.80	2.86	0.61	-1.11	7.13	10.50	1.47	-0.05	10.85	-0.34	-0.28	-0.28	-0.34	-0.31	-0.23	-0.41	-0.16

Table 27. 0.2 mm (8 mils), PR=0.4, medium inlet preswirl, and 15,350 RPM

	Test Data								Uncertainties							
Freq Hz	Re H_{xx}	Re H_{xy}	Re H_{yx}	Re H_{yy}	Im H_{xx}	Im H_{xy}	Im H_{yx}	Im H_{yy}	Re H_{xx}	Re H_{xy}	Re H_{yx}	Re H_{yy}	Im H_{xx}	Im H_{xy}	Im H_{yx}	Im H_{yy}
9.77	-1.07	1.32	-1.69	-1.12	0.53	-0.10	0.06	0.54	-0.16	-0.15	-0.15	-0.14	-0.23	-0.12	-0.24	-0.12
19.53	-0.91	1.41	-1.64	-1.27	0.98	0.01	0.00	0.97	-0.17	-0.08	-0.13	-0.08	-0.13	-0.11	-0.12	-0.10
29.30	-0.99	1.40	-1.62	-1.08	1.44	0.02	0.02	1.50	-0.12	-0.17	-0.15	-0.08	-0.10	-0.12	-0.08	-0.12
39.06	-0.86	1.41	-1.71	-1.10	1.93	-0.02	0.10	2.04	-0.10	-0.20	-0.11	-0.15	-0.10	-0.10	-0.09	-0.10
48.83	-0.73	1.31	-1.70	-0.77	2.45	-0.04	0.00	2.41	-0.11	-0.14	-0.14	-0.10	-0.12	-0.12	-0.13	-0.11
58.59	-0.59	1.55	-1.59	-0.78	2.97	-0.24	-0.14	3.00	-0.11	-0.12	-0.18	-0.17	-0.12	-0.10	-0.21	-0.18
68.36	-0.47	1.34	-1.73	-0.36	3.24	-0.10	-0.19	3.50	-0.13	-0.23	-0.12	-0.25	-0.10	-0.16	-0.15	-0.18
78.13	-0.41	1.28	-1.62	-0.36	3.80	-0.21	-0.05	3.88	-0.08	-0.10	-0.13	-0.10	-0.08	-0.10	-0.09	-0.12
87.89	-0.09	1.44	-1.58	-0.15	4.20	-0.26	-0.13	4.37	-0.08	-0.09	-0.07	-0.11	-0.06	-0.07	-0.05	-0.07
97.66	0.19	1.39	-1.68	0.07	4.58	-0.18	-0.11	4.68	-0.10	-0.09	-0.07	-0.12	-0.07	-0.09	-0.09	-0.10
107.42	0.49	1.35	-1.83	0.36	4.79	-0.19	0.03	4.95	-0.10	-0.13	-0.11	-0.10	-0.06	-0.09	-0.09	-0.10
117.19	0.67	1.34	-1.72	0.53	5.13	-0.28	-0.20	5.42	-0.09	-0.11	-0.11	-0.09	-0.05	-0.10	-0.07	-0.07
126.95	0.74	1.27	-1.75	0.88	5.52	-0.11	0.03	5.68	-0.11	-0.14	-0.07	-0.17	-0.09	-0.19	-0.11	-0.14
136.72	0.93	1.40	-1.79	1.11	5.72	-0.25	0.05	5.93	-0.05	-0.10	-0.10	-0.09	-0.07	-0.12	-0.06	-0.10
146.48	0.79	1.16	-2.35	1.19	9.33	-0.60	-0.68	5.99	-0.28	-0.12	-0.08	-0.12	-0.10	-0.11	-0.07	-0.16
156.25	1.32	1.43	-1.93	1.42	6.40	-0.26	-0.01	6.81	-0.06	-0.12	-0.07	-0.11	-0.10	-0.11	-0.10	-0.10
166.02	0.82	1.52	-1.42	0.88	6.76	-0.52	-0.22	7.24	-0.08	-0.14	-0.08	-0.13	-0.06	-0.16	-0.07	-0.19
175.78	1.62	1.31	-2.08	2.00	6.50	-0.49	0.05	7.13	-0.09	-0.12	-0.08	-0.09	-0.08	-0.13	-0.06	-0.11
185.55	1.83	1.54	-1.64	1.80	7.28	-0.31	-0.05	7.22	-0.07	-0.08	-0.07	-0.08	-0.05	-0.10	-0.08	-0.07
195.31	2.22	1.28	-1.93	2.28	7.37	-0.30	0.08	7.56	-0.05	-0.09	-0.06	-0.10	-0.06	-0.07	-0.05	-0.08
205.08	2.75	1.48	-2.58	1.98	7.83	-0.59	-0.02	8.05	-0.21	-0.23	-0.18	-0.20	-0.16	-0.33	-0.10	-0.26
214.84	2.80	1.22	-2.06	2.57	7.78	-0.20	0.28	8.11	-0.06	-0.12	-0.06	-0.09	-0.09	-0.09	-0.05	-0.10
224.61	2.72	1.11	-2.21	2.94	8.25	-0.30	0.29	8.30	-0.08	-0.10	-0.05	-0.10	-0.09	-0.10	-0.09	-0.09
234.38	3.12	1.11	-1.94	3.09	8.30	-0.12	0.58	8.37	-0.08	-0.12	-0.06	-0.11	-0.10	-0.15	-0.09	-0.10
244.14	3.26	0.93	-1.91	3.31	8.46	-0.16	0.29	9.19	-0.24	-0.19	-0.09	-0.12	-0.13	-0.24	-0.08	-0.11
253.91	2.77	1.06	-2.03	4.54	8.01	2.32	1.34	9.38	-1.47	-2.55	-0.51	-0.27	-2.25	-1.55	-0.23	-0.38
263.67	3.48	1.32	-1.97	4.30	8.97	0.06	0.71	9.21	-0.35	-0.26	-0.11	-0.15	-0.33	-0.33	-0.18	-0.12
273.44	3.82	1.60	-2.22	4.18	9.18	-0.22	0.49	9.02	-0.15	-0.15	-0.08	-0.16	-0.15	-0.18	-0.14	-0.10
283.20	4.26	2.01	-2.18	4.76	9.15	0.28	0.67	9.72	-0.12	-0.24	-0.15	-0.17	-0.14	-0.21	-0.08	-0.17
292.97	4.35	1.18	-4.11	0.99	9.79	0.31	1.61	13.70	-0.14	-0.17	-0.19	-0.49	-0.15	-0.14	-0.27	-0.38
302.73	6.10	0.41	-3.06	6.09	9.78	0.99	0.59	8.44	-0.11	-0.15	-0.08	-0.11	-0.13	-0.13	-0.11	-0.13
312.50	5.16	0.79	-2.19	5.72	11.77	-1.56	-0.51	10.56	-0.18	-0.21	-0.19	-0.19	-0.21	-0.16	-0.12	-0.17
322.27	5.35	1.82	-2.23	5.02	10.38	-0.70	0.41	10.63	-0.15	-0.15	-0.16	-0.14	-0.26	-0.15	-0.13	-0.15
332.03	4.67	1.37	-1.59	5.52	10.97	-0.48	0.54	11.08	-0.22	-0.16	-0.15	-0.16	-0.18	-0.13	-0.12	-0.12
341.80	3.31	1.49	-0.38	7.53	12.46	1.75	1.14	12.67	-0.20	-0.28	-0.19	-0.23	-0.16	-0.15	-0.18	-0.17

Table 28. 0.2 mm (8 mils), PR=0.4, medium inlet preswirl, and 20,200 RPM

	Test Data								Uncertainties							
Freq Hz	Re H_{xx}	Re H_{xy}	Re H_{yx}	Re H_{yy}	Im H_{xx}	Im H_{xy}	Im H_{yx}	Im H_{yy}	Re H_{xx}	Re H_{xy}	Re H_{yx}	Re H_{yy}	Im H_{xx}	Im H_{xy}	Im H_{yx}	Im H_{yy}
9.77	-1.11	1.99	-2.14	-1.15	0.60	-0.05	0.00	0.57	-0.17	-0.15	-0.15	-0.18	-0.20	-0.10	-0.20	-0.08
19.53	-0.95	2.14	-2.24	-1.18	1.06	-0.09	0.07	1.07	-0.19	-0.07	-0.12	-0.10	-0.11	-0.11	-0.11	-0.08
29.30	-1.06	2.09	-2.18	-0.86	1.57	-0.21	0.08	1.63	-0.11	-0.14	-0.10	-0.11	-0.10	-0.15	-0.09	-0.15
39.06	-0.84	1.94	-2.06	-1.01	2.14	-0.33	0.14	2.18	-0.08	-0.15	-0.10	-0.13	-0.10	-0.20	-0.11	-0.22
48.83	-0.62	2.10	-2.25	-0.76	3.08	-0.53	0.16	2.69	-0.49	-0.44	-0.28	-0.17	-0.66	-0.58	-0.23	-0.15
58.59	-0.51	2.19	-2.19	-0.62	3.25	-0.42	-0.05	3.42	-0.14	-0.12	-0.17	-0.16	-0.12	-0.11	-0.15	-0.14
68.36	-0.34	1.99	-2.33	-0.12	3.57	-0.30	0.20	3.67	-0.14	-0.14	-0.12	-0.19	-0.10	-0.18	-0.19	-0.22
78.13	-0.21	1.91	-1.99	-0.22	4.02	-0.44	0.27	4.24	-0.08	-0.11	-0.08	-0.12	-0.11	-0.11	-0.09	-0.11
87.89	0.05	1.95	-2.07	0.00	4.47	-0.50	0.10	4.59	-0.07	-0.08	-0.05	-0.11	-0.07	-0.06	-0.05	-0.06
97.66	0.34	1.97	-2.08	0.30	4.74	-0.44	0.23	4.93	-0.08	-0.12	-0.11	-0.09	-0.09	-0.12	-0.08	-0.08
107.42	0.64	1.89	-2.28	0.52	5.28	-0.49	0.33	5.37	-0.10	-0.09	-0.15	-0.14	-0.08	-0.12	-0.13	-0.12
117.19	0.90	1.73	-2.08	0.84	5.45	-0.53	0.13	5.65	-0.12	-0.10	-0.11	-0.11	-0.11	-0.08	-0.09	-0.09
126.95	1.12	1.94	-2.09	0.97	6.01	-0.66	0.04	6.12	-0.10	-0.13	-0.06	-0.14	-0.08	-0.14	-0.08	-0.14
136.72	1.37	1.72	-2.23	1.27	6.13	-0.66	0.21	6.39	-0.10	-0.12	-0.06	-0.11	-0.06	-0.12	-0.05	-0.09
146.48	1.53	1.87	-2.58	1.55	9.70	-1.01	-0.12	6.26	-0.14	-0.23	-0.08	-0.15	-0.12	-0.15	-0.07	-0.13
156.25	1.84	1.83	-2.11	1.69	6.82	-0.62	0.12	7.14	-0.06	-0.09	-0.08	-0.13	-0.12	-0.11	-0.08	-0.12
166.02	1.14	1.94	-1.79	1.81	7.24	-0.76	0.01	7.41	-0.07	-0.08	-0.08	-0.13	-0.05	-0.14	-0.06	-0.14
175.78	1.87	1.99	-2.26	1.92	6.95	-0.71	0.06	7.62	-0.09	-0.15	-0.10	-0.13	-0.09	-0.10	-0.09	-0.16
185.55	2.46	1.84	-1.99	2.31	7.81	-0.73	0.04	7.75	-0.07	-0.15	-0.07	-0.11	-0.09	-0.08	-0.07	-0.11
195.31	2.78	1.70	-2.27	2.82	7.79	-0.67	0.30	8.01	-0.07	-0.11	-0.05	-0.08	-0.08	-0.07	-0.06	-0.07
205.08	3.64	1.34	-2.54	3.01	7.81	-1.61	0.54	8.44	-0.16	-0.22	-0.15	-0.20	-0.16	-0.31	-0.19	-0.28
214.84	3.53	1.60	-2.48	3.35	8.08	-0.69	0.58	8.66	-0.06	-0.10	-0.08	-0.07	-0.07	-0.12	-0.04	-0.09
224.61	3.32	1.49	-2.29	3.69	8.42	-0.60	0.64	8.59	-0.09	-0.12	-0.08	-0.11	-0.06	-0.12	-0.06	-0.11
234.38	3.75	1.45	-2.30	3.73	8.64	-0.63	0.68	8.80	-0.09	-0.14	-0.06	-0.13	-0.10	-0.15	-0.06	-0.08
244.14	3.95	1.39	-2.07	3.95	9.10	-0.47	0.41	9.49	-0.15	-0.20	-0.11	-0.13	-0.14	-0.20	-0.06	-0.10
253.91	5.24	1.33	-2.28	4.98	9.00	1.55	0.30	9.54	-1.12	-2.22	-0.18	-0.16	-1.72	-1.49	-0.12	-0.23
263.67	4.77	1.98	-2.36	5.01	9.14	-0.02	0.65	9.25	-0.28	-0.28	-0.14	-0.09	-0.28	-0.31	-0.15	-0.15
273.44	4.52	2.07	-2.44	4.96	9.11	-0.37	0.84	9.42	-0.09	-0.23	-0.08	-0.13	-0.15	-0.15	-0.11	-0.16
283.20	4.91	2.60	-2.14	5.24	9.79	-0.77	0.85	9.95	-0.13	-0.15	-0.08	-0.10	-0.11	-0.22	-0.07	-0.12
292.97	5.00	1.05	-3.05	1.47	9.85	-0.31	1.50	11.43	-0.12	-0.16	-0.14	-0.17	-0.10	-0.14	-0.13	-0.23
302.73	6.59	0.36	-3.04	7.39	10.20	0.61	0.81	8.73	-0.16	-0.15	-0.13	-0.13	-0.15	-0.15	-0.12	-0.12
312.50	5.59	1.08	-1.92	6.68	12.56	-2.76	-0.89	11.93	-0.25	-0.18	-0.24	-0.16	-0.19	-0.20	-0.21	-0.30
322.27	6.81	2.77	-2.50	5.50	10.97	-1.44	0.17	10.72	-0.20	-0.19	-0.11	-0.15	-0.21	-0.18	-0.17	-0.17
332.03	5.60	1.56	-1.67	7.35	11.42	1.05	0.68	10.95	-0.28	-0.45	-0.22	-0.17	-0.29	-0.32	-0.21	-0.37
341.80	4.91	2.72	-0.91	7.39	12.46	-0.94	0.13	11.52	-0.30	-0.31	-0.24	-0.17	-0.26	-0.22	-0.24	-0.15

Table 29. 0.2 mm (8 mils), PR=0.5, medium inlet preswirl, and 10,200 RPM

	Test Data								Uncertainties							
Freq Hz	Re H_{xx}	Re H_{xy}	Re H_{yx}	Re H_{yy}	Im H_{xx}	Im H_{xy}	Im H_{yx}	Im H_{yy}	Re H_{xx}	Re H_{xy}	Re H_{yx}	Re H_{yy}	Im H_{xx}	Im H_{xy}	Im H_{yx}	Im H_{yy}
9.77	-1.04	0.88	-0.93	-1.06	0.36	0.11	0.06	0.41	-0.14	-0.14	-0.15	-0.16	-0.21	-0.10	-0.20	-0.10
19.53	-0.71	0.87	-1.17	-1.15	0.84	0.13	-0.08	0.77	-0.16	-0.08	-0.13	-0.10	-0.11	-0.12	-0.09	-0.09
29.30	-0.81	0.82	-1.00	-0.82	1.28	0.04	-0.10	1.40	-0.11	-0.15	-0.12	-0.17	-0.12	-0.12	-0.12	-0.18
39.06	-0.76	0.69	-1.12	-0.80	1.78	-0.20	0.01	1.76	-0.07	-0.14	-0.09	-0.20	-0.10	-0.15	-0.09	-0.08
48.83	-0.80	0.95	-1.08	-0.56	2.38	0.23	0.07	2.34	-0.14	-0.12	-0.21	-0.17	-0.10	-0.15	-0.21	-0.21
58.59	-0.47	0.83	-1.09	-0.72	2.60	0.01	-0.23	2.66	-0.12	-0.12	-0.16	-0.19	-0.12	-0.12	-0.15	-0.12
68.36	-0.29	0.93	-1.12	-0.50	2.80	0.13	-0.19	3.05	-0.12	-0.19	-0.12	-0.19	-0.14	-0.22	-0.15	-0.12
78.13	-0.36	0.87	-1.06	-0.43	3.44	0.02	-0.16	3.61	-0.08	-0.08	-0.11	-0.11	-0.09	-0.12	-0.11	-0.09
87.89	-0.12	0.95	-1.13	-0.23	3.71	0.01	-0.24	3.91	-0.07	-0.10	-0.05	-0.11	-0.07	-0.07	-0.08	-0.08
97.66	0.14	0.95	-1.15	-0.10	4.10	-0.08	-0.17	4.27	-0.10	-0.09	-0.08	-0.14	-0.12	-0.11	-0.14	-0.09
107.42	0.21	0.98	-1.33	0.14	4.32	0.01	-0.08	4.58	-0.10	-0.08	-0.09	-0.14	-0.09	-0.11	-0.10	-0.09
117.19	0.44	0.94	-1.31	0.40	4.75	-0.10	-0.12	4.88	-0.13	-0.08	-0.08	-0.09	-0.10	-0.08	-0.08	-0.09
126.95	0.52	1.00	-1.25	0.50	5.00	0.03	-0.30	5.18	-0.12	-0.24	-0.08	-0.15	-0.10	-0.24	-0.07	-0.17
136.72	0.54	0.92	-1.27	0.63	5.18	-0.11	-0.16	5.50	-0.11	-0.15	-0.08	-0.14	-0.10	-0.11	-0.07	-0.12
146.48	0.83	1.13	-1.19	0.82	5.77	-0.01	0.04	5.58	-0.14	-0.24	-0.13	-0.17	-0.09	-0.15	-0.11	-0.11
156.25	1.00	0.97	-1.12	0.98	5.96	0.09	-0.30	6.05	-0.31	-0.28	-0.16	-0.20	-0.23	-0.34	-0.17	-0.20
166.02	-0.34	3.05	-0.10	-0.75	8.06	-2.01	-1.36	6.64	-0.62	-0.91	-0.53	-1.20	-0.57	-1.35	-0.57	-0.88
175.78	0.94	0.98	-0.99	0.85	6.18	-0.09	-0.19	6.89	-0.51	-0.63	-0.28	-0.52	-0.51	-0.64	-0.40	-0.39
185.55	1.50	1.02	-1.37	1.68	7.00	-0.15	-0.37	6.97	-0.23	-0.22	-0.16	-0.20	-0.20	-0.26	-0.14	-0.20
195.31	1.46	0.97	-1.41	1.78	6.89	-0.01	-0.04	7.10	-0.16	-0.15	-0.10	-0.11	-0.16	-0.16	-0.07	-0.15
205.08	1.86	0.63	-1.82	1.69	7.05	-0.35	-0.21	7.39	-0.26	-0.31	-0.19	-0.20	-0.22	-0.47	-0.16	-0.32
214.84	2.36	0.90	-1.74	2.29	7.25	-0.16	0.14	7.56	-0.10	-0.13	-0.09	-0.10	-0.09	-0.13	-0.05	-0.13
224.61	2.16	0.88	-1.63	2.38	7.62	-0.03	0.17	7.52	-0.10	-0.12	-0.05	-0.11	-0.17	-0.14	-0.10	-0.11
234.38	2.44	1.00	-1.50	2.37	7.90	0.18	0.31	7.75	-0.10	-0.17	-0.05	-0.09	-0.13	-0.14	-0.06	-0.13
244.14	2.62	1.05	-1.42	2.49	8.37	0.21	-0.09	8.71	-0.21	-0.20	-0.12	-0.15	-0.16	-0.32	-0.11	-0.20
253.91	3.50	1.03	-1.45	3.45	8.25	1.92	0.00	8.82	-1.19	-2.19	-0.19	-0.19	-1.70	-1.52	-0.13	-0.23
263.67	3.11	0.99	-1.58	3.71	8.49	0.17	0.17	8.76	-0.29	-0.26	-0.11	-0.14	-0.28	-0.38	-0.09	-0.16
273.44	3.04	1.11	-1.69	3.51	8.64	0.14	0.28	8.64	-0.12	-0.18	-0.11	-0.15	-0.12	-0.21	-0.13	-0.17
283.20	3.39	1.65	-1.66	3.78	8.85	0.07	0.28	9.51	-0.09	-0.18	-0.09	-0.18	-0.19	-0.18	-0.10	-0.17
292.97	3.86	1.23	-1.39	4.85	8.94	-0.27	0.85	9.04	-0.15	-0.20	-0.12	-0.17	-0.13	-0.17	-0.18	-0.10
302.73	3.68	0.76	-1.25	4.65	9.09	0.77	0.49	8.39	-0.14	-0.18	-0.14	-0.16	-0.17	-0.12	-0.10	-0.13
312.50	4.29	1.01	-1.83	4.05	9.45	-0.75	0.22	9.94	-0.19	-0.19	-0.15	-0.14	-0.15	-0.22	-0.15	-0.18
322.27	4.21	1.36	-1.66	4.14	9.75	-0.10	0.23	10.17	-0.18	-0.20	-0.16	-0.18	-0.17	-0.21	-0.12	-0.15
332.03	3.80	0.95	-1.12	4.68	9.93	-0.05	0.49	10.76	-0.27	-0.35	-0.31	-0.38	-0.32	-0.30	-0.35	-0.32
341.80	2.83	0.04	-1.49	5.91	10.68	1.40	-0.08	11.69	-1.14	-0.75	-1.41	-0.91	-1.10	-0.72	-1.65	-1.00

Table 30. 0.2 mm (8 mils), PR=0.5, medium inlet preswirl, and 15,350 RPM

	Test Data								Uncertainties							
Freq Hz	Re H_{xx}	Re H_{xy}	Re H_{yx}	Re H_{yy}	Im H_{xx}	Im H_{xy}	Im H_{yx}	Im H_{yy}	Re H_{xx}	Re H_{xy}	Re H_{yx}	Re H_{yy}	Im H_{xx}	Im H_{xy}	Im H_{yx}	Im H_{yy}
9.77	-1.14	1.42	-1.50	-1.05	0.41	-0.04	0.14	0.44	-0.21	-0.14	-0.18	-0.14	-0.24	-0.13	-0.25	-0.14
19.53	-0.87	1.43	-1.66	-1.14	0.90	-0.11	0.14	0.89	-0.16	-0.08	-0.14	-0.08	-0.12	-0.11	-0.10	-0.10
29.30	-1.04	1.41	-1.52	-0.83	1.33	-0.16	0.00	1.58	-0.08	-0.13	-0.12	-0.10	-0.08	-0.17	-0.09	-0.12
39.06	-0.88	1.39	-1.64	-0.77	1.74	-0.07	0.12	1.92	-0.10	-0.15	-0.10	-0.12	-0.10	-0.14	-0.08	-0.15
48.83	-0.88	1.29	-1.52	-0.69	2.41	-0.02	-0.18	2.32	-0.10	-0.15	-0.11	-0.13	-0.13	-0.09	-0.09	-0.09
58.59	-0.69	1.32	-1.55	-0.56	2.87	-0.13	-0.16	2.75	-0.11	-0.13	-0.18	-0.14	-0.13	-0.09	-0.22	-0.18
68.36	-0.48	1.28	-1.62	-0.41	3.12	-0.21	-0.01	3.26	-0.18	-0.20	-0.11	-0.19	-0.15	-0.18	-0.14	-0.13
78.13	-0.43	1.26	-1.61	-0.25	3.64	-0.13	-0.09	3.70	-0.07	-0.10	-0.11	-0.11	-0.09	-0.11	-0.12	-0.12
87.89	-0.13	1.37	-1.61	-0.13	3.98	-0.16	-0.12	4.11	-0.05	-0.10	-0.04	-0.08	-0.06	-0.09	-0.06	-0.07
97.66	0.05	1.39	-1.70	-0.04	4.30	-0.10	-0.09	4.36	-0.07	-0.10	-0.08	-0.11	-0.07	-0.08	-0.08	-0.08
107.42	0.19	1.45	-1.81	0.26	4.65	-0.15	0.00	4.69	-0.09	-0.11	-0.12	-0.12	-0.09	-0.06	-0.14	-0.10
117.19	0.53	1.31	-1.76	0.47	5.05	-0.18	-0.31	5.08	-0.08	-0.07	-0.12	-0.10	-0.11	-0.09	-0.07	-0.09
126.95	0.58	1.41	-1.66	0.54	5.33	-0.25	-0.18	5.56	-0.09	-0.14	-0.07	-0.09	-0.07	-0.11	-0.10	-0.14
136.72	0.73	1.39	-1.82	0.89	5.52	-0.29	-0.03	5.86	-0.07	-0.09	-0.05	-0.10	-0.06	-0.07	-0.06	-0.09
146.48	1.11	1.43	-1.74	0.79	6.07	-0.13	0.19	5.75	-0.08	-0.13	-0.07	-0.12	-0.08	-0.10	-0.05	-0.14
156.25	1.20	1.40	-1.79	1.33	6.15	-0.15	0.11	6.39	-0.06	-0.08	-0.09	-0.10	-0.09	-0.08	-0.07	-0.09
166.02	0.95	1.68	-1.75	0.99	6.39	-0.11	0.06	6.77	-0.05	-0.14	-0.08	-0.20	-0.06	-0.07	-0.09	-0.15
175.78	1.33	1.30	-2.04	1.66	6.81	-0.42	-0.18	7.06	-0.08	-0.12	-0.07	-0.10	-0.09	-0.11	-0.07	-0.08
185.55	1.68	1.60	-1.69	1.49	7.19	-0.16	-0.10	7.09	-0.09	-0.08	-0.05	-0.08	-0.05	-0.11	-0.07	-0.08
195.31	1.83	1.41	-1.83	1.97	7.32	-0.21	0.07	7.47	-0.06	-0.10	-0.05	-0.09	-0.08	-0.08	-0.05	-0.06
205.08	2.40	1.39	-2.13	2.07	7.57	-0.65	0.06	7.56	-0.09	-0.30	-0.11	-0.16	-0.19	-0.20	-0.10	-0.14
214.84	2.54	1.38	-2.09	2.25	7.78	-0.21	0.22	8.01	-0.05	-0.10	-0.06	-0.10	-0.06	-0.12	-0.05	-0.11
224.61	2.47	1.36	-2.09	2.50	8.10	-0.19	0.18	8.23	-0.09	-0.16	-0.08	-0.11	-0.15	-0.12	-0.07	-0.12
234.38	2.82	1.54	-1.99	2.48	8.26	-0.24	0.52	8.42	-0.11	-0.26	-0.06	-0.11	-0.14	-0.14	-0.08	-0.10
244.14	2.89	1.34	-1.76	2.73	8.74	-0.41	0.02	9.24	-0.29	-0.41	-0.13	-0.23	-0.24	-0.35	-0.14	-0.22
253.91	4.25	-0.68	-1.24	4.31	9.90	1.58	-0.26	10.52	-2.89	-4.09	-1.20	-1.57	-3.27	-3.66	-1.23	-1.51
263.67	4.05	1.54	-1.95	3.87	8.92	-0.41	0.17	9.11	-0.54	-0.57	-0.44	-0.31	-0.53	-0.47	-0.24	-0.35
273.44	3.55	1.83	-2.07	3.79	8.89	-0.09	0.64	9.12	-0.20	-0.29	-0.16	-0.18	-0.28	-0.28	-0.12	-0.15
283.20	3.57	2.15	-1.86	4.19	9.45	-0.15	0.74	9.70	-0.10	-0.20	-0.11	-0.15	-0.14	-0.19	-0.10	-0.12
292.97	4.01	1.93	-1.64	5.73	9.49	-0.42	1.19	9.63	-0.13	-0.19	-0.11	-0.15	-0.16	-0.15	-0.14	-0.09
302.73	4.43	1.45	-1.89	5.12	9.52	0.80	0.63	8.82	-0.14	-0.14	-0.09	-0.21	-0.15	-0.18	-0.14	-0.09
312.50	4.69	1.70	-1.91	4.57	10.24	-1.09	0.47	10.33	-0.16	-0.16	-0.14	-0.14	-0.16	-0.19	-0.10	-0.14
322.27	4.41	1.66	-1.80	4.61	10.37	-0.43	0.66	10.70	-0.21	-0.13	-0.17	-0.15	-0.17	-0.18	-0.16	-0.14
332.03	4.42	1.77	-1.51	5.25	10.97	-0.60	0.62	11.04	-0.19	-0.16	-0.17	-0.15	-0.14	-0.19	-0.19	-0.20
341.80	3.54	1.02	-1.45	5.67	11.62	-0.01	0.17	10.90	-0.17	-0.18	-0.14	-0.11	-0.19	-0.17	-0.23	-0.08

Table 31. 0.2 mm (8 mils), PR=0.5, medium inlet preswirl, and 20,200 RPM

	Test Data								Uncertainties							
Freq Hz	Re H_{xx}	Re H_{xy}	Re H_{yx}	Re H_{yy}	Im H_{xx}	Im H_{xy}	Im H_{yx}	Im H_{yy}	Re H_{xx}	Re H_{xy}	Re H_{yx}	Re H_{yy}	Im H_{xx}	Im H_{xy}	Im H_{yx}	Im H_{yy}
9.77	-1.01	1.89	-1.97	-1.03	0.48	-0.06	0.06	0.56	-0.19	-0.12	-0.17	-0.18	-0.25	-0.09	-0.18	-0.08
19.53	-0.77	1.99	-2.12	-1.12	1.01	0.03	-0.02	0.95	-0.21	-0.10	-0.16	-0.08	-0.14	-0.11	-0.10	-0.07
29.30	-0.89	1.98	-1.99	-0.94	1.52	-0.19	-0.03	1.54	-0.10	-0.14	-0.10	-0.14	-0.08	-0.16	-0.09	-0.12
39.06	-0.75	1.96	-2.03	-0.85	1.94	-0.22	0.13	2.04	-0.12	-0.14	-0.11	-0.13	-0.08	-0.14	-0.12	-0.19
48.83	-0.80	1.89	-1.92	-0.76	2.27	0.01	-0.01	2.57	-0.63	-0.63	-0.19	-0.19	-0.75	-0.71	-0.15	-0.24
58.59	-0.56	2.01	-1.95	-0.65	2.98	-0.27	0.01	3.09	-0.10	-0.13	-0.18	-0.14	-0.15	-0.10	-0.15	-0.16
68.36	-0.54	2.14	-1.87	-0.52	3.54	-0.28	0.10	3.30	-0.15	-0.21	-0.11	-0.21	-0.13	-0.13	-0.16	-0.14
78.13	-0.29	1.80	-1.94	-0.27	3.92	-0.31	0.12	4.00	-0.07	-0.09	-0.09	-0.10	-0.11	-0.07	-0.13	-0.13
87.89	-0.03	1.80	-1.98	-0.02	4.27	-0.40	-0.02	4.47	-0.06	-0.09	-0.06	-0.10	-0.06	-0.08	-0.07	-0.10
97.66	0.25	1.90	-1.99	0.06	4.81	-0.37	0.13	4.66	-0.09	-0.12	-0.10	-0.13	-0.10	-0.06	-0.10	-0.09
107.42	0.45	1.78	-2.05	0.41	5.13	-0.36	0.14	5.17	-0.08	-0.12	-0.10	-0.12	-0.12	-0.07	-0.15	-0.10
117.19	0.76	1.77	-2.15	0.68	5.31	-0.42	0.12	5.48	-0.07	-0.11	-0.06	-0.07	-0.12	-0.07	-0.05	-0.09
126.95	1.00	1.88	-2.03	0.86	5.74	-0.39	0.03	5.96	-0.12	-0.15	-0.08	-0.14	-0.10	-0.21	-0.09	-0.12
136.72	1.04	1.83	-2.08	1.02	6.07	-0.55	0.15	6.17	-0.10	-0.11	-0.09	-0.12	-0.07	-0.10	-0.05	-0.10
146.48	1.74	2.07	-1.99	1.17	6.56	-0.48	0.29	6.31	-0.11	-0.12	-0.08	-0.13	-0.06	-0.18	-0.14	-0.13
156.25	1.65	1.66	-2.07	1.60	6.57	-0.51	0.18	6.84	-0.08	-0.10	-0.10	-0.12	-0.06	-0.11	-0.08	-0.12
166.02	1.32	1.76	-2.12	1.81	6.81	-0.44	0.25	7.19	-0.05	-0.18	-0.06	-0.11	-0.07	-0.07	-0.07	-0.11
175.78	1.67	2.01	-2.19	1.84	7.26	-0.70	0.09	7.50	-0.07	-0.12	-0.09	-0.14	-0.08	-0.14	-0.09	-0.12
185.55	2.25	1.94	-2.07	2.12	7.68	-0.58	-0.01	7.81	-0.10	-0.12	-0.08	-0.13	-0.08	-0.15	-0.08	-0.10
195.31	2.30	1.77	-2.03	2.55	7.84	-0.40	0.10	7.84	-0.05	-0.13	-0.04	-0.10	-0.08	-0.08	-0.07	-0.07
205.08	3.12	1.91	-2.46	2.34	8.15	-0.94	0.13	8.15	-0.15	-0.28	-0.15	-0.27	-0.15	-0.20	-0.15	-0.20
214.84	3.13	1.59	-2.41	3.00	8.07	-0.53	0.47	8.60	-0.07	-0.15	-0.06	-0.13	-0.07	-0.10	-0.09	-0.10
224.61	3.02	1.69	-2.26	3.31	8.54	-0.45	0.54	8.51	-0.09	-0.11	-0.09	-0.11	-0.07	-0.13	-0.07	-0.10
234.38	3.29	1.67	-2.14	3.42	8.69	-0.36	0.53	8.61	-0.08	-0.24	-0.04	-0.10	-0.10	-0.15	-0.06	-0.14
244.14	3.55	1.30	-2.05	3.69	9.03	-0.39	0.31	9.45	-0.20	-0.32	-0.09	-0.19	-0.15	-0.28	-0.10	-0.15
253.91	4.74	1.72	-2.24	4.59	9.31	1.60	0.27	9.46	-1.16	-2.26	-0.19	-0.16	-1.74	-1.52	-0.13	-0.25
263.67	4.46	2.26	-2.40	4.45	9.16	-0.05	0.75	9.21	-0.32	-0.38	-0.08	-0.18	-0.28	-0.34	-0.20	-0.14
273.44	3.97	2.44	-2.39	4.57	9.12	-0.17	0.98	9.32	-0.18	-0.31	-0.12	-0.15	-0.19	-0.27	-0.15	-0.21
283.20	4.36	2.77	-2.23	4.69	9.92	-0.67	0.70	10.18	-0.16	-0.23	-0.14	-0.18	-0.17	-0.28	-0.12	-0.18
292.97	4.88	2.26	-1.72	6.93	9.81	-0.54	1.64	10.27	-0.17	-0.22	-0.20	-0.20	-0.18	-0.20	-0.13	-0.18
302.73	5.06	1.81	-1.92	5.94	10.29	0.43	0.87	9.27	-0.24	-0.23	-0.27	-0.20	-0.31	-0.29	-0.14	-0.21
312.50	5.41	2.16	-2.28	5.42	11.18	-1.18	0.49	10.54	-0.54	-0.56	-0.29	-0.33	-0.58	-0.70	-0.41	-0.34
322.27	6.46	2.72	-2.11	5.41	11.13	-0.86	0.20	10.82	-1.09	-0.68	-0.36	-0.55	-0.83	-0.98	-0.67	-0.39
332.03	5.66	5.05	-4.06	4.66	7.07	-1.88	1.62	10.11	-3.26	-3.22	-1.68	-1.76	-2.04	-2.72	-1.46	-1.72
341.80	1.88	1.44	-2.18	6.87	9.54	-0.41	2.25	13.02	-2.78	-1.42	-1.86	-1.03	-2.16	-1.89	-1.24	-1.02

Table 32. 0.2 mm (8 mils), PR=0.6, medium inlet preswirl, and 10,200 RPM

	Test Data								Uncertainties							
Freq Hz	Re H_{xx}	Re H_{xy}	Re H_{yx}	Re H_{yy}	Im H_{xx}	Im H_{xy}	Im H_{yx}	Im H_{yy}	Re H_{xx}	Re H_{xy}	Re H_{yx}	Re H_{yy}	Im H_{xx}	Im H_{xy}	Im H_{yx}	Im H_{yy}
9.77	-0.76	0.90	-0.90	-0.89	0.53	-0.10	-0.11	0.48	-0.20	-0.10	-0.20	-0.12	-0.22	-0.10	-0.20	-0.09
19.53	-0.65	0.87	-1.02	-0.92	0.87	-0.05	-0.06	0.89	-0.16	-0.11	-0.19	-0.10	-0.07	-0.09	-0.10	-0.11
29.30	-0.63	0.70	-1.00	-0.65	1.23	-0.07	-0.11	1.47	-0.12	-0.11	-0.18	-0.10	-0.10	-0.08	-0.10	-0.14
39.06	-0.63	0.74	-1.03	-0.75	1.68	-0.15	0.08	1.81	-0.11	-0.12	-0.10	-0.11	-0.08	-0.11	-0.09	-0.16
48.83	-0.33	0.78	-1.15	-0.49	2.06	0.05	-0.06	2.21	-0.17	-0.13	-0.21	-0.15	-0.25	-0.15	-0.22	-0.23
58.59	-0.32	0.77	-1.01	-0.44	2.54	-0.06	-0.27	2.70	-0.11	-0.13	-0.17	-0.16	-0.11	-0.08	-0.19	-0.15
68.36	-0.11	0.97	-1.15	-0.36	2.75	0.04	-0.10	2.98	-0.19	-0.18	-0.16	-0.16	-0.12	-0.15	-0.22	-0.19
78.13	-0.27	0.82	-0.94	-0.25	3.14	-0.04	-0.30	3.44	-0.11	-0.10	-0.11	-0.10	-0.11	-0.16	-0.14	-0.13
87.89	-0.05	0.93	-1.10	-0.10	3.52	0.00	-0.12	3.71	-0.07	-0.09	-0.07	-0.11	-0.07	-0.07	-0.07	-0.08
97.66	0.21	0.88	-1.26	0.16	3.89	0.02	-0.15	3.91	-0.07	-0.10	-0.11	-0.12	-0.07	-0.09	-0.07	-0.10
107.42	0.25	0.89	-1.42	0.31	4.27	-0.02	-0.16	4.32	-0.08	-0.09	-0.09	-0.12	-0.10	-0.09	-0.15	-0.10
117.19	0.57	0.88	-1.12	0.43	4.47	-0.03	-0.17	4.64	-0.14	-0.09	-0.09	-0.09	-0.08	-0.09	-0.14	-0.08
126.95	0.59	0.99	-1.04	0.42	4.77	-0.02	-0.30	4.86	-0.11	-0.17	-0.09	-0.20	-0.08	-0.14	-0.08	-0.14
136.72	0.68	0.94	-1.11	0.66	4.98	-0.04	-0.29	5.34	-0.08	-0.14	-0.08	-0.12	-0.09	-0.12	-0.06	-0.12
146.48	0.84	1.01	-1.46	1.14	5.35	-0.13	-0.13	5.38	-0.10	-0.16	-0.10	-0.12	-0.10	-0.18	-0.10	-0.13
156.25	0.91	0.94	-1.09	1.01	5.65	-0.16	-0.27	5.99	-0.20	-0.22	-0.11	-0.18	-0.19	-0.22	-0.11	-0.16
166.02	0.77	0.86	-1.19	0.71	6.61	-0.76	-1.07	7.17	-0.48	-1.03	-0.38	-0.64	-0.47	-0.72	-0.34	-0.83
175.78	0.39	1.50	-0.95	1.18	6.02	0.14	0.04	6.27	-0.38	-0.44	-0.23	-0.30	-0.36	-0.51	-0.23	-0.34
185.55	1.38	1.18	-1.22	1.33	6.45	-0.23	-0.09	6.72	-0.15	-0.15	-0.12	-0.15	-0.13	-0.18	-0.11	-0.11
195.31	1.65	0.85	-1.40	1.79	6.55	-0.17	-0.04	6.95	-0.10	-0.11	-0.09	-0.08	-0.09	-0.10	-0.05	-0.12
205.08	1.85	1.02	-1.64	2.18	6.95	-0.09	0.16	7.22	-0.21	-0.25	-0.18	-0.24	-0.18	-0.33	-0.12	-0.23
214.84	2.07	0.94	-1.61	2.09	7.08	-0.24	0.17	7.44	-0.07	-0.10	-0.06	-0.11	-0.06	-0.10	-0.08	-0.12
224.61	2.27	0.73	-1.57	2.43	7.43	-0.04	0.05	7.41	-0.10	-0.12	-0.12	-0.10	-0.06	-0.13	-0.08	-0.08
234.38	2.46	1.05	-1.43	2.57	7.65	0.29	0.37	7.72	-0.07	-0.15	-0.09	-0.13	-0.14	-0.15	-0.07	-0.10
244.14	2.60	1.24	-1.52	2.52	7.84	-0.06	0.20	8.01	-0.15	-0.19	-0.06	-0.15	-0.15	-0.26	-0.07	-0.16
253.91	3.58	1.19	-1.49	2.83	8.24	0.14	0.19	8.40	-0.80	-1.06	-0.17	-0.23	-0.72	-0.97	-0.14	-0.19
263.67	2.91	1.20	-1.24	3.06	8.29	0.24	0.43	8.41	-0.27	-0.41	-0.12	-0.15	-0.28	-0.31	-0.17	-0.20
273.44	2.93	1.11	-1.31	3.25	8.84	0.03	0.19	8.50	-0.18	-0.24	-0.13	-0.15	-0.13	-0.18	-0.13	-0.11
283.20	3.39	1.33	-1.64	3.42	9.09	0.08	0.21	8.91	-0.14	-0.17	-0.10	-0.12	-0.12	-0.19	-0.08	-0.11
292.97	3.60	1.22	-1.46	4.04	9.23	-0.03	0.71	9.21	-0.18	-0.17	-0.13	-0.11	-0.12	-0.15	-0.11	-0.18
302.73	3.35	1.03	-1.24	3.89	9.59	0.48	-0.06	9.04	-0.17	-0.19	-0.13	-0.16	-0.19	-0.16	-0.10	-0.18
312.50	4.51	1.30	-1.78	4.38	9.70	-0.07	0.71	9.77	-0.14	-0.21	-0.13	-0.16	-0.20	-0.14	-0.17	-0.15
322.27	4.62	1.86	-1.33	4.29	9.75	-0.28	0.11	9.82	-0.19	-0.19	-0.15	-0.24	-0.33	-0.21	-0.23	-0.21
332.03	4.34	1.21	-1.58	4.32	9.88	-0.50	0.47	10.46	-0.31	-0.38	-0.24	-0.31	-0.43	-0.18	-0.49	-0.26
341.80	4.56	0.80	-3.06	4.58	12.54	1.10	-2.25	9.47	-1.60	-1.14	-2.05	-1.38	-1.89	-0.79	-2.19	-0.98

Table 33. 0.2 mm (8 mils), PR=0.6, medium inlet preswirl, and 15,350 RPM

	Test Data								Uncertainties							
Freq Hz	Re H_{xx}	Re H_{xy}	Re H_{yx}	Re H_{yy}	Im H_{xx}	Im H_{xy}	Im H_{yx}	Im H_{yy}	Re H_{xx}	Re H_{xy}	Re H_{yx}	Re H_{yy}	Im H_{xx}	Im H_{xy}	Im H_{yx}	Im H_{yy}
9.77	-0.93	1.31	-1.43	-0.79	0.34	0.00	0.05	0.47	-0.19	-0.18	-0.17	-0.15	-0.23	-0.08	-0.23	-0.11
19.53	-0.71	1.46	-1.53	-0.98	0.92	0.02	-0.04	0.85	-0.17	-0.09	-0.15	-0.09	-0.08	-0.09	-0.10	-0.11
29.30	-0.82	1.38	-1.43	-0.65	1.33	-0.15	-0.10	1.48	-0.12	-0.11	-0.13	-0.16	-0.09	-0.08	-0.09	-0.18
39.06	-0.69	1.37	-1.46	-0.74	1.81	-0.22	0.09	1.88	-0.11	-0.13	-0.08	-0.14	-0.11	-0.12	-0.11	-0.13
48.83	-0.57	1.29	-1.50	-0.51	2.27	-0.18	-0.13	2.27	-0.13	-0.10	-0.10	-0.09	-0.12	-0.08	-0.14	-0.13
58.59	-0.35	1.33	-1.44	-0.46	2.76	-0.15	-0.25	2.70	-0.14	-0.10	-0.20	-0.15	-0.10	-0.09	-0.17	-0.18
68.36	-0.14	1.55	-1.75	-0.36	3.06	-0.31	-0.30	3.25	-0.14	-0.10	-0.12	-0.20	-0.10	-0.19	-0.20	-0.29
78.13	-0.36	1.32	-1.40	-0.18	3.41	-0.08	-0.16	3.46	-0.08	-0.13	-0.18	-0.11	-0.12	-0.10	-0.13	-0.14
87.89	0.01	1.39	-1.55	-0.13	3.87	-0.05	-0.12	3.76	-0.06	-0.07	-0.12	-0.09	-0.06	-0.09	-0.06	-0.10
97.66	0.16	1.37	-1.56	0.12	4.15	-0.08	0.02	4.02	-0.09	-0.08	-0.10	-0.15	-0.09	-0.08	-0.09	-0.10
107.42	0.56	1.35	-1.69	0.31	4.42	-0.14	0.07	4.46	-0.11	-0.12	-0.12	-0.09	-0.11	-0.07	-0.13	-0.09
117.19	0.55	1.37	-1.66	0.49	4.77	-0.09	-0.13	4.86	-0.10	-0.10	-0.10	-0.09	-0.11	-0.07	-0.08	-0.09
126.95	0.65	1.29	-1.56	0.48	5.12	-0.12	-0.10	5.02	-0.06	-0.15	-0.06	-0.16	-0.10	-0.14	-0.10	-0.17
136.72	0.85	1.22	-1.69	0.75	5.31	-0.22	-0.11	5.59	-0.06	-0.13	-0.09	-0.09	-0.05	-0.06	-0.07	-0.12
146.48	1.26	1.36	-1.68	0.97	5.71	-0.18	0.07	5.70	-0.07	-0.09	-0.08	-0.11	-0.07	-0.07	-0.08	-0.11
156.25	1.27	1.40	-1.66	1.32	5.83	-0.17	-0.05	6.11	-0.08	-0.09	-0.10	-0.10	-0.06	-0.11	-0.08	-0.10
166.02	1.38	1.45	-1.86	0.77	6.04	0.07	0.14	6.72	-0.06	-0.12	-0.07	-0.14	-0.06	-0.14	-0.07	-0.12
175.78	1.31	1.57	-1.98	1.83	7.05	-0.82	-0.42	7.08	-0.08	-0.14	-0.11	-0.16	-0.08	-0.09	-0.07	-0.13
185.55	1.68	1.78	-1.62	1.31	6.99	-0.35	0.06	6.89	-0.11	-0.11	-0.07	-0.12	-0.06	-0.10	-0.08	-0.08
195.31	1.86	1.48	-1.82	1.80	7.15	-0.33	-0.04	7.30	-0.06	-0.13	-0.05	-0.12	-0.08	-0.08	-0.07	-0.08
205.08	2.18	1.34	-2.22	2.14	7.32	-0.52	0.41	7.66	-0.18	-0.37	-0.15	-0.29	-0.22	-0.18	-0.17	-0.24
214.84	2.45	1.44	-1.92	2.20	7.51	-0.43	0.30	7.67	-0.11	-0.18	-0.07	-0.14	-0.09	-0.15	-0.08	-0.12
224.61	2.33	1.38	-1.93	2.48	7.96	-0.27	0.20	7.90	-0.13	-0.23	-0.09	-0.12	-0.18	-0.14	-0.10	-0.12
234.38	2.59	1.61	-2.02	2.56	8.15	-0.29	0.65	8.15	-0.20	-0.47	-0.16	-0.29	-0.23	-0.22	-0.13	-0.16
244.14	2.82	1.57	-1.74	2.83	8.53	-0.27	0.34	8.50	-0.47	-0.84	-0.20	-0.41	-0.44	-0.52	-0.27	-0.32
253.91	3.61	5.43	-1.55	-0.39	9.28	-5.35	0.52	8.17	-2.99	-2.88	-1.80	-1.66	-3.26	-3.64	-1.32	-1.49
263.67	3.53	1.87	-1.75	3.84	8.67	0.39	0.64	8.77	-1.12	-0.94	-0.56	-0.88	-0.85	-1.24	-0.55	-0.34
273.44	3.32	1.75	-1.73	3.65	9.24	-0.35	0.44	8.56	-0.36	-0.61	-0.25	-0.26	-0.39	-0.32	-0.14	-0.19
283.20	3.63	1.85	-1.91	3.85	9.49	-0.14	0.68	9.41	-0.28	-0.27	-0.12	-0.29	-0.28	-0.49	-0.19	-0.18
292.97	4.09	2.08	-1.41	5.45	9.76	-0.12	1.27	9.91	-0.21	-0.26	-0.19	-0.16	-0.24	-0.24	-0.15	-0.21
302.73	4.67	1.59	-1.80	5.01	9.84	0.75	0.49	8.77	-0.26	-0.25	-0.15	-0.21	-0.29	-0.25	-0.13	-0.15
312.50	5.18	1.81	-2.14	4.61	10.18	-1.27	0.74	10.42	-0.32	-0.31	-0.14	-0.14	-0.22	-0.21	-0.16	-0.21
322.27	5.03	2.43	-1.87	4.55	9.93	-1.44	0.63	10.57	-0.19	-0.17	-0.16	-0.15	-0.17	-0.16	-0.18	-0.17
332.03	4.24	1.12	-1.58	4.93	10.32	-1.49	0.99	11.09	-0.28	-0.25	-0.18	-0.15	-0.19	-0.14	-0.19	-0.21
341.80	4.19	0.78	-1.08	6.15	11.48	-0.25	0.24	10.96	-0.31	-0.23	-0.17	-0.12	-0.27	-0.20	-0.23	-0.12

Table 34. 0.2 mm (8 mils), PR=0.6, medium inlet preswirl, and 20,200 RPM

	Test Data								Uncertainties							
Freq Hz	Re H_{xx}	Re H_{xy}	Re H_{yx}	Re H_{yy}	Im H_{xx}	Im H_{xy}	Im H_{yx}	Im H_{yy}	Re H_{xx}	Re H_{xy}	Re H_{yx}	Re H_{yy}	Im H_{xx}	Im H_{xy}	Im H_{yx}	Im H_{yy}
9.77	-0.92	1.91	-1.74	-0.91	0.58	-0.07	-0.12	0.52	-0.23	-0.13	-0.17	-0.14	-0.21	-0.07	-0.22	-0.10
19.53	-0.64	1.90	-2.00	-0.94	0.91	-0.11	0.10	0.99	-0.20	-0.09	-0.14	-0.08	-0.11	-0.11	-0.11	-0.10
29.30	-0.81	1.96	-1.88	-0.73	1.29	-0.14	0.04	1.48	-0.12	-0.15	-0.14	-0.08	-0.11	-0.15	-0.12	-0.15
39.06	-0.65	1.95	-1.94	-0.83	1.80	-0.24	0.24	1.95	-0.11	-0.17	-0.10	-0.11	-0.09	-0.13	-0.11	-0.20
48.83	-0.66	1.73	-2.07	-0.45	2.81	-0.27	0.04	2.31	-0.75	-0.75	-0.22	-0.19	-0.83	-0.47	-0.21	-0.24
58.59	-0.32	1.93	-1.84	-0.35	2.91	-0.28	-0.11	2.96	-0.12	-0.13	-0.19	-0.19	-0.12	-0.09	-0.16	-0.17
68.36	-0.28	2.07	-1.92	-0.19	3.12	-0.38	-0.05	3.30	-0.13	-0.21	-0.16	-0.20	-0.11	-0.16	-0.19	-0.16
78.13	-0.19	1.89	-1.87	-0.10	3.64	-0.50	0.11	3.67	-0.12	-0.09	-0.11	-0.11	-0.08	-0.15	-0.12	-0.13
87.89	0.13	1.78	-1.92	-0.05	4.02	-0.43	0.08	4.12	-0.07	-0.08	-0.07	-0.11	-0.04	-0.10	-0.07	-0.08
97.66	0.15	1.78	-1.86	0.20	4.52	-0.40	0.12	4.47	-0.10	-0.12	-0.10	-0.11	-0.12	-0.12	-0.09	-0.10
107.42	0.48	1.88	-1.80	0.30	5.02	-0.35	0.07	4.93	-0.15	-0.13	-0.08	-0.09	-0.14	-0.09	-0.13	-0.11
117.19	0.78	1.82	-1.92	0.59	5.16	-0.38	-0.05	5.29	-0.11	-0.10	-0.10	-0.11	-0.10	-0.07	-0.06	-0.09
126.95	0.91	1.86	-1.94	0.86	5.52	-0.41	0.00	5.69	-0.07	-0.14	-0.10	-0.16	-0.06	-0.11	-0.09	-0.13
136.72	1.18	1.75	-2.04	1.10	5.76	-0.51	0.00	5.93	-0.10	-0.10	-0.09	-0.10	-0.07	-0.06	-0.06	-0.09
146.48	1.84	1.80	-2.23	1.38	6.23	-0.37	0.12	5.97	-0.09	-0.13	-0.10	-0.14	-0.10	-0.11	-0.07	-0.12
156.25	1.60	1.65	-2.06	1.55	6.32	-0.38	0.14	6.52	-0.06	-0.09	-0.09	-0.10	-0.06	-0.08	-0.05	-0.08
166.02	1.81	1.77	-2.21	1.69	6.59	-0.50	0.34	7.08	-0.09	-0.12	-0.09	-0.11	-0.05	-0.13	-0.05	-0.16
175.78	1.72	1.92	-2.36	2.02	7.45	-0.95	-0.40	7.41	-0.09	-0.16	-0.08	-0.10	-0.10	-0.11	-0.06	-0.11
185.55	2.03	1.92	-2.15	1.91	7.38	-0.57	0.17	7.47	-0.08	-0.11	-0.08	-0.12	-0.08	-0.09	-0.07	-0.09
195.31	2.24	1.74	-2.16	2.40	7.64	-0.52	0.19	7.74	-0.06	-0.12	-0.05	-0.10	-0.08	-0.08	-0.06	-0.09
205.08	2.74	1.50	-2.37	2.57	7.78	-0.69	0.39	7.91	-0.15	-0.22	-0.14	-0.24	-0.12	-0.20	-0.11	-0.22
214.84	3.11	1.81	-2.30	2.75	8.10	-0.63	0.46	8.26	-0.09	-0.12	-0.05	-0.11	-0.06	-0.09	-0.10	-0.13
224.61	2.99	1.64	-2.31	3.16	8.39	-0.51	0.47	8.29	-0.11	-0.14	-0.10	-0.11	-0.12	-0.13	-0.12	-0.09
234.38	3.23	1.68	-2.22	3.21	8.53	-0.50	0.70	8.37	-0.09	-0.17	-0.09	-0.14	-0.09	-0.16	-0.08	-0.16
244.14	3.52	1.51	-2.13	3.48	8.91	-0.37	0.56	9.30	-0.18	-0.23	-0.08	-0.14	-0.17	-0.25	-0.08	-0.16
253.91	4.77	1.83	-1.99	4.20	9.43	-0.13	0.44	9.42	-0.77	-1.05	-0.17	-0.20	-0.71	-0.94	-0.13	-0.19
263.67	4.64	2.10	-2.21	4.56	9.14	-0.16	0.75	9.12	-0.34	-0.46	-0.10	-0.21	-0.31	-0.29	-0.19	-0.09
273.44	4.38	2.21	-2.23	4.27	9.21	-0.41	0.69	9.12	-0.19	-0.23	-0.09	-0.17	-0.18	-0.18	-0.13	-0.12
283.20	4.38	2.50	-2.14	4.60	9.66	-0.74	0.88	10.06	-0.15	-0.23	-0.12	-0.18	-0.14	-0.25	-0.12	-0.17
292.97	4.86	2.20	-1.65	6.57	9.76	-0.88	1.64	10.72	-0.24	-0.19	-0.19	-0.10	-0.20	-0.17	-0.15	-0.13
302.73	4.80	1.25	-2.27	5.76	10.06	0.17	0.85	9.02	-0.18	-0.24	-0.13	-0.12	-0.28	-0.24	-0.14	-0.15
312.50	6.03	2.30	-2.48	5.02	11.25	-1.27	0.56	10.67	-0.48	-0.32	-0.22	-0.24	-0.41	-0.43	-0.23	-0.20
322.27	5.01	2.31	-1.87	5.43	11.22	-1.21	0.93	11.06	-0.71	-0.52	-0.38	-0.31	-0.66	-0.49	-0.40	-0.27
332.03	5.19	1.79	-1.29	5.94	12.04	-1.24	1.23	11.52	-3.23	-2.11	-1.23	-1.19	-2.12	-2.29	-1.69	-1.18
341.80	5.26	1.57	-1.64	6.89	10.78	-0.82	0.76	11.09	-1.53	-1.17	-1.39	-0.75	-2.83	-1.20	-0.99	-0.61

Table 35. 0.2 mm (8 mils), PR=0.4, high inlet preswirl, and 10,200 RPM

	Test Data								Uncertainties							
Freq Hz	Re H_{xx}	Re H_{xy}	Re H_{yx}	Re H_{yy}	Im H_{xx}	Im H_{xy}	Im H_{yx}	Im H_{yy}	Re H_{xx}	Re H_{xy}	Re H_{yx}	Re H_{yy}	Im H_{xx}	Im H_{xy}	Im H_{yx}	Im H_{yy}
9.77	-1.58	3.33	-3.78	-1.57	1.36	0.07	-0.15	1.04	-0.20	-0.10	-0.19	-0.10	-0.23	-0.12	-0.21	-0.16
19.53	-1.52	3.21	-3.68	-1.50	2.13	0.07	-0.10	2.17	-0.18	-0.13	-0.14	-0.11	-0.12	-0.11	-0.15	-0.16
29.30	-1.44	3.35	-3.87	-1.41	3.39	-0.19	-0.38	3.38	-0.11	-0.14	-0.17	-0.15	-0.10	-0.13	-0.12	-0.18
39.06	-1.32	3.47	-3.58	-1.33	4.31	0.01	-0.17	4.28	-0.10	-0.13	-0.09	-0.15	-0.12	-0.16	-0.11	-0.21
48.83	-1.15	3.54	-3.58	-0.99	5.42	-0.07	-0.24	5.11	-0.20	-0.11	-0.17	-0.11	-0.22	-0.15	-0.16	-0.15
58.59	-0.58	3.27	-3.49	-0.75	6.07	0.10	-0.48	6.21	-0.20	-0.13	-0.23	-0.19	-0.12	-0.12	-0.15	-0.22
68.36	-0.34	3.65	-3.60	-0.53	7.20	0.19	-0.38	7.41	-0.18	-0.16	-0.11	-0.19	-0.15	-0.15	-0.14	-0.19
78.13	-0.33	3.42	-3.85	-0.25	8.01	-0.07	-0.64	8.41	-0.12	-0.12	-0.14	-0.12	-0.08	-0.16	-0.13	-0.23
87.89	0.20	3.52	-3.89	0.44	9.11	0.11	-0.58	9.32	-0.10	-0.14	-0.06	-0.12	-0.07	-0.12	-0.09	-0.18
97.66	0.64	3.55	-3.74	0.71	9.90	0.13	-0.72	9.87	-0.13	-0.09	-0.11	-0.14	-0.11	-0.11	-0.12	-0.20
107.42	1.16	3.79	-3.91	1.15	10.66	0.09	-0.67	10.40	-0.13	-0.15	-0.16	-0.12	-0.11	-0.09	-0.15	-0.25
117.19	1.77	3.81	-4.09	1.64	11.44	0.08	-0.86	11.39	-0.10	-0.09	-0.08	-0.11	-0.12	-0.10	-0.08	-0.18
126.95	2.13	3.78	-4.21	1.72	12.17	-0.07	-0.99	11.95	-0.14	-0.31	-0.08	-0.22	-0.15	-0.20	-0.14	-0.26
136.72	2.62	3.54	-4.65	2.59	12.75	-0.16	-0.86	12.94	-0.07	-0.16	-0.11	-0.14	-0.12	-0.09	-0.08	-0.19
146.48	2.01	4.51	-4.46	1.88	13.25	0.22	-0.55	13.38	-0.11	-0.13	-0.18	-0.22	-0.10	-0.19	-0.13	-0.17
156.25	2.48	5.82	-3.06	0.89	13.79	-1.16	-0.47	15.59	-0.28	-0.14	-0.16	-0.11	-0.26	-0.23	-0.19	-0.28
166.02	4.19	3.11	-4.56	4.66	14.39	0.51	-0.20	13.65	-0.65	-1.21	-0.52	-0.93	-0.62	-1.15	-0.45	-0.91
175.78	4.60	3.77	-5.15	4.27	15.09	0.02	-0.65	15.59	-0.44	-0.63	-0.30	-0.40	-0.52	-0.49	-0.41	-0.51
185.55	4.94	3.78	-5.03	4.76	15.84	-0.02	-0.56	16.16	-0.17	-0.24	-0.15	-0.21	-0.12	-0.26	-0.13	-0.33
195.31	5.22	3.97	-5.08	4.84	16.71	0.07	-0.85	16.64	-0.17	-0.12	-0.12	-0.14	-0.14	-0.16	-0.09	-0.18
205.08	5.57	3.57	-5.14	5.72	17.33	-0.05	-0.43	17.57	-0.23	-0.22	-0.16	-0.23	-0.17	-0.20	-0.10	-0.26
214.84	6.29	3.95	-5.10	5.93	17.52	-0.12	-0.28	18.26	-0.13	-0.11	-0.09	-0.13	-0.08	-0.11	-0.08	-0.18
224.61	6.46	3.93	-5.70	6.38	18.17	-0.09	-0.65	18.78	-0.16	-0.13	-0.14	-0.12	-0.20	-0.13	-0.14	-0.19
234.38	7.07	4.03	-5.74	6.99	18.71	-0.27	-0.38	19.20	-0.09	-0.18	-0.12	-0.16	-0.12	-0.23	-0.11	-0.25
244.14	7.85	4.02	-5.63	7.40	19.22	0.16	-0.13	20.09	-0.19	-0.19	-0.11	-0.17	-0.15	-0.31	-0.08	-0.20
253.91	9.17	4.09	-5.56	8.34	19.85	0.29	-0.24	20.58	-0.76	-1.03	-0.16	-0.20	-0.67	-0.99	-0.10	-0.27
263.67	9.04	3.64	-6.04	9.27	20.17	0.02	-0.47	20.63	-0.22	-0.39	-0.16	-0.17	-0.29	-0.29	-0.24	-0.18
273.44	8.81	3.69	-5.98	9.74	19.68	0.56	-0.18	20.26	-0.19	-0.21	-0.18	-0.19	-0.17	-0.26	-0.11	-0.22
283.20	8.03	4.16	-6.05	9.30	20.61	1.13	-0.09	20.41	-0.19	-0.26	-0.15	-0.23	-0.14	-0.20	-0.14	-0.21
292.97	8.12	4.35	-6.12	9.44	22.18	0.66	-0.31	21.44	-0.15	-0.16	-0.15	-0.14	-0.17	-0.20	-0.14	-0.20
302.73	9.17	4.16	-6.95	10.79	23.62	1.61	-0.94	20.47	-0.19	-0.21	-0.15	-0.16	-0.26	-0.18	-0.19	-0.19
312.50	9.34	4.55	-6.53	9.21	24.19	1.98	-0.94	21.59	-0.11	-0.20	-0.18	-0.14	-0.19	-0.19	-0.13	-0.29
322.27	10.84	5.91	-5.80	9.40	25.63	2.30	-2.78	21.72	-0.12	-0.19	-0.15	-0.20	-0.21	-0.19	-0.25	-0.23
332.03	11.21	6.48	-7.02	9.19	25.37	3.16	-3.21	21.40	-0.31	-0.23	-0.21	-0.34	-0.27	-0.26	-0.32	-0.24
341.80	13.27	12.56	-14.00	-3.43	25.87	0.71	-3.05	30.98	-1.42	-0.95	-2.09	-1.47	-1.27	-0.89	-1.86	-1.27

Table 36. 0.2 mm (8 mils), PR=0.4, high inlet preswirl, and 15,350 RPM

	Test Data								Uncertainties							
Freq Hz	Re H_{xx}	Re H_{xy}	Re H_{yx}	Re H_{yy}	Im H_{xx}	Im H_{xy}	Im H_{yx}	Im H_{yy}	Re H_{xx}	Re H_{xy}	Re H_{yx}	Re H_{yy}	Im H_{xx}	Im H_{xy}	Im H_{yx}	Im H_{yy}
9.77	-1.70	4.32	-4.95	-1.72	1.18	0.15	-0.06	0.99	-0.20	-0.10	-0.17	-0.14	-0.26	-0.15	-0.22	-0.18
19.53	-1.80	4.41	-4.86	-1.79	2.18	-0.05	0.08	2.24	-0.18	-0.09	-0.12	-0.11	-0.11	-0.08	-0.11	-0.15
29.30	-1.64	4.35	-4.72	-1.62	3.28	-0.11	0.10	3.22	-0.13	-0.15	-0.14	-0.12	-0.12	-0.15	-0.14	-0.17
39.06	-1.59	4.47	-4.68	-1.53	4.43	-0.14	0.00	4.51	-0.16	-0.17	-0.11	-0.12	-0.15	-0.12	-0.12	-0.20
48.83	-1.21	4.40	-4.61	-1.17	5.31	-0.19	-0.17	5.56	-0.19	-0.14	-0.13	-0.13	-0.15	-0.12	-0.15	-0.16
58.59	-0.81	4.34	-4.79	-0.72	6.29	-0.21	-0.22	6.34	-0.12	-0.22	-0.20	-0.17	-0.12	-0.16	-0.19	-0.23
68.36	-0.53	4.38	-4.71	-0.27	7.54	0.26	-0.11	8.21	-0.21	-0.20	-0.14	-0.25	-0.14	-0.31	-0.18	-0.25
78.13	-0.41	4.53	-4.80	-0.04	8.45	-0.39	-0.43	8.89	-0.12	-0.12	-0.14	-0.14	-0.11	-0.14	-0.15	-0.24
87.89	-0.01	4.43	-4.95	0.38	9.32	-0.02	-0.48	9.72	-0.06	-0.10	-0.10	-0.10	-0.09	-0.12	-0.08	-0.19
97.66	0.33	4.54	-4.77	1.01	10.42	-0.08	-0.43	10.42	-0.14	-0.08	-0.12	-0.12	-0.13	-0.11	-0.08	-0.18
107.42	0.98	4.60	-4.88	1.22	11.14	-0.08	-0.59	11.26	-0.12	-0.15	-0.13	-0.12	-0.17	-0.09	-0.09	-0.21
117.19	1.92	4.57	-5.13	1.75	11.93	-0.18	-0.83	11.88	-0.11	-0.10	-0.08	-0.12	-0.09	-0.16	-0.08	-0.18
126.95	2.02	4.56	-5.10	2.06	12.65	0.01	-0.73	12.38	-0.09	-0.19	-0.09	-0.22	-0.11	-0.24	-0.12	-0.18
136.72	2.46	4.35	-5.40	2.74	13.27	-0.08	-0.59	13.36	-0.07	-0.13	-0.07	-0.12	-0.06	-0.11	-0.07	-0.17
146.48	1.85	5.36	-5.47	2.24	13.59	0.18	-0.37	13.80	-0.14	-0.17	-0.10	-0.11	-0.12	-0.09	-0.11	-0.19
156.25	1.94	6.79	-3.66	0.99	14.20	0.32	-0.24	14.52	-0.20	-0.13	-0.16	-0.13	-0.12	-0.14	-0.09	-0.20
166.02	4.15	3.51	-5.68	5.41	14.84	1.00	-0.01	13.10	-0.11	-0.20	-0.18	-0.21	-0.12	-0.17	-0.09	-0.28
175.78	4.56	4.52	-5.98	4.69	15.91	-0.24	-0.63	16.21	-0.10	-0.19	-0.13	-0.12	-0.11	-0.13	-0.09	-0.23
185.55	4.79	4.78	-6.05	5.01	16.62	-0.21	-0.68	16.86	-0.09	-0.17	-0.11	-0.16	-0.16	-0.10	-0.08	-0.21
195.31	5.43	5.06	-6.45	5.26	17.46	-0.35	-0.67	17.44	-0.11	-0.11	-0.08	-0.14	-0.10	-0.10	-0.08	-0.17
205.08	5.59	4.43	-6.21	6.07	18.10	-0.24	-0.40	18.22	-0.14	-0.22	-0.12	-0.21	-0.15	-0.14	-0.15	-0.26
214.84	6.47	4.83	-6.41	6.24	18.22	-0.52	-0.50	19.11	-0.10	-0.12	-0.09	-0.12	-0.08	-0.12	-0.13	-0.22
224.61	6.95	4.89	-6.65	7.02	19.18	-0.66	-0.41	19.58	-0.20	-0.12	-0.13	-0.13	-0.16	-0.14	-0.12	-0.18
234.38	7.67	4.68	-6.69	7.76	19.47	-0.71	-0.18	20.17	-0.17	-0.20	-0.22	-0.20	-0.17	-0.15	-0.11	-0.22
244.14	8.35	4.96	-6.89	8.03	19.87	-0.51	-0.20	21.00	-0.39	-0.28	-0.28	-0.14	-0.37	-0.27	-0.18	-0.19
253.91	10.06	3.31	-6.65	9.66	21.29	0.02	-1.04	21.93	-3.00	-1.58	-1.13	-0.53	-2.31	-1.44	-1.69	-0.62
263.67	9.48	3.94	-7.54	9.64	20.99	-0.38	-0.43	21.76	-0.84	-0.46	-0.43	-0.24	-0.74	-0.35	-0.44	-0.25
273.44	8.91	4.52	-7.56	10.29	20.51	0.58	0.31	21.25	-0.38	-0.31	-0.25	-0.16	-0.29	-0.19	-0.20	-0.22
283.20	8.39	5.48	-7.21	9.55	22.11	0.81	0.38	21.19	-0.18	-0.22	-0.17	-0.18	-0.26	-0.24	-0.16	-0.26
292.97	8.52	5.35	-7.16	10.60	23.41	0.44	0.04	22.52	-0.20	-0.18	-0.13	-0.12	-0.20	-0.17	-0.13	-0.19
302.73	9.59	5.91	-8.02	10.74	25.19	1.38	-0.97	21.83	-0.27	-0.21	-0.21	-0.19	-0.28	-0.17	-0.15	-0.17
312.50	9.92	6.35	-8.00	10.01	25.58	1.24	-1.02	22.67	-0.14	-0.16	-0.15	-0.14	-0.20	-0.17	-0.12	-0.19
322.27	11.91	7.15	-7.74	10.48	27.10	1.52	-2.58	22.94	-0.24	-0.15	-0.17	-0.20	-0.16	-0.17	-0.23	-0.24
332.03	12.20	7.13	-9.40	10.03	27.10	3.05	-3.41	21.50	-0.25	-0.17	-0.22	-0.16	-0.19	-0.21	-0.20	-0.24
341.80	13.55	15.57	-16.10	-7.81	27.38	0.55	-4.31	32.36	-0.24	-0.24	-0.26	-0.29	-0.33	-0.25	-0.37	-0.57

Table 37. 0.2 mm (8 mils), PR=0.4, high inlet preswirl, and 20,200 RPM

	Test Data								Uncertainties							
Freq Hz	Re H_{xx}	Re H_{xy}	Re H_{yx}	Re H_{yy}	Im H_{xx}	Im H_{xy}	Im H_{yx}	Im H_{yy}	Re H_{xx}	Re H_{xy}	Re H_{yx}	Re H_{yy}	Im H_{xx}	Im H_{xy}	Im H_{yx}	Im H_{yy}
9.77	-1.74	5.17	-5.99	-1.84	1.07	0.10	-0.06	1.17	-0.21	-0.10	-0.19	-0.14	-0.22	-0.09	-0.21	-0.16
19.53	-1.86	5.30	-5.96	-1.76	2.19	-0.02	-0.01	2.44	-0.12	-0.11	-0.16	-0.13	-0.14	-0.10	-0.11	-0.19
29.30	-1.69	5.44	-5.87	-1.90	3.45	-0.27	-0.06	3.47	-0.13	-0.20	-0.10	-0.11	-0.15	-0.20	-0.11	-0.21
39.06	-1.58	5.40	-5.83	-1.45	4.51	-0.31	0.06	4.91	-0.14	-0.14	-0.10	-0.15	-0.14	-0.12	-0.17	-0.22
48.83	-0.54	4.77	-5.47	-0.93	4.58	-1.11	0.10	5.69	-0.52	-0.39	-0.14	-0.16	-0.28	-0.42	-0.19	-0.18
58.59	-0.81	5.14	-5.51	-1.13	6.41	-0.50	-0.15	6.80	-0.14	-0.16	-0.20	-0.20	-0.16	-0.18	-0.21	-0.28
68.36	-0.79	5.92	-5.53	-0.26	7.92	-0.29	0.00	8.26	-0.23	-0.26	-0.22	-0.32	-0.22	-0.18	-0.18	-0.41
78.13	-0.58	5.44	-5.79	-0.14	8.65	-0.61	-0.02	8.86	-0.12	-0.11	-0.15	-0.21	-0.09	-0.12	-0.15	-0.22
87.89	-0.25	5.32	-5.80	0.31	9.79	-0.46	-0.08	10.13	-0.11	-0.10	-0.08	-0.10	-0.08	-0.12	-0.09	-0.17
97.66	0.20	5.42	-5.88	1.00	11.00	-0.46	0.01	10.99	-0.25	-0.19	-0.24	-0.28	-0.20	-0.25	-0.24	-0.31
107.42	1.10	5.29	-5.74	1.59	11.54	-0.68	0.07	11.84	-0.17	-0.11	-0.11	-0.13	-0.15	-0.20	-0.18	-0.20
117.19	1.47	5.28	-5.92	2.03	12.32	-0.52	-0.22	12.43	-0.19	-0.12	-0.11	-0.20	-0.14	-0.18	-0.10	-0.19
126.95	2.34	5.09	-5.96	2.38	13.13	-0.72	-0.30	13.19	-0.11	-0.26	-0.13	-0.22	-0.15	-0.19	-0.11	-0.22
136.72	2.44	5.12	-6.31	3.01	13.76	-0.56	-0.32	14.16	-0.17	-0.13	-0.11	-0.14	-0.12	-0.19	-0.11	-0.19
146.48	2.30	5.92	-6.10	2.84	14.37	-0.24	0.06	14.27	-0.16	-0.15	-0.18	-0.15	-0.16	-0.21	-0.14	-0.25
156.25	2.48	7.57	-4.19	1.33	14.93	-0.53	0.40	15.39	-0.13	-0.17	-0.25	-0.16	-0.15	-0.17	-0.11	-0.20
166.02	4.37	4.45	-6.81	6.51	15.50	0.58	0.45	13.81	-0.16	-0.30	-0.22	-0.20	-0.21	-0.33	-0.17	-0.36
175.78	4.84	5.01	-6.82	5.43	16.49	-0.62	-0.34	16.80	-0.14	-0.22	-0.13	-0.15	-0.11	-0.21	-0.18	-0.27
185.55	5.19	5.38	-6.62	5.79	17.12	-0.36	-0.01	17.38	-0.08	-0.13	-0.09	-0.15	-0.09	-0.14	-0.09	-0.20
195.31	5.67	5.53	-6.90	5.71	17.86	-0.75	-0.49	17.92	-0.09	-0.14	-0.09	-0.13	-0.08	-0.13	-0.07	-0.18
205.08	5.82	4.87	-6.93	6.91	18.58	-0.40	-0.09	18.78	-0.12	-0.21	-0.16	-0.27	-0.13	-0.19	-0.16	-0.30
214.84	7.00	5.31	-6.88	6.95	18.73	-0.84	-0.05	19.61	-0.08	-0.14	-0.11	-0.17	-0.10	-0.09	-0.08	-0.16
224.61	7.05	5.35	-7.46	7.93	19.67	-0.91	0.04	20.18	-0.12	-0.13	-0.12	-0.13	-0.10	-0.10	-0.10	-0.15
234.38	8.01	5.29	-7.46	8.45	20.40	-1.12	0.23	20.53	-0.17	-0.21	-0.17	-0.14	-0.13	-0.17	-0.10	-0.24
244.14	8.72	5.34	-7.54	8.70	20.71	-0.51	0.37	21.56	-0.20	-0.24	-0.14	-0.13	-0.17	-0.27	-0.13	-0.23
253.91	9.81	5.52	-7.49	10.01	21.10	-0.10	-0.22	22.22	-0.77	-1.05	-0.18	-0.22	-0.77	-1.02	-0.23	-0.25
263.67	9.98	5.23	-7.89	10.97	21.84	-0.42	0.41	21.92	-0.26	-0.44	-0.13	-0.22	-0.31	-0.31	-0.16	-0.21
273.44	9.39	5.00	-7.68	11.40	21.20	0.28	0.37	21.34	-0.23	-0.32	-0.13	-0.26	-0.19	-0.17	-0.20	-0.23
283.20	9.15	6.38	-7.64	10.19	22.93	0.21	0.20	21.82	-0.19	-0.21	-0.13	-0.17	-0.13	-0.19	-0.17	-0.26
292.97	9.55	6.02	-7.82	11.06	23.76	-0.48	0.16	22.83	-0.32	-0.24	-0.23	-0.11	-0.17	-0.34	-0.14	-0.28
302.73	10.42	6.15	-8.88	11.52	25.65	0.43	-0.73	22.13	-0.27	-0.28	-0.31	-0.14	-0.44	-0.40	-0.23	-0.32
312.50	10.99	6.02	-8.07	10.62	25.82	0.58	-0.88	22.96	-0.27	-0.42	-0.25	-0.16	-0.56	-0.34	-0.29	-0.39
322.27	13.06	7.95	-8.37	11.14	28.29	1.64	-2.81	23.50	-0.73	-0.40	-0.36	-0.28	-0.83	-0.59	-0.61	-0.40
332.03	14.79	7.50	-10.19	9.97	27.33	0.64	-4.36	23.28	-2.58	-2.21	-1.05	-0.42	-2.14	-1.02	-1.46	-1.36
341.80	15.01	13.93	-19.17	-0.49	26.22	-1.50	-4.52	32.68	-2.84	-1.72	-1.21	-1.13	-1.40	-0.68	-2.46	-1.62

Table 38. 0.2 mm (8 mils), PR=0.5, high inlet preswirl, and 10,200 RPM

	Test Data								Uncertainties							
Freq Hz	Re H_{xx}	Re H_{xy}	Re H_{yx}	Re H_{yy}	Im H_{xx}	Im H_{xy}	Im H_{yx}	Im H_{yy}	Re H_{xx}	Re H_{xy}	Re H_{yx}	Re H_{yy}	Im H_{xx}	Im H_{xy}	Im H_{yx}	Im H_{yy}
9.77	-1.02	2.83	-3.59	-1.24	1.08	0.18	-0.23	1.09	0.18	0.10	0.16	0.13	0.25	0.12	0.18	0.17
19.53	-1.03	2.89	-3.54	-1.19	1.78	0.32	-0.27	2.10	0.10	0.08	0.09	0.12	0.13	0.12	0.14	0.17
29.30	-0.79	3.00	-3.75	-1.05	2.91	0.15	-0.15	3.08	0.11	0.15	0.09	0.17	0.11	0.19	0.11	0.21
39.06	-0.73	3.02	-3.63	-0.98	3.93	0.19	-0.25	4.04	0.10	0.12	0.07	0.14	0.11	0.11	0.15	0.20
48.83	-0.76	3.41	-3.77	-0.61	4.84	0.08	-0.28	5.08	0.29	0.23	0.26	0.21	0.32	0.18	0.18	0.17
58.59	-0.19	3.00	-3.50	-0.32	5.65	0.35	-0.40	5.86	0.15	0.23	0.17	0.19	0.21	0.19	0.19	0.25
68.36	-0.09	3.10	-3.40	-0.51	6.62	0.23	-0.37	7.31	0.22	0.39	0.16	0.28	0.22	0.29	0.13	0.24
78.13	-0.22	3.29	-3.75	0.16	7.53	0.13	-0.59	8.05	0.16	0.16	0.10	0.09	0.13	0.15	0.13	0.18
87.89	0.32	3.19	-3.78	0.58	8.30	0.43	-0.60	9.00	0.12	0.09	0.10	0.15	0.09	0.13	0.06	0.18
97.66	0.67	3.58	-3.75	0.92	9.31	0.36	-0.79	9.69	0.18	0.11	0.11	0.11	0.13	0.11	0.08	0.16
107.42	1.11	3.70	-4.04	1.38	10.03	0.33	-0.71	10.18	0.13	0.13	0.10	0.15	0.10	0.13	0.15	0.24
117.19	1.50	3.60	-4.04	1.69	10.96	0.17	-0.70	10.87	0.10	0.13	0.10	0.12	0.12	0.10	0.10	0.18
126.95	1.81	3.60	-4.19	2.02	11.67	-0.04	-1.06	11.66	0.15	0.30	0.11	0.16	0.11	0.25	0.10	0.30
136.72	2.53	3.39	-4.53	2.63	12.31	0.09	-0.68	12.55	0.13	0.11	0.14	0.17	0.07	0.15	0.08	0.16
146.48	2.18	4.50	-4.54	1.86	12.63	0.32	-0.54	12.71	0.14	0.14	0.11	0.15	0.19	0.18	0.12	0.20
156.25	1.80	6.20	-2.48	0.36	13.22	0.19	-0.18	13.92	0.28	0.24	0.32	0.23	0.31	0.28	0.26	0.28
166.02	3.33	3.94	-4.63	4.64	14.05	1.23	-0.30	12.84	0.80	1.39	0.66	0.91	0.76	1.30	0.62	1.13
175.78	4.15	3.57	-4.76	4.11	15.20	-0.04	-0.71	14.94	0.50	0.51	0.39	0.44	0.50	0.59	0.38	0.53
185.55	4.43	3.85	-4.76	4.58	15.62	0.35	-0.69	15.64	0.17	0.19	0.14	0.16	0.21	0.25	0.19	0.30
195.31	4.87	3.93	-5.07	4.67	16.10	0.12	-0.84	16.27	0.16	0.15	0.11	0.18	0.15	0.13	0.12	0.26
205.08	5.00	3.51	-5.18	5.37	16.95	0.60	-0.60	16.89	0.17	0.18	0.12	0.30	0.15	0.35	0.17	0.33
214.84	5.89	4.21	-4.92	5.43	17.01	0.03	-0.66	17.47	0.12	0.11	0.14	0.18	0.10	0.16	0.08	0.21
224.61	6.24	4.05	-5.40	6.07	17.70	-0.10	-0.60	18.19	0.16	0.16	0.16	0.11	0.18	0.15	0.08	0.19
234.38	6.76	4.29	-5.48	6.42	18.37	-0.12	-0.54	18.87	0.12	0.21	0.10	0.19	0.12	0.26	0.11	0.21
244.14	7.13	4.02	-5.54	6.84	18.68	-0.13	-0.37	19.59	0.20	0.23	0.14	0.18	0.17	0.29	0.10	0.20
253.91	8.74	2.43	-5.22	7.96	20.21	0.71	-0.76	20.36	2.07	2.62	0.28	0.32	1.38	1.69	0.45	0.57
263.67	8.08	3.59	-5.87	8.41	19.70	0.29	-0.62	20.40	0.36	0.36	0.18	0.22	0.33	0.46	0.17	0.19
273.44	7.60	3.74	-5.88	9.18	19.47	0.71	-0.46	20.28	0.19	0.16	0.11	0.16	0.17	0.31	0.14	0.21
283.20	7.38	4.49	-5.77	8.29	20.59	0.50	-0.34	20.23	0.20	0.22	0.16	0.23	0.16	0.21	0.16	0.20
292.97	7.44	4.23	-6.02	9.15	21.80	0.47	-0.53	21.21	0.16	0.21	0.11	0.19	0.16	0.19	0.17	0.22
302.73	8.34	4.26	-6.89	9.11	23.59	1.49	-1.20	20.90	0.19	0.23	0.14	0.18	0.17	0.19	0.25	0.19
312.50	8.73	4.81	-6.33	8.95	23.62	1.51	-1.07	21.66	0.31	0.23	0.19	0.16	0.17	0.20	0.27	0.23
322.27	10.08	5.90	-5.79	9.03	25.69	2.32	-2.88	21.82	0.35	0.21	0.16	0.21	0.18	0.19	0.13	0.25
332.03	10.75	6.11	-6.89	9.37	25.50	3.20	-3.43	20.65	0.34	0.31	0.26	0.27	0.32	0.28	0.40	0.31
341.80	11.03	13.85	-10.81	-9.30	26.24	2.25	-4.62	25.11	0.92	0.57	1.09	0.87	1.22	0.86	1.88	1.21

Table 39. 0.2 mm (8 mils), PR=0.5, high inlet preswirl, and 15,350 RPM

	Test Data								Uncertainties							
Freq Hz	Re H_{xx}	Re H_{xy}	Re H_{yx}	Re H_{yy}	Im H_{xx}	Im H_{xy}	Im H_{yx}	Im H_{yy}	Re H_{xx}	Re H_{xy}	Re H_{yx}	Re H_{yy}	Im H_{xx}	Im H_{xy}	Im H_{yx}	Im H_{yy}
9.77	-1.45	4.21	-4.65	-1.63	1.30	0.03	-0.21	1.08	0.17	0.13	0.18	0.14	0.24	0.16	0.15	0.15
19.53	-1.61	4.22	-4.52	-1.73	1.98	0.02	-0.18	2.15	0.09	0.07	0.09	0.12	0.12	0.12	0.09	0.16
29.30	-1.22	4.01	-4.76	-1.51	3.24	-0.21	-0.18	3.22	0.08	0.13	0.09	0.15	0.11	0.20	0.11	0.17
39.06	-1.36	4.42	-4.57	-1.31	4.35	-0.30	-0.29	4.48	0.11	0.12	0.07	0.15	0.12	0.11	0.18	0.19
48.83	-0.98	4.23	-4.47	-1.17	5.29	-0.20	-0.20	5.36	0.14	0.12	0.19	0.16	0.18	0.12	0.21	0.25
58.59	-0.80	4.01	-4.57	-0.80	6.09	-0.05	-0.38	6.35	0.14	0.15	0.15	0.21	0.12	0.11	0.20	0.24
68.36	-0.24	3.88	-4.40	-0.56	7.22	-0.11	-0.03	7.67	0.20	0.24	0.20	0.24	0.22	0.30	0.13	0.27
78.13	-0.51	4.32	-4.66	-0.25	8.28	-0.11	-0.50	8.64	0.10	0.16	0.14	0.17	0.13	0.12	0.14	0.22
87.89	0.15	4.30	-4.81	0.25	9.16	-0.15	-0.57	9.54	0.12	0.08	0.10	0.15	0.06	0.12	0.12	0.19
97.66	0.47	4.30	-4.77	0.84	9.98	0.04	-0.68	10.34	0.14	0.11	0.11	0.12	0.12	0.13	0.07	0.20
107.42	1.02	4.45	-4.84	1.23	10.77	-0.11	-0.83	10.93	0.12	0.13	0.14	0.12	0.12	0.13	0.14	0.26
117.19	1.65	4.54	-5.11	1.65	11.54	-0.13	-0.83	11.74	0.06	0.09	0.13	0.12	0.10	0.10	0.11	0.17
126.95	1.74	4.27	-5.12	1.94	12.33	0.18	-0.83	12.28	0.11	0.20	0.09	0.21	0.12	0.17	0.11	0.24
136.72	2.54	4.40	-5.52	2.58	13.24	-0.17	-0.84	13.22	0.09	0.09	0.10	0.11	0.08	0.14	0.13	0.16
146.48	1.92	5.26	-5.58	2.07	13.44	0.07	-0.28	13.73	0.13	0.14	0.11	0.15	0.11	0.12	0.10	0.16
156.25	1.94	6.63	-3.75	0.91	13.64	0.43	0.24	14.04	0.16	0.20	0.17	0.18	0.13	0.13	0.14	0.20
166.02	3.97	3.76	-6.07	6.28	14.70	1.28	0.02	13.14	0.16	0.28	0.20	0.21	0.18	0.24	0.16	0.32
175.78	4.36	4.42	-6.21	4.65	15.72	0.09	-0.67	16.10	0.16	0.16	0.14	0.19	0.13	0.12	0.17	0.30
185.55	4.73	4.59	-6.15	4.75	16.25	0.04	-0.77	17.00	0.11	0.14	0.07	0.12	0.13	0.17	0.13	0.16
195.31	5.29	4.94	-6.28	4.85	17.20	-0.19	-0.70	17.45	0.12	0.12	0.14	0.17	0.11	0.15	0.14	0.19
205.08	5.29	4.48	-6.48	5.29	17.91	0.31	-0.89	18.18	0.19	0.31	0.17	0.25	0.24	0.28	0.18	0.33
214.84	6.09	4.91	-6.30	5.95	17.82	-0.27	-0.52	18.85	0.14	0.18	0.11	0.14	0.16	0.16	0.11	0.26
224.61	6.45	4.82	-6.57	6.62	18.69	-0.27	-0.33	19.49	0.14	0.22	0.16	0.15	0.19	0.15	0.11	0.22
234.38	7.29	4.85	-6.73	6.97	19.32	-0.50	-0.24	20.15	0.26	0.34	0.21	0.26	0.27	0.37	0.18	0.25
244.14	7.76	4.61	-6.98	7.70	19.48	-0.29	-0.43	21.13	0.45	0.45	0.31	0.32	0.50	0.49	0.27	0.36
253.91	11.64	2.68	-8.26	10.07	20.02	2.57	-2.15	21.10	5.73	5.38	1.62	2.27	3.25	4.29	2.98	2.49
263.67	8.60	3.93	-7.83	9.19	20.31	0.40	-0.55	21.90	1.08	0.81	0.56	0.45	0.77	0.82	0.54	0.54
273.44	7.87	4.62	-7.58	9.79	20.32	0.77	0.10	21.35	0.42	0.45	0.39	0.28	0.41	0.41	0.22	0.41
283.20	7.77	6.05	-6.90	8.70	22.08	0.78	-0.07	21.53	0.22	0.29	0.18	0.26	0.29	0.28	0.13	0.29
292.97	8.01	5.21	-7.05	9.87	23.26	0.09	-0.55	22.32	0.20	0.29	0.13	0.20	0.24	0.24	0.20	0.26
302.73	8.70	5.83	-7.96	9.51	24.95	1.02	-0.76	22.37	0.30	0.25	0.24	0.27	0.34	0.25	0.28	0.25
312.50	9.28	6.48	-7.67	9.78	25.78	0.75	-1.43	23.07	0.30	0.26	0.13	0.17	0.34	0.22	0.18	0.23
322.27	11.33	7.04	-6.96	10.06	27.52	1.48	-3.15	23.02	0.29	0.21	0.18	0.19	0.19	0.16	0.18	0.21
332.03	11.68	7.01	-8.95	10.06	27.33	3.09	-3.66	21.67	0.35	0.21	0.22	0.14	0.18	0.30	0.10	0.18
341.80	12.45	15.67	-13.98	-7.97	27.10	2.94	-3.71	21.97	0.40	0.24	0.28	0.15	0.54	0.23	0.29	0.24

Table 40. 0.2 mm (8 mils), PR=0.5, high inlet preswirl, and 20,200 RPM

	Test Data								Uncertainties							
Freq Hz	Re H_{xx}	Re H_{xy}	Re H_{yx}	Re H_{yy}	Im H_{xx}	Im H_{xy}	Im H_{yx}	Im H_{yy}	Re H_{xx}	Re H_{xy}	Re H_{yx}	Re H_{yy}	Im H_{xx}	Im H_{xy}	Im H_{yx}	Im H_{yy}
9.77	-1.64	5.01	-5.83	-1.69	1.24	0.01	-0.15	1.07	0.18	0.10	0.20	0.13	0.23	0.11	0.19	0.18
19.53	-1.59	5.04	-5.69	-1.58	2.16	-0.09	-0.06	2.17	0.11	0.12	0.10	0.11	0.15	0.14	0.13	0.18
29.30	-1.34	4.98	-5.79	-1.63	3.31	-0.10	0.06	3.31	0.14	0.11	0.11	0.18	0.13	0.10	0.10	0.22
39.06	-1.48	5.12	-5.55	-1.24	4.22	-0.34	-0.01	4.47	0.12	0.13	0.08	0.15	0.13	0.16	0.12	0.17
48.83	-2.94	4.85	-5.93	-1.44	6.37	1.49	-0.03	5.28	0.25	0.27	0.22	0.16	0.33	0.11	0.14	0.16
58.59	-0.87	4.83	-5.48	-0.99	6.17	-0.35	0.06	6.35	0.18	0.24	0.16	0.18	0.20	0.16	0.16	0.19
68.36	-0.50	4.95	-5.32	-0.39	7.15	-0.09	0.04	7.87	0.22	0.31	0.22	0.24	0.17	0.25	0.23	0.23
78.13	-0.41	5.17	-5.48	-0.17	8.06	-0.72	-0.07	8.33	0.10	0.16	0.16	0.19	0.13	0.17	0.12	0.22
87.89	0.01	4.89	-5.62	0.05	9.01	-0.60	-0.10	9.81	0.09	0.08	0.07	0.14	0.07	0.13	0.09	0.15
97.66	-0.22	5.20	-6.03	1.03	10.22	-0.41	-0.10	10.67	0.16	0.14	0.10	0.10	0.14	0.14	0.10	0.21
107.42	1.08	4.72	-5.52	1.12	10.78	-0.66	-0.20	11.19	0.15	0.15	0.13	0.15	0.09	0.14	0.17	0.23
117.19	1.32	4.87	-5.74	1.81	11.73	-0.62	-0.04	11.99	0.11	0.13	0.12	0.11	0.07	0.12	0.07	0.17
126.95	1.73	4.70	-5.84	2.35	12.51	-0.11	-0.58	13.16	0.13	0.15	0.10	0.20	0.18	0.28	0.13	0.32
136.72	2.54	4.69	-5.91	2.55	13.41	-0.54	-0.62	13.71	0.13	0.11	0.16	0.10	0.11	0.13	0.08	0.17
146.48	2.36	5.85	-5.92	1.91	13.97	-0.55	-0.31	14.07	0.18	0.12	0.18	0.17	0.13	0.18	0.17	0.33
156.25	1.96	7.45	-4.32	0.92	14.32	-0.38	0.22	14.92	0.27	0.18	0.24	0.19	0.18	0.28	0.24	0.17
166.02	3.71	4.61	-6.47	5.86	14.89	1.17	0.29	13.22	0.18	0.20	0.22	0.23	0.16	0.34	0.13	0.39
175.78	4.33	4.72	-6.77	4.96	15.82	-0.13	-0.19	16.18	0.15	0.21	0.13	0.16	0.15	0.12	0.12	0.25
185.55	4.95	4.90	-6.42	4.89	16.47	-0.40	-0.42	17.05	0.09	0.20	0.08	0.16	0.14	0.12	0.13	0.17
195.31	5.20	5.32	-6.64	5.29	17.08	-0.55	-0.24	17.58	0.13	0.13	0.11	0.17	0.18	0.11	0.11	0.18
205.08	5.73	4.84	-6.80	6.02	18.01	-0.48	-0.36	18.23	0.13	0.42	0.13	0.29	0.28	0.30	0.18	0.27
214.84	6.55	5.26	-6.48	6.26	18.12	-0.72	-0.21	18.89	0.12	0.17	0.09	0.11	0.12	0.13	0.10	0.21
224.61	6.56	5.18	-7.14	6.87	19.01	-0.50	-0.30	19.50	0.08	0.16	0.11	0.13	0.11	0.13	0.09	0.25
234.38	7.18	5.12	-7.41	7.43	19.65	-0.63	0.18	20.33	0.16	0.18	0.13	0.15	0.12	0.15	0.07	0.25
244.14	8.00	5.16	-7.14	7.87	19.87	-0.23	0.24	20.99	0.20	0.21	0.16	0.16	0.18	0.31	0.15	0.20
253.91	9.28	3.91	-7.26	9.30	21.46	0.74	-0.26	22.03	2.08	2.61	0.34	0.35	1.37	1.68	0.46	0.55
263.67	9.22	5.21	-7.47	10.11	21.33	-0.38	0.32	21.52	0.41	0.41	0.18	0.18	0.33	0.43	0.27	0.21
273.44	8.53	4.98	-7.44	10.27	20.65	0.40	0.29	21.07	0.27	0.18	0.17	0.20	0.25	0.29	0.18	0.24
283.20	8.12	6.41	-7.37	9.25	22.12	0.20	-0.13	21.57	0.26	0.31	0.18	0.27	0.18	0.32	0.18	0.32
292.97	8.49	5.73	-7.65	10.10	23.49	-0.24	-0.10	22.79	0.26	0.24	0.14	0.14	0.19	0.30	0.14	0.25
302.73	9.78	6.18	-8.74	10.65	24.99	0.42	-0.39	22.10	0.34	0.31	0.26	0.27	0.27	0.33	0.32	0.33
312.50	9.64	6.01	-7.65	10.00	25.54	0.50	-0.71	23.17	0.40	0.43	0.23	0.26	0.37	0.44	0.27	0.28
322.27	11.74	7.60	-7.40	10.53	28.02	1.85	-2.31	23.59	0.56	0.52	0.50	0.32	0.89	0.51	0.47	0.39
332.03	12.77	8.34	-8.46	10.65	27.62	2.61	-3.72	22.19	2.10	1.88	1.45	1.19	2.73	2.10	1.38	1.09
341.80	14.34	14.33	-14.70	-3.98	27.36	-1.66	-6.11	32.07	2.21	1.40	1.98	1.12	1.88	1.35	2.04	1.75

Table 41. 0.2 mm (8 mils), PR=0.6, high inlet preswirl, and 10,200 RPM

	Test Data								Uncertainties							
Freq Hz	Re H_{xx}	Re H_{xy}	Re H_{yx}	Re H_{yy}	Im H_{xx}	Im H_{xy}	Im H_{yx}	Im H_{yy}	Re H_{xx}	Re H_{xy}	Re H_{yx}	Re H_{yy}	Im H_{xx}	Im H_{xy}	Im H_{yx}	Im H_{yy}
9.77	-1.20	3.02	-3.29	-0.91	1.07	0.04	-0.24	0.86	0.20	0.14	0.17	0.15	0.24	0.14	0.20	0.19
19.53	-0.95	3.03	-3.50	-0.84	1.72	0.14	-0.13	1.82	0.15	0.14	0.14	0.10	0.12	0.12	0.10	0.15
29.30	-0.86	3.20	-3.49	-0.79	2.85	0.14	-0.16	2.88	0.13	0.15	0.13	0.19	0.11	0.19	0.13	0.20
39.06	-0.72	3.08	-3.29	-0.65	3.88	0.10	-0.19	3.82	0.10	0.23	0.13	0.16	0.16	0.12	0.10	0.20
48.83	-0.35	3.32	-3.42	-0.57	4.81	0.08	-0.41	4.92	0.22	0.18	0.18	0.10	0.24	0.13	0.20	0.21
58.59	-0.46	3.21	-3.46	-0.18	5.37	0.30	-0.27	5.37	0.17	0.19	0.18	0.19	0.18	0.21	0.17	0.20
68.36	0.07	3.25	-3.27	0.07	6.57	0.42	-0.41	6.92	0.18	0.26	0.18	0.26	0.22	0.23	0.19	0.30
78.13	-0.02	3.47	-3.50	0.07	7.19	0.08	-0.71	7.56	0.15	0.14	0.09	0.16	0.12	0.13	0.14	0.23
87.89	0.34	3.43	-3.45	0.62	8.08	0.24	-0.55	8.37	0.13	0.09	0.08	0.14	0.15	0.13	0.09	0.17
97.66	0.82	3.40	-3.53	1.19	8.90	0.18	-0.83	9.29	0.11	0.12	0.15	0.10	0.12	0.12	0.11	0.18
107.42	1.05	3.54	-3.85	1.39	9.66	-0.05	-0.83	9.60	0.14	0.12	0.14	0.14	0.15	0.14	0.10	0.18
117.19	1.51	3.46	-3.87	1.62	10.41	0.04	-0.85	10.54	0.07	0.11	0.12	0.13	0.10	0.10	0.08	0.20
126.95	1.98	3.71	-3.94	1.90	11.14	0.16	-0.99	11.09	0.11	0.21	0.09	0.20	0.09	0.12	0.10	0.27
136.72	2.35	3.50	-4.23	2.33	11.75	0.02	-0.96	11.96	0.07	0.14	0.08	0.17	0.08	0.11	0.09	0.18
146.48	1.86	4.24	-4.23	1.64	12.22	0.37	-0.50	12.20	0.11	0.11	0.09	0.12	0.11	0.13	0.11	0.23
156.25	2.03	5.92	-2.46	0.11	12.92	-0.86	-0.69	14.25	0.20	0.09	0.24	0.12	0.21	0.19	0.18	0.18
166.02	3.69	2.64	-4.49	4.33	13.64	0.62	-0.82	13.23	0.19	0.26	0.26	0.21	0.18	0.25	0.15	0.29
175.78	4.16	3.01	-4.95	3.93	14.04	0.31	-0.93	14.63	0.13	0.15	0.09	0.15	0.15	0.09	0.07	0.21
185.55	4.39	3.79	-4.66	4.02	14.67	0.06	-0.82	15.06	0.08	0.12	0.08	0.17	0.06	0.08	0.11	0.20
195.31	4.50	3.93	-4.92	4.34	15.54	0.19	-0.96	15.66	0.08	0.11	0.08	0.16	0.12	0.11	0.08	0.20
205.08	4.60	3.75	-5.07	4.87	16.08	0.42	-0.70	16.69	0.17	0.36	0.17	0.24	0.17	0.26	0.16	0.27
214.84	5.06	3.89	-4.73	5.02	16.36	-0.10	-0.55	17.13	0.09	0.12	0.09	0.18	0.13	0.15	0.07	0.21
224.61	5.52	4.08	-4.90	5.45	17.33	-0.04	-0.99	17.64	0.15	0.11	0.12	0.12	0.15	0.16	0.13	0.21
234.38	6.06	4.02	-5.28	5.80	17.74	-0.25	-0.44	18.19	0.16	0.13	0.12	0.18	0.16	0.19	0.11	0.15
244.14	6.26	4.35	-5.28	6.01	18.31	0.02	-0.70	18.96	0.24	0.26	0.15	0.14	0.14	0.34	0.10	0.23
253.91	5.45	5.31	-5.00	7.07	20.35	0.61	-0.53	19.38	1.62	2.25	0.38	0.34	1.21	0.95	0.40	0.65
263.67	7.86	3.64	-5.46	7.68	19.41	-0.15	-1.15	19.76	0.23	0.21	0.24	0.19	0.51	0.53	0.16	0.27
273.44	7.22	4.12	-5.62	8.18	18.72	0.46	-0.62	19.89	0.21	0.20	0.11	0.17	0.29	0.28	0.19	0.27
283.20	5.83	4.37	-5.65	7.57	19.82	0.74	-0.81	19.61	0.18	0.21	0.14	0.19	0.15	0.26	0.14	0.24
292.97	5.94	4.08	-5.88	8.16	21.73	0.60	-0.99	20.95	0.14	0.23	0.12	0.16	0.16	0.15	0.12	0.16
302.73	7.30	4.48	-7.22	8.20	23.54	1.93	-1.62	19.98	0.15	0.27	0.20	0.13	0.22	0.17	0.12	0.22
312.50	7.52	4.80	-6.25	7.82	24.33	1.59	-1.78	21.53	0.19	0.21	0.15	0.16	0.24	0.20	0.17	0.26
322.27	8.90	6.06	-6.41	8.06	26.01	2.35	-3.18	21.64	0.20	0.24	0.16	0.13	0.20	0.14	0.14	0.24
332.03	10.33	7.33	-7.86	7.69	26.69	3.70	-3.64	21.11	0.22	0.22	0.18	0.18	0.19	0.24	0.36	0.25
341.80	12.91	13.47	-14.28	-6.53	26.39	0.17	-3.36	28.41	0.68	0.25	0.89	0.27	0.71	0.33	0.83	0.48

Table 42. 0.2 mm (8 mils), PR=0.6, high inlet preswirl, and 15,350 RPM

	Test Data								Uncertainties							
Freq Hz	Re H_{xx}	Re H_{xy}	Re H_{yx}	Re H_{yy}	Im H_{xx}	Im H_{xy}	Im H_{yx}	Im H_{yy}	Re H_{xx}	Re H_{xy}	Re H_{yx}	Re H_{yy}	Im H_{xx}	Im H_{xy}	Im H_{yx}	Im H_{yy}
9.77	-1.19	3.79	-4.17	-1.48	0.96	0.25	-0.16	0.96	0.16	0.10	0.18	0.11	0.22	0.08	0.19	0.18
19.53	-1.18	3.93	-4.18	-1.38	1.86	0.19	-0.09	2.02	0.15	0.12	0.15	0.14	0.15	0.10	0.10	0.16
29.30	-0.90	4.07	-4.42	-1.45	2.99	0.18	-0.33	3.28	0.15	0.15	0.12	0.13	0.13	0.15	0.12	0.24
39.06	-0.92	3.91	-4.05	-1.11	3.92	-0.04	-0.45	4.10	0.12	0.21	0.13	0.16	0.14	0.15	0.19	0.17
48.83	-0.69	4.09	-4.28	-1.09	4.87	-0.08	-0.28	5.13	0.14	0.12	0.19	0.15	0.21	0.13	0.14	0.21
58.59	-0.42	3.88	-4.41	-0.84	5.38	0.07	-0.43	6.04	0.12	0.21	0.14	0.22	0.14	0.21	0.21	0.22
68.36	0.21	3.75	-4.24	-0.20	6.84	0.11	-0.35	7.74	0.22	0.22	0.18	0.27	0.20	0.30	0.23	0.32
78.13	-0.18	4.04	-4.56	-0.06	7.52	0.02	-0.68	8.39	0.19	0.15	0.11	0.20	0.16	0.14	0.13	0.22
87.89	0.21	4.00	-4.51	0.21	8.44	0.04	-0.75	9.22	0.13	0.12	0.07	0.13	0.07	0.11	0.10	0.19
97.66	0.66	4.08	-4.46	0.74	9.38	0.15	-0.85	10.09	0.11	0.11	0.14	0.11	0.15	0.10	0.16	0.19
107.42	1.10	4.01	-4.77	1.20	9.91	0.01	-0.90	10.56	0.16	0.14	0.15	0.16	0.10	0.12	0.10	0.20
117.19	1.46	4.16	-4.93	1.49	10.87	0.09	-1.07	11.32	0.11	0.08	0.12	0.13	0.11	0.14	0.13	0.17
126.95	1.95	4.12	-4.81	1.69	11.69	0.10	-1.13	11.92	0.08	0.20	0.10	0.19	0.14	0.21	0.15	0.33
136.72	2.44	4.09	-5.37	2.37	12.17	0.07	-0.89	12.88	0.09	0.14	0.09	0.14	0.09	0.14	0.07	0.19
146.48	1.95	5.02	-5.20	1.76	12.72	0.31	-0.63	13.26	0.12	0.14	0.09	0.13	0.12	0.11	0.14	0.27
156.25	2.16	6.41	-3.67	0.77	12.82	0.62	-0.37	13.69	0.25	0.12	0.27	0.16	0.14	0.16	0.23	0.23
166.02	3.87	3.52	-5.77	5.34	13.97	1.05	-0.22	12.51	0.22	0.25	0.16	0.36	0.10	0.29	0.21	0.32
175.78	4.01	4.06	-5.92	4.28	14.96	0.44	-0.83	15.54	0.12	0.14	0.11	0.25	0.14	0.14	0.14	0.22
185.55	4.53	4.53	-5.88	4.26	15.32	0.10	-0.93	16.23	0.09	0.17	0.09	0.17	0.08	0.17	0.12	0.20
195.31	4.78	4.67	-6.21	4.45	16.13	0.04	-0.83	16.90	0.14	0.12	0.12	0.10	0.13	0.16	0.08	0.16
205.08	4.66	4.57	-6.08	5.09	17.02	0.44	-0.56	17.93	0.20	0.45	0.18	0.30	0.22	0.24	0.14	0.36
214.84	5.46	4.72	-6.15	5.41	17.15	-0.30	-0.56	18.38	0.08	0.16	0.11	0.15	0.08	0.14	0.07	0.23
224.61	5.91	4.82	-6.41	6.11	18.32	-0.22	-0.46	19.06	0.15	0.17	0.11	0.12	0.17	0.15	0.13	0.16
234.38	6.61	4.80	-6.62	6.50	18.61	-0.55	-0.48	19.65	0.21	0.14	0.20	0.23	0.17	0.16	0.21	0.22
244.14	6.94	5.03	-6.75	6.91	19.13	-0.29	-0.62	20.68	0.32	0.27	0.19	0.16	0.24	0.37	0.16	0.21
253.91	7.24	4.82	-7.09	8.58	20.71	0.96	-0.78	21.10	2.59	2.62	1.13	0.62	2.49	1.49	1.21	0.97
263.67	8.28	4.07	-7.33	8.51	19.98	-0.39	-0.59	21.56	0.49	0.33	0.40	0.23	0.60	0.57	0.36	0.34
273.44	7.20	4.97	-7.27	9.10	19.17	0.67	-0.21	21.09	0.29	0.22	0.17	0.21	0.34	0.32	0.15	0.29
283.20	6.58	5.58	-6.88	8.27	21.59	0.85	-0.37	21.03	0.21	0.27	0.13	0.17	0.19	0.22	0.17	0.22
292.97	6.70	5.59	-6.97	9.12	23.30	0.24	-0.69	22.30	0.13	0.20	0.16	0.16	0.18	0.15	0.09	0.18
302.73	7.94	6.17	-8.18	8.63	25.02	1.31	-1.37	22.19	0.22	0.28	0.18	0.17	0.24	0.18	0.15	0.30
312.50	8.33	6.23	-8.02	8.81	26.15	1.26	-2.15	23.06	0.17	0.24	0.17	0.17	0.29	0.20	0.12	0.22
322.27	10.63	7.15	-7.85	9.18	28.03	2.09	-3.82	22.49	0.27	0.34	0.29	0.24	0.29	0.12	0.15	0.26
332.03	12.11	8.71	-10.18	8.35	28.28	3.86	-3.79	21.59	0.22	0.17	0.25	0.27	0.25	0.21	0.33	0.32
341.80	13.87	17.64	-16.71	-12.66	27.61	0.84	-3.34	25.76	0.29	0.17	0.27	0.40	0.32	0.31	0.43	0.50

Table 43. 0.2 mm (8 mils), PR=0.6, high inlet preswirl, and 20,200 RPM

	Test Data								Uncertainties							
Freq Hz	Re H_{xx}	Re H_{xy}	Re H_{yx}	Re H_{yy}	Im H_{xx}	Im H_{xy}	Im H_{yx}	Im H_{yy}	Re H_{xx}	Re H_{xy}	Re H_{yx}	Re H_{yy}	Im H_{xx}	Im H_{xy}	Im H_{yx}	Im H_{yy}
9.77	-0.96	4.61	-5.48	-1.35	1.09	0.05	0.02	1.01	0.17	0.13	0.20	0.15	0.22	0.13	0.20	0.18
19.53	-1.11	4.65	-5.26	-1.41	1.84	0.05	-0.09	2.07	0.18	0.12	0.14	0.11	0.17	0.10	0.08	0.14
29.30	-0.87	4.93	-5.33	-1.32	3.11	-0.05	-0.06	3.11	0.12	0.18	0.12	0.19	0.13	0.12	0.18	0.20
39.06	-0.82	4.62	-5.13	-1.30	3.98	-0.14	-0.16	4.37	0.12	0.19	0.12	0.15	0.12	0.15	0.15	0.20
48.83	0.95	3.90	-4.95	-1.08	4.20	-0.05	0.09	5.18	0.39	0.29	0.21	0.20	0.56	0.55	0.17	0.22
58.59	-0.30	4.77	-5.46	-0.81	5.90	-0.36	-0.19	5.95	0.16	0.25	0.13	0.19	0.18	0.22	0.25	0.29
68.36	0.01	5.29	-5.39	0.03	6.66	-0.07	-0.45	7.51	0.25	0.29	0.18	0.23	0.27	0.26	0.19	0.40
78.13	-0.26	5.08	-5.54	-0.20	7.55	-0.51	-0.29	8.21	0.15	0.14	0.14	0.15	0.13	0.14	0.17	0.23
87.89	0.11	4.76	-5.27	-0.03	8.54	-0.58	-0.07	9.26	0.15	0.11	0.09	0.14	0.08	0.14	0.10	0.21
97.66	0.58	4.66	-5.49	0.65	9.64	-0.54	-0.34	10.26	0.31	0.27	0.21	0.22	0.30	0.26	0.36	0.31
107.42	1.11	4.76	-5.34	0.93	10.56	-0.49	-0.47	10.93	0.17	0.08	0.13	0.19	0.19	0.16	0.11	0.25
117.19	1.39	4.67	-5.44	1.63	11.35	-0.23	-0.28	11.73	0.15	0.14	0.13	0.14	0.14	0.15	0.15	0.16
126.95	1.93	4.60	-5.25	2.18	12.15	-0.03	-0.59	12.23	0.16	0.30	0.12	0.22	0.14	0.30	0.13	0.33
136.72	2.56	4.63	-5.80	2.56	12.69	-0.28	-0.62	13.39	0.11	0.15	0.12	0.15	0.11	0.13	0.11	0.16
146.48	2.17	5.44	-5.98	2.05	13.07	0.09	-0.39	13.55	0.13	0.13	0.15	0.14	0.22	0.19	0.22	0.29
156.25	2.16	7.19	-4.31	0.41	13.79	-0.73	-0.46	15.14	0.16	0.14	0.20	0.20	0.13	0.14	0.16	0.18
166.02	3.69	4.12	-6.15	5.62	14.18	1.22	0.04	13.10	0.15	0.31	0.19	0.24	0.19	0.13	0.12	0.25
175.78	4.27	4.75	-6.63	4.75	15.36	0.03	-0.31	16.05	0.11	0.22	0.12	0.19	0.14	0.19	0.13	0.22
185.55	4.69	4.84	-6.40	4.72	16.14	-0.08	-0.66	16.78	0.09	0.14	0.09	0.15	0.11	0.16	0.11	0.20
195.31	4.94	5.28	-6.55	4.92	16.69	-0.24	-0.65	17.07	0.08	0.15	0.12	0.15	0.14	0.10	0.12	0.18
205.08	5.36	4.56	-6.66	5.90	17.46	0.01	-0.55	18.36	0.18	0.37	0.13	0.25	0.20	0.28	0.18	0.32
214.84	6.21	5.16	-6.44	5.91	17.57	-0.69	-0.26	18.84	0.09	0.19	0.11	0.13	0.11	0.14	0.11	0.21
224.61	6.30	5.27	-7.04	6.67	18.54	-0.36	-0.38	19.34	0.13	0.17	0.07	0.14	0.10	0.18	0.10	0.23
234.38	6.82	5.42	-7.28	7.16	19.18	-0.69	0.06	20.17	0.20	0.20	0.08	0.20	0.09	0.21	0.11	0.18
244.14	7.40	5.25	-7.14	7.47	19.63	-0.32	0.13	20.87	0.25	0.25	0.12	0.20	0.15	0.38	0.14	0.21
253.91	6.53	6.66	-6.71	8.68	21.64	0.50	-0.26	21.35	1.60	2.25	0.41	0.33	1.17	0.96	0.38	0.62
263.67	9.05	5.17	-7.36	9.72	20.96	-0.62	0.07	21.86	0.28	0.26	0.20	0.24	0.55	0.51	0.16	0.34
273.44	7.90	5.44	-7.18	10.02	20.33	0.40	-0.05	20.80	0.16	0.26	0.23	0.22	0.34	0.32	0.18	0.27
283.20	7.61	6.47	-7.09	9.06	21.97	0.45	-0.02	21.31	0.26	0.29	0.14	0.23	0.26	0.32	0.13	0.27
292.97	7.63	6.08	-7.46	9.99	23.44	-0.29	-0.30	22.60	0.22	0.26	0.24	0.17	0.23	0.24	0.11	0.24
302.73	8.83	6.31	-8.60	10.45	25.11	0.77	-0.90	21.73	0.22	0.34	0.19	0.18	0.26	0.31	0.18	0.24
312.50	9.13	6.18	-7.87	9.65	25.72	0.45	-1.48	23.08	0.33	0.30	0.20	0.22	0.33	0.33	0.20	0.35
322.27	11.47	8.14	-7.96	9.93	28.25	2.08	-2.79	23.26	0.69	0.47	0.45	0.36	0.55	0.47	0.34	0.38
332.03	12.36	7.89	-9.57	9.55	28.05	1.98	-4.06	23.33	1.71	1.55	0.99	0.78	1.67	1.47	0.94	0.92
341.80	14.45	15.27	-17.16	-3.74	27.24	-0.79	-4.71	27.84	1.54	1.14	1.03	0.59	1.40	1.00	1.07	0.78

VITA

Name:	Michael Lloyd Vannarsdall
Address:	Michael Vannarsdall c/o Dr. Dara Childs Turbomachinery Laboratory Texas A&M University 3254 TAMU College Station, Texas 77843-3254
Email Address:	mlvann3@yahoo.com
Education:	B.S., Biosystems and Agricultural Engineering, University of Kentucky, 2007 M.S., Mechanical Engineering, Texas A&M University, 2011